Specific molecular mechanisms differentiating GABAergic from glutamatergic synaptogenesis

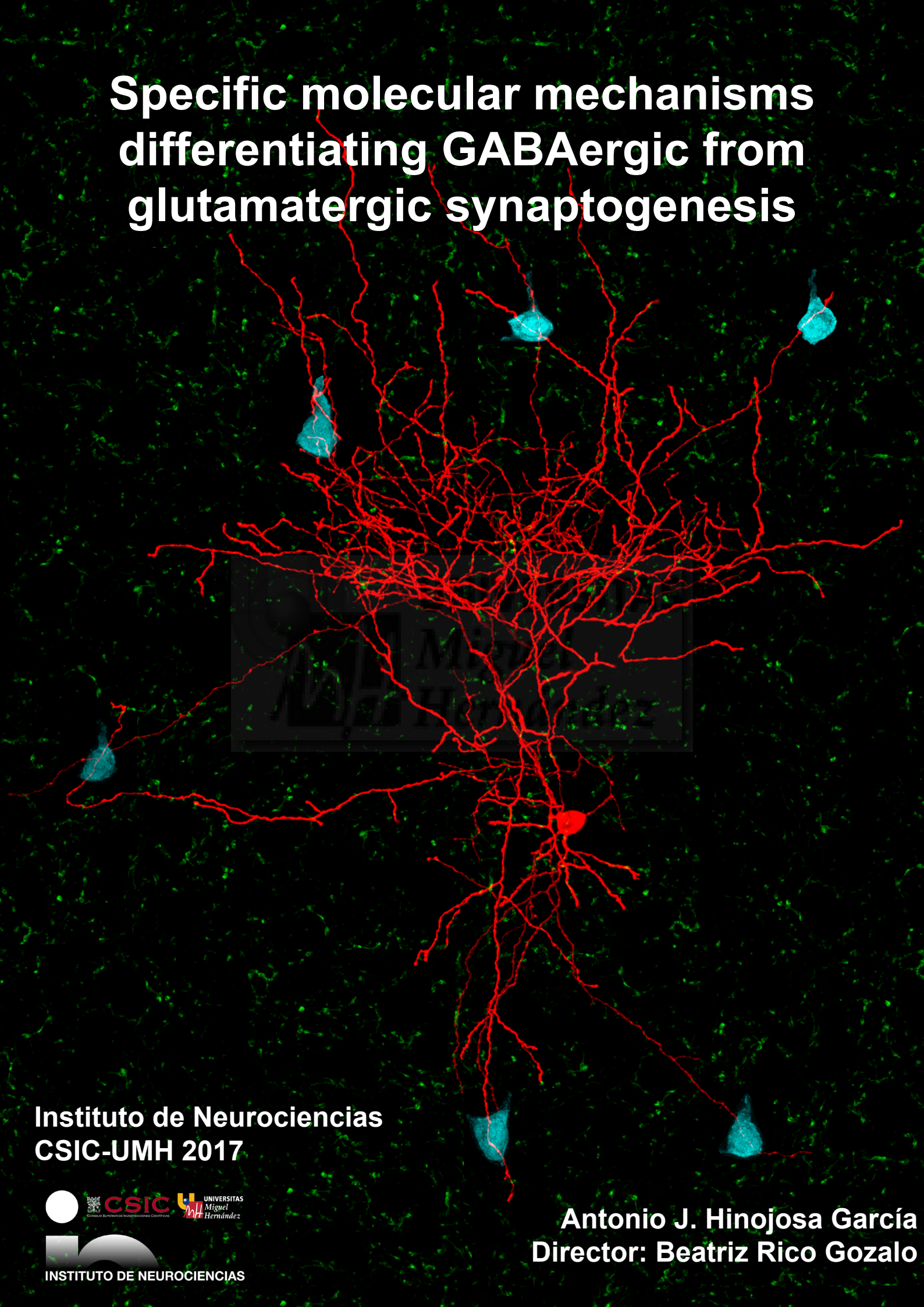

Instituto de Neurociencias
CSIC-UMH 2017

Antonio J. Hinojosa García
Director: Beatriz Rico Gozalo

Specific molecular mechanisms differentiating GABAergic from glutamatergic synaptogenesis

Antonio Jesús Hinojosa García

Director: Beatriz Rico Gozalo

Instituto de Neurociencias CSIC-UMH 2017

INSTITUTO DE NEUROCIENCIAS

EXCELENCIA SEVERO OCHOA

Consejo Superior de Investigaciones Científicas
Universidad Miguel Hernández
Instituto de Neurociencias

Prof. Salvador Martínez
Director

Prof. Salvador Martínez Pérez, Director del Instituto de Neurociencias, centro mixto de la Universidad Miguel Hernández, UMH y la Agencia Estatal Consejo Superior de Investigaciones Científicas, CSIC,

CERTIFICA :

Que la Tesis Doctoral titulada: *" Specific molecular mechanisms differentiating GABAergic from glutamatergic synaptogenesis"* ha sido realizada por D. Antonio Jesús Hinojosa García (NIF 30991778-Z) bajo la dirección del Dr. Beatriz Rico Gozalo, y da su conformidad para que sea presentada a la Comisión de Doctorado de la Universidad Miguel Hernández.

Para que así conste a los efectos oportunos, firma el presente certificado en San Juan de Alicante, a 26 de junio de 2017

Salvador Martínez
Director

direccion.in@umh.es
direccion.in@csic.es
www.ina.umh.es

Tel : +34 965 919220 (s)
+ 34 965 919221 (d)
Fax: +34 965 919561

Av Ramón y Cajal s/n
Campus de San Juan
03550 SAN JUAN DE ALICANTE– ESPAÑA

Department of Developmental Neurobiology

KING'S College LONDON

Department of Developmental
Neurobiology
4th floor, New Hunt's House
Guy's Campus
London SE1 1UL

Direct line: 00-44-20 78486036
E-M: beatriz.rico@kcl.ac.uk

3 July 2017

Dª BEATRIZ RICO, Professor of Developmental Neurobiology at King's College London,

CERTIFICA:

Que D ANTONIO JESUS HINOJOSA GARCIA, DNI/Pasaporte 30991778Z, ha realizado bajo su dirección el trabajo experimental que recoge la Tesis Doctoral titulada: "**Specific molecular mechanisms differentiating GABAergic from glutamatergic synaptogenesis**", y que ha revisado los contenidos científicos y los aspectos formales del trabajo dando su conformidad para que la misma sea presentada a la Comisión de Doctorado de la Universidad Miguel Hernández.

Para que así conste a los efectos oportunos, firma el presente certificado en Londres, a 26 de Junio de 2017.

Fdo.:
Fdo. Beatriz Rico

An important part of this thesis was carried out at the

Centre for Developmental Neurobiology, King's College London (United Kingdom)

ACKNOWLEDGEMENTS

Alguien me contó una vez que el protocolo para ser un buen científico hace uso simplemente de tres reactivos: inteligencia, trabajo duro y suerte. Sin embargo, en esta vida uno nunca consigue las cosas solo, todos nuestros logros se los debemos a quienes recorren el camino con nosotros de una u otra forma. Esta tesis es el fruto de muchos años de esfuerzo, errores y aprendizaje que espero que hayan hecho de mí, al menos, un esbozo de buen científico; pero hoy no estaría escribiendo estas líneas de no ser por aquellos que han ido formándome y apoyándome. Por eso, quiero expresarles mi agradecimiento.

Cuan inteligentes somos nos viene impuesto, primero, por la genética familiar y segundo, por lo que se nos va enseñando. Mi madre y mi padre han sido siempre para mí un ejemplo de tenacidad y esfuerzo por el trabajo. Mi hermano me enseñó a ser curioso y mi hermana a manejar mis sentimientos. Más allá de la familia, algunos profesores de la infancia dejaron una profunda marca en mí: Fanny me enseñó a ser creativo, Margarita me enseñó que era eso de la ciencia y Eduardo me enseñó a pensar más allá.

Desde el día que comencé esta tesis, la primera y principal lección que aprendí es que hay que trabajar al máximo de tus posibilidades para conseguir lo que te propones. Beatriz, con su ejemplo y estímulo, me ha enseñado a no parar de trabajar y a sacar lo máximo de mí mismo. Gracias por no dejar que me durmiera en los laureles ni que la incertidumbre me consumiera y, sobre todo, gracias por esta oportunidad. Oscar también ha sido de una gran ayuda en el diseño de este proyecto y le agradezco sus sabios consejos y críticas. En Valencia, gracias también a Nuria por sus consejos y al Club de Antonio por su apoyo incondicional. Sin embargo, ningún proyecto científico es exitoso sin ponerse la bata y mancharse de ciencia hasta las cejas. Con Ana aprendí lo que eso significa: como extraer orden del caos aparente que la naturaleza nos muestra, y le agradeceré esta lección eternamente. Además, he tenido la suerte de contar con una compañera que comenzó su tesis un día después que yo y la acabará un día antes y que ha supuesto cada día un modelo para mí, Emilia. Con ella he aprendido no sólo a no dejar de trabajar sino también a saber sacar lo mejor de cada persona. Thanks to Rubén, Catarina, Isabel, Cristina, Lynette and André for explaining so many experiments to me and for sharing your experiences in and outside the lab with me. Finally, thanks in general to all the present and past members of Beatriz and Oscar labs for enriching discussions, your help and your smiles (Thanks to Patri, Gabrielle, Giorgia, Verona, Nathalie, Jorge, Ignasi, Alfredo, Diana, Trini, Nasrat, Anna, Verónica, Ian, Aida, Marian, Sandra, Veronique, Virtu, Amanda, Carol, Nines, Malik, Clémence, Fong, Martijn, Alberto, David, Maddalena, Monika, Adrian, Antonio, Giovanna, Kinga and sorry if I forgot about someone).

Y es que, más allá del trabajo, es la suerte de encontrarse con buena gente lo que nos hace felices y nos permite ser buenos en aquello que nos propongamos. Gracias a mis amigos de Córdoba, en especial a Alberto, Xema, Isa y Natalia por vuestra amistad constante e inmutable a lo largo de los años. He tenido la suerte de nacer en una familia que, a pesar de ser muy grande, siempre se ha mantenido unida y me ha llenado de cariño. Gracias por hacerme sentir como si estuviera ahí con vosotros a pesar de la distancia. Me hubiera gustado realizar mi sueño en mi ciudad con ellos, pero fue imposible. No obstante, la gente del laboratorio ha hecho que nunca me haya sentido solo ni en Alicante ni en Londres. Patri, gracias por tus abrazos y por esa sonrisa que parece imborrable en tu cara. Gracias por las canciones y los bailes y, sobre todo, gracias por escucharme. Thanks to her and to Alfredo, Ana, Giorgia, Amanda, Catarina, Marian, Aida, Emilia, Ruben, Fong and every person who made me laugh

and created happy moments in the lab. Finally, thanks to all the friends I have made outside the lab during this time. Sandra, Sergio, Puri, Alejandro, Shaik, Marilyn, Jesh, Kris, Tim and Vincent thanks for the good moments that allowed me to forget about the lab for a while.

Thank you all for helping me to be a better scientist and a better person in one way or another.

SUMMARY / RESUMEN

Synapse formation is one of the most critical events in brain circuit wiring. Glutamatergic pyramidal cells and GABAergic interneurons in the cortex form their synaptic connections through a series of highly orchestrated events. Different genetic programs in both cells leads to basic differences in the process of synapse formation that includes targeted axonal pathfinding. While glutamatergic axons are rather straight and form their synapses through the subsequent extension of protrusions, GABAergic axons are more tortuous and form relatively more crossings with their synaptic targets. This body of data suggests that GABAergic axons look more actively for their synaptic targets while growing. However, little is known about the molecular mechanisms that generate these basic differences. In the present study, we carried out for the first time a high-throughput screening for genes differentially upregulated during synapse formation in both populations of cells. Subsequently, the role of the most striking genes in synaptogenesis was assessed by loss-of-function experiments. We found that Nek7, a kinase involved in microtubule polymerization, is specifically expressed in a high proportion of parvalbumin (PV) cells during synaptogenesis. Targeted elimination of *Nek7* from PV interneurons causes a reduction in the number of synaptic boutons they form onto pyramidal cells, as well as a reduction in the size of their neuritic arbour *in vivo*. Furthermore, axons lacking Nek7 show a more meandering path when grown *in vitro*. Galectin-1 (*Lgals1*), another gene found in the screening, is expressed by somatostatin and PV interneurons. In contrast with Nek7, removing *Lgals1* does not cause any synaptic deficit. Altogether, these data show that our screening is capable of identifying molecules differentially involved in GABAergic interneuron wiring. Moreover, Nek7 findings suggest that the kinase may be involved in a novel molecular mechanism by which PV interneuron axons guide their growth through the formation of synapses.

La formación de sinapsis es uno de los procesos más determinantes durante la formación de circuitos entre neuronas. Las células piramidales glutamatérgicas y las interneuronas GABAergicas de la corteza forman sus conexiones sinápticas a través de una serie de eventos altamente organizados. Programas genéticos diferentes entre los dos tipos celulares llevan a diferencias básicas en el proceso de formación sináptica que incluye la búsqueda de rutas axonales hacia la diana sináptica. Mientras que los axones glutamatérgicos son notablemente rectos y forman sinapsis a través de la extención de protuberancias posteriormente, los axones GABAérgicos son más tortuosos y forman relativamente más cruces con sus dianas sinápticas. Este conjunto de datos sugiere que los axones GABAérgicos buscan sus dianas sinápticas más activamente mientras crecen. En cambio, poco es sabido acerca del mecanismo molecular que genera estas diferencias básicas. En el presente estudio, llevamos a cabo por primera vez un escrutinio genético de alto rendimiento en busca de genes regulados positivamente durante sinaptogénesis en ambas poblaciones celulares. Posteriormente, el papel de los genes más notables en sinaptogénesis fue evaluado mediante experimentos de pérdida de función. Encontramos que Nek7, una quinasa involucrada en la polimerización de los microtúbulos, es expresada por una alta proporción de células parvalbumina (PV) positivas durante la sinaptogénesis. La eliminación dirigida de *Nek7* de las interneuronas PV causa una reducción en el número de botones sinápticos que estas forman sobre las células piramidales, así como una reducción en el tamaño de su árbol neurítico *in vivo*. Además, los axones con niveles reducidos de Nek7 crecen describiendo rutas más serpenteantes *in vitro*. Galectina-1 (*Lgals1*), otro gen encontrado en el escrutino genético, es expresado por interneuronas somatostatina (SST) y PV. Contrario a Nek7, la eliminación de *Lgals1* no genera un déficit sináptico. En general, estos datos muestran que nuestro escrutinio genético es capaz de identificar moléculas involucradas diferencialmente en la formación de circuitos GABAérgicos. Además, los descubrimientos llevados a cabo en Nek7 sugieren que esta quinasa podría estar mediando un nuevo mecanismo molecular mediante el cual los axones de las interneuronas PV guían su crecimiento a través de la formación de sinapsis.

INDEX

ABBREVIATIONS

AC	Auditory cortex
AMPA	α-amino-3-hydroxy-5-methyl-4-isoxazole
APC	Adenomatous polyposis coli
ASD	Autism spectrum disorders
BDNF	Brain-derived neurotrophic factor
BMP	Bone morphogenetic protein
C	Growth cone central domain
CA	*Cornus ammonis*
CAM	Cell adhesion molecule
CCK	Cholecystokinin
CDH	Cadherin
CGE	Caudal ganglionic eminence
CNS	Central nervous system
CRD	Carbohydrate binding domain
Cre	Cyclization recombinase
DEPC	diethyl pyrocarbonate
DIV	Days *in vitro*
DLPFC	Dorsolateral prefrontal cortex
E15.5	Embrionic day 15.5
ECM	Extracellular matrix
EGFP	Enhanced green fluorescent protein
Eph	Eph receptor tyrosine kinase
F	Forward
FACS	Fluorescence-activated cell sorting
FDR	False discovery rate
FGF	Fibroblast growth factor
FITC	Fluorescein isothiocyanate channel in FACS
FS	Fast spiking
FSC-A	Forward scattered light
G30	GAD65-GFP Transgenic mice
GABA	Gamma-aminobutirin acid
$GABA_A$	Gamma-aminobutirin acid receptor A
$GABA_B$	Gamma-aminobutirin acid receptor B
GAD65	Glutamate decarboxylase 65
GAD67	Glutamate decarboxylase 67
Gal	Galactose
Gal-1	Galectin 1 (Protein)
Gal-3	Galectin3 (Protein)
GalNAc	N-acetylgalactosamine
Geph	Gephyrin
GFP	Green fluorescent protein
GFP^-	GFP positive cells
GFP^+	GFP negative cells
GIN	GAD67-GFP Transgenic mice
Glc	Glucosamine
GlcNAc	N-acetylglucosamine

GO	Gene ontology
GOF	Gain of function
GSK-3β	glycogen synthase kinase 3 beta
HA	Human influenza hemagglutinin
HANek7	Nek7 fussion protein construct with an HA tag
Hip	Hippocampus
IN P0	Experimental group of interneurons at postnatal day 0
IN P10	Experimental group of interneurons at postnatal day 10
KO	Knockout
Lgals1	Galectin 1 (gene)
Lgals3	Galectin 3 (gene)
LGE	Lateral ganglionic eminence
Lhx6	LIM homeobox protein 6
LOF	Loss-of-function
LTP	Long-term potentiation
MAPs	Microtubule associated proteins
MECP2	Methyl-CpG-binding protein 2
MGE	Medial ganglionic eminence
mNek7	Nek7 synonimously mutated and tagged with Flag
mRNA	Messenger ribonucleic acid
Narp	Neuronal pentraxin-2
NCAM	Neural cell adhesion molecule
NEK	NIMA (never in mitosis A)-related kinases
Nex	Neurogenic differentiation protein 6
NGF	Nerve growth factor
NIMA	Never in mitosis gene A
Nkx2.1	NK2 homeobox protein 1
NLG	Neuroligin
NMDA	N-metil-D-aspartato
NP1	Neuronal pentraxin-1
Npas4	neuronal PAS domain protein 4
NPY	Neuropeptide Y
NSF	NEM sensitive factor
NUSE	Normalized Unscaled Standard Error
P	Growth cone peripheral domain
PBS	phosphate buffer saline
PBS-T	Phosphate buffer saline with tween
PBV	Piccolo-Bassoon transport vesicles
PCA	Principal component analysis
PCDH	Protocadherin
PEI	Poly(ethylenimine)
PFA	Paraformaldehyde
PFC	Prefrontal cortex
PI3K	Phosphoinositide 3-kinase
PlxnB1	Plexin B1
PSA	Polysialic acid

PV	Parvalbumin
PX	Postnatal day X
Pyr P0	Experimental group of pyramidal cells at postnatal day 0
Pyr P12	xperimental group of pyramidal cells at postnatal day 12
qPCR	Quantitative PCR
R	Reverse
RMA	Robust Multiarray Average
S.E.M.	Estándar error of the mean
SALMS	Synaptic cell adhesion-like molecules
SAM	Significance analysis of microarrays
SCV	Small clear vesicles
Shh	Sonic-hedgehog
SSC	Somatosensory cortex
SSC-A	Side scattered light
SST	Somatostatin
Syt1	Synaptotagmin 1
Syt2	Synaptotagmin 2
v/v	% volume/volume
VC	Visual cortex
VIP	Vasointestinal peptide
w/v	% weight/volume
w/w	% weight/weight
Wnt	wingless-type MMTV integration site family
WT	Wild type

1. INTRODUCTION

1.1. Organization of the cerebral cortex

1.1.1. Structure and function of the cerebral cortex

Since ancient times, the cerebral cortex has been considered one of the structures most related to cognitive function (Rocca, 2003). However, its pivotal role was not demonstrated and recognized until the 19th century, when important breakthroughs were made using electrical stimulation in cortical areas showing its role in sensory and motor functions (Gross, 2007). The sensory information received in the primary cerebral cortices is then processed to give rise to complex cognitive functions. This requires the integration of information from several cortical areas and takes place in the associative cortices (Kandel, 2013). Therefore, all information processing essential to support the biological bases of sensory perception, movement and complex functions such as motor planning, working memory or even consciousness culminates in the cerebral cortex.

Thus, it is not difficult to foresee that dysfunctions in the cerebral cortex lead to a broad range of neurological disorders such as schizophrenia, autisms, mental disability, depression, bipolar disorder, or dementia (Pandya *et al.*, 2015). In all these diseases, cognitive function is dramatically impaired and, therefore, the quality of life of people suffering from them. This is why a detailed knowledge of the cerebral cortex is essential to understanding not only the biological basis of cognition but also the aetiology of different diseases.

During development, the most anterior part of the neural tube swells from the forebrain, which will later give rise to the telencephalon and diencephalon. The cerebral cortex arises from the telencephalon. Coordinated BMP (Bone morphogenetic protein) and Shh (sonic-hedgehog) signalling, from the dorsal epidermis and the ventral part respectively, differentiate the pallium (dorsal region) from the subpallium (ventral region). Then, an active proliferation within the subpallium results in the emergence of three structures: the medial, lateral and caudal ganglionic eminences (MGE, LGE and CGE respectively) (Rallu *et al.*, 2002). In particular, a combination of secreted factors will induce the expression of different transcription programs in the MGE, LGE and ventricular zone at the cortical primordium. This will activate differential gene expression profiles and give rise to completely different types of cells. For example, in the MGE Shh produces the expression of Nkx2.1 (Lupo *et al.*, 2006).

Although the primary source of neurons that populates the cerebral cortex comes from the pallial region, there is an important contribution of neurons from the subpallium. Subpallial neurons migrate tangentially, parallel to the proliferative area of origin, to reach the pallial region. In contrast, Pallial cells are originated in the subventricular zone and they migrate radially, orthogonal to the proliferative area, to reach their final destination into the cortex (Marín and Rubenstein, 2003). The intrinsic developmental program of cortical cells orchestrates a constellation of events that will lead to the formation of a fully functional cortex. Therefore, knowing how the cortex is formed will allow us to understand both its functions and also how small modifications in this program can alter these.

Differential aspects in the development of cortical regions lead to a diverse cytoarquitecture across cortices (Cho *et al.*, 2016). Cortical areas can be classified by the number of layers they have. According to this criterion, we can distinguish: six-layered neocortex, archeocortex, with three to four

layers (i.e. entorhinal and retrosplenial cortex, subiculum and hippocampus) and paleocortex with three layers (i.e. piriform cortex).

Although the functional significance of layer number is not known, it seems plausible that complexity increases with the number of layers. Neocortex is the newest addition to our brain, and is the biggest and the most widely used for cognitive functions in mammals. Nevertheless, it is important to mention that, there are also multiple complex functions, such as memory, coded by less complex cortices like the hippocampus.

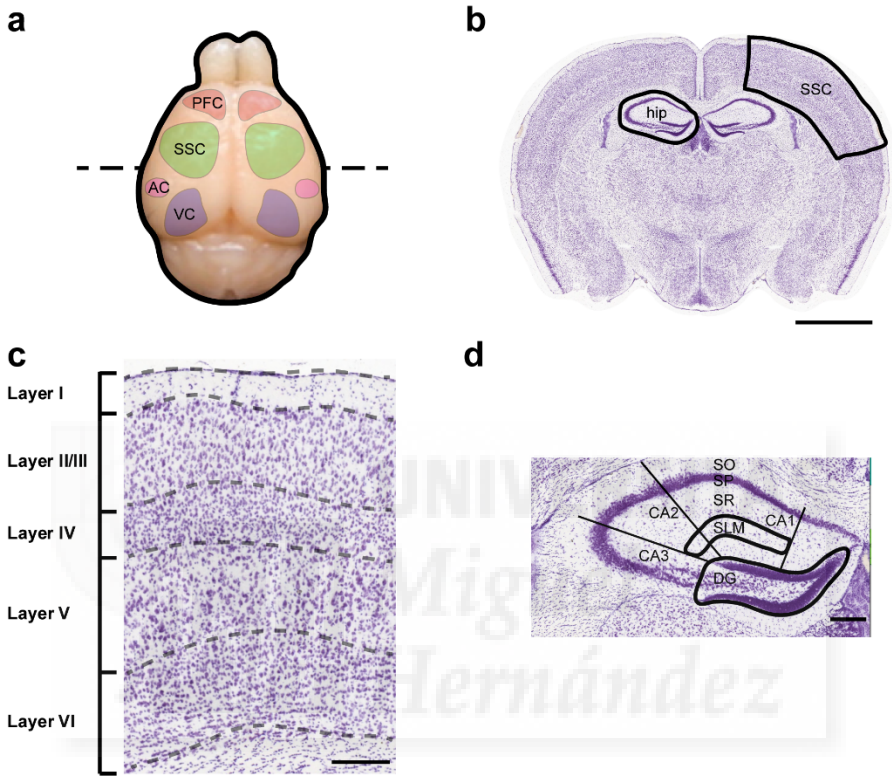

Figure 1.1. Structural features of the cerebral cortex. (a) Schematic of a mouse brain. Different neocortical regions are shown, from anterior to posterior: PFC prefrontal cortex, SSC Somatosensory cortex (S1), AC auditory cortex (A1), VC visual cortex (V1). Dashed line: coronal section showed in (c-d). (b) Nissl staining of the coronal section marked in (a). Hippocampus (hip). (c) Layer organization of the somatosensory cortex. (d) Regions differentiated in the rostral hippocampus. Radially from the centre: Stratum lacunosum moleculare (SLM), stratum radiatum (SR), stratum piramidale (SP) and stratum oriens (SO). Anticlockwise from the right: dentate gyrus (DG), CA3, CA2 and CA1 (*cornus ammonis 1-3)*. Scale bars: (b) 2 mm (c,d) 200 µm.

50 different cortical regions can be further differentiated looking at the thickness, density or other histological features of cortical layers. (For the most important ones see Fig. 1.1a) Layers in the neocortex are numbered with roman numbers (I-VI) from the pial surface to the ventricle (Fig. 1.1b, c). However, layers II and III in the mouse are fused in one unique layer named II/III. It is well known that the layering division in the cerebral cortex reflects a difference in their connectivity: layer I contains mainly neuropil, layer II/III project to other cortical regions, layer IV receives thalamic input and layer V and layer VI primarily projects to subcortical areas and to the thalamus, respectively (Fig. 1.1c). These structural features reflect functional differences. For example, motor cortex does not have a defined

layer IV because the thalamus does not project to this cortical area (Purves, 2011). Furthermore, neocortical neurons are organized radially in modules known as cortical columns. In sensory cortices, these modules group neurons that share a given receptive field and encode for similar features (Purves, 2011).

Finally, it is important to briefly describe the organisation of one of the most studied cortical areas closely related to the neocortex, the hippocampus (Fig.1.1b, d). The hippocampus can be divided in dentate gyrus, formed by the *fascia dentata* and hilus; and *cornu ammonis* (CA), formed by the subregions CA1, CA2 and CA3 (Fig. 1.1d). In the CA regions several layers from radial to central can be differentiated: stratum oriens, stratum pyramidale, stratum lucidum (present in CA3), stratum radiatum, stratum lacunosum-moleculare and hippocampal sulcus that separates CA1 from dentate gyrus (Andersen, 2007; Fig. 1.1d).

1.1.2. Cell types in the cerebral cortex

Two main cell type populations are present in the cerebral cortex: excitatory pyramidal cells, of pallial origin, and inhibitory interneurons, of subpalial origin. Pyramidal cells account for an 80% of cortical neurons, they are excitatory and classified as projection neurons (i.e. project to other brain areas). They are more homogeneous morphologically compared to interneurons, although subtypes can be found regarding their projection targets. There are pyramidal cells projecting to other ipsilateral cortical areas (associative), contralateral cortical regions (callosal) or subcortical areas (corticofugal). These subpopulations are originated from different progenitors and have a differentiated molecular programme that generate their diversity (Lodato and Arlotta, 2015; Molyneaux *et al.*, 2007). An example of these differences is the expression of the transcription factors Ctip2 and Satb2 that are related to callosal and corticospinal projection neurons, respectively (Alcamo *et al.*, 2008; Arlotta *et al.*, 2005; Britanova *et al.*, 2008). However, the richest diversity among the neurons populating the cortex is found in the remaining 20% population formed by interneurons.

As opposed to pyramidal cells, interneurons project locally and use gamma-aminobutiric acid (GABA) as inhibitory neurotransmitter. Various attempts have been made to classify interneurons and it is a topic of continuous debate. Although numerous criteria can be used, often the existent ones seem to be sometimes arbitrarily chosen. Furthermore, the nomenclaure varies among researchers in different areas of knowledge what often makes communication difficult. In spite of this, there is a rather consensuated classification according to three main features: 1. Morphology, 2.Genetic markers and 3. Electrophysiological properties. Ideally a global classification should span the three of them, although they are not always compatible. It would be important for example, to stick to a classification that gives us information about the functionality of each type of interneuron in the cortical circuitry. This classification is of course dynamic and has to be constantly updated in a joined effort from the scientific community (Ascoli *et al.*, 2008).

Increasing evidence suggests that disruption of the excitatory–inhibitory balance maintained by pyramidal cells and interneurons is linked to the aetiology of different neurological and psychiatric disorders. (Dani *et al.*, 2005; Levitt, 2005; Lewis *et al.*, 2005; Rubenstein and Merzenich, 2003; Verret *et al.*, 2012). In particular, several studies suggest that some forms of autism are caused by an increased ratio of excitation/inhibition. These changes in the network would affect sensory, mnemonic, social and emotional capacities of individuals (Rubenstein and Merzenich, 2003). The opposite imbalance is

thought to take place in Rett syndrome because this effect is observed in mice mutant for the causative gene, methyl-CpG-binding protein 2 (MECP2) (Dani *et al.*, 2005). Furthermore, mutations on *ErbB4*, a gene linked to schizophrenia, cause deficits in the wiring of a subpopulation of interneurons, an increase in cortical excitability, abnormal oscillatory activity and cognitive deficits (Fazzari *et al.*, 2010; Del Pino *et al.*, 2013). Also, deficits in the expression of receptors or voltage-channels particularly enriched in interneurons leads to phenotypes that are associated with epilepsy (Sun *et al.*, 2016). Finally, mouse models indicate that an unbalance between inhibition and excitation could also be underlying some of the cognitive deficits found in neurodegenerative disorders like Alzheimer (Verret *et al.*, 2012).

1.1.3. Origin of interneuron types

As mentioned above, knowing the developmental program of a neuron can give us information about its later function. Interneurons in the cortex are produced in several areas, where they are subject to different signals. These are the medial ganglionic eminence (MGE), caudal ganglionic eminence (CGE) and preoptic area (POA) (Gelman and Marín, 2010).

The MGE generates most of the parvalbumin (PV), basket and chandelier cells, and somatostatin (SST) expressing cells. The progenitors present in this area express NK2 homeobox protein 1 (Nkx2.1) and LIM homeobox protein 6 (Lhx6) (Gelman and Marín, 2010). Both are transcription factors and Lhx6 is downstream of Nkx2.1. CGE produces two populations of cells: bipolar and double-bouquet cells, which express vasointestinal peptide (VIP) and calretinin; and multipolar cells, which express reelin and neuropeptide Y (NPY). The last region, POA, produces also cells with multipolar morphology and a small fraction of PV and SST cells that does not express Lhx6 but express Nkx2.1. (Gelman and Marín, 2010).

It has been shown that altering the developmental program of interneurons affects their identity. For example, suppressing *Shh* signaling in the telencephalon, and thus repressing Nkx2.1 expression, reduces the number of parvalbumin (PV) and somatostatin (SST) expressing cells in the cortex (Xu *et al.*, 2005). This shows that the developmental program of a cell is essential for knowing the later identity and function of an interneuron and for their classification (See section 1.1.5 for a full description of the interneuron types mentioned).

1.1.4. Interneuron subtypes based on morphology

Santiago Ramón y Cajal and, afterwards, Lorente de Nó did the first classification of interneurons with Golgi-based preparations (Lorente de Nó, 1922; Ramón y Cajal, 1899). A finest morphological resolution has been achieved since then and numerous features can be used to classify interneurons looking at the soma, neurites and cell connectivity (Petilla Interneuron Nomenclature Group *et al.*, 2008).

Somas can vary in shape (sphericity), size (diameter) or orientation of their main axis in relation with cortical radial axis. However, the main morphological feature of neurons resides in the projections that emerge from the soma: the neurites. Multiple variables in branching metrics have been defined to help in this classification. For example, for neurite thickness and length can be measured to compare between different cell types. Branches are generated all along neurite extension, so the frequency of branching points can be measured as well as the branching angle. In addition, the neurite can meander

during its path, which can be measured with tortuosity. Finally, Sholl analysis is used to quantify the complexity of a neuritic arbour in a single measure by quantifying the number of intersections with concentric circles centred in the soma (Ascoli *et al.*, 2008; Sholl, 1953).

Among the different neurite types, axon and dendrites, the first is the major determinant of connectivity and is used as the principal classification criteria. The reason is that axonal morphology features are correlated with both developmental origin and synaptic physiology. Axon originates from the soma or a primary dendrite and has a distinctive axonal initial segment. There are some specific branching features of the axon, for example, they can branch either close to the soma or far from it in other regions such as different layers. Related to this, terminal branches can be curved or straight and be clustered or independent. Another distinctive feature of the axon whose distribution can be used to classify neurons is the distribution of myelin along its length. Finally, we can characterize a neuron by the distribution of its synaptic boutons. While terminal boutons are located at the end of the axon, *en passant* boutons can be found in the middle of the branch (Criteria described in Ascoli *et al.*, 2008).

Interneuron dendrites have simpler morphology compared to both pyramidal cell dendrites and interneuron axons. For this reason, they are secondary in the classification as compared to the axon. The number of dendrites that emerge from the soma varies among the interneurons. According to this, we can find unipolar, bipolar or multipolar cells. The distribution of these dendrites around the soma is also a distinctive feature. For example, there are bitufted cells that have two clusters of branches in opposite directions. Similarly, the directionality can change and they can be radial or tangential respect to the cortical radial axis. Finally, synaptic input distribution of both excitatory and inhibitory inputs can vary as well as the presence of dendritic spines, described as spiny or aspiny neurons (Ascoli *et al.*, 2008).

Altogether, the different morphological features of a cell reflect the type of connections it makes, and therefore, this criterion can be used to classify interneurons functionally. A wider criterion can be applied by using the connectivity of the cell based on either its inputs (dendrites and soma) or its outputs (axon). The subcellular location of their outputs is also different among interneurons, some cells connect to the soma while others connect to the axon or dendrites. Within these compartments, connections can be distributed evenly, following a so called “distributed” pattern, or forming groups, “clustered”. Lastly, dendritic shafts or spines can be the recipients of synaptic contacts in the postsynaptic dendrite.

Although most of this detailed analysis has been originally done in hippocampus most of the aspects are also found across the entire cortex. However, most of the information here is referred to neocortex. Using these criteria interneurons have been classified by many different researchers who have generated diverse groups. While most of the defined groups are consensuated some have been misused in the last years. However, the criteria by which some types have stopped being use is not clear and, for this reason are included in this list (For a sum up of morphological types examples see fig. 1.2).

Basket cells: this population accounts for 50% of all inhibitory interneurons. They can be divided in three main subclasses based on their axonal and dendritic morphology (Markram *et al.*, 2004), although this subclassification has not been used in the latest studies (Jiang *et al.*, 2015; Tremblay *et al.*, 2016; Wamsley and Fishell, 2017). All of them have in common their connectivity pattern: they target the soma and proximal dendrites of pyramidal cells and interneurons. Their name comes from the so-called basket-like structure they form when many of their axons, which have a curved shape in the

terminal portion, contact the soma of pyramidal cells (Jiang *et al.*, 2015; Markram *et al.*, 2004). Their connectivity is classified as pyramidal-neuron-targeting because they project to local pyramidal neurons and receive a strong excitation from them. They project also to interneurons of the same morphological type (Jiang *et al.*, 2015; Fig. 1.2). In the hippocampus, basket cells typically branch in the pyramidal cell layer (Somogyi and Klausberger, 2005).

Large basket cells: these cells have a bipolar, bitufted or even sometimes a pyramidal dendritic arbor without spines. Their axonal arbor is quite extensive with a low bouton density. This is related to its connectivity: their axon can reach other layers or cortical columns what makes them the main source of lateral inhibition; i.e. intercolumnar (Markram *et al.*, 2004).

Small basket cells: the dendritic arbour is bitufted or bipolar in layer II/III and multipolar in layer IV. Compared to large basket cells, their axons form more branches, are more curve and extend mainly locally. Yet, a few collaterals extend out of the local axonal cluster occasionally. There is as well a high density of lumps, or varicosities, that contain synaptic boutons. Consequently, they form the highest number of synapses onto pyramidal cells (Markram *et al.*, 2004).

Nest basket cells: their arbour resembles the nest of a bird. They are hybrids between large and small basket cells regarding axonal morphology. A local axonal cluster is extended locally, like small basket cells, and further axonal collaterals with a lower bouton density are formed resembling those of large basket cells (Markram *et al.*, 2004).

Shrub cell: this cell type is specific from layer V and was described in visual cortex (Jiang *et al.*, 2015). While their dendrites have a multipolar morphology, their axon emerges from the soma and ascends shortly before branching profusely forming a shrub like axonal field. As basket cells, their connectivity pattern let them be classified into the pyramidal-neuron-targeting group (Fig.1.2).

Horizontally elongated cell: as the previous population, it was described in layer V of visual cortex and its dendritic arbour is usually multipolar. Conversely, their axon is quite thick and arborises mostly horizontally within the same layer (Jiang *et al.*, 2015). They are also pyramidal-neuron targeting interneurons (Fig.1.2).

Chandelier cells: Chandelier cells often have a fusiform soma. Their axon has high branching density formed at shallow angles. Bouton density is high and clustered in rows forming a structure like a chandelier and their terminal portion is straight. This structure reflects their unique connectivity: they contact the axonal initial segment of pyramidal cells (Jiang *et al.*, 2015; Markram *et al.*, 2004; Fig. 1.2). Similar features are found in a subset of hippocampal interneurons (Somogyi and Klausberger, 2005).

Martinotti cells: Martinotti cells have the most elaborate dendritic tree among all the interneurons being usually bitufted in morphology. This cell type has also an axonal morphology that reflects its connectivity. They arborise mainly in layer I where they contact the distal dendrites of pyramidal cells, spanning even neighbouring and distant columns. However, they target other multiple domains like proximal dendrites and soma (Markram *et al.*, 2004). Regarding the cellular connectivity, they can be classified as master regulators because they connect non-specifically to every cell type in the cortex, although they avoid inhibiting other Martinotti cells. They receive strong input from pyramidal cells and inhibition from neurogliaform and bipolar cells (Jiang *et al.*, 2015; Fig. 1.2). Oriens lacunosum-moleculare (O-LM) interneurons have similar connectivity in the hippocampus. Their soma is located in

stratum oriens and they contact the apical dendrites of pyramidal cell in stratum lacunosum-moleculare (Somogyi and Klausberger, 2005).

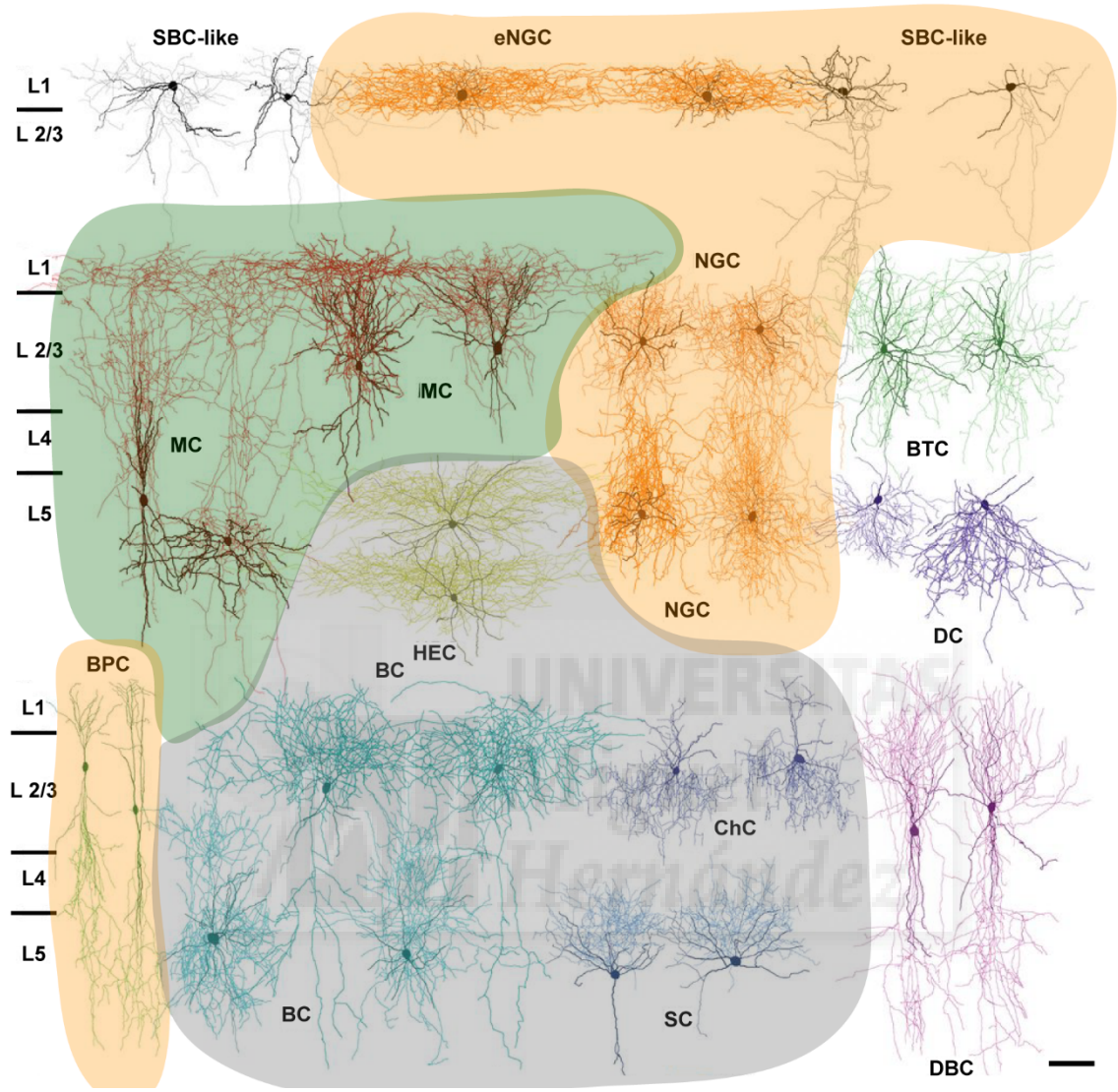

Figure 1.2. Morphologically defined types and marker expression. Examples of the main interneuron types described in the cortex grouped by the expression of non-overlaping molecular markers. Martinotti cell, MC; neurogliaform cell, NGC; basket cell, BC; single-bouquet cell-like cell, SBC-like; bitufted cell, BTC; bipolar cell, BPC, double-bouquet cell, DBC; chandelier cell, ChC; shrub cell, SC; horizontally elongated cell, HEC; deep-projecting cell, DC. Grey area, parvalbumin expressing cells; green area, somatostatin expressing cells; orange area, 5HT3aR expressing cells; excluded cells have not been clearly labelled by specific markers. Scale bar, 100 µm. Extracted from Jiang *et al.*, 2015.

Bipolar cells: this subpopulation of interneurons has a spindle or ovoid soma. They are named after their dendritic bipolar or bitufted morphology that holds a narrow vertical extension. Similarly, the axon emerges from a primary dendrite and forms a narrow band that crosses all layers. Bouton density is quite low in these cells. Consequently, they connect with a few cells, contacting usually with the basal dendrites of pyramidal cells (Markram *et al.*, 2004). They fall into the connectivity group named interneuron-selective interneurons which are cells that project specifically to other interneurons avoiding pyramidal cells. More specifically, they project to Martinotti cells and avoid self-inhibition. Little input is

received from local pyramidal cells or local inhibitory cells; thus, they may be primarily controlled by long-range inputs (Jiang *et al.*, 2015; Fig. 1.2).

Double bouquet cells: like the previous group, they have a bitufted dendritic arbor. However, their axonal morphology is quite distinctive. They form fascicles in a cylindrical shape similar to a horsetail and the most distant branches are thicker than the ones that are closer to the soma. Along its length, they form multiple varicosities and branches. They connect to the basal dendrites of pyramidal cells but, opposite to other pyramidal targeting cells, they do not receive strong excitatory input (Jiang *et al.*, 2015; Markram *et al.*, 2004; Fig. 1.2).

Bitufted cells: they have two primary dendrites that emerge from opposite poles of an ovoid soma. While the dendritic arbor is similar to bipolar and double bouquet cells, the axonal morphology is what distinguish them. While they are not very large in the radial axis, they extend their branches mainly tangentially, although not as much as horizontally elongated cells. Consequently, their connectivity stays in the same layer but extends to neighboring columns. They are dendritic-targetting cells, falling in the category of cells targeting pyramidal neurons , but they do not project to other bitufted cells (Jiang *et al.*, 2015; Markram *et al.*, 2004; Fig. 1.2).

Deep-projecting cell: while their dendritic arbor has a multipolar morphology, the axon descends towards deeper cortical layers. They can be found in layer V and their connectivity is interneuron-selective (Jiang *et al.*, 2015; Fig. 1.2).

Neurogliaform cells: these cells are the smallest among interneurons. They form a very symmetrical and spherical dendritic arbor. Furthermore, they are short and spiny, with many small bead-like structures, but limited branching points. Conversely, their axon arborises densely short after emerging from the soma, forming numerous small synaptic boutons (Markram *et al.*, 2004). They are master regulators because of their nonspecific connectivity. But contrary to Martinotti cells, they receive little input from pyramidal cells or local inhibitory cells. Thus, they are thought to mediate their connections through volume transmission (Jiang *et al.*, 2015; Fig. 1.2).

Layer I interneurons: all the previous interneurons populate layers II to VI with variable densities. Layer I is just sparsely populated by particular subtypes of interneurons. During development, Cajal-Retzius cells are the only neuron subtype allocated into layer I. They have extensive axonal arbors that horizontally contact the dendrites of pyramidal cells through several columns, however, they are confined to layer I (Markram *et al.*, 2004).

In the adult, two subclasses of interneuron are exclusively found in layer I: the neurogliaform cells and a curious type called multipolar. These are named after their multipolar dendritic morphology, which can be rather large. Their axon descends from layer I reaching as far as layer V (Gentet, 2012). In other study, a cell type with similar morphological features is described and named single-bouquet cell like (Jiang *et al.*, 2015; Fig. 1.2). This type is classified as an interneuron-selective interneuron, like bipolar or descending cells. Conversely, they inhibit other interneurons but Martinotti cells.

1.1.5. Interneuron subtypes based on molecular markers

Interneurons can also be classified by their gene expression pattern. Compared to morphology, this classification criterion is less ambiguous and prone to controversy. There are several markers that allow a classification of interneurons in a robust and non-overlapping manner. These are mainly

transcription factors, neurotransmitters or their synthesizing enzymes, neuropeptides, calcium-binding proteins, receptors, structural proteins, cell-surface markers, ion-channels, connexins or transporters (either plasma membrane or vesicular) (Ascoli *et al.*, 2008).

A different gene expression profile is often synonym of a distinct developmental origin. Having non-overlapping populations characterized by the expression of a set of genes can give us information about their developmental program as well as their later function (Tremblay *et al.*, 2016). Such classification exists for interneurons, for example, all the cells expressing glutamate decarboxylase 67 (GAD67), the enzyme that synthesizes GABA, can be classified by the expression of three non-overlapping markers. The relationship with the morphological types is described here. However, some of the morphologies have not been fully characterized (Fig. 1.2).

Parvalbumin (PV): 40% of all interneurons express this calcium binding protein. We can find it in most of the basket cells, in shrub and horizontally extending cells (Jiang *et al.*, 2015; Tremblay *et al.*, 2016). It is also expressed by approximately 30% of Chandelier cells although the percentage varies in different cortical regions (Taniguchi *et al.*, 2013; Fig. 1.2).

Somatostatin (SST): 30% of all interneurons express this neuropeptide. The main population of cells expressing SST are Martinotti cells. The rest of SST positive cells have different morphologies but have not been fully classified (Ma *et al.*, 2006; Wang *et al.*, 2004). The last study carried out by Tolias *et al.* reveals that a 25% of SST positive cells have a basket morphology (Jiang *et al.*, 2015; Fig. 1.2).

Ionotropic serotonin receptor 5HT3aR: they account for the remaining 30% of interneurons. Many of the morphological subtypes are represented in this population, including bipolar, neurogliaform, multipolar, single-bouquet like cells and a subpopulation of basket cells (Jiang *et al.*, 2015; Tremblay *et al.*, 2016; Fig. 1.2).

Although non-overlapping, these three subpopulations do not give a complete profile of the interneurons expressing each marker. For example, different morphological or functional subtypes share them. However, they are the starting point of a hierarchical classification where other markers can further subdivide these categories. In fact, there are other molecular markers that are not expressed in non-overlapping populations but, together with the previous ones, can define subpopulations (Tremblay *et al.*, 2016).

Vasointestinal peptide (VIP): this neuropeptide is expressed by 40% of 5HT3aR cells and all the cells expressing it contain 5HT3aR. VIP 5HT3aR expressing cells are PV negative small basket cells, bipolar and multipolar. Conversely, single-bouquet like, PV negative large basket cells and neuroglia form do not express VIP (Tremblay *et al.*, 2016).

Calbindin (CB): it is a calcium binding protein expressed in subpopulations of PV basket and Martinotti cells (Tremblay *et al.*, 2016).

Calretinin (CR): this calcium binding protein is expressed in subsets of VIP and Martinotti cells (Tremblay *et al.*, 2016).

Cholecystokinin (CCK): this neuropeptide labels a subpopulation of basket cells that does not express parvalbumin but 5HT3aR instead. Given their known connectivity, CCK may depend more on

subcortical input while PV basket cells are more driven by the local pyramidal cell input (Tremblay *et al.*, 2016).

Neuropeptide Y (NPY): this neuropeptide is present in some neurogliaform and Martinotti cells.

Several attempts have been made to fully characterise the expression profile of isolated interneurons using single-cell sequencing (Cadwell *et al.*, 2016; Fuzik *et al.*, 2016; Tasic *et al.*, 2016; Zeisel *et al.*, 2015). Single-cell transcriptomic signatures can be associated with specific electrophysiological properties. However, the technique has still low efficiency in detecting the whole transcriptome of the cell.

Althogether, these approaches comprise a powerful tool to classify interneurons. Nevertheless, it is difficult to interpret the functional meaning of these groups because the specific function that these molecules have in interneurons are not known.

1.1.6. Interneuron subtypes based on their electrophysiological properties

A key feature to classify interneurons is their electrophysiological properties. To understand how they fire provides information about how they control the activity in the network influencing the final computation of the circuitry. However, a problem often found is that these properties change with the experimental conditions and thus a rigorous standardization of the techniques used must be applied to compare different experiments (DeFelipe *et al.*, 2013; Tremblay *et al.*, 2016). Although many variables can be selected to characterize an interneuron, we will just describe here the most commonly used properties.

Passive properties where no modification is applied to the neuron, like the membrane potential, are frequently recorded. Subthreshold properties, where small changes in cell voltage are applied without triggering an action potential, are also assessed. These properties include the electrical resistance to a given injected current of either the whole cell (input resistance) or the cell membrane only. An additional measurement is the minimal current injected for the cell to fire an action potential, named rheobase (Ascoli *et al.*, 2008).

Also, different steps of current injection can be carried out *in vitro* to characterize the cell response. It is important to take into account these conditions and the age of the animal since the cell response can change with these variables. Once a depolarizing step is applied, the individual action potential features can be measured: voltage threshold for firing, spike amplitude and half-width or, after the action potential, other parameters including afterhyperpolarization or afterdepolarization can be assessed. In addition, the firing pattern of a cell can be obtained when multiple action potentials are fired.

The cell response can be divided in two phases: the onset, the initial part, and the steady-state, the response of the cell to an extended current injection. The firing frequency and inter-spike interval can be registered in both phases. The main feature measured at the onset of the cell response is when the cell starts firing; for example, a delayed cell will not fire its first action potential immediately after the current is injected. This particular parameter provides specific properties to some interneuron subtypes like the parvalbumin cells. Often the cell initially responds with a short train of action potentials at a higher frequency than normal. This train is called burst and it can also happen during the steady-state phase.

Many different patterns can be observed at steady-state and this is one of the main features to classify interneurons (Ascoli *et al.*, 2008):

Amplitude accommodation: decrease in amplitude during a train of action potentials.

Spike frequency adaptation: decrease in firing frequency along the train.

Fast spiking (FS): this firing pattern consist on a continuous high frequency set of brief action potentials and a fast deep afterhyperpolarization.

Regular spiking: this pattern displays a continuous and homogeneous frequency contrary to an irregular spiking pattern.

Stuttering: this one consists on short trains of spikes with short inter-spike intervals alternated with longer periods without activity.

Spiking can also be measure extracellularly. This methodology let us measure the phase relationship between the interneuron action potentials and local field oscillations. Other features that vary among interneurons are the postsynaptic responses. The profile of inhibitory and excitatory postsynaptic currents can be measured as well as their spatial and temporal summation. Furthermore, these currents can be subject to short and long-term plasticity mechanisms. Finally, the effect of neuromodulators or the presence of gap junctions can affect interneurons in different ways.

How do the morphological types fit with electrophysiological patterns? Although some morphological categories mostly correspond to a specific firing pattern, a morphologically identified neuron can have many discharge behaviours (Markram *et al.*, 2004). These are the most known patterns:

PV Basket cells: they have mostly fast spiking firing properties. However, we can find a diversity of delayed, non-delayed and stuttering behaviours (Tremblay *et al.*, 2016).

Chandelier cell: they are fast spiking with a slower firing frequency than basket cells (Tremblay *et al.*, 2016).

SST Martinotti cells: they have low threshold spiking and high input resistance although we can also find bursting or regular spiking cells. They show a low maximum firing frequency and spike frequency adaptation. After a hyperpolarizing step, they can show a rebound spike (depolarization) (Tremblay *et al.*, 2016),

SST non-Martinotti cells: these cells are described as quasi fast spiking, being like these but with spike frequency adaptation (Tremblay *et al.*, 2016).

5HT3Ar, VIP Bipolar cells: there is a wide variety of firing patterns in this population (irregular, regular and bursting) all of them with a strong adaptation. Single-bouquet cells in layer one also display this pattern (Tremblay *et al.*, 2016).

5HT3aR Neurogliaform: these cells have a high input resistance. They display a late-spiking pattern, *i.e.* a slow ramp depolarization preceding firing, with a moderate adaptation (Tremblay *et al.*, 2016).

Even though our understanding of the wide variety of interneuron types is limited, is obvious that it must be a reflection of different functions carried out in different neocortical circuits. Contributions of these cells to network dynamics, cortical computations, cognitive processes and behaviour have been

proven (Tremblay *et al.*, 2016). For example, a subset of SST interneurons fire preferentially when the mouse is in a reward zone while PV interneurons fire when it leaves this zone (Kvitsiani *et al.*, 2013). The main body of knowledge linking directly cortical neurons firing and cognitive function comes from recordings in the visual cortex when presenting visual stimuli to mice. Interneurons like SST or PV are less selective to variables like orientation or direction than VIP interneurons and pyramidal cells (Hofer *et al.*, 2011; Kerlin *et al.*, 2010; Liu *et al.*, 2010; Sohya *et al.*, 2007). In PV interneurons, the selectivity was shown to be inversely correlated with the dendritic arbour size (Runyan and Sur, 2013). Interestingly, this finding suggests that the increased selectivity to sensory stimulus could be related to the arbour size which is smaller in PV interneurons and bigger in VIP and pyramidal cells (Runyan and Sur, 2013). However, we still lack an understanding of how interneuron activity contributes to the complex computations underlying behaviour.

Interneurons are also known to contribute to the generation of cortical fast oscillations (Buzsáki and Wang, 2012). More specifically, PV expressing basket cells have critical roles in gamma, theta and ripple oscillations (Cardin *et al.*, 2009; Sohal *et al.*, 2009; Stark *et al.*, 2013, 2014). Gamma band oscillations reflect the synchronized firing of neuronal networks at 30-80 Hz and they are sustained in the dorsolateral prefrontal cortex (DLPFC) during working memory tasks (Lagler *et al.*, 2016; Tallon-Baudry *et al.*, 1998). Schizophrenia patients showed abnormal high frequency oscillatory activity (Uhlhaas and Singer, 2010). The working memory deficits observed in these patients are thought to be linked to an impaired gamma activity (Spencer *et al.*, 2003). Interestingly, schizophrenic individuals showed a reduction in one of the enzymes that synthesize GABA, GAD67 and in the GABA transporter, GAT-1, both enriched in the PV expressing basket and chandelier cells (Knable *et al.*, 2002). These data prove that an impairment in the function of different interneuron types can affect the normal cognitive function, leading to neurodevelopmental disorders like Schizophrenia.

1.2. Synapse structure and function

Neurons transmit information as electrical impulses. However, to transfer this electrical code to other neuron in the circuit, the cell membrane functions as an insulator and does not allow current transmission. Neurons establish connections between them using specialized structures called synapses. These structures, allow the communication between all neurons in both the peripheral and central nervous system. We can find two different types of connections, electrical and chemical.

Electrical synapses are membrane junctions, named gap junctions, that bind contacting cells by establishing a link between the cytoplasm of both cells (Revel and Karnovsky, 1967). They are composed of protein complexes of 8 nm in diameter named connexons. Connexons are arranged in crystalline hexagonal structures formed by 6 homologous monomers, the connexins. Oppossed cells align their connexons to form a continuous pore in the membrane, thus allowing the diffusion of soluble molecules between both cells. Molecules up to 1 kD can pass through these pores and permeability can be regulated with Ca^{2+} reducing the size of the pore (Unwin, 1989).

Given the size of ions, they can easily diffuse through connexons and allow the transmission of action potentials. This flow is passive, bidirectional, occurs without delay and cannot be saturated. Consequently, communication is so rapid that cells can discharge synchronously (Scolding, 1999). Gap junctions are not the preferred route of connection between neurons in the cortex, however, they have been found in GABAergic interneurons from development to adulhood. FS (prospective PV cells)

interneurons and late spiking cells (prospective SST cells) form gap junctions with interneurons of the same subtype (Galarreta and Hestrin, 1999; Gibson *et al.*, 1999). Conversely, pyramidal cells do not form this type of connections in adult cortex, although they have been found during their development (Galarreta and Hestrin, 1999; Gibson *et al.*, 1999; Meyer *et al.*, 2002).

The main type of connection found in the nervous system is the chemical synapse. Opposed to the previous ones, chemical synapses cause a delay in electric impulse transmission because membrane depolarization must be converted into secretion of molecules in the transmitter cell and back to electric signal in the receptor neuron (Scolding, 1999; Fig. 1.3).

These organelles specialized in cell-cell communication were first observed in the early 1950s with electron microscopy (Peters *et al.*, 1991). The observed structures were named synaptic complex and is formed by three compartments with different structure and composition: the presynaptic element, in the transmitter neuron; the postsynaptic component, in the receptor cell; and the synaptic cleft separating both. This structural and chemical organization is designed to fulfill the neurons functional requirements: (1) Fast emission of chemical messengers, (2) rapid messenger diffusion and (3) directed interaction with postsynaptic receptors. (Scolding, 1999; Fig. 1.3).

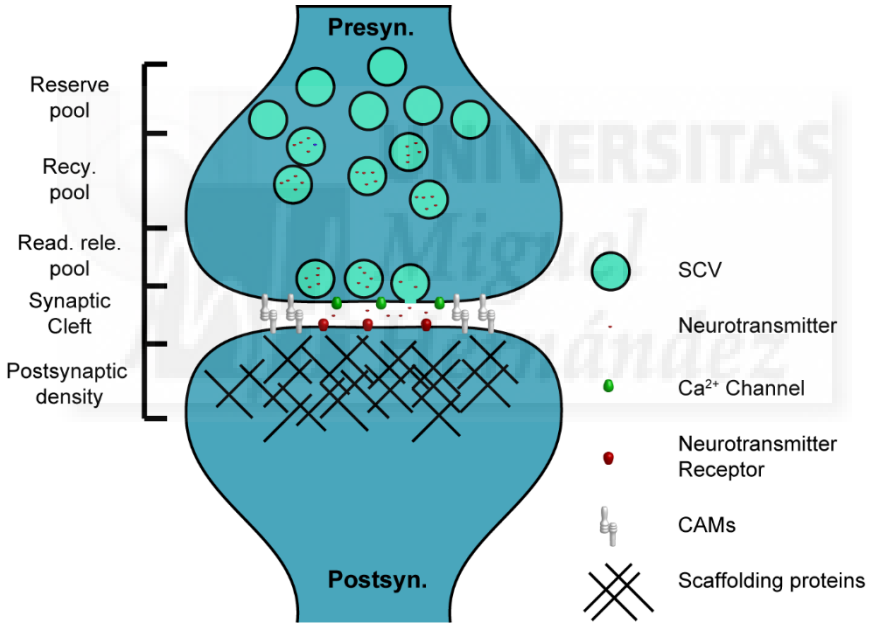

Figure 1.3. Synaptic structure and function. Schematic of the main components of a glutamatergic synapse and the main processes involving synaptic transmission. Presynaptically (top) a large number of vesicles (SCV) are specialized in neurotransmitter release and are divided in different pools. The large majority are not ready to be secreted (reserve pool), other group of them are filled with neurotransmitter (recycling pool) but far from the membrane and a small number is next to the membrane ready for being released upon an action potential (ready releasable pool). When the neurotransmitter is released binds the receptors in the postsynaptic compartment (bottom). This compartment contains a dense matrix of proteins that holds neurotransmitter receptors in place. Pre and postsynaptic compartments are joined by different CAMs (cell adhesion molecules).

1.2.1. Presynaptic compartment

The presynaptic compartment has a characteristic shape that can be recognized by electron microscopy. Organelles like mitochondria, smooth endoplasmic reticulum, cytoskeleton and synaptic vesicles can be identified within the synapse. The first studies in synapsis were carried out at the neuromuscular junction, the synapse formed between motor neurons and muscles (Couteaux and Pecot-Dechavassine, 1970). It was there where the active zone was defined as an electrodense material next to the presynaptic membrane. This structure is formed by the membrane and a presynaptic vesicular grid (Couteaux and Pecot-Dechavassine, 1970; Fig. 1.3).

1.2.2. Synaptic vesicles

The most distinctive elements in the presynaptic differentiation are the synaptic vesicles. It was observed that without stimulation small synaptic currents, named miniature potentials, were generated in the postsynaptic cell. These vesicles were postulated to be the containers of the chemical elements whose stochastic secretion lead to miniature potentials (Peters *et al.*, 1991). The presence of U shaped structures, resembling a fusing vesicle, in the presynaptic membrane contributed to this view (Fig. 1.3).

Different types of vesicles can be distinguished by electron microscopy. The most common type, small clear vesicles (SCVs), are small vesicles whose core is clearer than the membrane. They form the main type of vesicle that localizes close to the presynaptic membrane to be secreted. Different pools of these vesicles can be distinguished according to its relative position to the presynaptic membrane and its functional state to be secreted. The total number of vesicles that can be found in hippocampal synapses ranges from 30 to several hundred vesicles (Schikorski and Stevens, 1997). These can be divided into the resting pool, far from the synaptic membrane, and the recycling pool, closer to it (Schweizer and Ryan, 2006; Sudhof, 2004). Recycling pool vesicles would be the total of vesicles used during sustained stimulation. Yet in this pool we can distinguish the reserve pool and the ready releasable pool, being the last one formed by vesicles ready to be secreted after an action potential. While 17 to 20 vesicles form the reserve pool just 2 to 8 vesicles are in the ready releasable pool (Murthy *et al.*, 1997; Siksou *et al.*, 2009; Fig. 1.3).

A different type of vesicle that can be found between the small clear ones and far from the synaptic complex are the dense core vesicles (Zhu *et al.*, 1986).They vary in size and while small ones, 40-85 nm in diameter, are mostly related to monoamines; large ones, 100-150 nm in diameter, are related to neuropeptides (Peters *et al.*, 1991; Riveros *et al.*, 1986).

1.2.3. Chemical composition of the presynaptic compartment

One of the most functionally determinant molecular component of the presynaptic compartment is the cytoskeleton. Actin filament, tubulin, myosin, spectrins and beta-catenin are present at the presynapse (Phillips *et al.*, 2001). In particular, actin co-localizes with SCVs at central nervous system synapses. Not only it acts as a scaffold structure to anchor vesicles but also segregate them in different pools (Morales *et al.*, 2000; Sankaranarayanan *et al.*, 2003). Synapsins regulate this process through their phosphorylation dependent interaction with actin, microtubules, spectrin and synaptic vesicles. Membrane depolarization alters the phosphorylation state of synapsin1a, mobilizing the vesicles to be part of the ready releasable pool (Fdez and Hilfiker, 2006). Actin dynamics regulate the recycling of

vesicles as well. While F-actin, the filamentous form of actin, negatively regulates exocytosis, it has the opposite effect in clathrin-mediated endocytosis (Dillon and Goda, 2005; Engqvist-Goldstein and Drubin, 2003) (For a complete description of exocytosis and recycling see section 1.2.8).

Scaffolding molecules like SAP90/97 and CASK are also present at the presynaptic compartment. These molecules link the cytoskeletal matrix with membrane proteins like ion channels and adhesion molecules (Maximov *et al.*, 1999; Wu *et al.*, 1998). Finally, many molecules participating in tethering, docking, priming and fusion of vesicles are present at the presynaptic structure (Hida and Ohtsuka, 2010).

One of the main family of chemical components present in the presynaptic terminal, more specifically contained in synaptic vesicles, are the neurotransmitters (Fig. 1.3). Neurotransmitters are the molecules responsible for nerve impulse transmission. Each type of neuron expresses mainly one type of neurotransmitter although there are exceptions to this rule. As mentioned above, pyramidal cells use glutamate while interneurons use the neurotransmitter GABA (Jones, 1986). However, not all the neurotransmitters found in the neocortex come from neurons located in it. There is a whole ensemble of nerve afferents from the brain-stem and basal forebrain that innervate all the cortex including serotonin, noradrenaline, dopamine and acetylcholine (Jones, 1986). All the mentioned neurotransmitters are simple molecules derived from aminoacids and are contained in the SCVs. However, a whole group of neurotransmitters are short peptides (neuropeptides) that are contained in the dense core vesicles and secreted mostly through volume transmission (See section 1.2.9). Interestingly, the vast mayority of the known cortical peptides are found in GABAergic interneurons (Jones, 1986). These include SST, VIP or NPY that are also used to classify them; but others like tachykinin have also been described (Bandler *et al.*, 2017; Tasic *et al.*, 2016).

1.2.4. Synaptic cleft

The synaptic cleft is the intercellular space that separates the pre and postsynaptic elements. It measures between 15 and 30 nm and is partially filled by an electron/dense material. Its structural features suggest that is not isotropic, i.e. its properties are regionally defined, and the neurotransmitters do not diffuse freely through it. Its main molecular component is glycoproteins like glycosaminoglycans, sialic residues and the glycocalyx of pre and postsynaptic membrane proteins (Scolding, 1999; Fig. 1.3).

1.2.5. Cell-adhesion molecules

Presynaptic and postsynaptic compartments must be stably aligned to communicate the chemical message efficiently (Fig. 1.3). Cell adhesion molecules (CAMs) stabilize synapse position by binding the two synaptic structures (pre- and post-) between them or with the extracellular matrix. These contacts are established through homophylic interactions with CAMs of the same type, or heterophilic interactions with either other CAMs or the extracellular matrix. Such interactions are taking place through the extracellular domains of CAMs. Furthermore, some of the adhesion molecules contain intracellular domains that further stabilize the synaptic structure by binding to scaffolding proteins or cytoskeletal components (Missler and Südhof, 1998; Sheng and Sala, 2001).

The main known cell adhesion molecules present at the synapse are neurexins/neuroligin, synaptic cell adhesion molecules (SynCAM), neural cell adhesion molecules (NCAMs), cadherins,

protocadherins and integrins (Dityatev and El-Husseini, 2006). Neurexins are specifically located at the presynaptic membrane and neuroligins at the postsynaptic membrane. While neurexins interact with the scaffolding protein CASK, neuroligins interact with PSD95, a scaffolding protein present at the postsynaptic compartment (Craig and Kang, 2007; Dalva *et al.*, 2007; Dean and Dresbach, 2006; Huang and Scheiffele, 2008). Conversely, SynCAMs has been found at both sides of the synapse binding to CASK and PSD95 at the presynaptic and postsynaptic compartment, respectively (Biederer *et al.*, 2002; Fogel *et al.*, 2007). NCAM is a member of the immunoglobulin superfamily of cell adhesion molecules. Its structural function is carried out through interactions of their different isoforms with microtubules, actin and spectrin cytoskeleton components: α and β tubulin, microtubule associated protein 1A (MAP1A), β-actin and α-actinin 1 (Leshchyns'ka and Sytnyk, 2016). Cadherins and protocadherins are quite similar structurally but they differ in their binding to the cytoskeleton. Cadherins bind to actin filaments through their interaction with actinin but protocadherins do not interact with the cytoskeleton (Hartsock and Nelson, 2008). Alterations in this interaction lead to changes in the cytoskeletal dynamics, synapse morphology and function (Arikkath and Reichardt, 2008; Bamji, 2005; Dillon and Goda, 2005; Kwiatkowski *et al.*, 2010). Finally, integrins interact with the extracellular matrix components (Giancotti and Ruoslahti, 1999).

Beyond their interaction with structural components, these adhesion molecules can activate intracellular signalling cascades that regulate several processes. For example, NCAM activates signalling pathways that regulate long-term potentiation (LTP) like AMPA (α-amino-3-hydroxy-5-methyl-4-isoxazole) receptors (Vaithianathan *et al.*, 2004). Another example is the activation of intracellular proteins that regulates different aspects of the cytoskeleton and are downstream of some of these cell adhesion molecules, as focal adhesion kinase (FAK) (Navarro and Rico, 2014).

A wide variety of other transmembrane proteins are present in the synapse and transduce extracellular signals:

Ephrins: they are proteins that activate Eph tyrosine kinase receptors, both ligands and receptors are transmembrane proteins present at the synapse. Upon ephrins binding these receptors phosphorylate different cytoplasmic residues, including the ones they have (Bliss and Collingridge, 1993; Hayashi *et al.*, 2000; Man *et al.*, 2000). Autophosphorylation of these receptors opens a binding site for SH2 domain containing proteins that initiates a constellation of signalling cascades (Huber *et al.*, 2002; Man *et al.*, 2000). Ephrins can also activate a reverse signalling in the cell where it is expressed. Whereas ephrins are often found at the presynaptic membrane, Eph receptor are mostly located postsynaptically. There are however several exceptions to this rule (Gurden *et al.*, 2000).

Semaphorins: Some classes of membrane-bound semaphorins are also present at the synapse, like Sema4b and Sema4d (Burkhardt *et al.*, 2005; Raissi *et al.*, 2013). PDZ binding domains, specific binding sites for postsynaptic molecules like PSD-95, are present in Sema4b, suggesting that this protein can activate signalling cascades through these interactions (He *et al.*, 2002).

Neuregulin 1/ErbB4: transmembrane forms of neuregulin 1 are present in synaptic vesicles, including those containing glutamate. After vesicles fuse to the presynaptic membrane the extracellular domain is cleaved and can activate their receptor, ErbB4. This tyrosine-kinase receptor has PDZ binding domains that can activate intracellular signalling cascades. (Garcia *et al.*, 2000; Mei and Nave, 2014).

Neurotrophins and their receptors: neurotrophins are secreted molecules that regulate many developmental and functional processes in neurons. Four are known to be expressed in the brain: nerve growth factor (NGF), brain-derived growth factor (BDNF) and neurotrophins 3 and 4 (NT-3, NT-4). As an example of neurotrophin synaptic localization, BDNF is present presynaptically, while its receptor TrkB is present postsynaptically (Dieni *et al.*, 2012; Yoshii and Constantine-Paton, 2010).

1.2.6. Postsynaptic compartment

The neuron that receives the neurotransmitter has a specialized machinery to transform this signalling in electrical currents. In the first observations made by electron microscopy an electron-dense filamentous material was observed below the postsynaptic membrane, which was named postsynaptic density. Some years later, higher resolution microscopy allowed to describe the presence of a fine filamentous network (Landis *et al.*, 1987).

The postsynaptic compartment can be located at different subcellular regions of the neuron, such as the soma, axon and dendrites. A specific structure, named dendritic spine, is generated in the dendrites of some cells. These are small protrusions typically formed by a thin neck that emerges from the dendritic shaft and a bulbous head where the synaptic contact is made (Harris and Kater, 1994). Interestingly, while glutamatergic synapses are usually formed on dendritic spines, most of GABAergic contacts are located in the dendritic shaft (Megías *et al.*, 2001). Another distinctive element of the postsynaptic compartments is the spine apparatus: sacs of smooth endoplasmic reticulum in continuity with the subjacent endoplasmic reticulum. This organelle sequesters free Ca^{2+} that enters the synapse after synaptic transmission (Andrews *et al.*, 1988). Interestingly, there is a whole body of research proving that mRNAs translate locally at dendritic spines (Aakalu *et al.*, 2001; Cajigas *et al.*, 2012). Synapse associated polyribosome complexes can be found where specific synaptic proteins are thought to be synthetised (Steward and Levy, 1982).

1.2.7. Chemical composition of the postsynaptic compartment

Its chemical composition differs from that of the presynaptic compartment because of their different functions. The main proteins associated with the postsynaptic compartment function are neurotransmitter receptors, which will receive and transmit the information in the postsynaptic neuron. Cytoskeletal proteins like microtubules, actin filaments and fodrin contribute to its structure (Kennedy, 1993). Furthermore, dynamin is another component that controls membrane endocytosis, a key process in receptor exchange and thus neurotransmission. The maintenance of the postsynaptic density requires a whole set of scaffolding proteins that anchor neurotransmitters receptors to the cytoskeleton. The main components are PSD95 in glutamatergic synapses and Gephyrin (Geph) in GABAergic synapses (Kennedy, 1993). Together with other proteins like Shank or Homer in the case of PSD95, PSD95 and Geph form a matrix structure that is responsible for the ultrastructural features of the postsynaptic density (Hayashi *et al.*, 2009).

Neurotransmitters at the synapses are usually secreted at low concentrations and receptors must be located right in front of the presynaptic release site to detect it (Scolding, 1999). Two main types of receptors can be found at the cortical excitatory synapse: ionotropic and metabotropic. Ionotropic receptors form an ion channel that opens upon ligand binding. This response happens in a timescale of 1 ms. Conversely, metabotropic receptors are coupled to effector proteins through at least one

intermediary protein. They are coupled to channels or other signalling proteins through GTP binding proteins (G proteins). Beyond its interaction with classical neurotransmitters, metabotropic receptors interact with neuropeptides mediating its effect in the cell (Scolding, 1999).

Glutamate receptors are the main receptors present at excitatory postsynaptic membranes in the cortex. Three families of ionotropic and one family of metabotropic receptors have been described, each with several subtypes and splice variants. They are named based on their affinity to selective agonists: AMPA, kainate and NMDA (N-metil-D-aspartato) receptors (Gasic and Hollmann, 1992). AMPA receptors (AMPAR) are formed by combinations of six subunits (GluR1-6); kainate receptors by the combination of two protomers GluR5 and 7 with KA1 and KA2; and NMDA receptors (NMDAR) by the association of NR1 and NR2A,B,C or D subunits (Gasic and Hollmann, 1992).

In cortical inhibitory synapses, we can find several types of GABA receptors. The metabotropic GABAb receptors have an importart role presynaptically. They open a K^+ channel and close Ca^{2+} channels which depolarizes the nerve terminal blocking the propagation of the action potential (Bowery, 1989; Zhang and Jackson, 1993). The ionotropic $GABA_A$ receptor open a chloride channel that hyperpolarizes the postsynaptic cell (Bormann *et al.*, 1987), this generates inhibitory postsynaptic potentials and can be modulated by barbiturates, benxodiazepines, steroids and ethanol (Olsen and Tobin, 1990). Combinations of their different subunits (alfa1-6, beta 1-4, gamma 1-3, delta and epsilon) form a pentameric structure, generating channels of different pharmacological and electrophysiological properties (Herb *et al.*, 1992).

1.2.8. Function: neurotransmission process

Synaptic vesicles are involved in a tightly regulated secretory pathway through Ca^{2+} dependent exocytosis (Südhof and Rizo, 2011; Fig. 1.3). There are two main secretory pathways in neurons: the classical one and a specialized secretory pathway that fits the special requirements of the synapse. Neuropeptides are secreted though the classic regulated secretory pathways where vesicles are originated from the Golgi apparatus (Burgess and Kelly, 1987).

However, for SCVs the amount of vesicles needed exceeds the number that could be available through the classic secretory pathway. The synaptic terminal is able to produce new vesicles from the nerve ending without the involvement of Golgi apparatus, which would take longer. SCVs are directly involved in local endo-exocytosis at the periphery of the cell, even the assembly is made locally (Südhof and Rizo, 2011). On the one hand, membrane proteins like synaptophysin are first sent by classic secretory pathways to the synaptic membrane and then assembled to synaptic vesicles (Régnier-Vigouroux *et al.*, 1991; Südhof and Rizo, 2011). On the other hand, neurotransmitters are filled up at the nerve terminal by vesicular transporters.

Three vesicular glutamate transporters have been described: VGlut1-3. VGlut1 and 2 are the predominant isoforms. They have a complementary distribution, being VGlut1 mainly expressed in the cerebellum and cortex and VGlut2 in the thalamus, brain stem and spinal cord (Fremeau *et al.*, 2004; Hioki *et al.*, 2003, 2004). VGlut3 has a more restricted expression, being present in CCK positive interneurons and serotoninergic cells at the Raphe nuclei (Jackson *et al.*, 2009; Somogyi *et al.*, 2004). The vesicular GABA transporter VGAT transfers GABA into vesicles in inhibitory terminals. GABA is also synthetized at the terminal by glutamate decarboxilases 65 and 67 (GAD65 and GAD67) where GAD65 interacts with VGAT (Jin *et al.*, 2003).

This rapid and constant exocytosis requires a balanced endocytosis for the membrane to keep its proper size and structure. Several models of vesicle recycling have been proposed. In the kiss and run model the vesicle transiently fuse to the membrane, releasing the neurotransmitter and being immediately recycled. Other models suggest the partial or total fusion of the vesicular components with the membrane with different intermediate steps (Rizzoli and Jahn, 2007).

1.2.9. Synaptic release

As previously described, vesicles in the synaptic terminal form different pools depending on their availability to be released. This special type of exocytosis is faster than the regular exocytic mechanisms taking place in other cells and, for this reason, requires a specialized machinery. The first step to transport a vesicle from the resting pool to the reserve pool is tethering. Proteins like Synapsins, Basoon or Piccolo keep these vesicles in the active zone by interactions with the cytoskeleton (Malsam *et al.*, 2008; Rettig and Neher, 2002; Südhof and Rothman, 2009; Fig 1.3).

Once vesicles are in the reserve pool they are "docked" to the membrane through a well-known molecular mechanism. Synaptotagmin 1 (Syt1) and VAMP (synaptobrevin) are transmembrane proteins present at the vesicle. During the docking process, they form a complex with SNAP-25 and Syntaxin, located in the presynaptic membrane, known as the SNARE complex (Malsam *et al.*, 2008; Rettig and Neher, 2002; Südhof and Rothman, 2009). Complexin and Syt1 clamp the fusion machinery and hold it in a primed state, i.e. not yet ready to be released. Upon Ca^{2+} increase, caused by an action potential; Syt1 leaves the complex and α-Snap and NSF (NEM sensitive factor) binds to it. Finally, a molecule of ATP release α-Snap/NSF and the fusion starts (Malsam *et al.*, 2008; Rettig and Neher, 2002; Südhof and Rothman, 2009). Ca^{2+} rises for a short period of around 200 ms and it diffuses slowly, therefore the precise localization of all these proteins next to the docked vesicles is critical (Llinás *et al.*, 1981). They are located at the presynaptic membrane forming clustered rows (Robitaille *et al.*, 1990).

It is worth mentioning that synaptotagmin-2 (Syt2), which functions in concert with other synaptotagmins in neurotransmitter release, has been shown to be specifically expressed in parvalbumin synaptic terminals in the cortex and its *in situ* hybridization pattern resembles the one of PV (Sommeijer and Levelt, 2012). In this study, it was also proved that Synaptotagmin-2 is a reliable marker for parvalbumin positive inhibitory boutons in mouse visual cortex (Sommeijer and Levelt, 2012). Furthermore, recent studies have demonstrated its particular role on ensuring fast and efficient feedforward inhibition in cerebellar cortical circuitries (Chen *et al.*, 2017).

Once the neurotransmitter is released and reaches the postsynaptic receptors, it changes the cell membrane potential. As previously explained, the receptors are clustered to increase its neurotransmitter binding efficiency. However, not all the neurotransmitter effect takes place at the postsynapse. Neuropeptides and monoamines like acetylcholine, serotonin or VIP are released far from the target membrane where their receptors are located. Such receptors, usually metabotropic, can be distributed in patches or disperse along the membrane. This process is called volume transmission and its onset and duration is slower than regular synaptic transmission (Scolding, 1999).

1.3. Cellular and molecular mechanisms of synapse formation and axonal development

Synaptic assembly during development provides the core substrate for cognitive processes. Conversely, abnormal formation or function of these synapses lead to different cognitive disorders including autism and schizophrenia (Dani *et al.*, 2005; Levitt, 2005; Lewis *et al.*, 2005; Rubenstein and Merzenich, 2003; Verret *et al.*, 2012). In rodents, synaptogenesis begins in the first postnatal week and extend till postnatal day 30 (De Felipe *et al.*, 1997). Although less profusely, neurons also form synapses during adulthood and this process is thought to contribute to learning and memory (Waites *et al.*, 2005). Overall, synaptogenesis requires the coordinated assembly of a large number of proteins through well differentiated cellular events that will later be required for synaptic transmission (McAllister, 2007). The initial formation is however imperfect and requires enough flexibility to be realigned until optimal connectivity is established (Garner *et al.*, 2006). In this chapter, the main steps of synapse formation are described with a special focus on GABAergic synapse formation (Fig. 1.4).

1.3.1. Cellular and molecular events of axonal development

After migration and establishment of their final location in the cortex, neurons become polarized extending both dendrites and axon. Axonal development can be divided in three steps. First, neurons become polarized and the axon differentiates from dendrites: axonal polarization and specification (Lewis *et al.*, 2013; Fig. 1.4). Second, the axon grows guided by different molecules secreted by the target or the surrounding tissue: axonal growth and guidance (Lewis *et al.*, 2013; Fig. 1.4). Finally, the extensive axonal branching takes place in parallel to presynaptic contact formation: axonal branching and presynaptic differentiation (Lewis *et al.*, 2013; Fig. 1.4).

Neuronal polarization and axon specification

Neuronal polarization consists on the disruption of the newly born cell symmetry to generate the asymmetric cellular structure that initiates axon and dendrite formation (Dotti and Banker, 1987; Fig. 1.4a). This process is molecularly controlled by extracellular cues; intracellular signalling cascades, including those altering the cytoskeleton; and subcellular organelle localization. Localized intracellular cues instruct which neurite will become the axon by activating intracellular signalling (Adler *et al.*, 2006; Randlett *et al.*, 2011; Shelly *et al.*, 2011; Yi *et al.*, 2010). A group of these intracellular signalling molecules are partition-defective proteins (PARs), which are required for polarization and axon formation (Barnes *et al.*, 2007; Chen *et al.*, 2013; Shelly *et al.*, 2007; Shi *et al.*, 2003, 2004). Organelle subcellular localization is a controversial issue. Initially it was thought that Golgi complex, centrosome, mitochondria and endosome position correlate with the neurite that will finally become the axon (de Anda *et al.*, 2005, 2010; Bradke and Dotti, 1997). However, more recent studies suggest that

centrosomal position is not required for neuronal polarization (Distel *et al.*, 2010; Nguyen *et al.*, 2011).

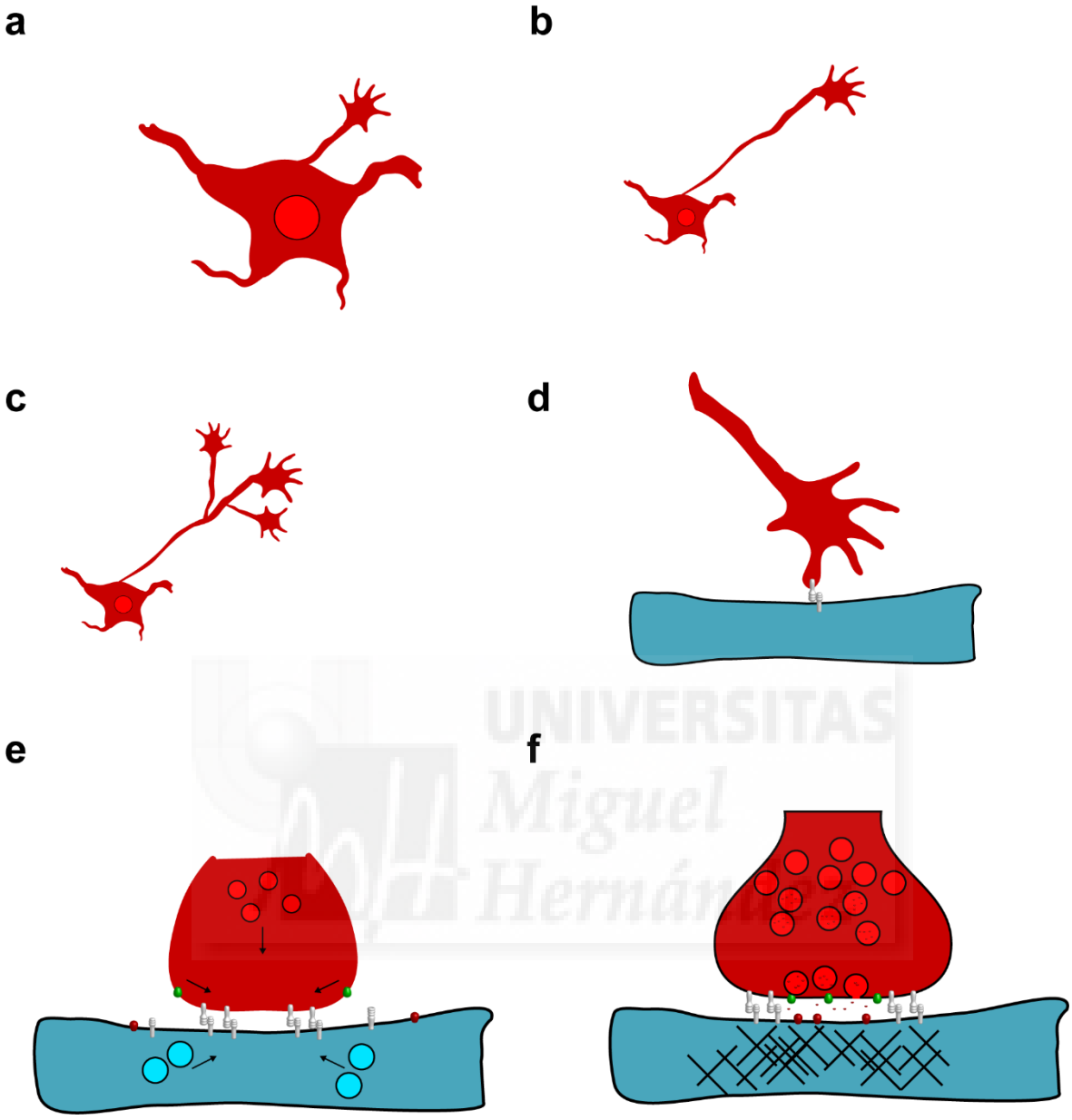

Figure 1.4. Cellular events of axonal development and synapse formation. (a) Axonal polarization: neurons develop neurites and one of them differentiates to become the axon. (b) Axonal growth and pathfinding: the axon grows guided by molecules present in the medium. (c) Axonal branching: the axon extends branches when arriving to the target area. (d) Synapse formation, initial contact: cell adhesion molecules permit the generation of specific contacts between the pre and postsynaptic cells. (e) Synapse differentiation: the elements that will form the synapse are recruited. (f) Synaptic maturation and maintenance: synapses finally defined their final morphology and functionality, being maintained, or not, for long periods of time. Presynaptic cell, red; postsynaptic cell, blue.

The cytoskeleton forms the core framework of the developing axon. On one hand, actin polymerization has an important role in specifying the axonal compartment (Hirokawa *et al.*, 2010). F-actin polymerisation and depolymerisation dynamics have a role in neurite outgrowth at the beginning of the process. Moreover, disruption of actin polymerization misplaces dendritically localized proteins to the axonal compartment (Lewis *et al.*, 2009; Song *et al.*, 2009; Winckler *et al.*, 1999). On the other hand,

microtubules distribute differently in axon and dendrites. While axonal microtubules distribute uniformly with the polymerizing end, termed plus end, pointing away from the cell body, dendrites lack such uniform microtubule network which is randomly directed (Baas *et al.*, 1988; Heidemann *et al.*, 1981). This orientation is essential for the organization of axonal transport through microtubules mediated by motor proteins. The main motor proteins are dyneins, minus end- directed, and kinesins like kinesin-1, plus end-directed (Lewis *et al.*, 2013). Interestingly, other MAPs are mainly localized in the axon, like Tau and MAP1B, or in the dendrite, like MAP2a-c family.

Axonal growth and guidance

Axonal growth is tightly linked to its guidance towards the proper postsynaptic targets (Lewis *et al.*, 2013). The growth cone is a dynamic structure at the tip of the growing neurite that is responsible of most of its growth and guidance (Lewis *et al.*, 2013; Fig. 1.4b). Its progression is the result of the balance between two opposite forces: the pushing force produced by slow axonal transport and polymerization of microtubules, and the pulling force generated by the retrograde flow of actin (Letourneau *et al.*, 1987; Suter and Miller, 2011). However, growth cone is unlikely to be the only elongation mechanism; axon stretching induces insterstitial axon elongation *in vitro* and *in vivo* (Abe *et al.*, 2004; Loverde *et al.*, 2011; Pfister *et al.*, 2004; Smith *et al.*, 2001). This requires the addition of new lipids, proteins, cytoskeleton elements and organelles that can be transported from the cell soma or, additionally, along the axon, like lipids (Hayashi and Su, 2004; Posse De Chaves *et al.*, 2000).

Also during this process, cytoskeletal dynamics has an essential role. Disrupting the actin cytoskeleton directly or indirectly has a limited effect on axon elongation but alters prominently axon guidance, *i.e.* the axon continues growing but not towards its target (Bentley and Toroian-Raymond, 1986; Chacón *et al.*, 2012; Marsh and Letourneau, 1984; Ruthel and Hollenbeck, 2000). Microtubule dynamics regulate axon growth mainly because it is required to sustain axon elongation and branching ((Lewis *et al.*, 2013), Letourneau 1987, Baas and Ahmad 1993). There are several molecules related to microtubules whose disruption affect axonal growth: plus-end microtubule-binding proteins such as EB1 and EB3 (Geraldo *et al.*, 2008; Jiménez-Mateos *et al.*, 2005; Zhou *et al.*, 2004), MAPs such as MAP1B (Black *et al.*, 1994; Dajas-Bailador *et al.*, 2012; Takei *et al.*, 2000; Tortosa *et al.*, 2013), kinases that phosphorilate in axonal MAPs like Tau (Morris *et al.*, 2011) or proteins regulating microtubule severing like KIF2A (Homma *et al.*, 2003). Beyond the growth cone, cytoskeletal polymerization along the axon shaft and axonal transport also contribute to axonal growth (Lewis *et al.*, 2013; Xia *et al.*, 2003; Yabe *et al.*, 1999).

Axon branching and presynaptic differentiation

The last steps of axonal development include terminal branching which will allow a single axon to connect to multiple postsynaptic targets (Lewis *et al.*, 2013; Fig. 1.4c). Two different mechanism can generate an axonal branch: splitting-bifurcation of the growth cone; or interstitial formation of collateral branches from the axon shaft after initial growth (Lewis *et al.*, 2013). The relative amount of branches generated through one or the other mechanism is highly divergent between different neuronal types (Bastmeyer and O'Leary, 1996; Matheson and Levine, 1999; Portera-Cailliau *et al.*, 2005). Interestingly, growth cones pause frequently *in vitro* and it has been shown that interstitial branching often occurs at the pause site (Szebenyi *et al.*, 1998). It is worth mentioning that presynaptic bouton formation seems

to be involved in axonal branching by the stabilization of nascent axonal branches *in vivo* (Meyer and Smith, 2006). Furthermore, new axon branches can emerge from existing presynaptic terminals (Alsina *et al.*, 2001; Javaherian and Cline, 2005; Panzer *et al.*, 2006).

Manipulations of the cytoskeleton often affect both axonal growth and branching (Chen *et al.*, 2011b; Homma *et al.*, 2003). Moreover, classical axon guidance molecules also influence branching behaviour. For example, members of the Rho family of GTPases (Rho, Rac or Cdc42) are important regulators of both processes (Hall and Lalli, 2010). Nevertheless, they constitute two separate phenomena and can be operationally separated. *In vivo*, glutamatergic cortical neurons initially elongate their axons through the corpus callosum, stop elongating and, subsequently, start forming collateral branches in the contralateral hemisphere (Mizuno *et al.*, 2007; Wang *et al.*, 2007). Several molecular players mediate these processes differentially. While axon elongation is primarily mediated by the severing protein katanin, branching is mostly dependent upon spastin activity (Qiang *et al.*, 2010). Another example is taxol, a compound that mediates microtubule stabilization and influences axon elongation but not branching (Gallo and Letourneau, 1999).

Different extracellular molecules had been demonstrated to influence axonal branching. For example, many guidance proteins such as Netrins, ephrins, semaphorins and Slit/Robo signalling has been shown to be required not only for axonal guidance but also for branching in the postsynaptic target area (Kalil and Dent, 2014). Growth factors like FGF (Fibroblast growth factor), NGF or BDNF also mediate axonal branching (Kalil and Dent, 2014). Finally, morphogens like several WNTs (wingless-type MMTV integration site family) has been also shown to promote terminal branching (Kalil and Dent, 2014).

These extracellular signals will activate different intracellular pathways. As an example, the activation of NGF trigger intracellular signalling cascades including phosphoinositide 3-kinase (PI3K), glycogen synthase kinase 3 beta (GSK-3β) and integrin linked- kinase (Zhou *et al.*, 2004). Specific kinases have been described to mediate axonal branching; NUAK1 and LKB1 control axon branching of mouse cortical neurons through the regulation of presynaptic mitochondria capture (Courchet *et al.*, 2013). Moreover, many extracellular cues that regulate axonal branching function upstream of FAK (Chacón *et al.*, 2010; Rico *et al.*, 2004; Tran *et al.*, 2009; Valiente *et al.*, 2011). FAK functions as an orchestra conductor for these multiple extracellular cues that modulate differently its activity. Netrin and BDNF induce opposite activity than Sema3A by phosphorylating FAK at different sites (Chacón *et al.*, 2010; Li *et al.*, 2004; Liu *et al.*, 2004; Myers and Gomez, 2011). FAK controls axonal behaviour by promoting activation of the Rho GTPase Cdc42 (Myers *et al.*, 2012) or the recruitment of the RhoGTPase activator p190RhoGEF and inhibitor p120GAP (Endo and Yamashita, 2009; Hata *et al.*, 2009; Rico *et al.*, 2004). As for the rest of processes leading to axonal development, many of these signalling pathways will exert its effect through the modulation of cytoskeletal dynamics.

Cytoskeletal reorganization in the nascent branch follows a well-established sequence. Initially, F-actin polymerization gives rise to protrusions, filopodia or lamellipodia, and microtubule invasion consolidate them (Gallo, 2011). Actin filaments accumulate along the axon and form patches that act as nucleators for axon protrusions (Ketschek and Gallo, 2010; Korobova and Svitkina, 2008; Mingorance-Le Meur and O'Connor, 2009). Proteins like FAK and ADF/Cofilin mediates its effect in branching mainly through regulation of actin polymerization (Chacón *et al.*, 2012; Kalil and Dent, 2014).

After the accumulation of actin, microtubules along the axon shaft, destabilise and fragment in pieces at these future branch points (Dent *et al.*, 1999; Gallo and Letourneau, 1998; Yu *et al.*, 2008). This process is thought to disrupt axonal transport locally to help trap molecules at the branch points (Lewis *et al.*, 2013). Subsequently, severed microtubules and organelles are transported into these branches to start branch stabilization (Ahmad *et al.*, 2006; Gallo and Letourneau, 1999; Hu *et al.*, 2012; Qiang *et al.*, 2010). Molecularly, this process is started by guidance cues like Slit or NGF (Kornack and Giger, 2005). More specifically, NGF is known to activate adenomatous polyposis coli (APC), a plus end-binding protein that is enriched in growth cones. Regulation of APC and GSK3β signalling modulates the stabilization of dynamic microtubules influencing axonal branching (Dent *et al.*, 2003; Gordon-Weeks, 2004). Other family of proteins, Kinesin I subfamily including KIF2A, possess a robust microtubule destabilising activity (Desai *et al.*, 1999). Consequently, KIF2A negatively regulates axonal branching (Kornack and Giger, 2005).

Actin and microtubule polymerization are closely coupled processes during axonal growth and branching (Kornack and Giger, 2005). Growth cone is organized into a peripheral (P) and a central (C) domain. The P domain includes filopodia and lamellipodia and its structure depends mainly on actin filaments. Conversely, microtubules are more abundant in the C-domain (Kornack and Giger, 2005). However, some highly dynamic microtubules, called pioneer microtubules, interact with actin filaments in the P domain (Kornack and Giger, 2005). It is known that interaction of the growth cone with molecules present in a permissive target leads to the strengthening of adhesion, attenuation of the retrograde actin flow and directed advance of microtubules towards the contact site (Suter *et al.*, 2004). Moreover, disruption of actin filaments in the P domain causes disappearance of pioneer microtubules, resulting in growth cone turning. Similarly, at axon branch sites microtubule severing is accompanied by focal accumulation of F-actin (Dent and Kalil, 2001). Consistently, axon branching is impaired by the selective inhibition of microtubules or actin dynamics (Dent and Kalil, 2001; Rodriguez *et al.*, 2003). Molecularly, the Rho-family of GTPases and their effectors are known to regulate not only actin reorganization but also the generation of pioneer microtubules (Etienne-Manneville and Hall, 2003; Fukata *et al.*, 2002; Wittmann *et al.*, 2003, 2004). Furthermore, microtubule-severing enzymes can also contribute to actin nucleation and filopodia formation (Hu *et al.*, 2012). In conclusion, all these studies support the idea that coordinated F-actin and microtubule dynamics are necessary for both growth cone steering and axon branching.

1.3.2. Cellular events of synapse formation

Neurons generate these specialized organelles, synapses, through a series of specific cellular events that lead to the formation of a functional synapse (Fig 1.4). The first step is the establishment of an initial contact. As explained above, axons undergo a guided pathfinding towards their synaptic targets and, once there, they make contacts through CAMs (Scheiffele, 2003). Once this first contact is established, bidirectional signalling in the pre and post-synaptic neurons induces the differentiation of the synapse (Garner *et al.*, 2006). Such differentiation consists on the progressive accumulation of synaptic proteins in the pre and post-synaptic compartments. Subsequently, further molecular events take place during a more prolonged period, leading to an increased stability and resistance to disassembly (Garner *et al.*, 2006). Finally, many of the newly formed synapses will remain stable over

days, weeks and even months due to different cellular and molecular mechanisms that are not yet well understood (Holtmaat *et al.*, 2005; Trachtenberg *et al.*, 2002; Zuo *et al.*, 2005a).

Axon pathfinding and initial contact

As explained in the previous section, after migration and establishment of their final location in the cortex, neurons become polarized extending both dendrite and axons (Fig 1.4d). These extensions will first grow towards an appropriate target area following specific guidance cues. Subsequently, they will follow gradients of guidance molecules, such as ephrin a and b for the axon (Dufour *et al.*, 2003; McLaughlin and O'Leary, 2005). These synapses are formed specifically in the target region because complementary surface proteins are recognized between the presynaptic and the postsynaptic cells. It is worth mentioning that against the traditional view that the axon is the only extension searching for the synaptic target, time lapse experiments in zebrafish have shown that both may contribute (Cline, 2001; Jontes *et al.*, 2000; Meyer and Smith, 2006; Niell *et al.*, 2004; Ruthazer *et al.*, 2006).

Axodendritic contacts can be initiated by either filopodia from axonal growth cones (Meyer and Smith, 2006; Washbourne *et al.*, 2002) or from dendritic growth cones (Sabo *et al.*, 2006). However, how strong is the relation between axonal growth and synapse formation? The synaptotropic hypothesis states that synaptic inputs control the elaboration of dendritic and axonal arbours and, consequently, the axons grow preferentially where synaptic contact can be established (Vaughn, 1989; Vaughn and Sims, 1978). In fact, experiments with retino-tectal axons in zebrafish show that there is a strong correlation between the generation of a synaptic bouton and axonal branch structure (Meyer and Smith, 2006). This data suggests that the growth of axonal and dendritic arbours is largely dictated by the formation of stable synaptic contacts (Meyer and Smith, 2006).

Once the initial paths are established, further synaptogenesis can be initiated by filopodia from already formed axons or dendrites to make *en passant* synapses (Ahmari *et al.*, 2000; Jontes *et al.*, 2000; Niell *et al.*, 2004; Washbourne *et al.*, 2002). Furthermore, synapses can also be assembled in locations where the axon and dendrite shafts are already in contact (Friedman *et al.*, 2000; Gerrow *et al.*, 2006; Washbourne *et al.*, 2002). Interestingly, it has been shown that GABAergic axons form transient protrusions but synaptic boutons are generated at pre-existing axo-dendritic crossings in hippocampal slice cultures (Wierenga *et al.*, 2008). Conversely, glutamatergic boutons are formed in stabilized filopodia (Wierenga *et al.*, 2008). Furthermore, the axons of interneurons exhibit high tortuosity and trajectories that correlate well with the positions of their synaptic target, while pyramidal cell axons show straighter pathways and less correlation with the postsynaptic partner (Stepanyants *et al.*, 2004). Considering all these data, a possible explanation is that the formation of inhibitory synapses is mainly the outcome of an axonal exploratory behaviour while pyramidal cells extend protrusions after forming their initial paths (Stepanyants *et al.*, 2004).

A small subset of these filopodia become stabilized and nascent synapses are subsequently formed at these sites. The signals that lead to filopodia stabilization, mainly cell adhesion molecules, are likely to be some of the first leading to synapse formation (Garner *et al.*, 2006). Interestingly, GABAergic synapses are formed in specific regions on the postsynaptic neuron. In the cerebellum, basket cells and stellate cells, two different types of GABAergic interneurons, restrict their synaptic contacts to subcellular locations of the Purkinje cell guided by the presence of neurofascin186 and $GABA_A$ receptors (Ango *et al.*, 2004; Fritschy *et al.*, 2006).

Differentiation: Recruitment of synaptic proteins

Upon the first contact, axon and dendrite initiate a constellation of signalling cascades that leads to the differentiation of the presynaptic bouton and post-synaptic specialization (Fig. 1.4e). The differentiation of presynaptic boutons includes the appearance of vesicular clusters and the formation of active zones; the differentiation of postsynaptic densities involves the accumulation of receptors, scaffolding proteins and other molecular components in the postsynaptic membrane. Most of our knowledge on this process is based on *in vitro* studies, where glutamatergic neurons are more abundant. In contrast, little is known about the mechanisms underlying GABAergic synapse assembly due to the low presence and undifferentiated morphology of interneurons in primary cultures (McAllister, 2007).

Presynaptic assembly depends mainly on preassembled protein complexes (Craig *et al.*, 2006; Waites *et al.*, 2005; Ziv and Garner, 2004). Proteins needed at the synapse form these complexes in the cell soma and are subsequently transported to the contact sites. Two main components accumulate during the assembly: SCV precursors and Piccolo-Bassoon transport vesicles (PBV). SCV precursors contain mainly synaptic vesicle proteins and are thought to arrive the first to the contact site (Hannah *et al.*, 1999; Huttner *et al.*, 1995; Waites *et al.*, 2005). PBVs contain multidomain scaffold proteins like Piccolo, Bassoon or others and they accumulate after SCVs (Ohtsuka *et al.*, 2002; Shapira *et al.*, 2003). Adhesion molecules, like SynCAM or neurexins, are known to induce synaptogenesis and neurexins are localized in the growth cone prior to synapse formation (Dean *et al.*, 2003).

There are not evidences of preassembled complexes in the postsynaptic density before or just after the first synaptic contact emerges. Conversely, proteins appear independently and stochastically at sites of axodendritic contact in order to be subsequently assembled (Garner *et al.*, 2006). The main identified elements at the postsynapses are both, NMDA and AMPA containing vesicles and PSD95 (Kennedy and Ehlers, 2006). Proteins accumulate gradually, beginning with the scaffolding protein, PSD95, and closely followed by independent NMDA and AMPA receptor accumulation (Bresler *et al.*, 2004; Ziv and Garner, 2004). Another set of key elements that accumulates at the postsynaptic compartment during its assembly are the endoplasmic reticulum and Golgi fragments together with ribosomes and mRNAs. The presence of these elements at the nascent as well as mature synapse suggests that the cytosolic and membrane proteins required for these processes can be synthesized locally (Aakalu *et al.*, 2001; Cajigas *et al.*, 2012; Steward and Levy, 1982; Sutton and Schuman, 2005). Therefore, local protein synthesis could contribute to the assembly of proteins like CaMKII-α, Shank or NMDA and AMPA receptors (Böckers *et al.*, 2004; Ju *et al.*, 2004; Steward and Schuman, 2001).

Presynaptic differentiation has been shown to often precede postsynaptic differentiation (Friedman *et al.*, 2000; Okabe *et al.*, 2001; Zhai *et al.*, 2001). However, dendrites seem to induce the formation of presynaptic specialization in the axon as well, at least *in vitro* (Ziv and Garner 2001). The accumulation of pre- and postsynaptic proteins is often used as readout of synaptogenesis time course (Waites *et al.*, 2005). However, since most of our information is based on *in vitro* studies, it would be essential to corroborate, whether the players and their spatial and temporal location match *in vivo*. This will be particularly relevant for GABAergic interneurons since they do not keep their normal morphology *in vitro* (unpublished observations).

Maturation and maintenance

Once the synaptic elements arrive to the synapse in a continuous manner the initial labile contacts become more stable due to a series of structural and functional changes (Ahmari and Smith, 2002; Garner *et al.*, 2006; Fig. 1.4f). This process takes places over a more protracted period of time, changing both the pre- and post-synaptic compartment. One of the most essential modifications is the change in stability. While nascent synapses stability depends on CAMs and is disrupted by actin depolimerizing drugs, mature synapse structure is not affected by these drugs or, for example, does not depend on N cadherin (Bozdagi *et al.*, 2004; Ruthazer *et al.*, 2006; Zhang and Benson, 2001).

At the pre-synaptic terminal, synaptic maturation increases the number of clustered SCVs two to threefold over the first month of cortical development (Vaughn, 1989). Conversely, there is a decrease in the probability of transmitter release (Bolshakov and Siegelbaum, 1995; Chavis and Westbrook, 2001). Postsynaptically, a pronounced density appears and there is a change in spine morphology. Live imaging studies have shown that the synapses are formed in filopodia-like structures that, later on, become mushroom and stubby spines with decreased mobility (Okabe *et al.*, 2001; Tada and Sheng, 2006; Yuste and Bonhoeffer, 2004; Ziv and Smith, 1996).

Pre and postsynaptic elements develop co-ordinately. Variables such as bouton volume, active zone area and postsynaptic density area are correlated in both synaptic sides (Harris and Stevens, 1989; Pierce and Mendell, 1993; Schikorski and Stevens, 1997). This suggests that the cell-adhesion complexes that span the cleft regulate these changes with reciprocal signalling as the synapse matures. Finally, there are also changes in both axonal and dendritic cytoskeleton, favouring stability over growth as maturation takes place.

The synapse can remain stable for days, weeks or even months (Holtmaat *et al.*, 2005; Trachtenberg *et al.*, 2002; Zuo *et al.*, 2005b). The cellular and molecular mechanism mediating synaptic maintenance are still not well understood and future studies will be required to decipher whether the same players support synapse formation and maintenance. It is important to mention that changes in the synaptic lifetime might be also prolonged by a reduction in the overall growth dynamics of neurons while they mature and not only by their strengthening.

Synaptic transmission and synaptogenesis

The nascent synapses are able to release the neurotransmitter presinaptically and detect it at the corresponding postsynaptic site within the first 30 min of initial contact (Buchanan *et al.*, 1989; Zhai *et al.*, 2001). When glutamate is completely removed from the vesicles, pyramidal cells in the hippocampus have smaller dendritic trees and form less synapses in some regions (Sando *et al.*, 2017). However, this does not affect the formation of either presynaptic terminals or dendritic spines (Sando *et al.*, 2017; Sigler *et al.*, 2017). GABAergic connectivity is established prior to glutamatergic connectivity in hippocampus and neocortex, although GABA shows excitatory actions (Hennou 2002, Tyzio 1999, Ben-Ari 2007). It has been shown that GABA regulates activity-dependent inhibitory synapse formation (Jin *et al.*, 2003).

1.3.3. Molecular players of synapse formation

The cellular mechanisms leading to synapse formation are mediated by specific molecular players that regulate the different stages of this process. However, is not always possible to know at which step of synapse formation a given protein exerts its function (Waites *et al.*, 2005). A combination of them are secreted molecules that are released to the extracellular compartment, steering the axon and the dendrite to their target (Waites *et al.*, 2005; Fig 1.5). Some others exert their action at the time of synaptic contact, tagging the appropriate target regions in the membrane and subsequently triggering intracellular signalling cascasdes (Waites *et al.*, 2005; Fig 1.5).

Extracellular molecules

Neurons encounter different proteins secreted mainly by the target neurons, and also by the surrounding glia. These secreted proteins can influence different aspects of synapse formation, but mostly they act locally to facilitate the generation of the first contact (Fig 1.5).

A handful of secreted proteins that have been previously involved in growth cone guidance like netrins, semaphorins and ephrins; are also involved in synapse formation (Bagri *et al.*, 2002; Pascual *et al.*, 2004; Tessier-Lavigne, 1995). These guidance molecules stimulate local arborisation and, overall, create a permissive environment for the formation of functional synapsis (Waites *et al.*, 2005). Netrin-1 and its receptor DCC are expressed during synapse formation and gain-of-function (GOF) experiments show that Netrin-1 increases the number of excitatory synapses and the complexity of axonal and dendritic arbours (Goldman *et al.*, 2013). Although Sema3A was shown to have a similar effect, increasing the number of dendritic spines and synapses *in vitro*, this phenotype has not been found *in vivo* (Tillo *et al.*, 2012; Tran *et al.*, 2009). Conversely, overexpression of Sema3F and its receptor neuropilin-2/Plexin-A3 increases spine number *in vivo* (Tran *et al.*, 2009). Finally, Ephs can induce synapse formation, the stabilization of glutamate receptors at nascent synapses and regulate dendritic spine morphology. In turn, activation of ephrins by Eph receptors induces synapse and spine formation (Hruska and Dalva, 2012).

A different group of secretable factors that promote neuronal maturation and induce globally the synaptogenetic activity of the cell are neurotrophins, including BDNF. BDNF acts as a priming molecule regulating the density of synaptic contacts and inducing both regional arborisation and synapse formation (Alsina *et al.*, 2001; Vicario-Abejón *et al.*, 1998). BDNF receptor TrkB has been found in axonal growth cones, dendritic filopodia and synapses, as well as in axonal and dendritic shafts (Drake *et al.*, 1999; McAllister, 2007). Comparing interneurons and pyramidal cells, while TrkB is expressed in both cells BDNF is exclusively expressed by pyramidal cells in the cortex (Cabelli *et al.*, 1996; Cellerino and Maffei, 1996; Miranda *et al.*, 1993). BDNF is known to accelerate presynaptic terminal maturation, increase GAD65/67 levels and increase the number of $GABA^+$ terminals (Aguado *et al.*, 2003; Huang *et al.*, 1999; Sánchez-Huertas and Rico, 2011). Furthermore, TrkB loss-of-function (LOF) experiments showed a decrease in the number of GABAergic synapses without altering the glutamatergic ones (Chen *et al.*, 2011a; Rico *et al.*, 2002). At later stages of synaptogenesis, TrkB signalling allows pre and postsynaptic proteins to cluster (Chen *et al.*, 2011a).

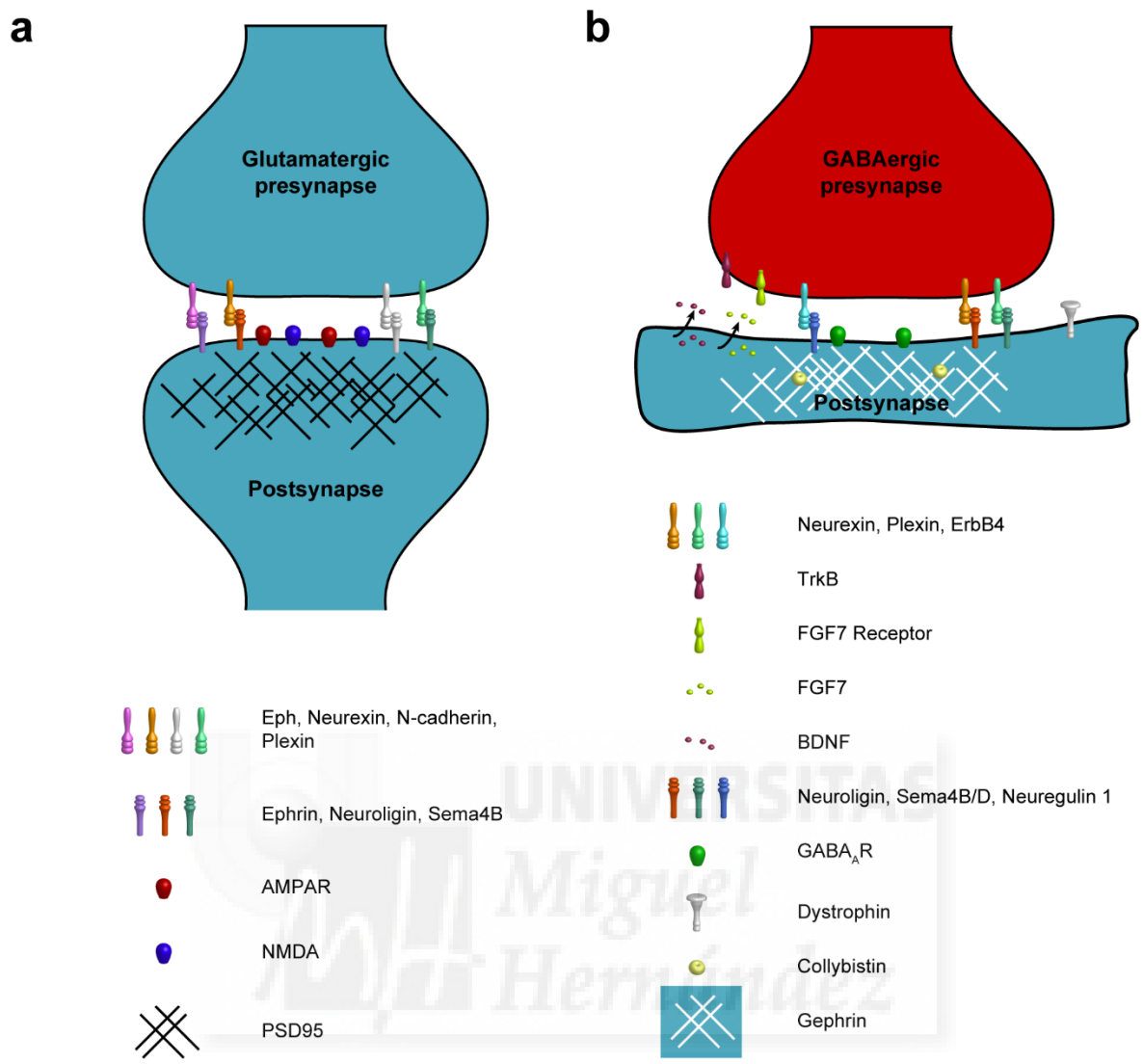

Figure 1.5. Molecular players in synapse formation. (a) Schematic of the main molecules involved in glutamatergic synapse formation in the different synaptic compartments (b) Same as in (a) for GABAergic synapses. Some of the represented molecules are involved in the formation of both types of synapses. Modified from Kuzirian and Paradis, 2011.

Wnt and FGF families also induce regional axon arborisation and synapse formation (Scheiffele, 2003). Wnt3 is known to induce arborisation of innervating sensory axons and Wnt7a induces clustering of synapsin1, associated to SCVs, in the mossy fiber axons in the cerebellum (Hall *et al.*, 2000). Consistent with the role of Wnt signaling in synapse formation, Dishevelled, one of Wnt receptors, has been shown to be required for presynaptic terminal differentiation (Ahmad-Annuar *et al.*, 2006). Besides this, FGF22 and the related family members FGF7 and FGF10 promote the formation of presynaptic boutons in the mossy fibre axons of the cerebellum (Umemori *et al.*, 2004). Interestingly, FGF7 represents, one of the few molecules implicated specifically in the presynaptic differentiation of GABAergic synapses (Kuzirian and Paradis, 2011). This protein localizes at the presynaptic terminal and induces the clustering of synaptic vesicles in the GABAergic synapse (Terauchi *et al.*, 2010). Moreover, deletion of the FGF2 receptor (FGFR2) inhibits presynaptic differentiation in the mossy fibres

of the cerebellum (Umemori *et al.*, 2004). Probably, all these molecules activate signalling cascades that trigger the synaptogenetic program of the cell. Another not so well known protein family that influences synapse formation are the secreted proteins pentraxins. Both family members Narp (Neuronal pentraxin-2) and neuronal pentraxin-1 (NP1) are known to have an effect on synapse formation, inducing AMPA and NMDA receptors clustering (O'Brien *et al.*, 1999; Xu *et al.*, 2003). Indeed, Narp participates in the formation of glutamatergic synapses onto interneurons and not onto pyramidal cells (Chang *et al.*, 2010).

As mentioned before, not only neurons secrete molecules that will guide or induce synapse formation but also there is an important contribution from glial cells. Thrombospondin-1 is one of these molecules that exerts its influence promoting the overall production of synapses in the cell (Ullian *et al.*, 2004). Besides secreted molecules, astrocytes make an essential contribution of cholesterol binding to ApoE protein during synapse formation (Mauch *et al.*, 2001). In the context of GABAergic synapses, neurons in culture increase the number of inhibitory synapses when grown with astrocytes due to an unknown protein that astrocytes secrete to the media (Elmariah *et al.*, 2004; Liu and Edwards, 1997).

Beyond diffusible molecules, synapses are surrounded by a protein meshwork that influences their formation: the extracellular matrix (ECM) (Barros *et al.*, 2011). The main system used to study such influence has been the neuromuscular junction. Components of the surrounding ECM like agrins (a heparin sulfate proteoglycan), laminins and collagen trigger intracellular signalling that activates several steps of synapse formation (Barros *et al.*, 2011). In the central nervous system (CNS), the ECM forms specific structures called perineuronal nets. They enwrap mainly the soma and processes of PV interneurons likely influencing synapse stabilization (Celio *et al.*, 1998).

Transmembrane proteins

The extracellular membrane constitutes the border of the synapse and thus the receptor of all the external signalling that will lead to synapse formation (Fig. 1.5). Similar to the previous functional classification done for secreted molecules, transmembrane proteins can be just involved in target recognition and initiation of synapses or induce a synaptogenetic state in the cell. While the first functional group is formed by CAMs, the second is formed by a series of receptors that can be called inducers (Waites *et al.*, 2005). They are attractive molecules to regulate synaptogenesis because they can initiate bidirectional signalling in both axon and dendrite.

CAMs exerts its synaptogenetic function both by generating the initial contact and by recruiting pre- and postsynaptic components after initiating intracellular signalling cascades (Bozdagi *et al.*, 2004; Brose *et al.*, 1999; Scheiffele *et al.*, 2000; Takeichi and Abe, 2005).

Cadherins (CDHs): cadherins mediate specific adhesion of pre and post-synaptic cells (Benson *et al.*, 2001; Shapiro and Colman, 1999). Their role in the initial stages of synaptogenesis is supported by their early appearance in the initial axodendritic contact sites, although they remain in the mature synapse (Benson and Tanaka, 1998; Benson *et al.*, 2001; Takai and Nakanishi, 2003; Williams *et al.*, 2011). Interestingly, different CDHs can be expressed by specific cell populations. For example, it has been shown that pyramidal cells in somatosensory cortex (SSC) express N-cadherin while septal granule cells and their thalamic inputs express CDH8 (Gil *et al.*, 2002). They lack an inductive role in synaptogenesis because, although the axons are mistargeted, synaptogenesis is taking place when blocking CDHs (Inoue and Sanes, 1997; Lee *et al.*, 2001). CDHs bind to intracellular catenins, like

p120catenin, that regulate actin cytoskeleton changes through the Rho-family of GTPases (Daniels *et al.*, 2001; Elia *et al.*, 2006; Ivanov *et al.*, 2001). After the first contact, CDH signalling also has other roles. For example, altering N-cadherin or β-catenin function causes a dispersion of synapsin clusters and SCV proteins respectively (Bamji *et al.*, 2003; Togashi *et al.*, 2002; Williams *et al.*, 2011; Ziv and Garner, 2004).

Protocadherins (PCDH): similar to cadherins, members of the PCDHγ subfamily localize to synaptic sites and are involved in target recognition rather than the induction of synapse formation (Lee *et al.*, 2003; Phillips *et al.*, 2003).

Nectins: Nectin-1 is expressed in axons and interacts with Nectin-3, present in dendrites, to promote synapse formation (Mizoguchi *et al.*, 2002; Togashi *et al.*, 2006). Such interactions are one of the first steps of the initial contact. They precede CDH interactions and are thought to promote their binding to the synapse (Mizoguchi *et al.*, 2002; Togashi *et al.*, 2006).

NCAM: NCAM is another classic cell adhesion molecule involved in target recognition during synapse formation (Dityatev and Schachner, 2006). It is among the first proteins that accumulate at nascent synapses (Fux *et al.*, 2003). Furthermore, this protein also has a role in the transport of trans-Golgi network organelles and its depletion reduces the number of synapses (Dityatev *et al.*, 2000; Sytnyk *et al.*, 2006). NCAM accumulates at contact sites between neighboring cells and probably exerts its action through interactions with proteins like heparin sulfate proteoglycans and FGF receptors (Dityatev *et al.*, 2004). The levels of NCAM are regulated by NMDA receptor activation and by kinesin-1 transport (Singh and Kaur, 2009; Wobst *et al.*, 2015). Its deficiency, produces thinner excitatory postsynaptic densities and reduced endocytosis of synaptic vesicles (Shetty *et al.*, 2013; Sytnyk *et al.*, 2006).

NCAM is post-translationally modified by the addition of the carbohydrate chain named long polysialic acid (PSA). Interestingly, PSA-NCAM is exclusively expressed by a subpopulation of interneurons in adult cerebral cortex (Gómez-Climent *et al.*, 2011). More specifically, 50-60% of these cells are SST positive and they exhibit reduced somatic boutons, dendritic arborisation and spine density (Gómez-Climent *et al.*, 2011). Moreover, removal of PSA increases the formation of dendritic spines in hippocampus (Guirado *et al.*, 2014). Other studies have shown that lack of NCAM impairs axonal branching and synaptic bouton formation of basket cells. Conversely, the phenotype is not altered when the removal occurs after synapse formation (Chattopadhyaya *et al.*, 2013).

Synaptic cell adhesion-like molecules (SALMS): this family of proteins is expressed in excitatory synapses of the CNS where they influence postsynaptic differentiation (Ko *et al.*, 2006; Wang *et al.*, 2006). More specifically, SALM1 is known to cluster both PSD95 and NMDA receptors at excitatory synapses and SALM2 interacts with PSD95 and induces AMPA receptor synaptic localization (Ko *et al.*, 2006; Wang *et al.*, 2006).

Molecules that induce the overall synaptogenetic activity of the cell can also be transmembrane receptors exerting this effect through ligand binding. These ligands usually are other membrane proteins present in the contacted neuron.

Neurexin/neuroligin: as previously explained, neurexins are present in the presynaptic membrane and neuroligin in the postsynaptic membrane. α and β neurexin families of cell surface proteins bind to neuroligin forming a complex that span the synapse (Boucard *et al.*, 2005; Ichtchenko *et al.*, 1995). In heterologous cell lines, neuroligins induce the differentiation of presynaptic boutons and

it requires β neurexin to exert this effect (Scheiffele *et al.*, 2000). In primary cultures, neuroligins induces presynaptic differentiation and β neurexin induces postsynaptic clustering of PSD95 and NMDA and GABA receptors (Graf *et al.*, 2004). *In vivo*, triple KO of *Nlg1,2* and *3* exhibits a modest reduction in synapse number but synaptic transmission is considerably decreased (Varoqueaux *et al.*, 2006). Single KO mice showed that *Nlg1* acts specifically to promote functional maturation of glutamatergic synapses while *Nlg2* promote GABAergic synapse maturation (Chubykin *et al.*, 2007; Poulopoulos *et al.*, 2009). This is consistent with the specific expression of NLG1 and 2 in glutamatergic and GABAergic synapses, respectively (Graf *et al.*, 2004; Varoqueaux *et al.*, 2004). Furthermore, neurexins impair the function of synaptic $GABA_A$ receptors, presumably, through a trans-synaptic mechanism (Zhang *et al.*, 2010). This body of work suggests that neurexins can regulate postsynaptic differentiation by recruiting the proper neuroligin isoform to forming synapses (Graf *et al.*, 2004).

SynCAM: expression of this homophylic receptor in neurons and heterologous cell lines exert a potent induction of synapse formation (Biederer *et al.*, 2002; Fogel *et al.*, 2011; Scheiffele, 2003). Intracellularly, it is known to bind to the scaffolding protein CASK like neuroligin (Biederer *et al.*, 2002).

EphB/ephrinB: beyond axonal guidance, activation of EphB receptor, through ephrinB activation, promotes postsynaptic clustering of NMDA and AMPA receptors (Dalva *et al.*, 2000; Martínez and Soriano, 2005; O'Brien *et al.*, 1999; Takasu *et al.*, 2002). Furthermore, ephinB1 promotes dendritic spine development (Murai and Pasquale, 2003). Triple KO mice of all EphBs showed a decrease in the number of excitatory synapses in the hippocampus (Henkemeyer *et al.*, 2003). Conversely, *ephrinB3* KO mice exhibit an increased number of excitatory synapses. Similarly to the functional diversity of ephrins in axonal guidance, different ephrins may be regulating different aspects of synapse formation (Rodenas-Ruano *et al.*, 2006).

Class 4 semaphorins: unlike Sema3 family, Sema4 are transmembrane proteins. Interestingly, depletion of Sema4B in the postsynaptic neuron leads to a decrease in both glutamatergic and GABAergic synapses in hippocampal cultures (Paradis *et al.*, 2007). Conversely, Sema4D and double, Sema4B and D, knockdown reduces exclusively GABAergic synapses (Kuzirian *et al.*, 2013; Paradis *et al.*, 2007; Raissi *et al.*, 2013). The best candidate to be mediating this effect is PlexinB1 (PlxnB1). Both interact in heterologous cells with high affinity and PlxnB1 is expressed by hippocampal neurons (Magdaleno *et al.*, 2006; Tamagnone *et al.*, 1999).

Neuregulin 1/ErbB4: neuregulins belong to the neurotrophic factor family and have been shown to play a role in the wiring of GABAergic interneurons through its receptor ErbB4. In particular, Neuregulin-ErbB4 signalling has been demonstrated to be involved in chandelier and CCK interneuron synapse formation as well as in the assembly of excitatory synapses into fast-spiking interneurons, including chandelier cells and basket PV cells as well as in CCK cells (Chang *et al.*, 2010; Fazzari *et al.*, 2010; Del Pino *et al.*, 2013, 2017; Ting *et al.*, 2011).

Intracellular molecules

Secreted molecules or other ligands activate transmembrane receptors to trigger intracellular signalling cascades. Although most of these cascades seem not to be fully specific for synapse formation, small differences in their regulation lead to the differential cellular and molecular events that underlie this process. However, some specific intracellular molecular players have been described during synapse formation.

As explained before, scaffolding proteins are a key component of the postsynaptic compartment. Interestingly, not only they contribute to its structure but they can also regulate some events during synapse formation. PSD95, at glutamatergic synapses, binds to neurotransmitter receptors at the postsynaptic density anchoring them (Kim and Sheng, 2004). Similar to PSD95, Geph molecules form clusters at the postsynaptic density of GABAergic synapses and is required for glycine receptor clustering (Feng *et al.*, 1998; Fritschy *et al.*, 2008). In contrast, the requirement of this protein to localize $GABA_A$ receptors is less clear (Kuzirian and Paradis, 2011).

One example of the specific signalling cascades regulated during GABAergic synapse formation is collybistin. Collybistin is a Rho-family guanine nucleotide exchange factor that is expressed specifically in the brain and it is known to be required for clustering of gephyrin and $GABA_A$ receptors (Harvey and Stephens, 2004; Kins *et al.*, 2000; Papadopoulos *et al.*, 2008). Interestingly, collybistin forms a complex with NLG2 and Geph that permits the recruitment of $GABA_A$ receptors (Poulopoulos *et al.*, 2009).

Dystrophin, another protein, forms a complex that is thought to connect the extracellular matrix to the actin cytoskeleton (Pilgram 2010). Dystrophin colocalizes and regulates the number of $GABA_A$ receptor α1 and α2 clusters in hippocampus and cerebellum (Brünig *et al.*, 2002; Knuesel *et al.*, 1999). Like dystrophin, many transmembrane proteins have in common the capacity to anchor to the actin cytoskeleton and, consistently, F-actin is concentrated at both pre and post- synaptic contacts (Dai *et al.*, 2000; Zhang and Benson, 2002). Furthermore, the coupling of dynamic microtubules to actin filaments is a key molecular event underlying the formation of growth cone filopodia that will produce the first contact of synapse formation (Geraldo and Gordon-Weeks, 2009).

Finally, even some transcription factors have been shown to regulate synaptogenesis specifically. Experiments with the myocyte enhancer factor 2 family, MEF2, demonstrate the involvement of some of its members in restricting synapse formation. More specifically, KO mice of MEF2A and D dramatically enhance synapse number while their overexpression decreases synaptic contacts (Flavell *et al.*, 2006). Another transcription factor, Npas4 (neuronal PAS domain protein 4), is specifically involved in GABAergic synapse formation (Lin *et al.*, 2008). While Npas4 depletion decrease the density of GABAergic synapses formed onto pyramidal cells, its overexpression increases synapse density (Lin *et al.*, 2008). This effect is partially dependent on BDNF, because Npas4 regulates its transcription (Lin *et al.*, 2008).

Link between cellular and molecular events

In conclusion, although a synaptogenetic role has been assigned to a large number of molecules, little is known about the mechanism used by any of them to signal the stabilization of the first contact or the assembly of synaptic proteins at new axodendritic contacts (McAllister, 2007). There are many signalling pathways that will likely converge in the actin cytoskeleton (Zito *et al.*, 2004) and, similarly, in microtubules. More knowledge is needed about how actin and microtubules dynamics regulate the different aspects of synapse formation to understand the whole cellular and molecular process.

1.3.4. Molecular mechanisms underlying GABAergic synaptogenesis

GABAergic cortical interneurons have a remarkable role in cognitive processes and their malfunction is closely linked to the aetiology of several neurodevelopmental disorders. The daunting variety of interneurons that are found must be a reflection of the different functions they are known to carry out. Moreover, small variations in the developmental program of interneurons can lead to the onset of these neurodevelopmental disorders. Therefore, there is a need to understand the development of the different interneuron types in order to shed some light on the circuitries that underlie different aspects of cognition.

Synapse formation is one of the most critical events in brain circuit wiring during development. The formation of a functional synapse will allow the communication between neurons and its specificity will determine the formation of proper circuits. GABAergic and glutamatergic synapses are not only different functionally but also the molecular mechanisms underlying these processes have essential differences. Whereas numerous molecular players have been proved to mediate synapse formation in pyramidal cells, few are the ones identified in interneurons as described in the above sections. An identification of the full complement of molecules that distinguish GABAergic from glutamatergic synapse formation would represent a major advance towards understanding these differences and the overall process of GABAergic synaptogenesis. Furthermore, dissecting the presence of these molecular players in different interneuron populations will contribute to understand how different cortical circuitries develop.

In the last years, the boost in the development of several tools to dissect interneurons and pyramidal cells have allowed us to explore these neurons in detail. We are now able to contribute to the knowledge about the molecular mechanisms that mediate GABAergic synapse formation in the cerebral cortex by searching for genes differentially implicated in this process. In this Thesis, using an unbiased screening, we have found some of these genes and we have demonstrated the specific function of one of them in the wiring of the GABAergic circuitry.

2. OBJECTIVES

The overall goal of this project is to identify the molecular mechanisms underlying the differential cellular events taking place during GABAergic synaptogenesis compared to glutamatergic synaptogenesis in the cerebral cortex. To this end, we have set the following sequential aims:

1. To perform a genome-wide screening for novel genes differentially and specifically expressed during GABAergic synaptogenesis but not during glutamatergic synaptogenesis.

2. To characterize the expression pattern of the novel genes in the main interneuron populations.

3. To investigate the involvement of the novel genes in synaptogenesis by loss of function experiments dissecting the molecular and/or cellular mechanisms mediating their prospective role in this process.

3. MATERIALS AND METHODS

3.1. Mice breeding

All the mice used in this thesis were maintained in a C57BL/6J background. Procedures were performed in strict accordance with Spanish, United Kingdom, and European Union regulations. The local ethical committees at the "Instituto de Neurociencias" (Alicante) and "King's College London" approved all experimental procedures involving mice.

For the initial genetic screening and subsequent Qpcr (quantitative polymerase chain reactionverification experiments, *Nkx2.1Cre* [Cyclization recombinase (Cre) under the promoter of NK2 homeobox protein 1 (*Nkx2.1*)] (Sussel *et al.*, 1999) and *NexCre* (*Nex*, neurogenic differentiation protein 6) (Goebbels *et al.*, 2006) mice were crossed with the CRE dependent reporter line R26R CAG-boosted EGFP (*RCE:LoxP*) (EGFP, enhanced green fluorescent protein)(Miyoshi *et al.*, 2010). Cortices from these litters were dissected at postnatal day 0 (P0) and P10 in *Nkx2.1Cre*;*RCE:LoxP*, to isolate GABAergic interneurons, and at P0 and P12 to isolate Glutamatergic pyramidal cells in *NexCre;RCE:LoxP* mice.

C57BL/6J wild type were used for the developmental time course experiments of Nek7 and the colocalization of candidate genes with interneuron markers. SST population *in situ*-immunohistochemistry colocalization with Nek7 was performed using *Sst-IRES-Cre knock-in* (Jackson Laboratory 013044) crossed with *RCE:loxP*. In both cases, mice were intracardially perfused at P30.

Nek7 loss of function experiments were done in *Lhx6Cre* mice (Fogarty *et al.*, 2007), which were always kept in heterozygosity. Mice were injected at P3 and perfused at P30 for this experiment. Morphological analysis was done injecting *Lhx6Cre* mice at embryonic day 15.5 (E15.5) and perfusing them at P21. Loss of function experiments of Lgals1 were done with the available knockout (*Lgals1*$^{-/-}$, Jackson Laboratory 006337). Heterozygous mice were used for breeding to perfuse homozygous and wild type littermates at P10 and P30.

Females were avoided in all the experiments involving synaptic bouton quantification given the previously reported variability found in the laboratory.

Finally, cortical cultures required the use of *Nkx2.1Cre* mouse line. These embryos were used from E16.5 to E18.5 being the preferred age E17.5.

3.2. DNA constructs

All the DNA constructs were cloned using standard molecular biology techniques that can be find in well documented manuals (Sambrook and Russell, 2001). The probe sequences used for *in situ* hybridization were obtained from Allen Brain Atlas database. Subsequently, they were checked for the absence of unspecific matchings, using BLAST, and secondary structures in the primers, using OligoAnalyzer 3.1 (Primerquest) (Nek7: RP_050725_01_H03, Fwd 5'-CGGAGGAGCTACGACAGC-3', Rev 5'-TGACTATCACGCCAGGCA-3'; Lgals1: RP_050725_01_F12, Fwd 5'-CCGCTTCTGACTGCTGGT-3', Rev 5'-CTCAAAGGCCACGCACTT-3').

RNA from P10 mouse cerebral cortex was extracted and retrotranscribed to serve as a template for the PCR reactions with these primers. PCR conditions were as stablished by the company (5Prime Manual HotMaster™ Taq DNA Polymerase) with annealing temperature 5° C lower than the melting temperature of the primers and 70° C as extension temperature. The resulting product was ligated with

pGEMT Easy vector (Promega A1360) where T7 and SP6 RNA polymerase promoters flanked the sequence.

shRNAs were designed with Block-IT (Thermo Fisher) against the open reading frame sequence (ORF) of Nek7 (Minimum G/C percentage, 35%; maximum G/C percentage, 55%). shRNAs are RNA sequences with complementary regions separated by a loop sequence. EcoRI and BlnI restriction sites were added in the 5' and 3' ends respectively. These were cloned first in pGEMT Easy vector and subsequently in pDIO-shRNA-mCherry digesting with EcoRI and BlnI.

pDIO-shRNA-mCherry was a construction designed by Ruben Deogracias merging the plasmid pDIO with an shRNA system available in the lab. Briefly, the sequence containing the distal and proximal elements of the U6 promoter spaced by the CDS for mCherry was PCR amplified using the oligos AH4-U6 FW 5'- TTCGCTAGCGGATCCGGAATAAC-3' and AH4-U6 RV 5'-CCAGAGGTTGATTGGTTTATCAGGC-3'. The resulting PCR product was cleaved in the introduced flanking restriction sites XbaI and EcoRI and subsequently clones into the pAAV-EF1a-DIO-mCherry vector (Kindly provided by Prof. Deisseroth) containing the same restriction sites. The resulting plasmids will be named *Nek7* shRNA, *gfp* shRNA and *lacZ* shRNA.

Full lengths sequences of Nek7 were amplified from P10 mouse cerebral cortex cDNA adding a HA (Human influenza hemagglutinin) tag (HANek7) in the N-terminus and cloned using the two steps previously described for shRNAs in pDIO-Cheta-TdTomato. The mutated form of Nek7 (*mNek7*) was designed introducing synonymous mutation in the five shRNA targeting sequences and adding 3 consecutive flag sequences in the C terminal end of the protein. This was synthetized with GeneArt Strings (Thermo Fisher), a-tailed and cloned in pGEMT Easy vector and subsequently in pDIO-Cheta-TdTomato where TdTomato was substituted by Nek7 cutting with the restriction enzymes AscI and NheI.

3.3. Fluorescent Activated Cell Sorting (FACS)

Fluorescently labelled population of cell were isolated by fluorescent activated cell sorting (FACS). The 4 conditions used in this thesis were GABAergic interneurons coming from *Nkx2.1Cre;RCE* mice at P0 and P10 (IN P0 and IN P10) and glutamatergic pyramidal cells from *NexCre;RCE* mice at P0 and P12 (Pyr P0 and Pyr P12).

Two to six mice were anesthetised either with ice, P0, or with pentobarbital, P10-P12, and decapitated. Importantly, all the solutions used in this protocol were filtered before being used to avoid contamination. Brains were dissected out with forceps, scalpel and a spatula. They were immediately immersed in ice cold dissociation media [10 mM $MgCl_2$, 2 mM HEPES buffer (Invitrogen 15630-106), 0.2 mM NaOH (Sigma S0899), 90 mM Na_2SO_4 (Sigma S6547), 30 mM K_2SO_4 (Sigma P9458), 36 mg/mL D-(+)-Glucose (Sigma G6152), 0.8 mM kynurenic acid (Sigma K337), 50 μM AP-V (Sigma A5282), 0.05 U/mL penicillin/streptomycin (Thermo Fisher 15140122)] to keep low temperature conditions during the rest of the process. Somatosensory cortex was dissected removing the meninges in *NexCre;RCE* mice while the whole neocortex was used in *Nkx2.1Cre;RCE* mice to increase cell yield. Dissected cortices were then cut in 1 mm^2 pieces to facilitate digestion.

Next, dissociation media was removed and the tissue was digested in a papain containing enzymatic solution [0.16 mg/mL cysteine (Sigma C9768), 7 U/mL Papain (Sigma P3125), 0.1 mg/mL DNAse (Qiagen 79254) diluted in dissociation media pH 7.35 ± 0.1] at 37˚ C during 30 minutes. The

tube was gently inverted every 5 minutes and the solution was changed after the first 15 minutes. All the solutions were added under a laminar flow hood after this step to avoid contamination. However, for the collection of cells for quantitative polymerase chain reaction (qPCR) everything was carried out without this protection and the results were not altered.

Enzymatic solution was then removed and inhibitor solution added [2.5 mg/mL Ovomucoid (Sigma T2011) and 2.5 mg/mL BSA (Sigma A4161) diluted in dissociation media pH 7.35 ± 0.1] twice during 1 minute at room temperature. Inhibitor was removed and washed out three times with complemented OptiMEM solution [3.6 mg/mL D-(+)-Glucose, 10 mM $MgCl_2$, 0.4 mM kynurenic acid, 25 μM AP-V, 0.04 mg/mL DNAse diluted in OptiMEM medium (Thermo Fisher, 31985) at pH 7.35 ± 0.1].

Tissue pieces were left in 2 mL of complemented OptiMEM solution and pipetted up and down six times with 1000 μL filter tip pipette. Pieces were left to sediment and the supernatant, consisting on a cell suspension, was separated in another round bottom tube. This step was repeated until all the tissue was broken up but never more than 3 times. Cells were harvested by centrifugation at 120 g for 5 minutes at 4˚ C to reduce the suspension volume and they were resuspended in 150-300 μL of fresh complemented OptiMEM by pipetting up and down 15 times. This cell suspension was passed through a 40 μm cell strainer (Thermo fisher, 22363547) to get a single cell suspension. The concentration at this step is key for the subsequent cytometric step, thus it should aim at getting around 1000-2000 events/s in the cytometer.

The single cell suspension was run in the sorter (BD FACS aria II, 644832). Cells were passed through a 488 nm laser beam and forward scattered (FSC-A), side scattered (SSC-A) and fluorescent (FITC) light were measured. FSC intensity is correlated with cell size while SSC is correlated with cell complexity which increases when cells are dying. First, we selected the population of events looking at the scatter plot of the area of these two variables. The population squared in the fig. correspond to healthy cells and was the selected one. Smaller or more scattered events are dead cells and bigger events correspond to double or triple cell aggregates, which were discarded. Second, we selected the cells with high fluorescence inside the previous population corresponding to the neurons expressing EGFP.

The sorter detector voltages and selected populations were calibrated previously with a cortex sample without fluorescent cells where the non-fluorescent population was stablished. Fluorescence signal was calibrated with 488 fluorescent beads. These were the settings stablished in the instrument: sort setup 85 μm (nozzle diameter), frequency 48.3, amplitude 32.1, phase 0, drop delay 28.8, attenuation off, precision 4-way purity, yield mask 0, purity mask 32, phase mask 0, single cell off, sweet spot on, first drop 241, target gap 11, plates voltage 5.500, voltage centering -39 and sheath pressure 45.

Sorted cells were collected in a tube with 2 mL of complemented OptiMEM. This suspension was transferred to an RNAse free Eppendorf and centrifuged at 1200 rpm for 10 minutes at 4˚ C. The supernatant was withdrawn, leaving the last 100 μL of medium; the samples were snap frozen in liquid nitrogen and stored at -80˚ C.

3.4. HEK293 cells culture and transfection

Downregulation effect of the generated shRNA plasmid was checked in HEK293 cells before being used in mice. These cells were kept at 37˚ C and 5% CO_2 in DMEM medium (Invitrogen 21969) containing 2 mM L- glutamin (Thermo Fisher 25030), 0.001% v/v (volume/volume) β-mercaptoethanol, 10% foetal bovine serum (Life technologies 10500056), 100 U/mL penicillin/streptomycin, HEPES 0.01 M and 1x MEM non-essential aminoacids (Thermo Fisher 11140050). To test the shRNA effect cells were replated and transfected when they were approximately 80% confluent. Culture medium was replaced by OptiMEM one hour before transfection. CRE, shRNA and full length plasmids were diluted at a total final concentration of 1 µg/mL in the transfection medium at equimolar rates. Poly(ethylenimine) (PEI; Sigma 408727) was used as transfection reagent at a rate of 4 µg per µg of DNA. Plasmids and PEI were diluted in OptiMEM, mixed and kept at room temperature during 25 minutes before being added to the plate. Cells were finally harvested 3 days after transfection, washed twice with phosphate buffer saline (PBS; 137 mM NaCl, 2.7 mM KCl, 8 mM Na_2HPO_4, 1.4 mM KH_2PO_4, pH 7.2) and frozen at -80˚ C.

3.5. AAV Viral production

HEK293 cell were used to produce adenoasociated viruses. To obtain a high titre, cells had to be replated several times after they became confluent to keep exponential growth. After this expansion, a total of 10 150mm diameter dishes (Sigma D8554) were transfected as described above. A plasmid containing the desired construct flanked by aav2 ITR sequences and the one expressing the adenoasociated capside 8 proteins (Plasmid Factory pDP8.ape) were cotransfected at a rate 1:4.

Cells were harvested after 3 days and viruses present in the media or intracellularly were collected. The cells were pelleted by centrifugation 10 minutes at 2200 rpm and lysated with lysis buffer [150 mM NaCl, 50 mM Tris, 2 mM $MgCl_2$ and 0.5% Na-Doc (Sigma D6750) pH 8.5]. Conversely, viruses secreted to the medium were precipitated adding ammonium sulphate (Sigma A4418) at a final concentration of 31.3 g/mL, incubated in ice during 30 minutes and centrifuged at 3200 g for 45 minutes at 4˚C. the precipitate was diluted in lysis buffer and added to lysated cells.

The solution was snap frozen in liquid nitrogen, defrosted and vortexed three times to further lysate the cells. Furthermore, benzonase (Sigma E1014) at a final concentration of 125 U/mL was applied during 30 minutes at 37˚C to break lysed DNA.

The solution was filtered and added on top of a iodixanol gradient (OptiPrep, SLS D1556). This gradient was stablished by different concentrations of iodixanol (15, 25, 40 and 58 % in descending order) diluted in gradient buffer (0.01M Tris, 0.15M NaCl, 0.01 M $MgCl_2$ pH 7.6). Next, the tubes were ultracentrifuged at 32,000 g in a ultracentrifugue (Beckman coulter, Optima L-100 XP; rotor SW32Ti) for 5 hours at 12˚C. After centrifugation, just the 40% gradient, containing the virus, was harvested. Iodixanol was washed with PBS using centrifugal filters (Millipore UFC710008 and UFC910024) by centrifugation at 3200 g at 4˚C until the minimum possible volume was obtained. The remaining virus was diluted in 100 µL of 5% w/v (weight/volume) sorbitol (Sigma S6021) and fast green (Sigma 408727).

Viruses were titred measuring the amount of viral DNA by qPCR using WPRE primers. Briefly, they were lysated with lysis buffer [100 mM NaCl, 0.5% SDS (Sigma L3771) in PBS] 1 hour at 95˚C and 3 µL of the lysed virus were used as a template for qPCR. Finally, the concentration of viral DNA was

calculated with a regression curve with serial dilutions of the plasmid used to be introduced in the virus. Just viruses with a titre higher than 10^{12} viruses/mL were used.

3.6. Postnatal viral injections

Lhx6Cre mice at P3-P4 were deeply anesthetised with 5% isoflurane for induction and 3% for maintenance at 0.5 L of O_2/min in a stereotaxic frame. The skin was cut opened and the skull was punctured with a 3 mm stab knife (WPI 501731) generating a small hole in it(1-2 mm). This hole was always located over somatosensory cortex: 2.2 mm lateral and 2.6 mm anterior to the interaural midpoint to conserve experimental conditions as much as possible.

Injections were carried out with microinjection capillaries (Drummond Scientific 3-000-203-G-X) pulled in a laser pooler (Sutter instruments P-97) with the following conditions: Heat 600, Filament 4, Velocity 35, Delay 140 and Pull 65. Right before the injection, a quarter of the tip was cut. Two injections were made then using a stereotaxic microinjector at 0.6 and 0.2 mm deep from the cortex surface. The total volume injected was 250 nL per injection site at 50 nL/min. The virus used contained either *Nek7* shRNA or the control shRNA, *gfp* shRNA, and was always used without any further dilution.

After this, the capillary was slowly withdrawn and the skin was sealed back with surgical glue (3M, 1469SB). Mice were finally left to recover in a recovery chamber at 37˚C and a topical analgesic (AstraZeneca EMLA cream) was applied in the affected area.

3.7. In utero viral injections

Lhx6Cre embryos at embryonic day 15.5 (E15.5) were used to label interneurons sparsely. Pregnant females were deeply anesthetised with 3.5% isoflurane for induction and 2% for maintenance at 1 L of O_2/min. Before starting the surgery, 100 μL of 14 mg/mL ritrodine (sigma r0758) diluted in 5% glucose were injected intraperitoneally to relax the uterus. The abdominal cavity was cut opened and the uterus extracted making the embryos accessible.

Viruses were diluted 1 in 30 (titre around $1.6 \cdot 10^{11}$ viruses/mL) and 1 μL was injected in one telencephalic lateral ventricle. To do so, capillaries were pooled as described above (laser pooler settings: Heat 410, Filament 5, Velocity 30, Delay 200 and Pull 120, tip cut half way) and they were inserted in a picospritzer (III, Parker). The injected solution was visible due to the presence of fast green. As in postnatal injections, the virus used contained either *Nek7* shRNA or the control shRNA, gfp shRNA.

The uteri were carefully placed back in the abdominal cavity and the incision sutured (aston pharma W9500T). After a couple of minutes exposed to the flow of oxygen without anesthetic the female was placed in a recovery chamber at 37˚C until fully recovered. As analgesic, buprex 0.1 mg/kg and carprofen 5 mg/kg were injected subcutaneously before and after surgery respectively.

3.8. Cortical cultures and transfection

Cortices from *Lhx6Cre* embryos at E17.5-E18.5 were used to grow primary cultures. All the solutions used were sterilized either by filtration or by autoclaving and every step was done as quick as

possible to improve cell survival. The heads of the embryos were kept at 4ºC while the genotype was determined by PCR because only the heterozygous mice were used for dissection.

After genotyping, 2-6 neocortices were dissected out removing the meninges. Next, tissue was digested with 1 mg/mL trypsin (Worthington Biochem. Corp. LS003707) diluted in HBSS (Life Technologies 14170112) for 15 minutes at 37ºC inverting the tube every 5 minutes. Digestion reaction was stopped adding trypsin inhibitor (Sigma T-9003) at a final concentration of 1 mg/mL. DNase I (Roche 10104159001) was also added at 0.05 mg/mL to break released DNA in the medium.

Cortical tissue was dissociated into single cells by gentle mechanical trituration, *i.e.* pipetting up and down 8 times with a 1000 µL pipette tip. Subsequently, the cell suspension was centrifuged at 32 x g for 10 minutes with the centrifuge brake off. The supernatant was removed and cells were resuspended in culture medium [500 mM Glutamax-I (Life Technologies 35050), 2% v/v B-27(Life Technologies 17504), 0.01 U/mL penicillin/streptomycin in Neurobasal A medium (Life Technologies 10888)] warmed at 37ºC.

To assess the number of viable cells in the cell suspension, trypan blue was added at 0.2% w/v and the number of cells excluding the dye were counted using a 20x objective. Finally, cells were platted at a density of 100.000 cells/cm^2. Glass-bottom plates(MatTek corporation P50G-1.5-30-F), had been previously treated with 0.5 mg/mL Poly-L-lysine (Sigma P2636), diluted in water (Sigma W4502), overnight at 37˚C.

Cultures were kept in incubators at 37˚C, 5% CO_2 and 100% humidity. Medium refreshment was carried out after the first week and every three days for the rest of the days. More specifically, half of the medium was withdrawn and replaced by a slightly higher volume of fresh medium to compensate water evaporation.

Cultures at day *in vitro* 4 (DIV4) were transfected with *Nek7* shRNA or *lacZ* shRNA using Lipofectamine 2000 (Invitrogen 11668) according to manufacturer's instructions. Culture medium was replaced by OptiMEM one hour before transfection. Plasmids were diluted at a total final concentration of 0.5 µg/mL in the transfection medium. Lipofectamin was used at a rate of 3 µL per µg of DNA and never after 6 months from manufacturing date. Plasmids and Lipofectamin were diluted in OptiMEM and left at room temperature during 5 minutes. Subsequently, they were mixed and kept at room temperature during 25 minutes before being added to the plate dropwise.

Cells were kept in the transfection medium during 3 hours in the incubator taking special care about keeping constant both temperature and CO_2 concentration. Next, the plates were washed with non-complemented Neurobasal-A medium twice and kept in a mix 1:1 of the medium withdrawn before transfection and fresh culture medium in the previous culture conditions.

3.9. RNA extraction

To carry out any protocol involving RNA all the surfaces were wiped with RNAse Zap (Ambion AM9780) and just water treated with diethyl pyrocarbonate (DEPC; Sigma D5758) was used to prepare all the solutions. Total RNA for microarray analysis was extracted and purified using Quiagen RNeasy Micro extraction kit (Quiagen 74004) following manufacturer's instructions with some modifications. The main reason to use this protocol was that microarray hybridization step is affected by traces of phenol,

although all the experiments involving sorted cells for qPCR were done with this protocol. To increase experiment speed and decrease RNA degradation, samples were processed independently.

Briefly, $1.5 \cdot 10^5$ cells were defrosted on ice and lysated adding 1 mL of buffer RLT (containing guanidine thiocyanate and 1% v/v β-mercaptoethanol) and passing the mix through a blunt 20-gauge needle. Next, 70% ethanol was added and the mix was homogenized and transferred to an extraction column. In this column, RNA molecules longer than 200 nucleotides, mostly mRNA, were bound passing the solution three times through it. After binding, treatment with DNAse, 4.22 units/µL during 15 minutes at room temperature, was carried out to eliminate DNA contamination. Several washing buffers were used in the column: RW1, two steps of RPE and 80% ethanol. For a complete washing all these buffers were left in the column for one minute and shaken vigorously before removing it by centrifugation. The column was finally dried to avoid contamination with the remaining ethanol. Finally, elution was performed with 14 µL of RNase-free water. The samples were stored at -80˚ C and shipped in dry ice.

Tri-reagent extraction method (Invitrogen AM9738) was used in the rest of experiments involving RNA following manufacturer's instructions. One mL of Tri-reagent was used per well of a 12-well plate in HEK cell experiments, for 35 mm dish in primary cultures and per dissected somatosensory cortex. These somatosensory cortices were dissected as previously described for FACS experiments. Homogenization was done simply pipetting Tri reagent over the plates with cells adhered or using the same procedure used to homogenize sorted cells with the dissected cortices.

After 5 minutes, 200 µL of chloroform (Sigma C2432) were added to separate the hydrophobic phase, containing mainly proteins, from the aqueous phase, containing RNAs. The superior colourless aqueous phase was separated in another tube avoiding the DNA present in the interphase. Subsequently, the RNA was precipitated adding 500 µL of isopropanol (Sigma I9516), centrifuged and the pellet was washed with 75% ethanol. Again, in this protocol elimination of remaining ethanol is quite important. Thus, the pellet was dried for 10 minutes after removing the maximum possible amount of ethanol. However, the pellet was never left to dry too much (what happen when it is transparent) to facilitate the subsequent solubility in water. The concentration and purity of the RNA was checked in a nanodrop spectrophotometer (Thermo Fisher E112352) and just the samples with concentration higher than 100 ng/µL, absorbance ratio 260/280 higher than 1.8 and absorbance ratio 260/230 higher than 1.3 were selected. After finishing the extraction, samples were also stored at -80˚ C.

3.10. Microarrays

RNA samples of the synaptogenesis genetic screening where sent to the genomics facility of "Centro de investigación del cancer" in Salamanca University for RNA purity analysis, microarray hybridization and bioinformatic analysis. Three replicates were done for all the 4 conditions assayed. mRNA integrity was assessed by capillary electrophoresis using Agilent 2100 Bioanalyzer (Agilent, Palo Alto, CA). Just samples with a rRNA ratio 28s/18s higher than 1.6 and a RNA Integrity Number (RIN) higher than 9 were selected.

Total RNA, 100-300 ng, was amplified using the wild type (WT) Expression Kit (Ambion, 4411973), labelled using the GeneChip WT Terminal Labeling Kit (Affymetrix, 900670) and hybridized to Mouse Gene 1.0 ST Array (Affymetrix, 902464). Washing and scanning were performed using

GeneChip System of Affymetrix formed by: GeneChip Hybridization Oven 640, GeneChip Fluidics Station 450 and GeneChip Scanner 7G.

Microarray fluorescence intensity data was analysed using the R package BioConductor (Ihaka and Gentleman, 1996). Normalization was carried out with the algorithm Robust Multiarray Average (RMA). Statistical significance for differential expression between the samples was measured with the statistical technique "Significance analysis of microarrays" (SAM) selecting the genes with a false discovery rate (FDR) of 0.05. Q-values where considered for significance instead of p-value because these are adjusted p-values that considers the multiple testing applied to every gene in the microarray. Since the samples could just be analysed in batches of 5 in the same experiment, there was a possibility of differences between experimental batches (batch effect). This effect was discarded comparing the "Normalized unscaled standard error" (Nuse) of the different samples and confirming that all of them were similar. Furthermore, the similarity among replicates of the same group was assessed using principal component analysis (PCA). This analysis let the multivariate data of each microarray be represented in 2 dimensions such that the spatial location of the points in the plot reflects the similarity between the arrays.

Three comparisons were done using SAM: IN P10 vs IN P0 for genes differentially expressed during GABAergic synaptogenesis, Pyr P12 vs Pyr P0 for genes differentially expressed during Glutamatergic synaptogenesis and IN P10 vs Pyr P12 for genes differentially expressed comparing both populations of cortical cells. Subsequently, these lists were compared among them using excel for genes upregulated specifically during GABAergic synapse formation, i.e. enriched in IN P10 with a small expression in the rest of the populations. Only those genes with a fold change greater than 2 in any of the comparisons were considered for analysis.

The populations compared was quantified using the specificity ratio (τ):

$$\tau = \frac{\sum_{i=1}^{n}(1-\hat{x_i})}{n-1}, \qquad \hat{x_i} = \frac{x_i}{\max\limits_{1\le i\le n}(x_i)}$$

Where $\hat{x_i}$ is the expression of the gene in tissue i and n is the number of conditions.

The criteria used to select the genes to study were: the specificity ratio, the expression pattern in Allen brain atlas, and the total levels in IN P10 (Lein *et al.*, 2007); see chapter 4).

Finallly, gene lists were analysized for possible known roles in the literature using Gene Ontology, KEGG and Reactome (Ashburner *et al.*, 2000; Fabregat *et al.*, 2016; Kanehisa *et al.*, 2017). To do this the package clusterProfiler inside Bioconductor was used in R (Ihaka and Gentleman, 1996). A q-value cut off of 0.05 was applied in all the analysis carried out. Similarly, for the heatmap data the package ggplots was used (Wickham, 2009).

3.11. qPCR

RNA samples to be used in the qPCR experiments were retronstranscribed into cDNA according to SuperScript IV protocol. One μg of total RNA was treated with DNAseI according to the manufacturer (1 U/reaction, 30 minutes at 37˚ C, Promega M6101). The DNAse step was done just in HEK293 samples because of their high DNA content but was not done in cortical or primary culture samples due to the low RNA yield.

Retrotranscription components were mixed in two steps. First, the nucleotidic components (oligonucleotides, RNA and dNTPs) were mixed, heated at 65˚ C during 10 minutes and quickly placed in ice afterwards to remove secondary structures. Second, the rest of components were added resulting in the following final concentrations: 0.025 µg/µL Oligo(dT) (15 nt Sigma), 7.5 µg/µL Random primers (Thermo Fisher N8080127), 0.5 mM dNTPs (Thermo Fisher R0191), RNA 0.05 µg/µL, 1x first strand buffer, 5 mM DTT, 10 U/µL Superscript IV (Thermo Fisher 18090050) and 2 U/ µL RNase OUT (Invitrogen 10777019). The reaction was left 5 minutes at 25˚ C for random primers to anneal and 30 minutes at 50˚ C for retrotranscription. Finally, the reaction was stopped heating at 70˚ C during 15 minutes and the cDNA diluted up to 200 µL in DEPC water.

The specificity and efficiency of the primers were assessed doing serial dilutions of a P10 cortical sample, which contained all the tested genes, and measuring their RNA levels by qPCR. From the regression curve slope the efficiency was calculated with the following equation:

$$\log_2 T_q = \log_2 T_0 - Cq * log_2(1+E) \;\; ; \;\; E = 2^{-b} - 1$$

Where T_0 and T_q are the number of transcripts initially and after the cycle Cq respectively, E is the efficiency of the reaction and b the slope of the showed straight-line equation. Only primers with efficiencies between 0.9 and 1 were used. The best concentrations for the primers were also assessed trying different combinations of three different final concentrations of the forward (F) and reverse (R) primers (50, 300 and 900 µM) and selecting the combinations with the highest yield. These were the used concentrations in the sample: 18S 0.3 µM F (forward) and R (reverse), Nek7 0.3 µM F and 0.9 µM R, WPRE 0.9 µM F and R, mCherry 0.9 µM F and 0.3 R and Lgals1 0.3 µM F and 0.9 R. These were the primers used:

Nek7 F	AGCCACAGAAGGCATTACGG
Nek7 R	CTACCGGCACTCCATCCAAG
Lgals1 F	CCAAGAGCTTTGTGCTGAACC
Lgals1 R	ATGGGCATTGAAGCGAGGAT
18s F	GTAACCCGTTGAACCCCATTCGT
18s R	GTGTGTACAAAGGGCAGGGACTTAA
mCherry F	CATCCTGTCCCCTCAGTTCATG
mCherry R	GAAGTTCATCACGCGCTCCCAC
WPRE F	GGCACTGACAATTCCGTGGT
WPRE R	CGCTGGATTGAGGGCCGAAG

Quantitative PCR reactions were done using 5 µL of FastStart Essential DNA Green Master (containing SyBRGreen, Roche 06402712001), 3 µL of the cDNA samples and the specific primers

diluted in 2 μL of water. The qPCR reaction was done in the qPCR thermal cycler LightCycler 96 (Roche) with a 3 steps amplification. Briefly, annealing temperature was 60˚ C and fluorescence was detected during the amplification step at 72˚ C. At the end of the qPCR protocol the product was subject to a temperature ramp from 65˚C to 97˚C and fluorescence was continuously measured. Only the primers whose product generated a single sharp peak signal in the melting curve at the expected melting temperature were considered.

Expression data was always normalized to a house keeping gene in all the samples, mainly 18s, and RNA expression was calculated with the following equation:

$$mRNA\ levels\ (a.u.) = \frac{2^{Cq_{18s}}}{2^{Cq_{gene}}}$$

In HEK cells transfection, levels of Nek7 were normalized to mCherry because the levels of both changed similarly with transfection efficiency and they none of them was expressed by non-transfected cells. 18s was not used in this case because HEK cells express it.

3.12. Immunohistochemistry

Mice were anesthetized with sodium pentobarbital and perfused with PBS followed by 4% paraformaldehyde (PFA) in PBS. Brains were dissected out the skull and postfixed 2 hours in 4% paraformaldehyde (PFA) at 4°C. Afterwards, they were cryoprotected in increasing concentrations of sucrose (15 % and 30%) and coronal slices were cut in a sliding microtome (Leica SM2010R) at 40 μm mainly or 100 μm for the morphology reconstruction experiments. These sections were kept in ethylene glycol solution at -20° C until their use.

Sections were blocked with a solution of 5% bovine serum albumin (BSA, Sigma A7906), 0.3% triton (Triton X-100 Sigma T8787) and, optionally, 5% Normal donkey or goat serum (Bio-Rad C06SBZ and C07SAZ), depending on the species of secondary antibody host, in PBS. Primary antibodies were then applied overnight at 4° C and secondary antibodies for 2 hours at room temperature. All the antibodies can be found in table I and were diluted in 1% BSA 0.3% triton in PBS. In the case of morphological analysis primary antibodies were applied during 2 nights at room temperature, secondary antibodies during 4 hours and triton concentration was increased to 1% to improve antibody penetrance. When any of the primary antibodies host was goat none of the secondary antibodies hosts was the same to avoid crossed reactivity.

DAPI solution (Sigma D9542) was applied to the sections at 5 μM except for the samples containing Streptavidin 405 antibody. PBS washes were done every time any of the solutions was changed and gentle horizontal shaking applied during the whole process. Sections were mounted using 0.05% w/v gelatin solution (Sigma G1890) in Tris-HCl pH 7.5 buffer and dried avoiding them from losing completely their moisture. Finally, mowiol/Dabco solution [100 g/L mowiol (Calbiochem 475904), 25 g/L Dabco (Sigma D2522), 40% v/v glycerol in PBS] was added and coverslips put on top before keeping the samples at 4° C.

Primary antibodies				
	Host	**Company**	**Reference**	**Concentration**
GAD65	Mouse IgG2a	Chemicon	MAB351R	1:500
VGlut1	Guinea-pig	Chemicon	AB5905	1:5000
SST	Rat	Chemicon	MAB354	1:200
PV	Rabbit	Swant	PV-25	1:5000
PV	Mouse	Sigma	P-3088	1:1000
PV	Chicken	SySy	195 006	1:500
PV	Goat			
DsRed	Rabbit	Clontech	632496	1:500
Geph	Mouse IgG1	SySy	147 011	1:500
Lgals1	Goat	R&D	AF1245	1:100
NeuN	Mouse IgG1	Millipore	MAB377	1:500
NeuN	Rabbit	Millipore	ABN78	1:500
Syt2	Mouse IgG2a	ZFIN	ZDB-ATB-081002-25	1:500 or 1:250 glycerol
mCherry	Goat	Antibodies-Online	ABIN1440057	1:500
GFP	Chicken	Aves labs	GFP-1020	1:1000
HA11	Mouse IgG1	BioLegend	901502	1:250 gly
Flag	Mouse IgG1	Sigma	F1804	1:500

Secondary antibodies				
	Host	**Company**	**Reference**	**Concentration**
Anti-Rat 488	Goat	Molecular Probes	A-11006	1:250
Anti-Rat 488	Donkey	Molecular Probes	A21208	1:200
anti-Rabbit Cy3	Donkey	Jackson	711-165-152	1:500
anti-Rabbit Biotin	Goat	Vector	BA-1000	1:200

anti-Rabbit 488	Donkey	Life Technologies	A21206	1:400
anti-Rabbit 647	Donkey	Molecular Probes	A31573	1:500
anti-Mouse Cy5	Donkey	Jackson	715-175-150	1:200
anti-Mouse 555	Donkey	Molecular Probes	A31570	1:500
anti-Mouse 488	Donkey	Molecular Probes	A21202	1:200
anti-Mouse 647	Donkey	Molecular Probes	A31571	1:500
anti-Mouse IgG2a 647	Goat	Molecular Probes	A21241	1:500
anti-Mouse IgG2a 488	Goat	Molecular Probes	A21131	1:500
anti-Mouse IgG2a 555	Goat	Molecular Probes	A21137	1:500
anti-Mouse IgG1 555	Goat	Molecular Probes	A21127	1:500
anti-Mouse IgG1 488	Goat	Molecular Probes	A-21121	1:500
anti-Goat 488	Donkey	Molecular Probes	A11055	1:500
anti-Goat 555	Donkey	Molecular Probes	A21432	1:250
anti-Goat Biotin	Horse	Vector	BA-9500	1:200
anti-Guinea Pig 488	Goat	Molecular Probes	A11073	1:500
anti-Guinea Pig 555	Goat	Molecular Probes	A21435	1:500
anti-Guinea Pig 647	Donkey	Jackson	706-605-148	1:250
anti-Chicken Cy2	Donkey	Jackson	703-225-155	1:250
anti-Chicken Biotin	Goat	Vector	BA-9010	1:200
Streptavidin 647		Jackson	016-600-084	1:200
Streptavidin DyLight 405		Jackson	016-470-084	1:400

Table 3.1. List of primary and secondary antibodies used. Full list of primary and secondary antibodies used in all the project. In the table are reported the antigen, antibody hosts species, producer company (with reference number) and concentration for use in immunohistochemistry. Antibodies are sorted according to antigen name.

3.13. Simultaneous In situ hybridization and immunohistochemistry

Mice brain slices were obtained in similar conditions to the immunohistochemistry protocol. We just changed the post-fixation to overnight and the thickness of the slices that were cut at 30 μm. Sections were mounted in superfrost slides (Thermo Fisher J1800AMNZ) using 0.5 % v/v Tween (Sigma P9416) in PBS (PBS-T) and fixed to these with PFA during 5 minutes. After three 5 minute washes with PBS-T, sections were digested with proteinase K (Sigma P2308) 5 μg/mL diluted in this same buffer, fixed again with PFA and washed with other three 5 minutes washes of PBS-T. Slides were then transferred to a sealed and moist hybridization chamber where they were incubated for 1 hour at 62° C with 500 μL of hybridization buffer [1x SALT solution (from a 10x stock with 2 M NaCl, 0.1 M Tris, 50 mM NaH_2PO_4, 50 Mm Na_2HPO_4, 50 Mm EDTA, pH 7.5), 1 x Denhardt's solution (from a 50x stock, Sigma D09905), 50% formamide (Ambion AM9342), 10 % w/w (weight/weight) dextran sulfate (Sigma D8906) and 0.2 % w/v yeast tRNA (Invitrogen 15401)]. Two to five μL of digoxigenin labelled RNA probes were heated at 80°C for 5 minutes, cooled in ice for the same period and diluted in prewarmed hybridization solution. Prehybridization solution was exchanged by the probe one and the slides were incubated overnight at 62°C.

The next day, slides were washed with washing solution [50% formamide, 0.5x SSC (Sigma S6639), 0.1% w/v tween] at 62° C first during 15 minutes and, after this, 3 more times during 30 minutes. Subsequently, slides were washed for 5 minutes in MABT buffer (0.1 M maleic acid, 0.2 M NaOH, 0.2 M NaCl, 0.5% v/v Tween) and 500 μL of blocking solution [10% v/v sheep serum (Bio-Rad), 5% BSA, 20% BBR (Roche 11096176001) in MABT] were added as a blocking step during 1 hour. Antibodies were diluted in antibody solution (blocking solution with 1% BSA) and incubated at 4˚ C overnight with a parafilm coat to keep the solution on the slide. The following antibodies were used: anti-digoxigenin 1:3500 (Roche 11093274910) for *in situ* signal and anti-GFP and anti-PV rabbit for immunohistochemistry being the concentration of these double than the used for the immunohistochemistry protocol.

The next day slides were tempered at room temperature, washed with MABT buffer 6 times for 30 minutes each wash and incubated during 2 hours with the immunohistochemistry secondary antibodies in antibody solution. Secondary antibodies used, anti-chicken 488 and anti-rabbit Cy3, were also at a concentration that was double the one used in the immunohistochemistry protocol. DAPI was also applied at the previously described concentration on top of the slide.

Subsequently, slides were washed in fluorescence detection buffer (100 mM Tris HCl pH 8, 0.1 M NaCl and 5 mM $MgCl_2$) during 2 washes of 10 minutes each at room temperature. Slides were then incubated in developing solution [0.1 mg/mL HNPP and 25 mg/mL Fast Red (Roche 11758888001) diluted in fluorescence detection buffer] during 2 to 3 hours until the signal was detectable.

Reaction was stopped washing 3 times during 5 minutes with EDTA 1 mM (Sigma ED2SS) diluted in PBS. The fluorescent precipitate was fixed in the slices with PFA 4%. Finally, excess PFA was

removed with two washes of PBS during 5 minutes each and all the slides were dried and mount with mowiol/dabco.

A similar protocol was carried out to develop the probe signal with a colorimetric staining. Differently, PBS-T and MAB-T buffer contained 0.1% Tween during the whole process. In the second day, the blocking buffer before the antibody was the same as described before but without BSA, and the same was used to incubate the anti-digoxigenin antibody. The main differences with the above protocol are found in the developing procedure that was done during the third day. Samples were washed during 3 times during 10 minutes in MABT buffer and 2 times in NTMT buffer (0.1 M NaCl, 0.1M Tris-HCl, 0.05 M $MgCl_2$, 0.1% Tween in H_2O at pH 9.5) during 10 minutes. Afterwards, the signal was developed with NBT-BCIP solution (Roche 11 681 451 001) diluted in NTMT. Developing times changed depending on the probe, specifically, for Nek7 probe the usual developing time was 5 hours. Reaction was stopped as in the previous protocol but samples were differently mounted. They were dehydrated in increasing concentrations of ethanol and xylol to be finally mounted using Kristalon mounting medium (Sigma 64969).

3.14. Confocal and fluorescence imaging

All the imaging experiments were done using a confocal microscope (Leica TCS SP8) or an fluorescence microscope (Zeiss) being blind to the experimental condition. It is important to note that the best imaging resolution was obtained when mowiol/dabco solution was dried which happened usually around 24 hours after mounting.

Confocal images were always acquired adjusting the detector beam to the fluorophore emission spectrum and restricting it according to the presence of other fluorophores in the sample that may also be excited. Laser intensities were usually 3% for 488 nm, 555 nm and 405 nm lasers and 6% for 647 nm laser. Offset was set to 0 and gain adjusted to the signal intensity trying to extend the dynamic range of the signal the maximum possible. Pixel resolution was set to 1024 x 1024 and bit depth to 8. Given the difference in intensity found in the z axis due to antibody penetrance, all images were taken starting at a z position 5 μm below the superior limit of the slice expanding it from this point to the centre of the slice in z-stacks.

All the images for cell quantification were done using 40x oil objective. In Nek7 loss of function (LOF) experiments, the number of infected PV cells in the area surrounding a pyramidal cell was quantified before imaging its somatic boutons. These images were taken at zoom 0.75.

Synaptic boutons were imaged with a 100x objective digital zoom 2.2. For quantifying synaptic density along development in layer II/III of SSC and in Lgals1 LOF quantification in layer I 15 fields of each condition were taken. In the somatic bouton quantifications, at least 20 cells were imaged either in 2D for Lgals1 or in 3D, doing z-stacks, for Nek7 experiments. Separation between stacks was set to 0.2 μm.

For reconstructing PV cell morphology, cells expressing mCherry and PV where found with the 20x objective, their positions recorded and imaged later with the 63x objective scanning in the x-y axis a grid of confocal fields (tilescan) and in z a stack spaning the size of each cell. Separation between stacks was set to 0.5 μm. Furthermore, Syt2 boutons were imaged within mCherry labelled neurites. 4

images were taken at different locations of the neuritic arbour in the same conditions as somatic Syt2 boutons (10 µm z-stacks).

Time lapse experiments were done in the same confocal model with an incubation chamber were cultures where kept at 37°C and 4% CO_2. Growth cones were identified and recorded at DIV7 with a 20x objective, resonant scanner set to 15% intensity and hybrid detector to reduce the scanning time and damage to the living cells. In every imaging session, around 15 growth cones were scanned in z-stacks during one hour with a 2.5 minutes inter-frame interval.

3.15. Somatic and neuropil bouton quantification.

As described above, synaptic boutons were identified with antibodies against presynaptic markers that accumulate in the presynaptic terminal forming a characteristic round bouton like shape. These boutons were quantified in the developmental timeline and Lgals1 experiments using the image analysis software ImageJ (Schindelin *et al.*, 2012; Schneider *et al.*, 2012).

First, images were filtered to improve the signal with subtract background (rolling=50) and enhance contrast (saturated=0.4). Given the variability in signal intensity between different boutons, the synaptic marker channel was converted to a binary mask. This mask was defined by an intensity threshold that was chosen from 0 to 255 according to the signal quality and was equal for all the conditions of a given experiment. The markers used were: GAD65, VGlut1 and SYT2 presynaptically and geph postsynaptically. Next, just particles with an area higher than 0.2 μm^2 (GAD65 and Syt2), 0.1 μm^2 (VGlut1) or 0.05 μm^2 (Geph) were filtered with the tool “analyse particles” and therefore considered synaptic boutons. In the synaptic development timeline experiments, GAD65 and VGlut1 were counted using the “Measure” tool.

Presynaptic and postsynaptic bouton colocalizations were done when there was no postsynaptic structure to appose the presynaptic terminals to. In 2d images this quantification was just done in Lgals1 KO for the quantification of GAD65 boutons in layer I. Once both boutons were masked and filtered they were colocalized and a colour threshold applied to select exclusively the colocalized particles. These particles were further filtered by an area filter of 0.01 μm^2 with “analyse particles” and quantified as before.

In both presynaptic and colocalized pre-postsynaptic bouton quantifications done in different cortical areas the number of boutons was expressed as boutons per 100 μm^2.

Somatic boutons were quantified around a region of interest (ROI) defined drawing a polygon following the border of the soma. The markers used were NeuN, PV and SST. Since SST does not define sharply the borders of the cell, NeuN was used to draw the limits of SST containing cells. The different channels were processed separately to avoid any possible bias and merged for quantification. Only the boutons whose pixels were contacting the defined borders of the cells were manually quantified. Bouton density was expressed as boutons per 100 µm of cell perimeter.

All cell quantifications where done with “Cell Counter” plug-in of ImageJ. Cell in the different channels were labelled independently and further compared when colocalization of several markers was needed. Finally, axonal growth movies recorded in time lapse experiments drifted along the duration of the experiment. This effect was corrected using ImageJ plug-in “Correct 3D Drift”.

3.16. Three-dimensional somatic bouton quantifications and morphological reconstruction

All the quantifications in Nek7 LOF experiments were done using the 3D image analysis software Imaris (Bitplane, Imaris 8.1.2). Image stacks were processed with background subtraction (13.2 µm) and Gaussian filtering (0.517) to enhance the signal. This software generates a set of objects based on the signal intensity: spots for synaptic boutons, surfaces for different structures like somas and neurites and filaments to trace the path of neurites. Imaris also uses a set of tools called XTensions that require Matlab (The MathWorks Inc. MATLAB R2016b).

For the analysis of somatic boutons, spots were identified from the Syt2 (presynaptic) channel with a diameter of 0.500 µm. Two surfaces were generated: mCherry neurites and 1 to 4 NeuN somas excluding those cells expressing mCherry and PV, area and volume of these surfaces was measured. "Spots close to surface" XTension was used to filter the Syt2 spots at 0.25 µm (one radium distance) from the NeuN surfaces, *i.e.* the somatic boutons. Finally, boutons coming from infected cells were quantified using the "Split spots into surfaces" XTension with somatic boutons in mCherry surface. Both all somatic boutons and those from infected cells were expressed as percentage of mCherry boutons and density of boutons per 100 μm^2 of soma.

Due to the variability in the number of PV cells infected the number of Syt2 boutons in mCherry containing axons changes. The proportion of $Syt2^+$ $mCherry^+$ boutons increases linearly with the number of PV infected. For this reason, we normalized both bouton percentages and densities to the number of infected PV cells in the surrounding area (See chapter 5). Images with less than 20% of PV infected were not considered.

To reconstruct PV basket cell morphology a unique surface was generated comprising the whole cell morphology. A binary mask was then created separating the signal contained in the cell and setting to 0 the possible signal outside the cell. Next, a filament was generated using the fully automated algorithm with the signal intensity in the masked channel. Finally, the XTension "Generate Convex Hull" was used to create a surface consisting on the minimal polyhedron containing the cell. All the available variables in the filament were compared and statistical significance was measured with t-test. However, from all these variables the main ones analysed were "sholl analysis", "branching points", "total length" and volume of the convex hull. Branching point density was expressed as number of branching points per 100 µm of neurite length.

The density of Syt2 boutons in these reconstructed cells was measured in different images to be able to have a comparable quantification of synaptic boutons. Briefly, spots were generated with Syt2 channel and a surface from mCherry channel. The number of presynaptic terminals in the cell neurites was measured with "Split spots into surfaces". Cell density was expressed as number of Syt2 boutons per 100 μm^2 of mCherry area.

Finally, growth cone dynamics were also measured using Imaris after drift had been corrected in ImageJ. The image was cropped to contain exclusively the axonal path and a filament was generated using the semiautomatic Autopath tool in every time point. Next, the "dendrite diameter" was rebuilt to analyse the filament track. Speed was expressed as µm/min and path length and displacement in µm.

Meandering of the axon during its growth was assessed measuring straightness, *i.e.* the result of dividing the total final displacement of the growth cone by the length of the path followed by it.

RESULTS

4. Identification of genes upregulated during GABAergic synapse formation

4.1. Introduction

Pyramidal cells and interneurons diverge remarkably from early times on their development. They are born at different places and have differentiated migratory behaviours. Once they are allocated in the cortex, they also make their connections differentially. Pyramidal cells extend long-range axons compared to interneurons, which have local connectivity. Such connections use distinct neurotransmitters: excitatory for pyramidal cells and inhibitory for interneurons. Furthermore, their outputs target different subcellular compartments, for example, pyramidal cells target the spines in other pyramidal cells while the interneurons rarely synapse in these structures. All these differential developmental processes, including synapse formation, may require distinctive molecular programs. Although many studies have shed some light into these differential mechanisms there has been few unbiased studies to date using high throughput genomic screenings. Such approach would be able to give a complete picture of the whole set of molecules mediating these processes in the mammalian cortex during development.

The absence of a high throughput analysis is more evident when the focus is placed in finding genes involved in synapse formation. There have been numerous genome-wide genetic screens in invertebrates (Aberle *et al.*, 2002; Featherstone and Broadie, 2000; Kurusu *et al.*, 2008; Schaefer *et al.*, 2000) and some in mammalian peripheral nervous system using biochemical approaches (Allen *et al.*, 2012; Christopherson *et al.*, 2005; Nitkin *et al.*, 1987; Peng *et al.*, 1991). Various studies have performed GABAergic synaptogenetic screens developing relatively high throughput techniques to quickly carry out LOF experiments of candidate genes and assess how they affect synapse formation (Paradis *et al.*, 2007; Sharma *et al.*, 2013). However, these studies can test a limited number of genes and their selection is subject to criteria based on previous knowledge, hence, being difficult to identify novel mechanisms. The main reason for this gap resides in the relatively low abundance of GABAergic synapses compared to glutamatergic synapses in cerebral cortex, which makes difficult the isolation of proteins or mRNAs participating in their development. The new generation of cell-type specific Cre lines together with the recently developed protocols that allow us to label and isolate subpopulations of neurons facilitate the separation of interneuron populations from the rest of cortical cells. This let us tackle different questions of interneuron development, including GABAergic synaptogenesis, with high throughput approaches.

Proteins participating in the formation of the synapse must be highly upregulated during this process, making possible the isolation of their transcripts from both the soma or the synapse where they are known to be transported (Cajigas *et al.*, 2012). To differentially isolate pyramidal cells and interneurons during synapse formation, we first studied temporal development of glutamatergic and GABAergic synapse formation (Fig. 4.1). Then, taking advantage of fluorescent reporter genes only expressed in each of these populations, we isolated both cell types by using fluorescent-activated cell sorting (FACS, Fig. 4.2). This method is highly reliable, repeatable and prevents the expression of apoptosis-related genes better than other methods. These features are even comparable to manual isolation of cells with the advantage of a much higher cell yield (Okaty *et al.*, 2011). The genetic profiles of both populations were obtained using microarray and subsequent bioinformatics analysis (Fig. 4.3-4.5). Finally, we selected candidate genes based on specific criteria to subsequently test their involvement in synapse formation (Fig. 4.6-4.10).

4.2. Quantification GAD65 and VGLUT1 Synaptic development

Synapse formation takes place during the first postnatal weeks (De Felipe *et al.*, 1997; McAllister, 2007; Waites *et al.*, 2005). Although several studies have previously analysed the developmental time course of synapse formation (Paradis *et al.*, 2007; Sharma *et al.*, 2013), none of them have carried out a comprehensive analysis of both glutamatergic and GABAergic synapses simultaneously at early stages of synapse formation. At these stages, protein transport packets accumulate at the synapse to form the synaptic bouton. Molecules like glutamate decarboxylases and vesicular transporters undergo this process and they are accumulated in synaptic boutons that can be identified by immunohistochemistry. Most of the proteins involved in the formation of the synapse may also be accumulated in these boutons, therefore, an increase in bouton number should parallel the accumulation of these synaptogenetic proteins. Thus, we used the vesicular transporter VGlut1 and the GABA synthetizing enzyme GAD65 to follow the time-course of glutamatergic and GABAergic synaptic bouton density respectively (Fig. 4.1). Compared to previous studies, this approach allows us to follow the synaptogenesis time-course independently of synaptic maturity.

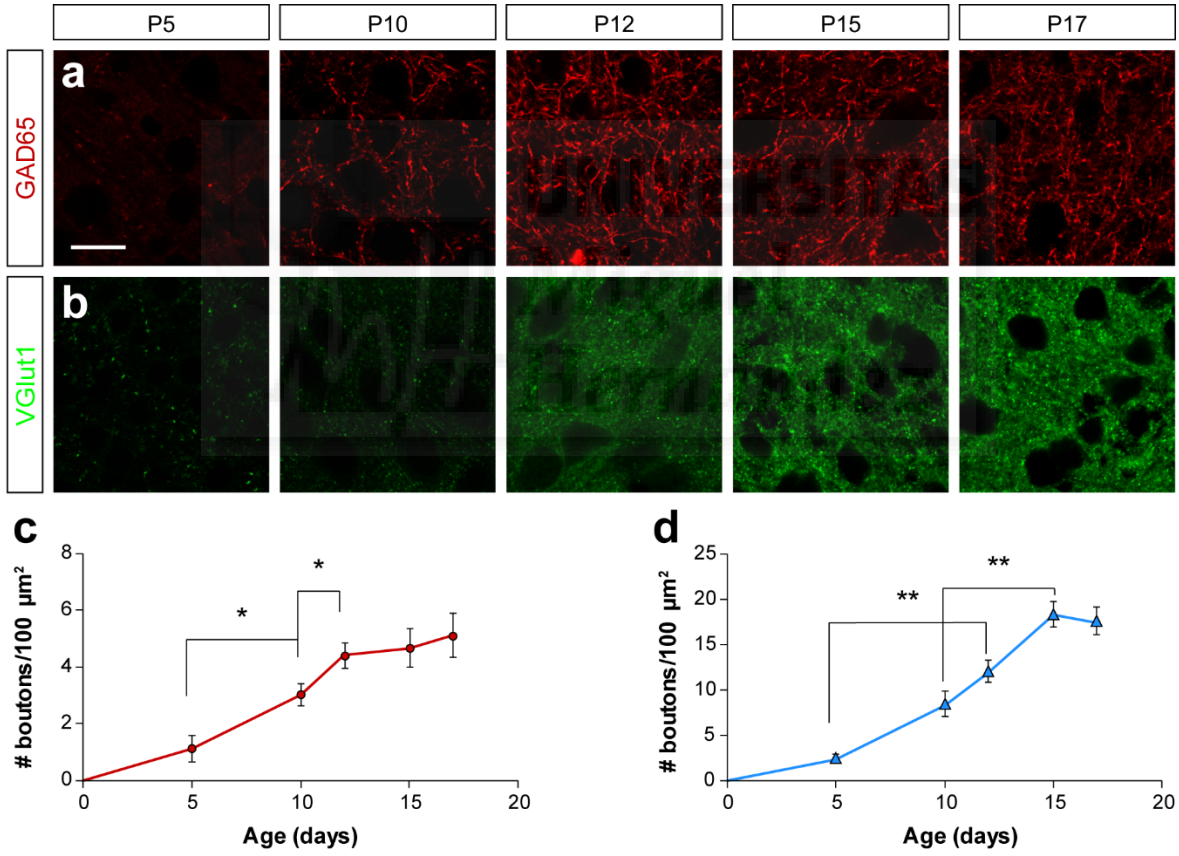

Figure 4.1. GABAergic and glutamatergic synaptogenesis time course. (a, b) Single confocal images showing GAD65 (a, red) and VGlut1 (b, green) staining at different timepoints of the first two postnatal weeks (P0-P17) in SSC layer II/III of C57BL/6 mice. (c, d) GAD65 (c, red) and VGlut1 (d, blue) bouton density in 100 µm^2 of cortical area as a function of postnatal age. One-way ANOVA, Post hoc Bonferroni, *p<0.05, **p<0.01 , n=3 brains per age. Scale bar: 10 µm. Data are expressed as mean±s.e.m.

We found an increase in bouton density from P5 to P20 in both GABAergic and glutamatergic synapses (Fig. 4.1). Such increase is higher during the first postnatal days reaching a plateau at later stages (at P15 for GABAergic and P17 for glutamatergic synapses; Fig. 4.1c, d). As previously described

(Ben-Ari, 2002), GABAergic synapses are formed a few days before glutamatergic synapses reaching the plateau earlier (Fig. 4.1c, d).

We next assessed when the highest synaptogenetic rate was taking place with the aim of isolating the cells expressing putatively the highest levels of synaptogenetic transcripts. For GABAergic interneurons, the highest rate occurs between P10 and P12 (6.90±1.41 bout/day·1000 μm^2, Fig.4.1c) while in pyramidal cells it occurs between P12 and P15 (20.86±1.41 bout/day·1000 μm^2, Fig.4.1d). Assuming that the highest quantities of synaptic proteins are going to be expressed during these time frames and considering that mRNA somatic transcription precede protein synaptic localization, we selected P10 for interneurons and P12 for pyramidal cells.

4.3. Fluorescent activated cell sorting (FACS)

We used green fluorescent protein reporter genes to specifically label GABAergic interneurons (*Nkx2.1:RCE*, Fig. 4.2, left) and pyramidal cells (*NexCre: RCE,* Fig. 4.2, right) for subsequent isolation using FACS sorting at P10 (IN P10) and P12 (Pyr 12) respectively (Fig. 4.2, top). To examine whether gene expression levels follow the dynamics of synapse formation we selected a different timepoint, P0, when synapses are not being formed yet (IN P0 and Pyr P0, Fig. 4.2, bottom). We expected that the levels of synaptogenetic genes would be mostly increased between P0 and P10/P12.

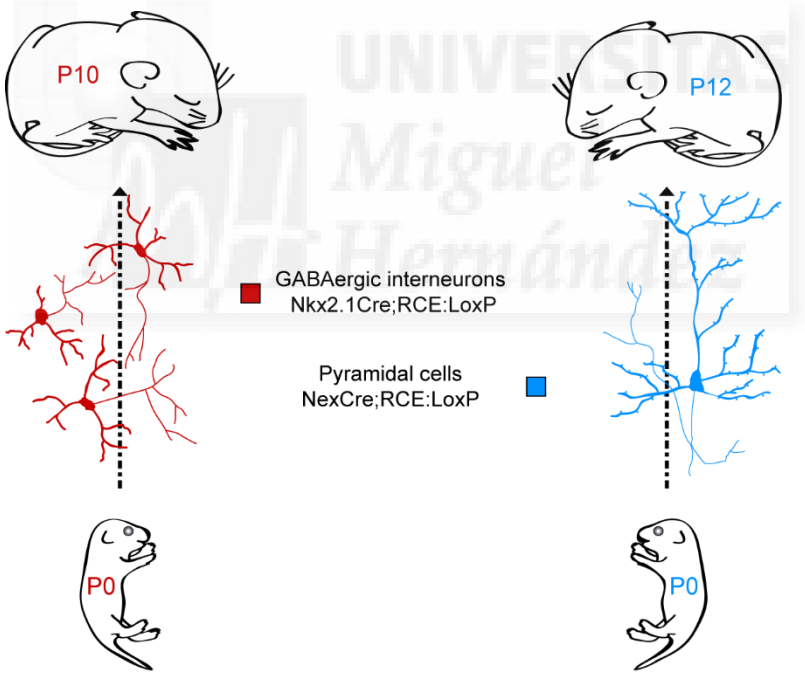

Figure 4.2. Experimental conditions used in the genetic screening. GABAergic interneurons (red) coming from *Nkx2.1Cre;RCE* mice were isolated when the highest synaptogenetic rate was taking place, P10, and at a timepoint when synaptogenesis has not started yet (P0). Similarly, glutamatergic pyramidal cells (blue) from *NexCre;RCE* mice were isolated at P12 and P0.

To assess the survival and purity of isolated cells several control sorting experiments were run. First, cells coming from a non-fluorescent mouse were isolated from the same experimental timepoints to identify the expected non-fluorescent cells (green fluorescent protein negative cells GFP$^-$; Fig. 4.3a,

a'). In all sorting experiments cells with a greater fluorescence than the defined GFP$^-$ population were considered GFP$^+$ (Fig. 4.3a', b'). As a second control, isolated fluorescent cells from the different conditions were sorted twice to corroborate that most of the cells were both alive and fluorescent. At IN P10 80.5% of the cells survive and 98.6% of the alive cells are GFP$^+$ (Fig. 4.3c, c').

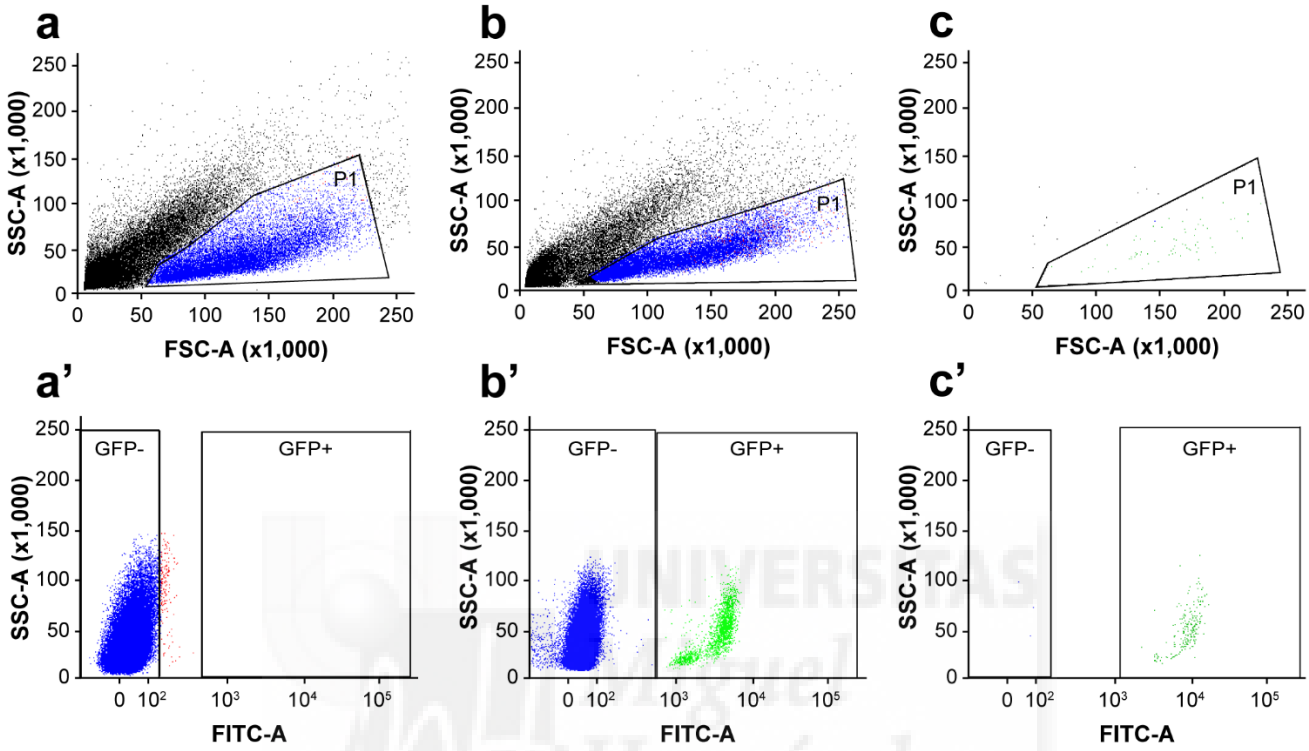

Figure 4.3. FACS purification control experiments. (a-a') Scatterplot showing the total population of cells sorted (a) of which P1 was selected to measure fluorescence (a') from wild type (WT) C57BL/6 mice at P10. *(b-b')* Same as in (c) from *Nkx2.1Cre;RCE* mice. (c-c') Same as in (a) and (b) of previously sorted GFP cells from *Nkx2.1Cre;RCE* mice. SSC-A, Side scattered light; FSC-A, Forward scattered light; FITC, Fluorescein isothiocyanate detection channel.

4.4. Microarray analysis: Genes upregulated during GABAergic synaptogenesis

Gene expression data was obtained from microarrays and differentially represented genes were identified comparing across cell types and ages. Initially, genes specifically expressed during GABAergic or Glutamatergic synaptogenesis were highlighted comparing P0 and P10 or P12 respectively (Fig. 4.4, blue and red gene sets). Separately, genes whose expression was cell type specific at the age of synaptogenesis were identified comparing GABAergic interneurons at P10 and pyramidal cells at P12 (Fig. 4.4, purple gene set).

These three groups of genes were further compared among them to obtain a list of genes specifically expressed in GABAergic interneurons during synaptogenesis. GABAergic and Glutamatergic synaptogenesis specific genes (Fig. 4.4, blue and red gene sets) were compared among them to identify both common and exclusively regulated genes. Finally, cell type specific genes that were exclusively regulated during GABAergic synaptogenesis were identified comparing the last-

mentioned list with the lists of cell type-specific genes (Fig. 4.4, non-overlapping red and purple dataset). This was the main gene set considered during the rest of the study (Fig. 4.4, Filtered gene set).

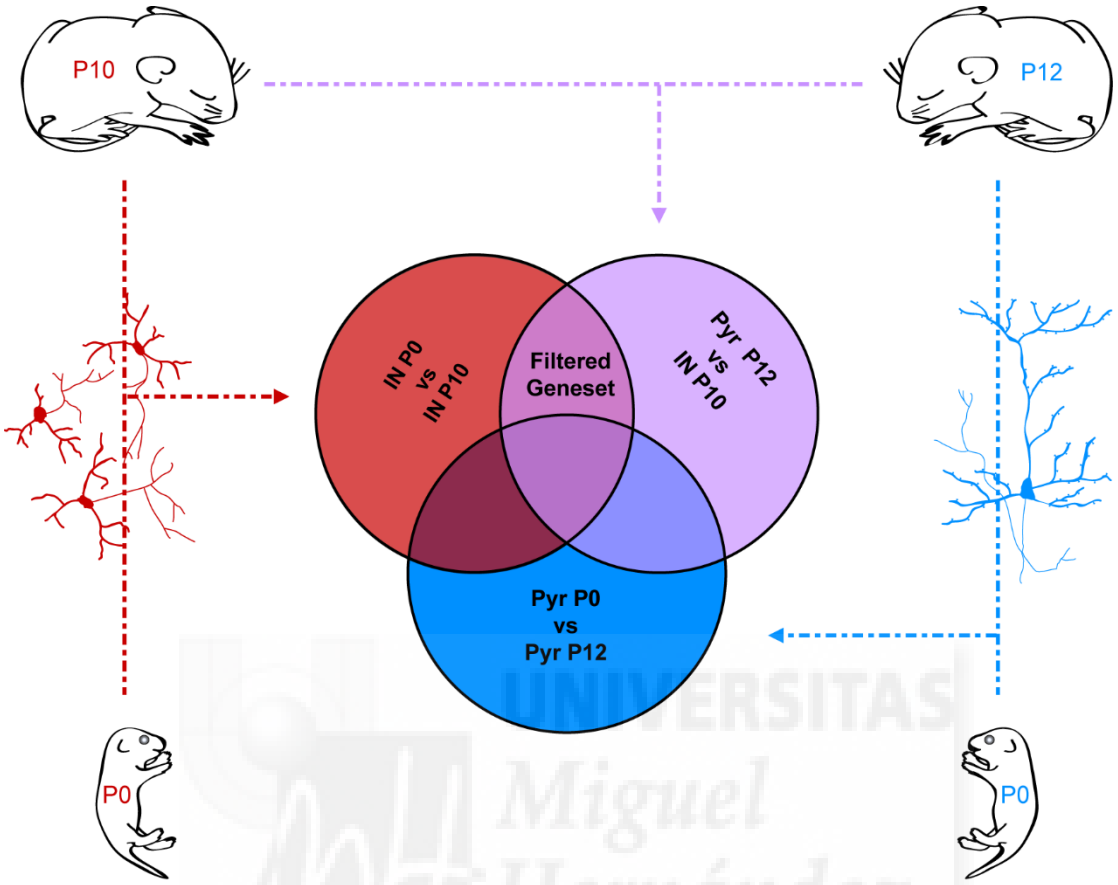

Figure 4.4. Bioinformatic comparisons of neuronal populations. First genes upregulated during GABAergic synaptogenesis (red gene set) were identified comparing the IN P0 and IN P10 experimental groups. Similarly, genes upregulated during glutamatergic synaptogenesis (blue gene set, Pyr P0 vs Pyr P12) were identified and subtracted from the first gene set. Finally, genes specifically expressed in interneurons during synaptogenesis (purple, Pyr P12 vs IN P10) were selected from the previous comparisons obtaining the final filtered gene set.

As a first control, we wanted to know whether the samples had a similar pattern of gene expression within the different experimental groups. The four conditions cluster together along the first two principal components as can be observed in the scatterplot (Fig. 4.5a). Moreover, clustering of samples uniquely based on the experimental condition discard any possible unintended cause of variability such as batch effects. We also tried to spot outlier samples comparing the signal intensity distributions of each microarray. All microarrays distributions had similar positions and widths and outliers were not detected (Fig. 4.5b).

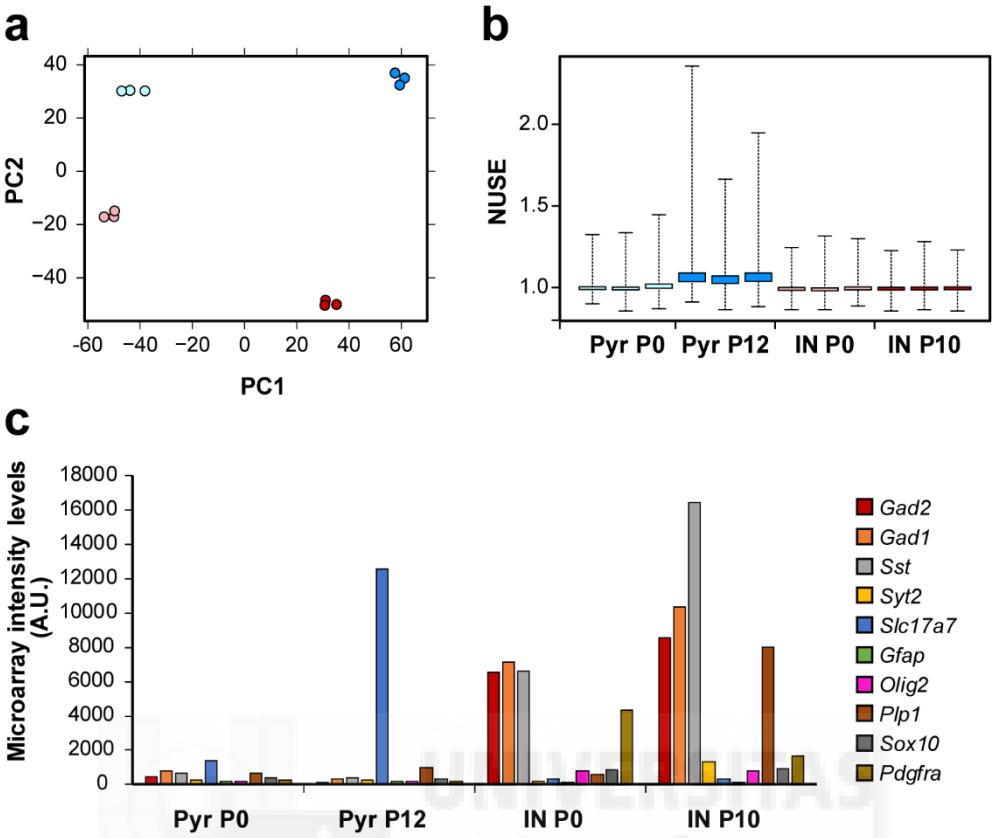

Figure 4.5. Quality control experiments for microarrays. (a) Scatterplot of the arrays along the first two principal components showing the distribution of the different microarray experiments. (b) Boxplot showing the individual probe error by normalizing the median values for each probe-set to 1 (NUSE: Normalized Unscaled Standard Error). Data are expressed as mean±s.e.m. (c) Microarray intensity levels of cell population specific markers [Interneurons: *Gad1* (GAD67), *Gad2* (GAD65), Sst and Syt2; pyramidal cells: *Slc17a7* (VGlut1); astrocytes: *Gfap*; oligodendrocytes: *Olig2*, *Plp1, Sox10, Pdgfra*] (U.A.: arbitrary units).

To assess the validity of the approach we selected genes known to be either cell type or synaptogenesis specific. Consistently, the transcript *VGlut1,* that was previously used to label Glutamatergic boutons, was specifically expressed in pyramidal cells and upregulated during synaptogenesis in these cells (Fig. 4.5c). Similarly, *Sst; Syt2; Gad65* and *Gad67* were expressed exclusively in interneurons and upregulated during GABAergic synaptogenesis (Fig. 4.5c). To test the possible contamination of non-neuronal cells we compared the levels of astrocytic, *GFAP,* and oligodendrocyte-specific, *Plp1* and *Olig2,* transcripts. Whereas *GFAP* and Olig2 did not show any expression in pyramidal cells or interneurons at any age, *Plp1* transcripts seem to be higher in the population of interneurons at P10. This could be explained by the presence of a small population of *Nkx2.1*-expressing oligodendrocytes produced postnatally (Nery *et al.*, 2001). Although this population had mostly disappeared by P10 (Kessaris *et al.*, 2006), there was still a reminiscent group of oligodendrocytes as it was also evidenced by the presence of *Pdgfra*. For this reason, we included an additional subtraction with a set of genes from the oligodendrocyte population at P10 (FACs sorted GFP+ cells from *Plp1-Cre;RCE* mice (Synapdomain database, Deogracias, Favuzzi, *et al.*, unpublished). Surprisingly, Plp1 was not among the subtracted genes and its levels in the mentioned *Plp1-Cre;RCE* line are close to zero. This may be due to the genetic modification introduced in the

mouse line but this has not been described before. Yet, the presence of other genes in this list proves that is a valid approach for identifying oligodendrocyte-specific genes.

The first and main comparison was aimed at identifying genes specifically upregulated during GABAergic synapse formation that were not expressed in Pyramidal cells at any of the tested stages (Table 4.1). A different manner of looking at the expression data of this selected population is quantifying the specificity of their expression in GABAergic interneurons at P10. In the table, the significance of the observed differences is expressed by the adjusted p-value (Q-value), the increase is expressed as fold change and specificity for IN P10 as tau (Table 4.1, See methods).

		INP0 vs INP10		INP10 vs PyrP12		
Genename	**Probeset**	**Q-value**	**Fold change**	**Q-value**	**Fold change**	**τ**
Tac1	10536363	0.044	17.900	0.039	61.607	0.971
Hapln1	10406519	0.044	27.553	0.039	15.673	0.954
Nek7	10358259	0.044	12.648	0.039	19.695	0.944
Rbp4	10467319	0.044	14.438	0.039	13.506	0.935
Crhbp	10411215	0.044	10.481	0.039	18.558	0.932
Lgals1	10425161	0.044	13.226	0.039	17.109	0.931
Akr1c18	10407435	0.044	7.571	0.039	18.970	0.919
Plp1	10601888	0.044	13.156	0.039	8.329	0.909
Pcp4l1	10360053	0.044	10.955	0.039	9.737	0.907
Th	10569370	0.044	8.353	0.039	8.551	0.882
Hpse	10531737	0.044	7.935	0.039	8.167	0.872
Steap2	10528008	0.044	5.150	0.039	7.226	0.856
Sparc	10386058	0.044	4.282	0.039	7.682	0.847
Sst	10438730	0.044	2.487	0.039	45.753	0.845
Ret	10547227	0.044	6.475	0.039	6.853	0.842
Igf1	10365559	0.044	4.006	0.039	9.341	0.841
Cnp	10381154	0.044	3.692	0.039	7.468	0.837
Gpx3	10376201	0.044	4.649	0.039	6.088	0.832
Gjd2	10485979	0.044	3.607	0.039	6.528	0.823
Syt2	10350077	0.044	6.159	0.039	5.317	0.823
Slc32a1	10478124	0.044	2.378	0.039	18.729	0.821
Nrsn2	10488617	0.044	6.333	0.039	3.761	0.814
Grin2d	10563421	0.044	3.223	0.039	7.047	0.812
Moxd1	10362186	0.044	3.790	0.039	5.691	0.811
Pdyn	10487613	0.044	5.898	0.039	4.309	0.810
Endod1	10590909	0.044	5.479	0.039	3.956	0.808
Mybpc1	10371627	0.044	5.144	0.039	4.897	0.803
Gpr83	10583286	0.044	5.038	0.039	4.653	0.799
Trmt2b	10606658	0.044	4.504	0.039	5.032	0.798
Zcchc12	10599187	0.044	2.612	0.039	8.489	0.798
Calb2	10581654	0.044	8.527	0.039	4.040	0.796
Nmbr	10361818	0.044	5.284	0.039	3.773	0.789
Oprd1	10516852	0.045	3.501	0.039	4.171	0.773

Pacsin2	10430997	0.044	4.949	0.039	3.109	0.769
Cnn2	10364593	0.044	3.602	0.039	4.961	0.766
Akr1b10	10537157	0.044	4.526	0.039	3.183	0.764
Adamts15	10591988	0.044	4.362	0.039	4.234	0.761
Ndrg2	10419578	0.045	2.510	0.039	7.708	0.759
Pnoc	10420853	0.044	3.341	0.039	5.230	0.758
Rassf4	10547177	0.044	3.435	0.039	5.002	0.758
Zfp804a	10473244	0.044	4.963	0.039	4.639	0.755
Lpl	10572130	0.044	16.734	0.039	2.390	0.750
Pdlim3	10571601	0.044	3.929	0.039	3.855	0.750
Mme	10492355	0.044	2.335	0.039	10.416	0.750
Cthrc1	10423836	0.044	3.551	0.039	3.857	0.747
Frmpd1	10504534	0.044	4.364	0.039	3.801	0.744
Alk	10452734	0.044	2.643	0.039	4.851	0.741
Sytl5	10598603	0.044	2.613	0.039	5.664	0.741
Sema5a	10423520	0.044	3.996	0.039	2.874	0.734
Filip1	10595298	0.044	4.430	0.039	2.740	0.729
Ptpre	10558410	0.044	3.456	0.039	3.307	0.728
Rnf128	10602009	0.044	4.885	0.039	2.470	0.726
Nnmt	10593219	0.044	3.796	0.039	3.562	0.724
Cplx1	10532180	0.044	4.292	0.039	2.718	0.723
Hap1	10391084	0.044	2.981	0.039	3.258	0.720
Ankrd29	10457536	0.044	3.376	0.039	3.274	0.719
Fam134b	10423333	0.044	4.010	0.039	2.596	0.719
Eya1	10353192	0.044	1.977	0.039	5.906	0.718
Vwc2	10374315	0.044	2.021	0.039	6.188	0.714
Pip5kl1	10471443	0.044	3.628	0.039	2.957	0.711
Igsf11	10435733	0.045	2.763	0.039	2.986	0.710
Ch25h	10467136	0.044	3.515	0.039	3.028	0.708
Adssl1	10398859	0.044	3.629	0.039	2.947	0.707
Ankrd34b	10406590	0.044	3.935	0.039	2.651	0.704
Cldn1	10438769	0.044	4.623	0.039	4.588	0.702
Egln3	10400304	0.044	2.301	0.039	6.583	0.701
Stac2	10390560	0.044	2.137	0.039	8.648	0.700
Adamts5	10440534	0.046	1.959	0.039	5.354	0.699
Btbd11	10365428	0.044	2.345	0.039	6.688	0.695
Arhgef6	10604713	0.044	2.447	0.039	4.205	0.694
Cd59a	10474229	0.045	3.261	0.039	2.887	0.694
Rab3b	10506883	0.044	2.805	0.039	3.261	0.693
Rcn1	10485645	0.044	3.935	0.039	2.581	0.692
Ptgs1	10471721	0.044	2.797	0.039	3.213	0.692
Gpr149	10498441	0.044	3.193	0.039	3.908	0.689
Klf3	10522051	0.044	2.136	0.039	6.698	0.685
Nacc2	10480901	0.044	2.290	0.039	3.502	0.685
Dmrt2	10462231	0.045	3.200	0.039	3.910	0.684

Pvt1	10424404	0.044	3.920	0.039	2.164	0.684
Ifit2	10462613	0.050	2.230	0.039	3.915	0.682
Thbs2	10447951	0.044	4.505	0.039	2.048	0.681
Ppif	10413222	0.044	2.884	0.039	3.283	0.681
Lypd6	10472034	0.044	2.586	0.039	3.589	0.680
Zim1	10559790	0.044	2.872	0.039	3.548	0.680
Flt3	10535780	0.044	3.764	0.039	2.261	0.675
Sfrp2	10492798	0.044	2.382	0.039	7.359	0.670
Grm1	10367830	0.044	2.394	0.039	3.162	0.666
Nefh	10383920	0.044	3.776	0.039	2.069	0.666
Id4	10404975	0.044	2.137	0.039	5.512	0.666
Kcnab1	10492402	0.044	8.561	0.039	2.133	0.665
Slc27a2	10475653	0.044	2.916	0.039	2.907	0.660
Aldh5a1	10408335	0.044	2.825	0.039	2.476	0.657
Doc2b	10388465	0.044	4.076	0.039	3.027	0.655
Alcam	10439895	0.044	3.266	0.039	2.335	0.651
Ndst3	10501924	0.044	5.214	0.039	2.368	0.645
Zfp385a	10433104	0.044	2.313	0.039	2.702	0.644
Myo5b	10456653	0.044	3.914	0.039	2.844	0.643
Phactr2	10367945	0.044	2.099	0.039	3.154	0.643
Ppapdc1a	10558049	0.044	2.180	0.039	3.363	0.642
Pgm2	10506188	0.044	2.049	0.039	2.787	0.640
Alox8	10387257	0.044	3.051	0.039	2.397	0.638
Rragb	10602692	0.044	3.048	0.039	2.288	0.636
Optn	10479833	0.044	3.082	0.039	2.670	0.634
Btn2a2	10408185	0.044	2.898	0.039	2.533	0.631
Adamts6	10406982	0.044	2.278	0.039	3.575	0.630
Drd2	10585169	0.044	2.433	0.039	3.023	0.628
Fa2h	10581824	0.044	2.498	0.039	2.782	0.627
Sema3c	10519886	0.045	3.229	0.039	2.020	0.619
Chrna2	10416071	0.045	2.605	0.039	2.591	0.619
Plch1	10498448	0.044	2.573	0.039	2.034	0.617
Crh	10497417	0.045	2.852	0.039	2.282	0.616
Pygb	10476969	0.044	3.053	0.039	2.589	0.616
Pdxk	10370497	0.044	2.423	0.039	2.046	0.615
Htr1d	10509238	0.044	2.567	0.039	2.414	0.608
Tmhs	10443383	0.044	2.706	0.039	2.633	0.606
Prdx3	10468869	0.046	2.663	0.039	2.242	0.604
Fam101b	10388488	0.044	2.716	0.039	2.010	0.603
Gys1	10552945	0.045	2.475	0.039	2.566	0.598
Acaa2	10456699	0.044	2.991	0.039	3.493	0.598
Kcnh2	10528548	0.044	2.146	0.039	2.885	0.591
Wif1	10366653	0.044	2.383	0.039	2.409	0.591
Dgkk	10598251	0.044	2.690	0.039	2.102	0.585
Tac2	10367024	0.048	2.440	0.039	2.167	0.582

Uprt	10601328	0.045	2.548	0.039	2.196	0.581
Acadl	10355246	0.044	2.529	0.039	2.074	0.579
Lypd6b	10472022	0.044	2.051	0.039	2.565	0.575
Shisa9	10433618	0.044	2.862	0.039	2.002	0.572
Fam195a	10449142	0.044	2.441	0.039	2.006	0.562
Prss23	10565456	0.044	2.218	0.039	2.168	0.561
Gm98	10465916	0.047	2.026	0.039	2.362	0.559
Tacr1	10539244	0.044	2.092	0.039	2.440	0.558
C330016O10Rik	10385709	0.044	2.013	0.039	2.702	0.555
Rerg	10548899	0.044	2.217	0.039	2.989	0.554
Arhgap18	10362294	0.044	2.450	0.039	2.242	0.554
Baiap3	10448878	0.044	2.056	0.039	2.354	0.552
Fam150b	10395136	0.045	1.980	0.039	2.095	0.528
Fam43a	10434932	0.045	2.030	0.039	2.065	0.519
Hpcal1	10394778	0.045	2.052	0.039	2.531	0.511
Timp3	10365482	0.044	2.732	0.039	3.302	0.509
Rgag1	10602196	0.044	2.185	0.039	2.747	0.107

Table 4.1. Genes differentially and specifically upregulated during GABAergic synapse formation. List of 140 genes upregulated during GABAergic synaptogenesis [Pairwise comparison IN P0 vs IN P10 using Significance analysis of microarrays (SAM), selecting genes with a false discovery rate (FDR) <0.05 and fold change higher than 2] and specifically expressed in interneurons (Pairwise comparison Pyr P12 vs IN P10 with the same previous criteria). In the table are reported gene name (official symbol), microarray probeset number, q-value (adjusted p-value) and fold change for both comparisons; and specificity ratio for IN P10 (τ). Genes are sorted according to τ.

It is important to mention that although our experimental design has provided a list enriched in synaptogenic genes, we could not exclude that some genes involved in other processes occurring in neurons between P0 and P10/P12 were also picked up. We focused on genes upregulated based on the rationale that those genes involved in synapse formation should be increasing their expression to play a function. Conversely, downregulated genes were excluded in our analysis, since it is not so straightforward to link them with a negative regulation of the process. For example, many of these genes may be mediating cellular and molecular processes that are taking place around P0 and not at the stage of synapse formation and, for this reason, they are downregulated at P10/P12.

Statistical significance for differential expression between the samples was measured with the statistical technique “Significance analysis of microarrays” (SAM) (Tusher *et al.*, 2001; Zhang, 2007). Since many studies use the algorithm Limma instead of SAM for microarray comparisons, we additionally carried out this analysis (Phipson *et al.*, 2016; Ritchie *et al.*, 2015), to examine whether other different genes were selected by this alternative method. Although we found a small difference in the fold change that consequently modified slightly the gene order in the list, all genes found in SAM appeared also in Limma. Previous studies have also shown that both are very robust methods and it is difficult to determine which one is better for a given experiment (Chrominski and Tkacz, 2015). Given these minimal differences, just the data resulting from SAM analysis are shown for brevity.

4.5. Microarray analysis: Similar to ErbB4

Even though most of the described genes involved in synaptogenesis increase their levels along postnatal development, there are some exceptions to this rule where levels remain unchanged. ErbB4

is one of the most characteristic examples (Fazzari *et al.*, 2010; Del Pino *et al.*, 2013, 2017; Yau *et al.*, 2003). Its involvement in interneuron migration and synaptogenesis keeps its levels relatively constant at the onset of synaptogenesis.

To identify other putative synaptogenic genes following this profile, we selected those with a specific expression in interneurons, i.e. fold change higher than 2 when comparing IN P10 and Pyr P12. This list was further filtered selecting just those genes that were not changing considerably between P0 and P10 in interneurons. 223 genes were identified following these criteria. We illustrate in Table 4.2 the genes with fold change higher than 4. Although this list can contain genes involved in synaptogenesis, only genes upregulated during synaptogenesis (Table I) were investigated due to their higher probability to function as synaptogenetic genes.

		Pyr P12 vs IN P10				Pyr P12 vs IN P10	
Genename	**Probeset**	**Q-value**	**Fold change**	**Genename**	**Probeset**	**Q-value**	**Fold change**
Erbb4	10355278	0.039	65.237	**Prkcq**	10469255	0.039	6.537
Gad2	10469672	0.039	59.775	**Stk32b**	10529636	0.039	6.478
Nxph1		0.039	53.256	**Elfn1**	10526968	0.039	6.314
Gad1	10472707	0.039	29.764	**Slc44a5**	10496975	0.039	6.303
Dusp10	10352448	0.039	15.649	**Pde5a**	10495794	0.039	5.799
Rpp25	10585703	0.039	15.182	**Ablim3**	10459262	0.039	5.765
Npy	10538247	0.039	14.938	**Tox3**	10580522	0.039	5.653
Reln	10528385	0.039	13.809	**AY172335.25**		0.039	5.553
Sox6	10567108	0.039	13.397	**4930431L04Rik**	10578796	0.039	5.183
Zfp536	10562532	0.039	12.252	**Olig1**	10436828	0.039	5.156
Ptprz1	10536667	0.039	10.873	**Ugt8a**	10501963	0.039	5.151
Erbb2ip	10411853	0.039	9.726	**Mfsd2a**	10516064	0.039	5.039
Dlx6	10536353	0.039	9.319	**Qk**	10447708	0.039	4.994
Cacna2d2	10588592	0.039	8.432	**Dgkg**	10438639	0.039	4.960
Kcnmb2	10491319	0.039	8.421	**Plekhh2**	10447190	0.039	4.745
Tmem132c	10525932	0.039	8.420	**D230039L06Rik**	10352143	0.039	4.687
St8sia4	10356880	0.039	8.101	**Tbc1d4**	10422028	0.039	4.536
Ubash3b	10592515	0.039	7.371	**Col19a1**	10353574	0.039	4.515
Afap1	10521440	0.039	6.977	**Scrg1**	10571865	0.039	4.478
Klhl13	10603896	0.039	6.954	**Olig2**	10436823	0.039	4.443
Pcdh18	10498018	0.039	6.831	**Timp4**	10547022	0.039	4.400
Bcan	10499285	0.039	6.716	**Lancl3**	10598575	0.039	4.337
Ank1	10570894	0.039	6.656	**Tmem176b**	10544596	0.039	4.277
AY172335.10	10598041	0.039	6.614	**Itpr2**	10549282	0.039	4.151
Klhl14	10457787	0.039	6.599				

Table 4.2. Genes specifically expressed in interneurons with similar levels between P0 and P10. List of 50 genes specifically expressed in interneurons (Pairwise comparison IN P0 vs Pyr P12 using SAM, selecting genes with an FDR <0.05 and fold change higher than 2) that keep constant their levels between P0 and P10 (|Fold change|>1.5). In the table are reported gene name (official symbol), microarray probeset number, q-value (adjusted p-value) and fold change between PyrP12 and INP10. Genes are sorted by fold change.

4.6. Microarray list data analysis: Gene Ontology and Enzymatic pathways

Once the individual genes upregulated during GABAergic synaptogenesis were identified, we decided to go beyond and analyse in a broader manner what molecular and cellular processes may be taking place during the formation of these synapses. To do so, we compared the main filtered gene list with the bioinformatic databases Gene Ontology (GO), KEGG and Reactome (Ashburner *et al.*, 2000; Fabregat *et al.*, 2016; Kanehisa *et al.*, 2017). These databases classify genes into groups according to the available literature, which will give us information about the most representative molecular and cellular processes present in our data.

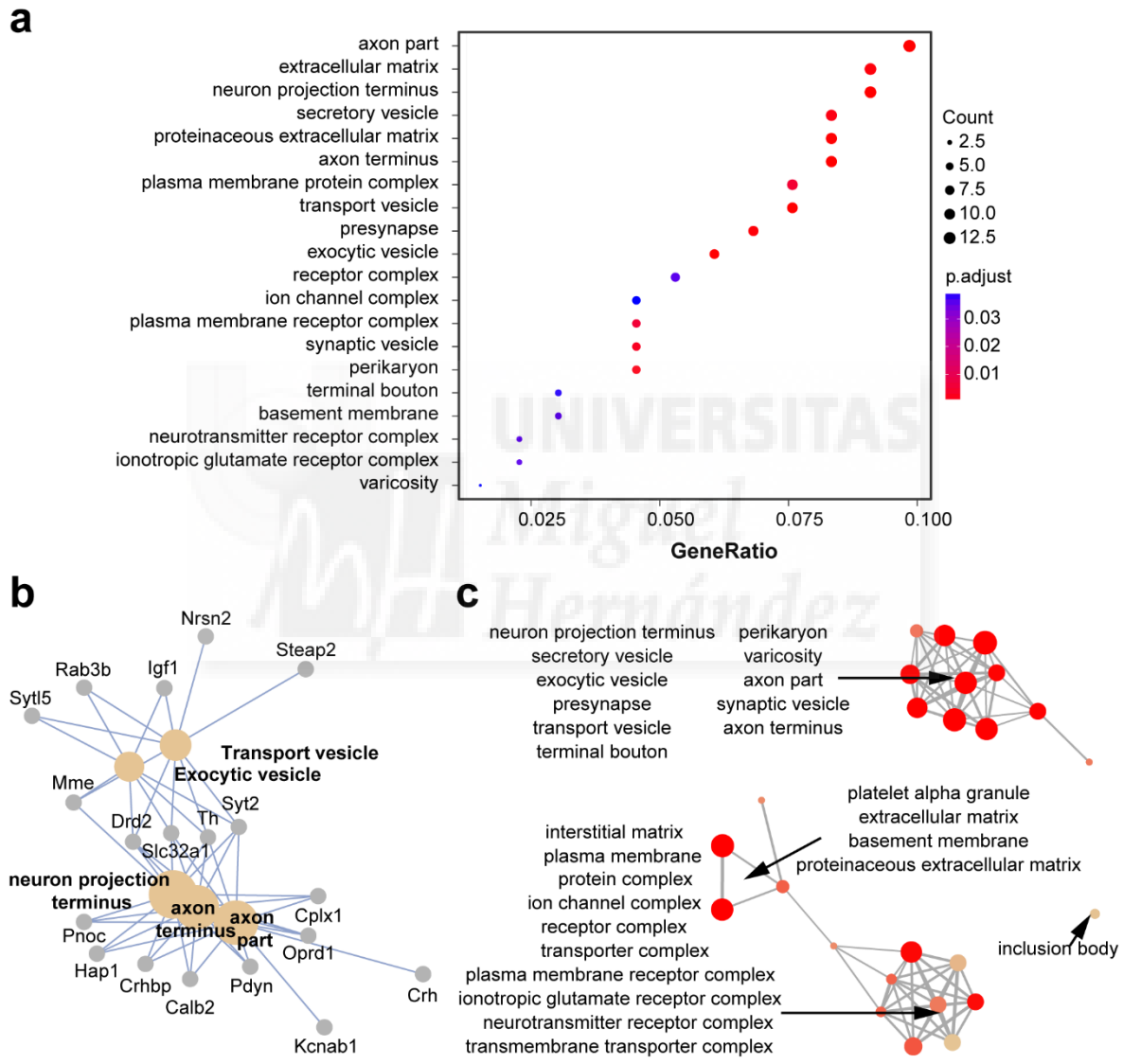

Figure 4.6. Cellular component domain of the GO analysis. (a) Ratio of genes from the filtered gene set belonging to the most representative categories of the cellular component domain. (b) Plot "function of gene concept net" showing the main genes that belong to the most representative categories and how these genes (legend from figure 4.6) are shared by different categories. (c) Enrichment map showing how different categories cluster together by the shared genes.

4.6.1. Gene ontology cellular compartment

Using the R package clusterProfiler (Yu *et al.*, 2012) we focused on the 20 most represented cellular compartments where the genes were allocated according to GO. The most represented compartments, axon part and extracellular matrix, can be used to cluster the rest of compartments in two main broader classes (Fig. 4.6a and c, Upper and lower clusters). These two classes were related because they shared some of the genes (Fig. 4.6b).

The first cluster was related to axon and secretion, which contained axon terminus, neuron projection terminus or axon part categories (Fig. 4.6c, upper cluster). Related to this, we also found gene sets associated with the synapse: presynapse, terminal bouton and synaptic vesicle (Fig. 4.6c, upper cluster). Finally, several groups included vesicles related processes: synaptic vesicle, transport vesicle, secretory vesicle and synaptic vesicle (Fig. 4.6b, c). The second cluster was related to extracellular matrix and cell membrane coding genes. Interestingly, in this cluster we found genes present in membrane transport, receptors and ion channel complexes (Fig. 4.6b, c). Consistent with our experimental design, the two main clusters contained gene sets that participate in cellular and molecular events required during the wiring of the neural circuits. This includes axonal and synapse development as well as genes that may influence the targeting and remodelling of these inputs.

4.6.2. Gene ontology Biological process

GO provides the possibility of classifying genes according to the biological process they are involved on. We found three main classes of processes among the 20 most represented ontological groups (Fig. 4.7a).

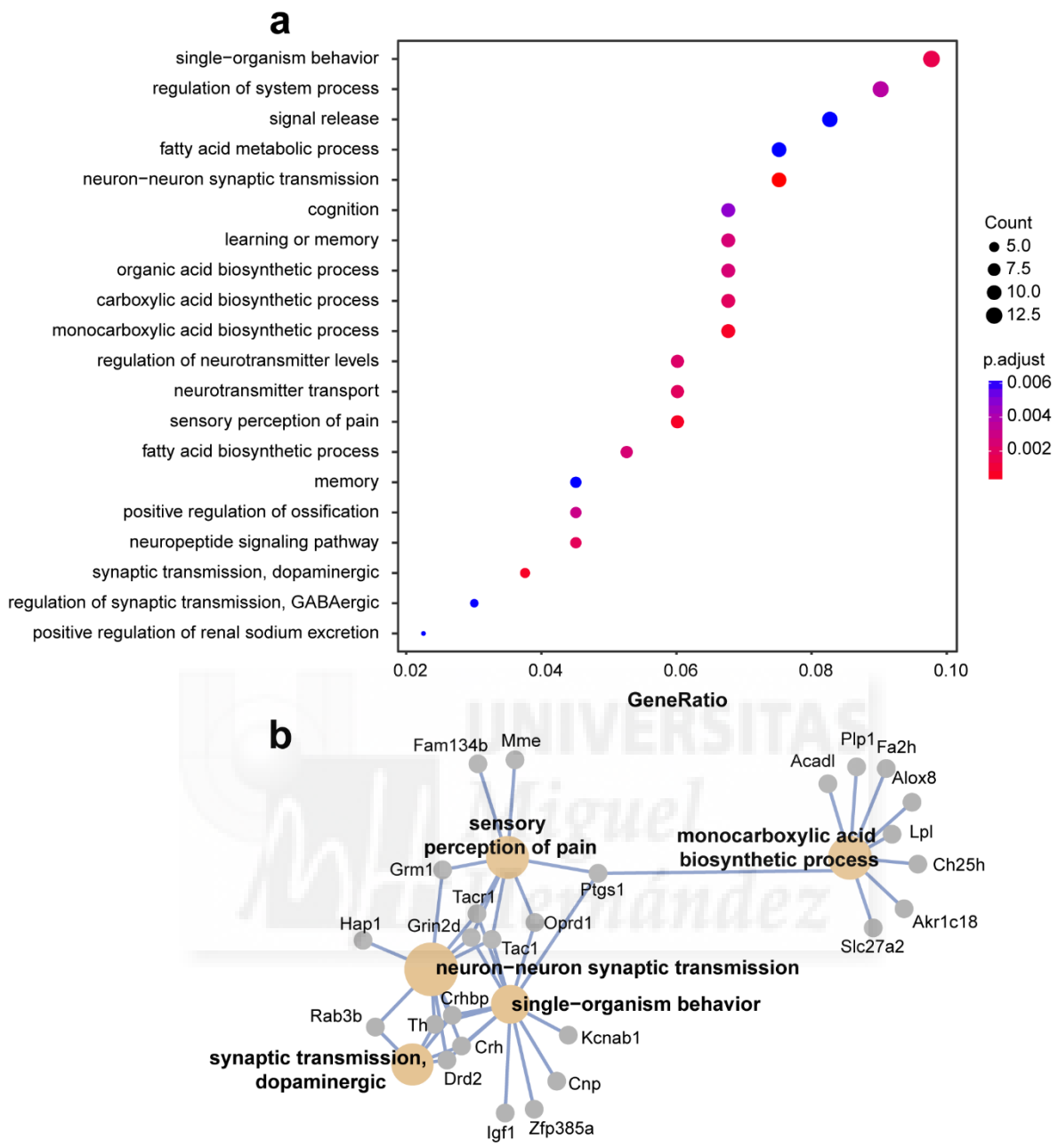

Figure 4.7. Biological process domain of the GO analysis. (a) Ratio of genes from the filtered gene set belonging to the most representative categories of the biological process domain. (b) Plot "function of gene concept net" showing the main genes that belong to the most representative categories and how these genes are shared by different categories.

Many of the genes were related to cognitive brain function as represented by the categories behaviour, cognition, learning, memory and sensory perception of pain (Fig.4.7b). Related to this, many other categories were linked to neurotransmission: neuropeptide signalling, GABAergic and DOPAminergic transmission or neurotransmitter level regulation (Fig.4.7a, b). In a completely different sphere, many of the genes were related to generic metabolic processes like fatty or monocarboxylic acid synthesis (Fig.4.7, top).

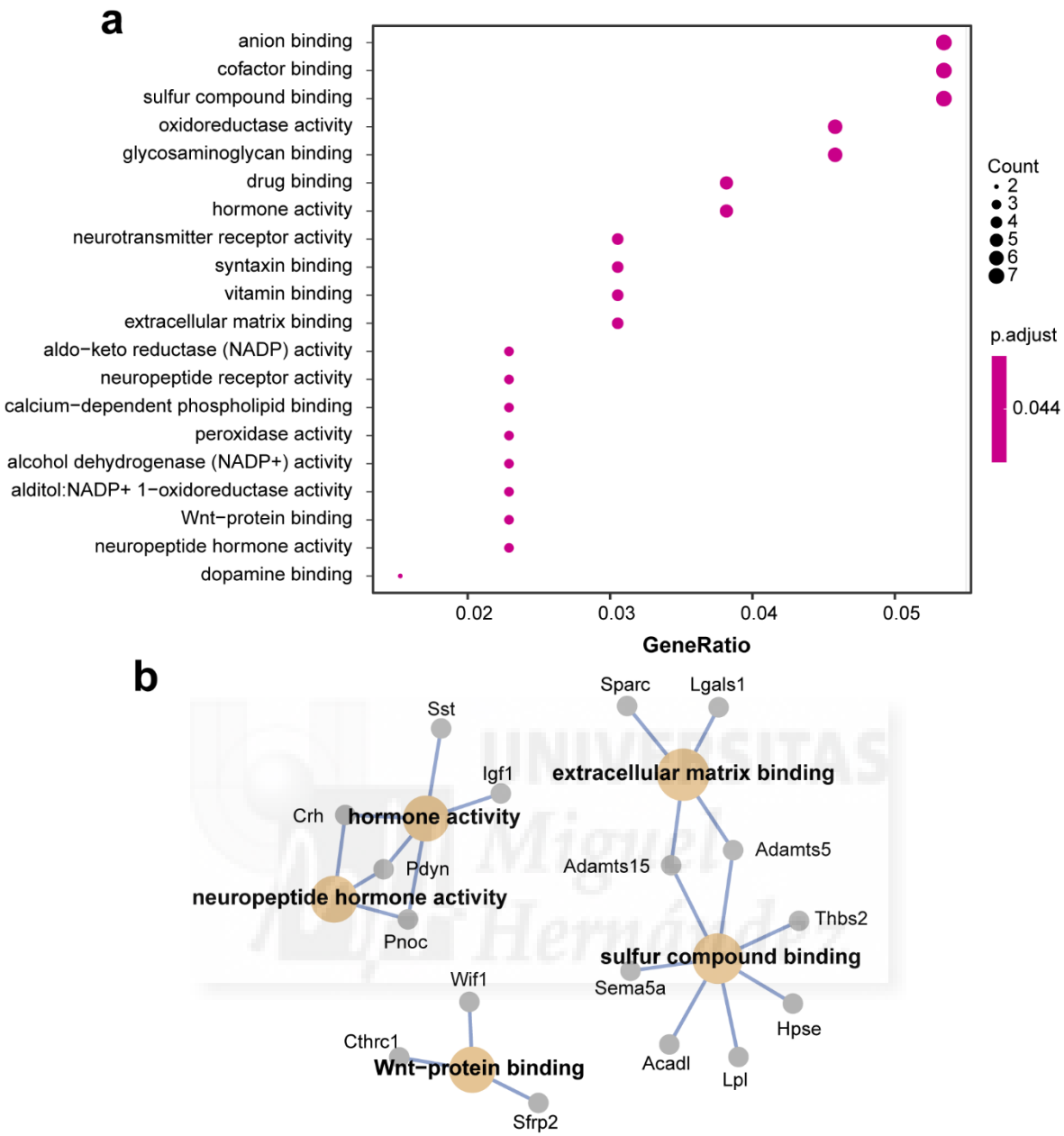

Figure 4.8. Molecular function domain of the GO analysis. (a) Ratio of genes from the filtered gene set belonging to the most representative categories of the molecular function domain. (b) Plot "function of gene concept net" showing the main genes that belong to the most representative categories and how these genes are shared by different categories.

4.6.3. Gene Ontology Molecular function

The last classification that GO project provides is by gene molecular function. Notably, the significance of none of the generated groups was far from the established threshold (Adj. p value>0.043), yet, some of the processes may be of interest. We found genes binding to anions, drugs or sulphur compounds (Fig.4.8a, b). We could also find again in this classification neuropeptides and hormone activity (Fig.4.8a, b). Interestingly, there were 3 genes in the list known to be binding to Wnt protein (Fig.4.8b, lower cluster), a family of proteins that has repeatedly been linked to synapse formation.

4.6.4. Molecular pathways

Different sets of databases are more focused in biochemically defined signalling pathways than GO. These databases can be of particular interest because they can unveil sets of genes that are upregulated during synaptogenesis as part of a whole signalling pathway. We used KEGG and Reactome projects using also Cluster Profiler algorithm. In KEGG, just two categories were found: neuroactive ligand-receptor interaction and cocaine addiction (Fig.4.9a). The first category is quite broad and includes many different pathways: dopamine (Drd2), serotonin (Htr1d), bombesin (Nmbr), opioids (Oprd1), substance P (Tacr1 and Tac1), glutamate receptors (metabotropic Grm1 and ionotropic Grin2d), N-acetylaspartyl-glutamate (Grin2d) and acetylcholine (Chrna2) (Fig. 4.9a).

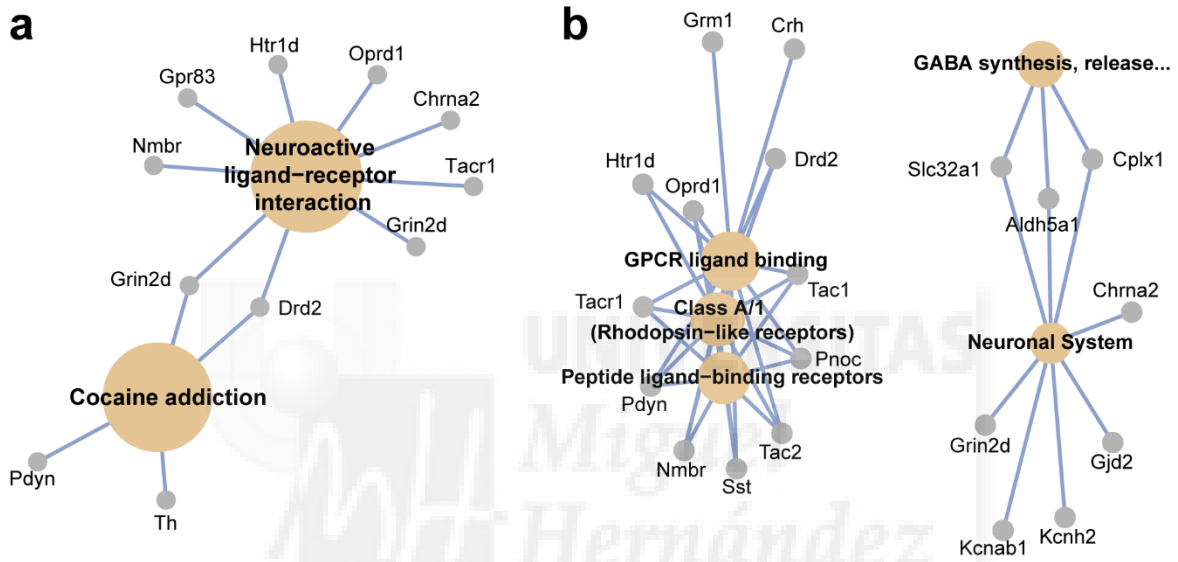

Figure 4.9. Signalling pathways analysis: KEGG and Reactome. (a) Plot "function of gene concept net" showing the main genes that belong to the most representative signalling pathways and how these genes are shared by different pathways in KEGG database. (b) Same as in (a) from Reactome database.

Finally, a pathway search using Reactome database (Fabregat *et al.*, 2016) gave also interesting gene sets that confirmed some of the categories identified in previous analysis. 10 of the genes were related to G coupled receptors (Grm1, Drd2 etc.; Fig.4.9b, right) as previously described with KEGG. A representative proportion of the genes were linked to peptide receptors: SST, Tac1 and 2, Nmbr, Pdyn and Pnoc. As expected some genes were related to GABA synthesis, release, reuptake and degradation (Fig.4.9b, top right cluster).

4.7. Microarray selection criteria

The first 30 genes were selected based on their higher specificity ratio (τ) which can be defined as the normalized mean expression within the population of interneurons at P10 compared with the maximum expression across other populations as described before (Kryuchkova-Mostacci and Robinson-Rechavi, 2017, see methods) (Table 4.3). More information was gathered to further filter and rank the list. This ranking was done based on different criteria that gave information about the feasibility for a particular gene to play a role in synapse formation.

Genename	τ	IN P10 Levels	Cellular pattern	Density (cells/mm^2)	Spec. Score	Level Score	Density Score	Total score
Nek7	0.94	3047.82	Scattered	164.08	28	22	29	79
Tac1	0.97	3902.33	Scattered	53.90	30	25	23	78
Sst	0.84	16419.43	Scattered	101.95	17	30	27	74
Lgals1	0.93	4254.69	Scattered	50.59	25	27	22	74
Rbp4	0.94	2761.47	Scattered	72.12	27	19	24	70
Slc32a1	0.82	4555.26	Scattered	274.81	10	28	30	68
Crhbp	0.93	2411.22	Scattered	46.12	26	17	20	63
Hapln1	0.95	2270.89	Scattered	41.31	29	16	18	63
Gjd2	0.82	3517.64	Scattered	76.10	12	23	26	61
Plp1	0.91	8002.17	Glial	0.00	23	29	7	59
Syt2	0.82	1292.30	Scattered	135.47	11	9	28	48
Akr1c18	0.92	1595.47	Scattered	12.13	24	12	11	47
Sparc	0.85	3747.90	Not detectable	0.00	18	24	5	47
Endod1	0.81	2912.80	Scattered	49.95	5	20	21	46
Igf1	0.84	2039.47	Scattered	16.64	15	15	12	42
Th	0.88	1519.10	Scattered	6.11	21	11	10	42
Grin2d	0.81	4143.18	Not detectable	0.00	8	26	6	40
Ret	0.84	1340.94	Scattered	22.70	16	10	13	39
Pcp4l1	0.91	1790.30	Pyramidal	0.00	22	13	2	37
Hpse	0.87	677.95	Scattered	23.06	20	1	14	35
Cnp	0.84	2741.15	Scatt. and glial	0.00	14	18	3	35
Nrsn2	0.81	3012.67	Pyramidal	0.00	9	21	4	34
Mybpc1	0.80	786.27	Scattered	72.55	4	3	25	32
Pdyn	0.81	974.86	Scattered	45.74	6	6	19	31
Zcchc12	0.80	2011.76	Scattered	30.43	1	14	16	31
Gpx3	0.83	1282.87	Scattered	4.63	13	8	9	30
Moxd1	0.81	968.09	Scattered	25.16	7	5	15	27
Steap2	0.86	1104.65	Not detectable	0.00	19	7	1	27
Gpr83	0.80	929.04	Scattered	36.52	3	4	17	24
Trmt2b	0.80	737.51	Not detectable	0.00	2	2	8	12

Table 4.3. Gene ranking for unbiased selection. List of the 30 most specific genes for GABAergic synaptogenesis (higher τ) from table 4.1. The table displays τ, intensity levels in IN P10 condition, expression pattern and density in Allen Brain Atlas, scores assigned for these three variables and total score. Scores were calculated by assigning points from 30-1 from the highest to the lowest value of the three variables separately. The scores were summed and the list is sorted by the total score.

The two criteria added to the selectivity ratio were related to the amount of transcript present in interneurons. High transcription levels in the present screening can be due to high levels in individual cells or to the presence of the mRNA in a high proportion of the isolated cells. Given the numerous synapses that are being formed at this stage of development we expected the level of proteins involved in synaptogenesis to be high compared with genes mediating other somatic processes occurring in parallel. We used then as first criteria the expression levels in interneurons at P10 (Table 4.3).

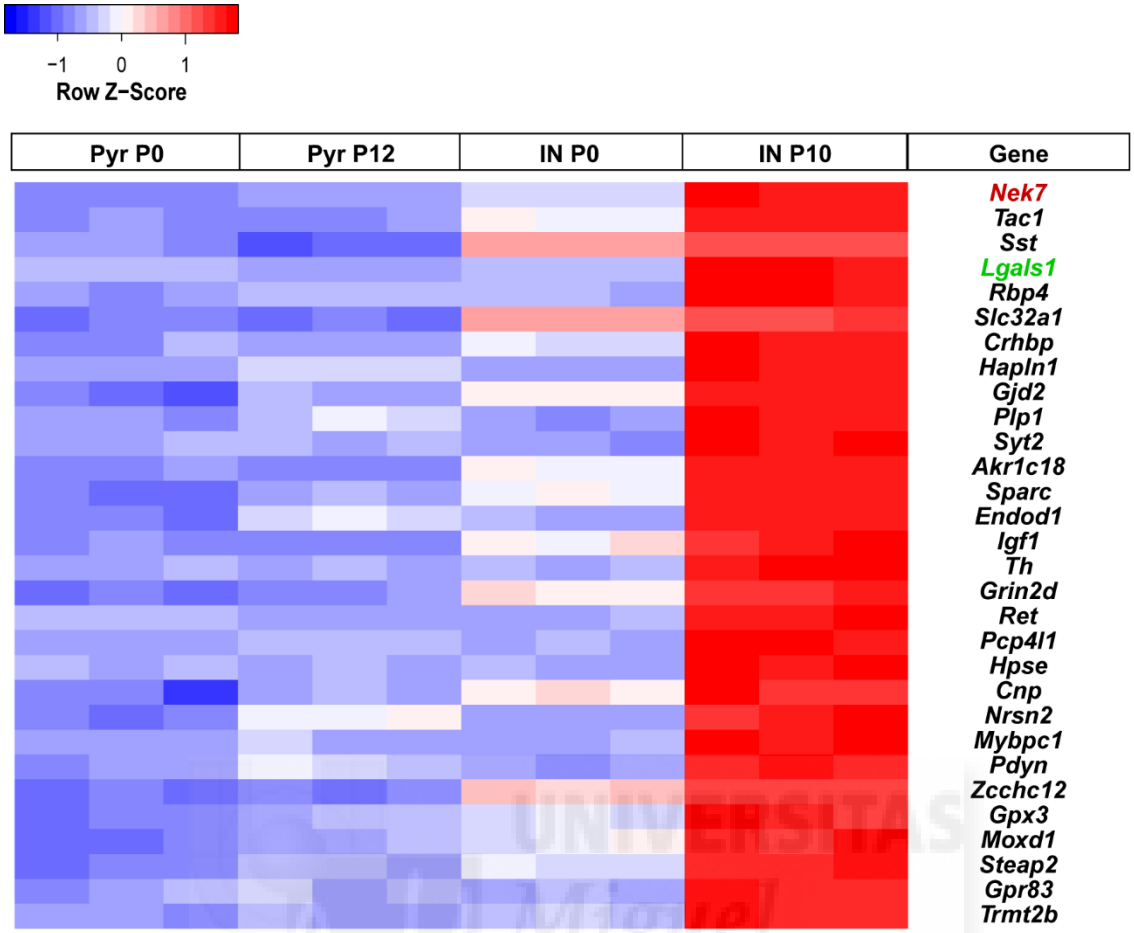

Figure 4.10. Heatmap of the main ranked genes. Expression levels of the 30 first ranked genes according to specificity and expression levels in IN P10 and estimation of cell density in Allen Brain Atlas (Row Z-score: standard deviation from each gene mean intensity values). The selected genes for analysis are marked in red (*Nek7*) and green (*Lgals1*).

However, this parameter did not provide information about the number of cells that was expressing the gene. We hypothesised that a generic molecular mechanism for GABAergic synapse formation would require that a large proportion of interneurons expressed the protein. To assess this, as third criteria, we searched available *in situ* hybridization data in Allen Brain Atlas database (Lein *et al.*, 2007). Only genes expressed in a scattered population of neurons in the cortex, which resembles the interneuron pattern, were considered and cell density was examined (Table 4.3, See Methods). It is worth mentioning that most of the information obtained from the Allen Brain Atlas was from adult brains, and the pattern of expression could be different during synaptogenesis. Yet, this approach was a good proxy to know how many cells are capable of expressing the protein since many synaptogenic proteins continue their expression during adulthood (Garner *et al.*, 2006).

Following these criteria, the genes were finally ranked and the first genes in the list were *Nek7, Tac-1, SST* and *Lgals1* (Table 4.3, Fig. 4.10). We selected *Nek7* and *Lgals1* for further investigations, and excluded the neuropeptides *Tac-1* and *SST* from our analysis because they were most likely playing a role in neurotransmission rather than in the formation of synapses (Table 4.3, Fig. 4.10).

RESULTS

5. Role of the kinase Nek7 in parvalbumin interneuron synapse formation and neurite morphology

5.1. Introduction

NIMA (never in mitosis A)-related kinases (Neks) are a family of serine/threonine kinases first discovered in *Aspergillus nidulans* (Morris, 1976; O'Connell *et al.*, 2003). 11 members of the family, NEK1 to 11, have been described in humans. While Nek2, Nek6, Nek7 and Nek9 are known to contribute to the formation of the microtubule based mitotic spindle; Nek1, Nek10 and Nek11 contribute to the DNA damage response (Fry *et al.*, 2012). Altogether, this provides Neks with key roles in mitotic entry, cytokinesis and cell cycle checkpoints. Moreover, additional roles have been described for some members of the family including Nek7 in the context of microtubules formation during interphase (Fry *et al.*, 2012; Quarmby and Mahjoub, 2005). For this reason, it is hypothethised that Neks may have evolved to mediate microtubule-dependent processes in both dividing and non-dividing cells. During cell division, the mitotic spindle is formed by a microtubule network that extends in the whole volume of the cell and it is organized from the centrosomes positioned at opposite extremes of the cell during cytokinesis. Nek7 has been described to be located at the centrosome and at the mitotic spindle (Kim *et al.*, 2007; Yissachar *et al.*, 2006). Its depletion causes cytokinesis failure due to fragile and multipolar mitotic spindles, which leads to the presence of multiple centrosomes and nuclei in the cell (Kim *et al.*, 2007; O'Regan and Fry, 2009; Salem *et al.*, 2010; Yissachar *et al.*, 2006). Consequently, cells are often arrested in mitosis and undergo apoptosis while chromosomes lag in their way to the poles causing tetraploidy and aneuploidy (O'Regan and Fry, 2009; Salem *et al.*, 2010). Furthermore, Nek7 is thought to regulate the microtubule nucleation activity of the centrosome as the decrease in γ-tubulin localized to this structure in Nek7 knockdown suggests.

During interphase, analogous functions of Nek7 have been described. Depletion of Nek7 reduces the accumulation of pericentriolar proteins around the centrioles, the microtubule structures that form the centrosome (Kim *et al.*, 2011). Moreover, ectopic expression of a Nek7 form that is directed to the centrosome produces extra centrioles (Kim *et al.*, 2011). Therefore, the function of Nek7 in the centrosome, the microtubule organizer centre of the cell, is observed in both, dividing as well as non-dividing cells. Beyond the centrosome, Nek7 accelerates microtubule instability in HELA cells and fibroblasts (Cohen *et al.*, 2013).

Microtubules exist in either polymerization or depolymerisation states, namely growth or shrinkage, but never reaches a steady-state length (Conde and Cáceres, 2009). This state is called dynamic instability and Nek7 downregulation decreases the growth and shrinkage rates (Cohen *et al.*, 2013). Interestingly, precise microtubule dynamics are key for the accurate formation of the mitotic spindle and structures like the cilium (Cohen *et al.*, 2013). It has been shown that Neks coevolved with centrioles and both can function as microtubule organizing centres and at the basal body of cilia (Quarmby and Mahjoub, 2005). Nek1, Nek7 and Nek8 are known to be involved in primary cilium formation through the control of microtubule dynamics (Shalom *et al.*, 2008). As described in cilia, microtubules are cytoskeletal components essential for the structure of axons and dendrites. Thus, it is appealing to hypothesise that Neks family could also play a role in the regulation of microtubule dynamics in neurons. It is worth mentioning that Nek3 is expressed in post-mitotic neurons and the mutation of its catalytic domain alters neuronal morphology including neuronal polarity and axon number (Chang *et al.*, 2009).

Nek7 is formed by a conserved C-terminal catalytic domain and a non-conserved disordered N-terminal regulator domain that is crucial to mediate the kinase interactions (de Souza *et al.*, 2014). It shares 76% sequence similarity with Nek6, its closest relative, which is also activated in mitosis and localises to the mitotic spindle (O'Regan and Fry, 2009). In addition, they both complex and increase their activity by their interaction with Nek9 (Haq *et al.*, 2015). Nek6 phosphorylates the kinesin Eg5 and, given their similarity, Nek7 is thought to do it as well (Rapley *et al.*, 2008). Interestingly, axons with depleted Eg5 grow longer and display more branches (Myers and Baas, 2007). In conclusion, Nek7 might be mediating the growth of the axon through Eg5.

What are the molecules upstream or downstream of Nek7? Nek7 interactome was obtained by both yeast two-hybrid and immunoprecipitation followed by mass spectrometry (de Souza *et al.*, 2014). RGS2, CC2D1A, TUBB2B, MNAT1, and Nek9 were found to interact and be substrates of Nek7. RGS2, TUBB2B, MNAT1, Nek9 and PLEKHA8 even localizes with Nek7 during the cell cycle (de Souza *et al.*, 2014). Intriguingly, Nek7 and Nek6 do not share common interactors, except Nek9. This, together with their different patterns of expression (Feige and Motro, 2002), suggests that they have different regulatory and functional properties (Minoguchi *et al.*, 2003; de Souza *et al.*, 2014). Depletion of the interactor RGS2 leads to similar mitotic phenotypes than Nek7, including reduced γ-tubulin in centrosomes (de Souza *et al.*, 2014). Thus, Nek7 and RGS2 may act cooperatively to ensure proper mitotic spindle organization.

Nek9 interacts with Nek7 and is activated during mitosis at centrosomes (Bertran *et al.*, 2011; de Souza *et al.*, 2014). Nek7 has an autoinhibited conformation where a tyrosine side chain blocks the active site (Richards *et al.*, 2009). Binding of Nek9 is needed for Nek7 activation which is thought to happen through Nek7 dimerization (Haq *et al.*, 2015).

The only known role of Nek7 in the brain to date is the variation of its levels after (LTP) protocols. Nek7 levels in dentate gyrus decreases after perforant path stimulation (Li *et al.*, 2014).

The involvement of Nek7 in the formation of microtubule-based structures together with its function in the regulation of microtubule dynamics suggest that Nek7 may be a good candidate to regulate different aspects of neuronal differentiation, including neurite development and synapse formation. Consistent with this, our screening pointed out Nek7 as a potential candidate to play a role in the early wiring of GABAergic circuitries.

5.2. Developmental time course of Nek7 expression

To confirm and validate the relative transcript levels obtained in the microarray experiments we carried out qPCR with specific primers for Nek7. We performed a new round of sorting experiments to isolate pyramidal cells and interneurons using the same conditions than before for microarray analysis (See section 4.3 and Material and methods). Consistent to our microarray data, qPCR results confirmed that interneurons expressed substantially more Nek7 than pyramidal cells (Fold change 22.02±4.56; Fig. 5.1a). Moreover, there was a prominent fold change increase in interneurons compared to pyramidal cells (12.03±1.29 versus 1.93±0.37; Fig. 5.1a) that correlated to the increment observed in synapse formation (Fig. 5.1a and Fig. 4.1). In all the comparisons, fold changes are similar between microarray and qPCR (Fig. 5.1a). Thus, we can conclude that transcript levels measured in the microarray faithfully reflect expression levels of Nek7 in cortical neurons.

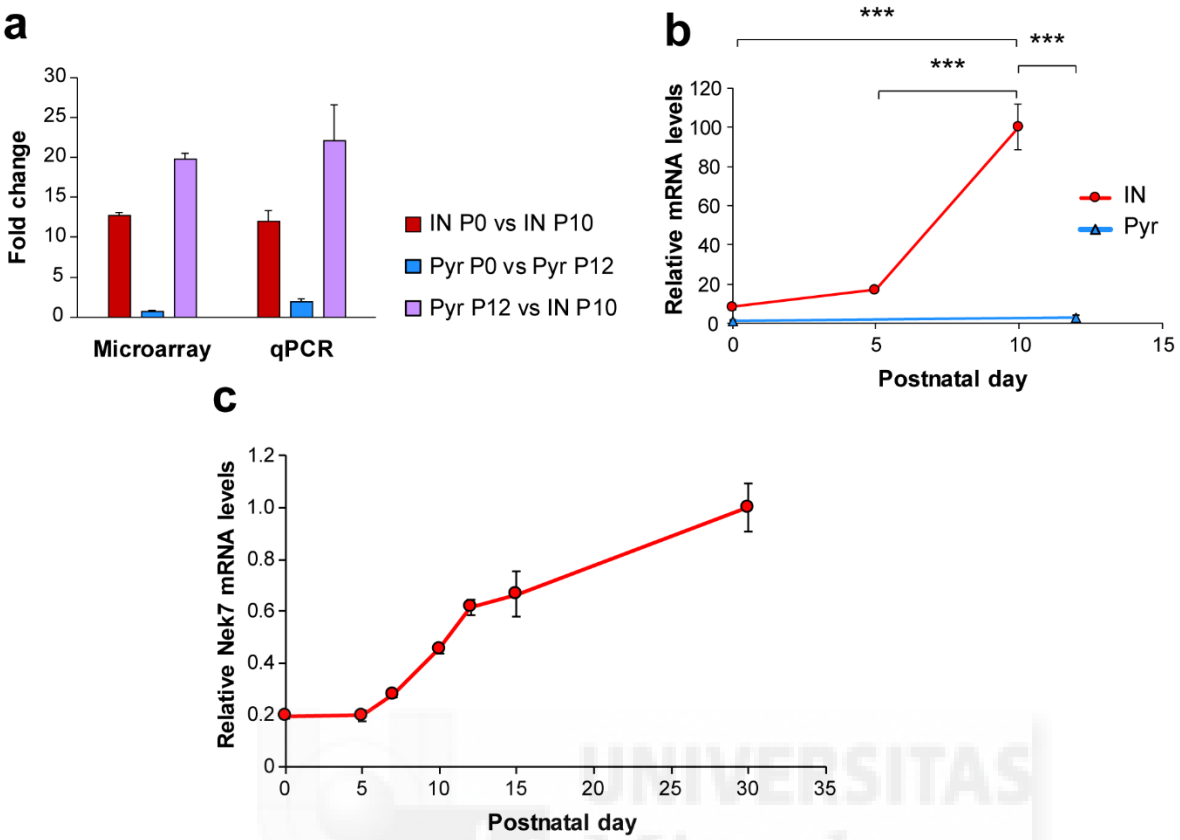

Figure 5.1. *Nek7* expression levels along development. (a) Fold changes in the different comparisons carried out bioinformatically between the sorted experimental groups [interneurons at P0 and P10 (IN P0, IN P10) and pyramidal cells at P0 and P12 (Pyr P0, Pyr P12)]. Both the data from microarray experiments and qPCR are shown. (b) *Nek7* mRNA levels measured by qPCR in sorted cortices from *Nkx2.1Cre;RCE* (IN, red) and *NexCre;RCE* (Pyr, blue) mice. One-way ANOVA, Post hoc Bonferroni, ***p<0.01 , n=3 brains per age. (c) Relative *Nek7* mRNA levels in whole cortices from C57BL/6 mice. n=4 brains per age. (a-c) Data are expressed as mean±s.e.m.

To increase the temporal resolution for Nek7 expression along development, we added a new time point to our experiments: P5. We observed that *Nek7* transcripts showed a small increase from almost undetectable levels at P0 to P5 (Fig. 5.1b) followed by a remarkable increment in expression from P5 to P10 (IN P0 8.5±1.13%; InP5 17±0.73% relative to InP10, Fig. 4.1b). In contrast, pyramidal cells displayed no detectable levels of *Nek7* transcript (Fig. 5.1b).

We further investigated Nek7 expression during postnatal development from birth, P0, to sexual maturity, P30. Since the increasing levels of myelin during development in the cortex makes sorting neurons a rather challenging experiment due to a reduction in cell survival (Guez-Barber *et al.*, 2012), we measured Nek7 RNA levels in whole-tissue somatosensory cortex (Fig. 5.1c). As we have shown that Nek7 expression is enriched in interneurons, we would expect that any difference along the time should indicate only a change in the levels of the kinase in interneurons. These whole-tissue qPCR experiments revealed that Nek7 levels increase from P0 to P10 as previously shown using the FACs sorted interneurons. Later on, the increase in expression seemed to slow down around P15 but it continued rising up to P30. At P30, Nek7 is expressed even at higher levels than during early postnatal development (Fig. 5.1c).

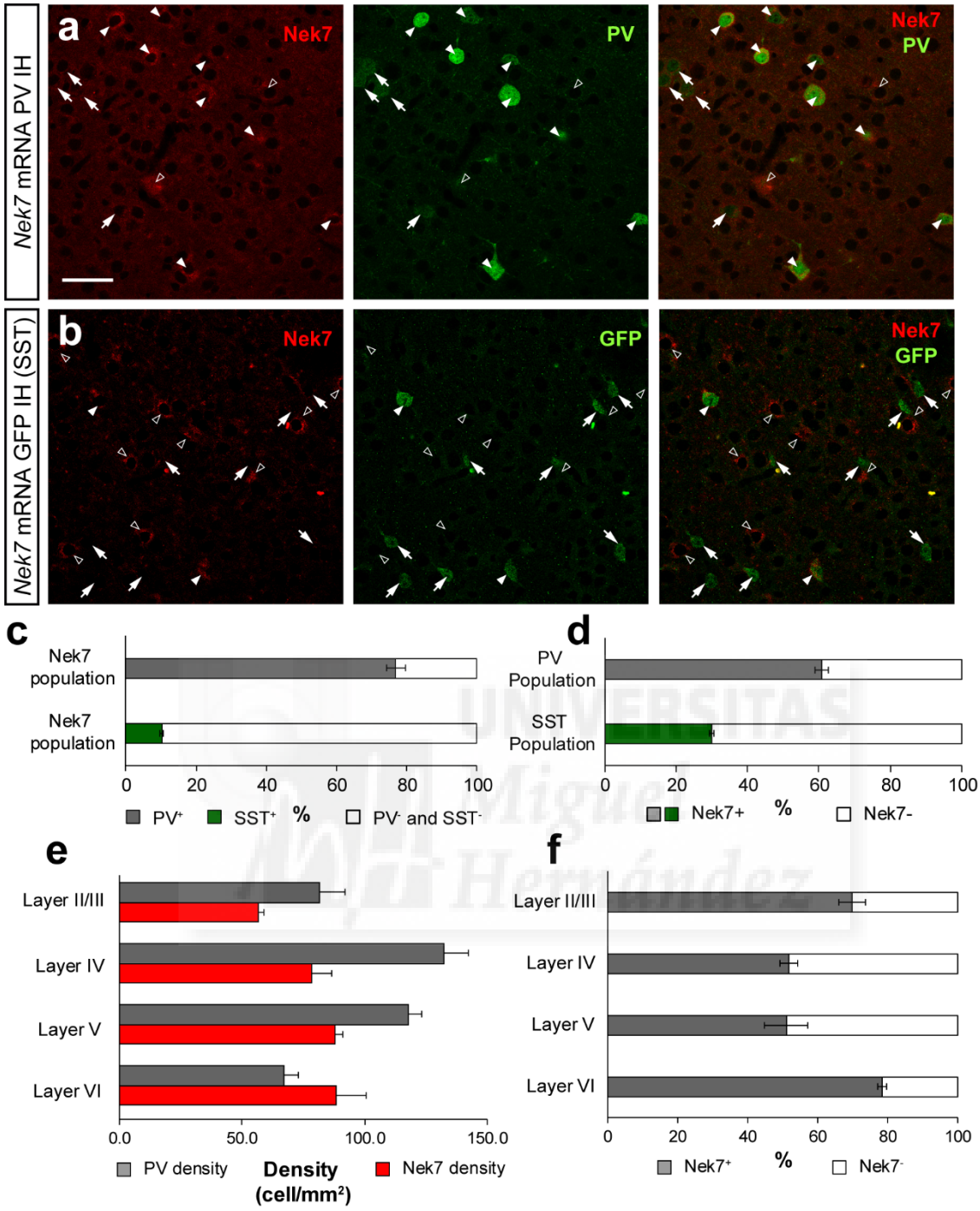

Figure 5.2. Interneuron populations expressing *Nek7*. (a) Single confocal images showing *in situ* hybridization for (*Nek7*, red) and immunohistochemistry (PV, green) colocalizations in SSC of P30 C57BL/6 mice. Colocalizing cells (filled arrowheads), PV+ *Nek-*$^{-}$ (arrows), PV- *Nek7*+ (open arrowheads). (b) Same as in (a) but GFP immunohistochemistry (green) in *SstCre;RCE*. (c) Percentage of PV (Grey) and SST (Green) among all *Nek7*-expressing cortical cells. (d) Percentage of *Nek7* among all PV (Grey) and SST (Green) cortical populations. (e) Cell density of PV (Grey) and *Nek7* (Red) expressing cells in the different cortical layers. (f) Percentage of *Nek7*+ cells among PV population in all cortical layers. Data are expressed as mean±s.e.m. Scale bar: 50 µm.

5.3. Nek7 is expressed in PV and SST interneurons in the cortex

The presence of *Nek7* in the Nkx2. expressing interneuron population can be due to the expression of the kinase in any of the two main populations that express this transcription factor: PV and/or SST expressing cells (Gelman and Marín, 2010). To study its expression in the two populations of interneurons, we performed *in situ* hybridization and immunohistochemistry, simultaneously, to colocalise Nek7 transcripts with the appropriate interneuron markers (Fig. 5.2).

PV was expressed in most of the Nek7 expressing cells (77.0±2.7%; Fig. 5.2a, c) and Nek7 was also expressed in a high proportion of the PV population (60.9±2.0%; Fig. 5.2a, d). Conversely, in the *Nek7* population there was a lower percentage of cells expressing SST (10.2±0.5%; Fig. 4.1b, c) and, similarly, SST population had fewer cells expressing *Nek7* (29.9±0.6%; Fig. 5.2b, d).

We next quantified the distribution of Nek7 positive cells across the different cortical layers to explore whether there was any layer specific enrichment of this population. Density of Nek7 follows the pattern of PV positive cells being less abundant in upper layers (layer II/III 56.5±2.3 cells/mm^2, layer IV 78.1±8.5 cells/mm^2, no Nek7 expressing cells in layer I; Fig. 5.2e) than in lower layers (layer V 87.9±3.0 cells/mm^2, layer VI 88.2±12.2 cells/mm^2; Fig. 5.2e). Nevertheless, Nek7 expressing fraction of PV population is slightly higher in layer II/III and VI than in layer IV and V (layer II/III 69.7±5.6%, layer IV 51.6±8.0%, layer V 51.0±2.7%, layer VI 78.3±1.7%; Fig. 5.2f).

In conclusion, we found that Nek7 expression is mostly specific for PV interneurons in the cortex and its distribution correlates with the normal expression pattern of the PV interneuron population.

5.4. Validation of the shRNA system for LOF experiments

To investigate the function of Nek7 in interneuron postnatal development, including neurite arborisation and synapse formation, we carried out loss of function experiments (LOF). It is key to identify additional markers expressed by Nek7 expressing cells because the protein itself cannot be used as a marker if we reduce its levels. Consequently, we decided to focus in synapses formed by PV positive cells to see the effect of the lack of Nek7 in this population.

Since there is no knock out (KO) or conditional mouse available, we designed a strategy to knockdown the expression of *Nek7* transcripts specifically in the interneuron population. For that, we drove a Cre-dependent LOF experiment in the somatosensory cortex (SSC) using stereotaxic viral injections. This type of approach requires a means to label the affected cells to know which ones were effectively infected and thus altered. Furthermore, synaptic bouton quantification in a specific interneuron population, i.e. infected PV cells, requires labelling their synaptic terminals to know where contacts are formed. For these reasons, a construct was designed in the lab to express mCherry under Cre recombination (Deogracias unpublished). An effective way for doing LOF are shRNAs (Ngo *et al.*, 2006; Paddison *et al.*, 2002). The used construct included an shRNA that, as mCherry, was expressed after a recombination event. This makes Nek7 shRNA expression specific for cells containing Cre and couples both LOF and fluorescent labelling. To test different aspects of the generated system we carried out several validation assays.

5.4.1. Knockdown of Nek7 in cell lines

As a rapid way of probing the knockdown effect of the designed shRNA constructs, we used HEK293 cells. A plasmid containing the shRNA construct was cotransfected with a Cre expressing plasmid together with a plasmid expressing the full-length coding sequence (CDS) of Nek7. Nek7 transcript levels were measured in these cells by qPCR. Endogenous expression of Nek7 was not detected in non-transfected HEK293 cells, thus, all the Nek7 signal came from the transfected plasmid. This signal almost disappeared when the full-length Nek7 was cotransfected with the assayed shRNA (Fig. 5.3a). The substantial knockdown effect is not due to a non-specific impairment in the cellular machinery caused by the shRNA because *Nek7* levels remain unaltered when using a control shRNA with no specific target in the cell line (Fig. 5.3b).

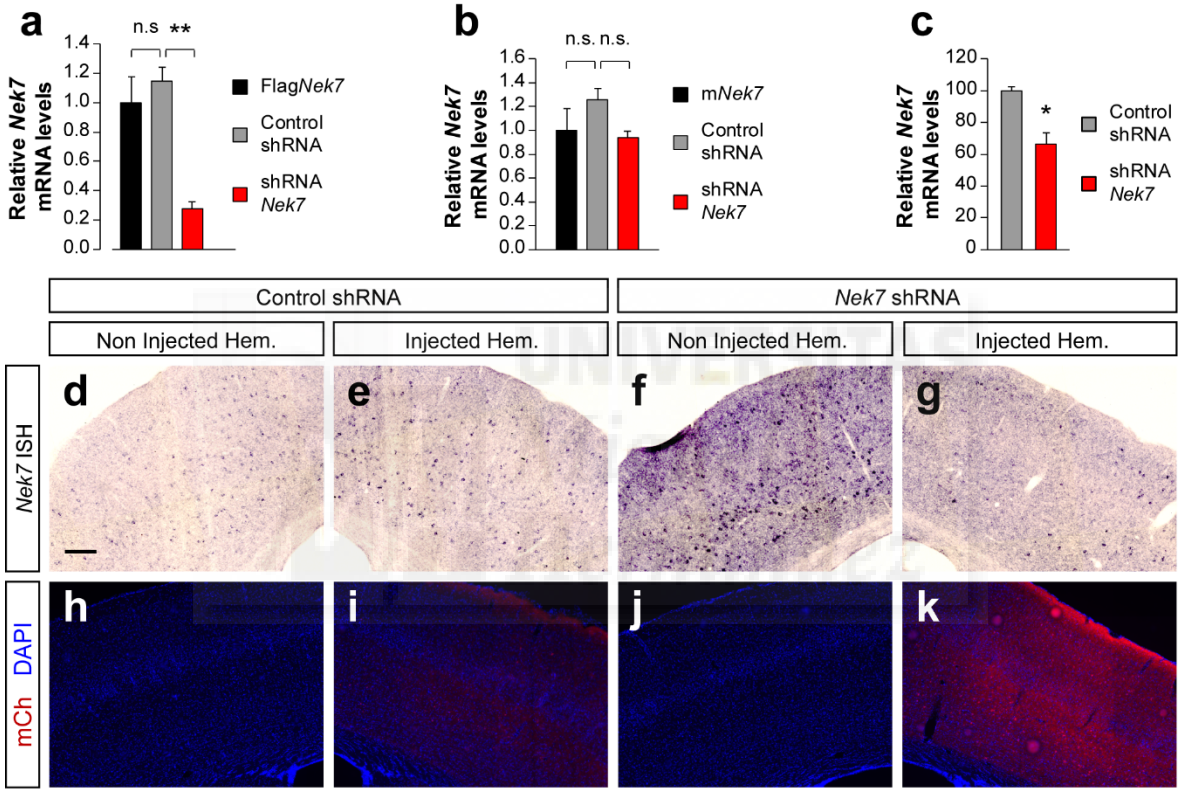

Figure 5.3. *Nek7* shRNA validation assays. (a) *Nek7* mRNA levels in HEK293 cells transfected with plasmids containing Cre, Flag*Nek7* and different shRNAs (grey and red) or no shRNA (black); three days after transfection. Levels relative to the non-shRNA condition (black). N= 5, 4 and 5 cultures for Cre+Flag*Nek7*, control shRNA and shRNA *Nek7* respectively. p (n.s.) =0.674. (b) Same as in (a) but using the synonymously mutated form of *Nek7*. N= 5, 4 and 3 cultures for Cre+m*Nek7*, control shRNA and shRNA *Nek7* respectively. p (n.s. m*Nek7*) = 1.00, p(n.s. shRNA *Nek7)* = 0.398. (c) *Nek7* mRNA levels in dissected cortices from P30 *Lhx6Cre* mice infected with an adenoasociated virus (AAV) containing different shRNAs. N= 3 and 4 brains for control shRNA and *Nek7* shRNA respectively. (d,f) Non-injected hemisphere of P30 *Lhx6Cre* mice infected with the shRNA AAVs. mRNA detected by colorimetric *in situ* hybridization. (e,g) Same as in (d,f) in the injected hemisphere. (h,j) Contiguous coronal sections to the ones used in (d-g) showing the mCherry (red) expressed by infected cells in the non-injected hemisphere. (i,k) Same as in (h,j) in the injected hemisphere. One-way ANOVA, Post hoc Bonferroni, *p<0.05, **p<0.01, n.s. not significant. Data are expressed as mean±s.e.m. Scale bar: 200 µm.

In addition, a mutated form of Nek7 (mNek7) was designed to be resistant to the downregulation effect of the shRNA. The mutations were always silent to avoid any modification in the aminoacidic composition of the protein and therefore, its function. The same experiment was carried out to see the

effect of shRNA in this resistant form of Nek7 and, consistently, its levels remained unaltered (Fig. 5.3b). Altogether, this data validates the downregulation effect of our shRNA construct as well as its lack of effect in mNek7.

5.4.2. Knockdown of Nek7 *in vivo*

The knockdown experiments in HEK293 cells proved the effect of the shRNA *in vitro*. To corroborate that the knockdown regulation strategy was also working in mouse neocortex we performed pilot experiments to check its efficiency *in vivo* (See section 5.5). Adenoasociated viruses (AAVs) containing Cre-dependent shRNA constructs were injected at P3 and the efficiency of down-regulation was measured at P30 using two different strategies.

First, we measured the levels of Nek7 from dissected cortices by qPCR. We observed a decrease in Nek7 transcript levels within the infected area (59.9±10% of the control shRNA condition; Fig. 5.3c). This decrease was lower than the one observed in HEK293 cells because not all the cells in the dissected area were infected and, therefore, the not infected cells still maintained *Nek7* expression.

To know whether this global downregulation was observed at a cellular level we performed *in situ* hybridization against Nek7 in the same previously described conditions. There is a considerable reduction in the density of cells labelled with Nek7 in the infected area, which is labelled with mCherry, as shown in the image (Fig. 5.3f, g, j, k). This downregulation is not caused by a non-specific effect of the shRNA because the control shRNA does not cause a reduction in Nek7+ cell density (Fig. 5.3d, e, h, i). Hence, the shRNA is efficiently knocking down Nek7 in our *in vivo* system and can be used for LOF experiments.

5.5. Loss of Nek7 impairs PV interneuron inhibitory synapse formation

To investigate Nek7 function during synapse formation, we expressed the shRNA during the first postnatal week with the aim to reduce the kinase levels just before synapse formation takes place. Although, Nek7 levels at P0 are very low, we ignore whether this protein has a role in previous developmental processes like cell migration. Furthermore, although no considerable levels of Nek7 have been found in pyramidal cells, the described Cre-dependent constructs allow us to guarantee that the possible effect would be due to the specific loss of Nek7 in interneurons expressing Cre and not to other compensatory mechanisms caused by pyramidal cells modifying their properties (Fig. 5.4a).

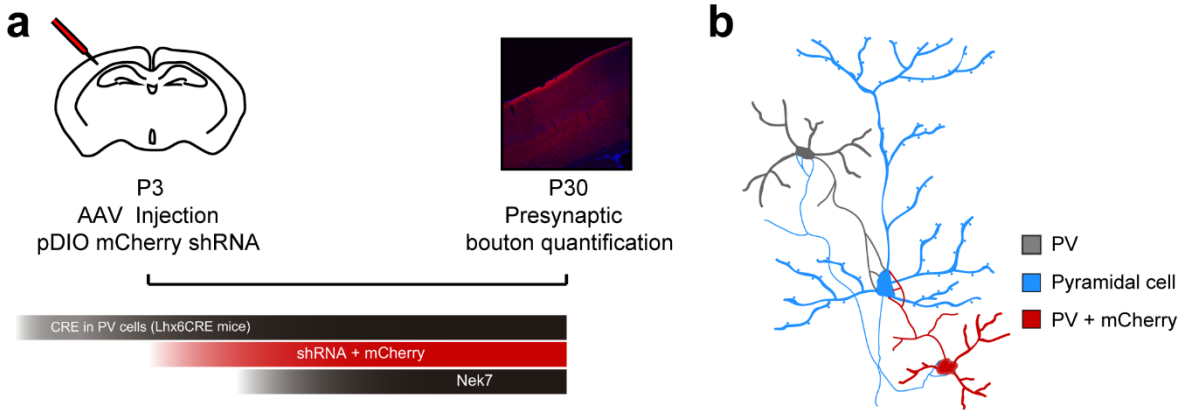

Figure 5.4. Experimental design of *Nek7* LOF for synaptogenesis. (a) P3 *Lhx6Cre* mice were infected to downregulate *Nek7* and express the fluorescent marker mCherry in PV interneurons. The effect was quantified at P30. (b) Both boutons coming from infected (red) and not infected (grey) PV cells were quantified using Syt2 in pyramidal cells (blue) somas.

Given the enrichment of Nek7 in PV cell population and the importance of these cells in sensing and fine-tuning the cortical network changes, we decided to focus in PV interneurons. However, PV is not expressed until P15-P20 (Vogt Weisenhorn *et al.*, 1998) and Cre expression under PV promoter would not allow the recombination of our shRNA construct on time. Thus, we used Lhx6 mouse that expresses Cre in both PV and SST interneurons at early postnatal stages ((Fogarty *et al.*, 2007); Fig. 5.4a). Despite the existence of a portion of SST cells expressing Nek7, this possible effect would difficultly affect synapses formed by PV interneurons given their small number (25%).

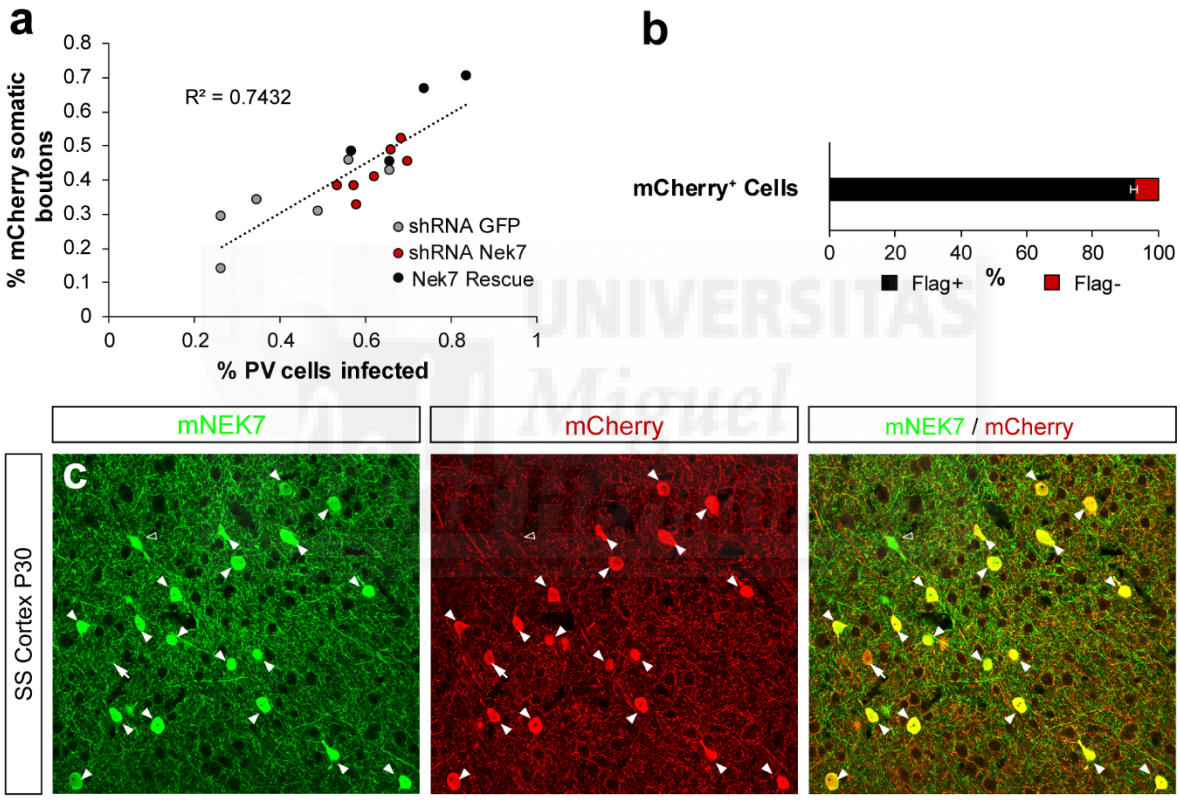

Figure 5.5. Validation assays for synaptic number quantification. (a) Percentage of mCherry positive somatic boutons (Syt2) as a function of the percentage of PV cells infected in the area. Data are expressed as mean. (b) Percentage of mCherry expressing cells that coexpress m*Nek7.* Data are expressed as mean±s.e.m. (c) Single confocal images showing FlagNek7 (green) and mCherry (red) staining of SSC of P30 *Lhx6Cre* mice coinfected with an AAV expressing *Nek7* shRNA and m*Nek7.* Colocalizing cells (filled arrowheads), mCherry- *Nek7*+ (open arrowheads).

To first explore whether Nek7 was involved in the wiring of PV interneurons, we focused in the main PV cell output, the soma of the pyramidal cells ((Markram *et al.*, 2004; Tremblay *et al.*, 2016, Fig. 5.4a,b). We used the synaptic bouton marker, synaptotagmin 2 (Syt2) that specifically labels PV terminals (Sommeijer and Levelt, 2012). To label the pyramidal cells we used Neuronal nucleai (NeuN). Although NeuN is a panneuronal somatic marker in the cortex and it also stains interneurons, quantifying them is unlikely due to the larger density of pyramidal cells and the fact that they can be distinguished

due to their smaller size compared to pyramidal cells. In addition, all the infected *Lhx6* positive cells and all PV positive cells were discarded in our quantifications. Thus, somatic inhibitory boutons belonging to the infected cells were spotted by their coexpression of Syt2 and mCherry ($Syt2^+$ and $mCherry^+$ boutons) and their contact with NeuN pyramidal cells ($NeuN^+$ cells; Fig 5.4b).

Due to the variability of viral infectivity among the different experiments, it was not possible to find a constant proportion of PV cells infected in the same precise area of the somatosensory cortex. This proportion affects the number of mCherry positive ($mCherry^+$) boutons and can bias the synaptic quantification depending on the infectivity of viruses used for the various conditions. However, we found that the percentage of somatic $mCherry^+$ boutons was linearly correlated with the percentage of putatively connected PV cells in the area (R^2=0.7432; Fig.5.5a). Therefore, we normalized the number of $mCherry^+$ boutons of each pyramidal cell to the percentage of infected PV cells in the area. In parallel experiments, we also attempted to rescue Nek7 knockdown by co-infecting the shRNA virus together with the shRNA-resistant wild-type Nek7 tagged with the epitope FLAG (mNek7). Co-infection took place in the majority of the labelled cells within the most densely infected area (92.7±1.0%; Fig. 5.5b, c). Because the large majority of cells expressing mCherry were also expressing mNek7, we carried out the same synaptic quantification for all three conditions.

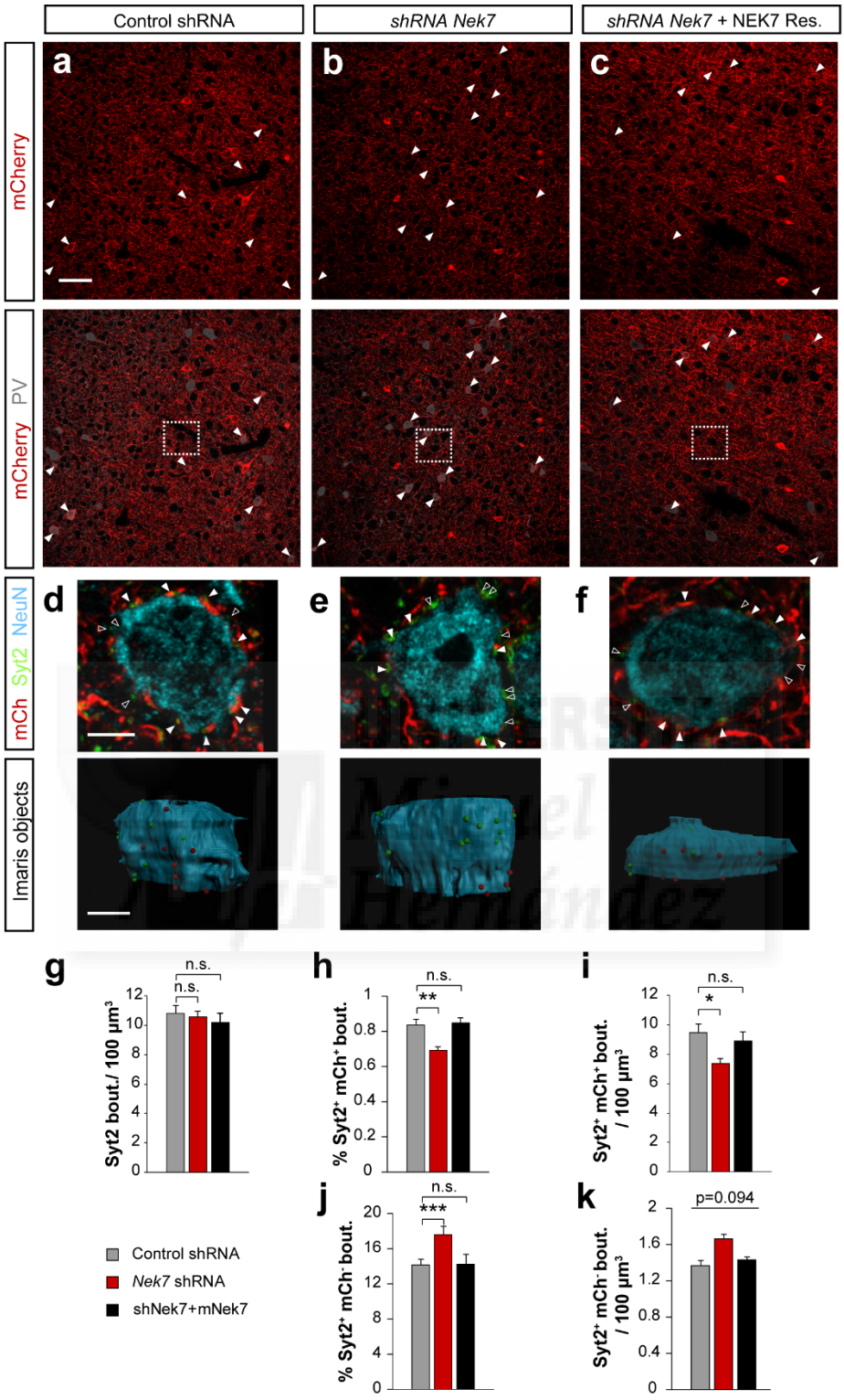

Figure 5.6. Loss of Nek7 impairs PV interneuron inhibitory synapse formation. (a-c) Single confocal images showing PV (Grey) and mCherry (red) staining of SSC layer V, P30 *Lhx6Cre* mice infected with the AAVs expressing shRNA. Collocalizing cells (filled arrowheads). (d-f) Top, confocal images from cells located in the centre of (a-c) showing Syt2 (Green), mCherry (red) and NeuN (Blue). Colocalizing boutons (filled arrowheads), Syt2+ mCherry- (open arrowheads). Bottom, 3D Imaris resconstructions of cells. Red spheres (colocalizing boutons), green spheres (Syt2+ mCherry- boutons). (g) Density of total somatic Syt2 boutons in pyramidal cells for the different experimental conditions. p (n.s.) = 1.00 (h) Percentage of Syt2+ mCherry+ somatic boutons in pyramidal cells normalized to the percentage of PV cells infected in the area. p (n.s.) = 1.00. (i) Same as in (g) for the boutons colocalizing Syt2 and mCherry nomalized to the percentage of PV

(legend from figure 5.6) cells infected in the area. p (n.s.) = 1.00 (j) Same as in (h) for Syt2+ mCherry- boutons and not infected cells. p (n.s.) = 0.163 (k) Same as in (i) for Syt2+ mCherry- boutons and not infected cells. Kruskal-Wallis test, pairwise comparisons. *p<0.05, **p<0.01, ***p<0.001, n.s. not significant. Control shRNA: N= 182 cells from 7 brains. *Nek7* shRNA: 200 cells from 6 brains. Scale bars: (a-c) 50 µm, (d-f, d'-f') 5 µm. Data are expressed as mean±s.e.m.

We found a decrease in the percentage of mCherry^{+} boutons in the Nek7 knockdown (Control shRNA, 83.7±3.1%; Nek7 shRNA, 69.1±2.0%; Fig. 5.6a, b, d, e, h), that was rescued by mNek7 indicating that the loss of PV synaptic boutons was specific (Fig. 5.6c, f, h). The same reduction was observed in mCherry^{+} bouton density (Fig. 5.6i). Nonetheless, the total density of Syt2 boutons remained constant in all the three conditions (Fig. 5.6g) which suggested a possible compensation of the loss of PV input. To confirm this, we quantified the percentage of Syt2^{+} somatic boutons not labelled by mCherry (mCherry^{-}) and normalised it to the percentage of not infected PV cells. The density of mCherry^{-} boutons was higher in Nek7 knockdown than in the control shRNA and rescue (Control shRNA, 14.2±0.6 bout/100 µm^2; Nek7 shRNA, 17.6±1.0 µm^2; Rescue, 14.2±1.1 µm^2; Fig. 5.6j,k). This suggested that the change in synaptic number may be compensated by other basket cells, either the population that did not express Nek7 or the one that expressed it but have not been infected.

5.6. Loss of Nek7 alters PV interneuron arborisation and synaptic density in vivo

Since Nek7 is involved in microtubule dynamic instability (Cohen *et al.*, 2013) it is very appealing to hypothesise that one of its functions might be the regulation of neurite differentiation, including axonal development. In our experimental approach, an alteration of PV cell morphology could indirectly affect the formation of inhibitory presynaptic terminals because the axon would not be able to reach its synaptic target. To explore whether the loss of synapses found in Nek7 knockdown was due to a deficient axonal formation, we carried out ventricular *in utero* injections of AAV at embryonic day 15.5 (E15.5; Fig. 5.7). Differently to the postnatal synaptic viral injections, the pre-natal ventricle infections allowed a lower infectivity of the virus due to the control of the viral titre and the dilution of the injected virus in the ventricle. This strategy allowed us to label isolated parvalbumin cells and reconstruct their morphologies (Fig.5.7).

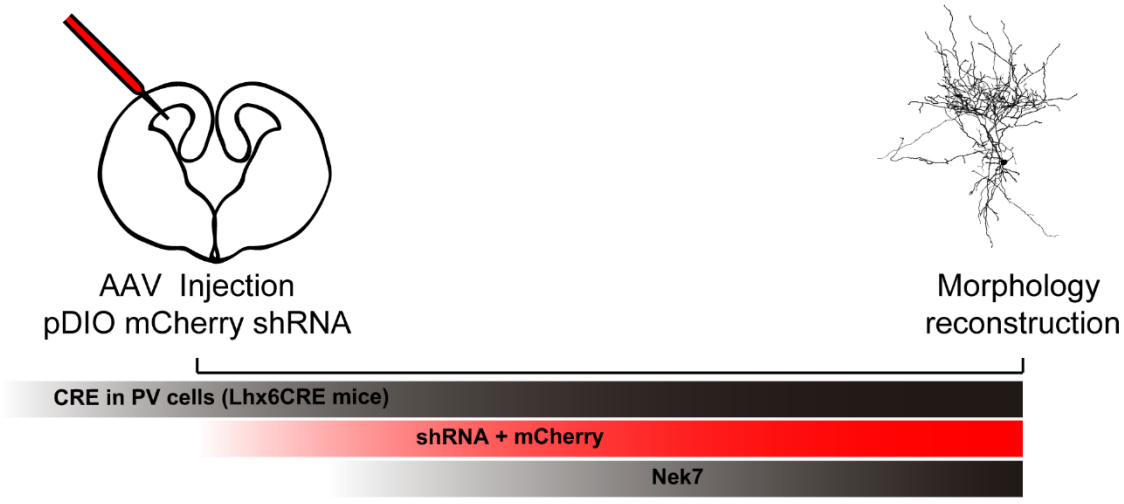

Figure 5.7. Experimental design of *Nek7* LOF experiments for PV cell morphological reconstruction. E15.5 *Lhx6Cre* mice were intraventricularly infected with AAVs to downregulate *Nek7*

and express the fluorescent marker mCherry in PV interneurons. The effect was quantified at P21 reconstructing their morphologies.

To reconstruct and analyse neuronal arbour morphologies we generated confocal images and processed them with the imaging software IMARIS software (Bitplane; Fig. 5.8a,b). The analysis of different parameters showed that down-regulation of Nek7 in PV cells caused a reduction in the cell volume (control shRNA, $3.81 \cdot 10^6$ μm^3; shRNA Nek7, $2.50 \cdot 10^6$ μm^3; Fig. 5.8c). However, neither their total neuritic length nor the density of branching points are significantly altered (Fig. 5.8d,e). One of the possible ways to reconcile the discrepancy between volume and length results is having differences in neurite tortuosity, i.e. how curve neurites are, between the two conditions. However, no differences were found in neuritic tortuosity between the two conditions (Fig. 5.8f). Finally, Sholl analysis was carried out to quantify how the branch morphology changes at different distances from the soma. In line with the volume data, PV cell branches lacking Nek7 are not able to reach the most remote locations (Fig. 5.8g).

Although mCherry did not let us differentiate between axon and dendrites, since most of the branches of PV interneurons belong to the axon (Jiang *et al.*, 2015), we can infer that the observed effect will mainly be caused by the effect of Nek7 knockdown in the axon.

Altogether, our data suggested that the observed synaptic phenotype could be just the consequence of mere axonal growth. For example, a smaller axon will not be able to reach the furthest cells to form synapses therefore the number of inhibitory boutons onto pyramidal cells will be reduced. Alternatively, the axon itself could have an impaired capability to form synapses. Both possibilities are not exclusive. To understand whether any or both of these scenarios were conceivable, we quantified the number of Syt2 boutons in neurites of previously reconstructed cells (Fig. 5.9). We found that PV neurons lacking Nek7 have a lower density of Syt2 boutons (control shRNA, 3.74±0.41 bout/100 μm^2 of neurite; Nek7 shRNA, 2.55±0.30 bout/100 μm^2 of neurite; Fig. 5.9a, b, c). Thus, Nek7 is somehow controlling the formation of both axon and synapses.

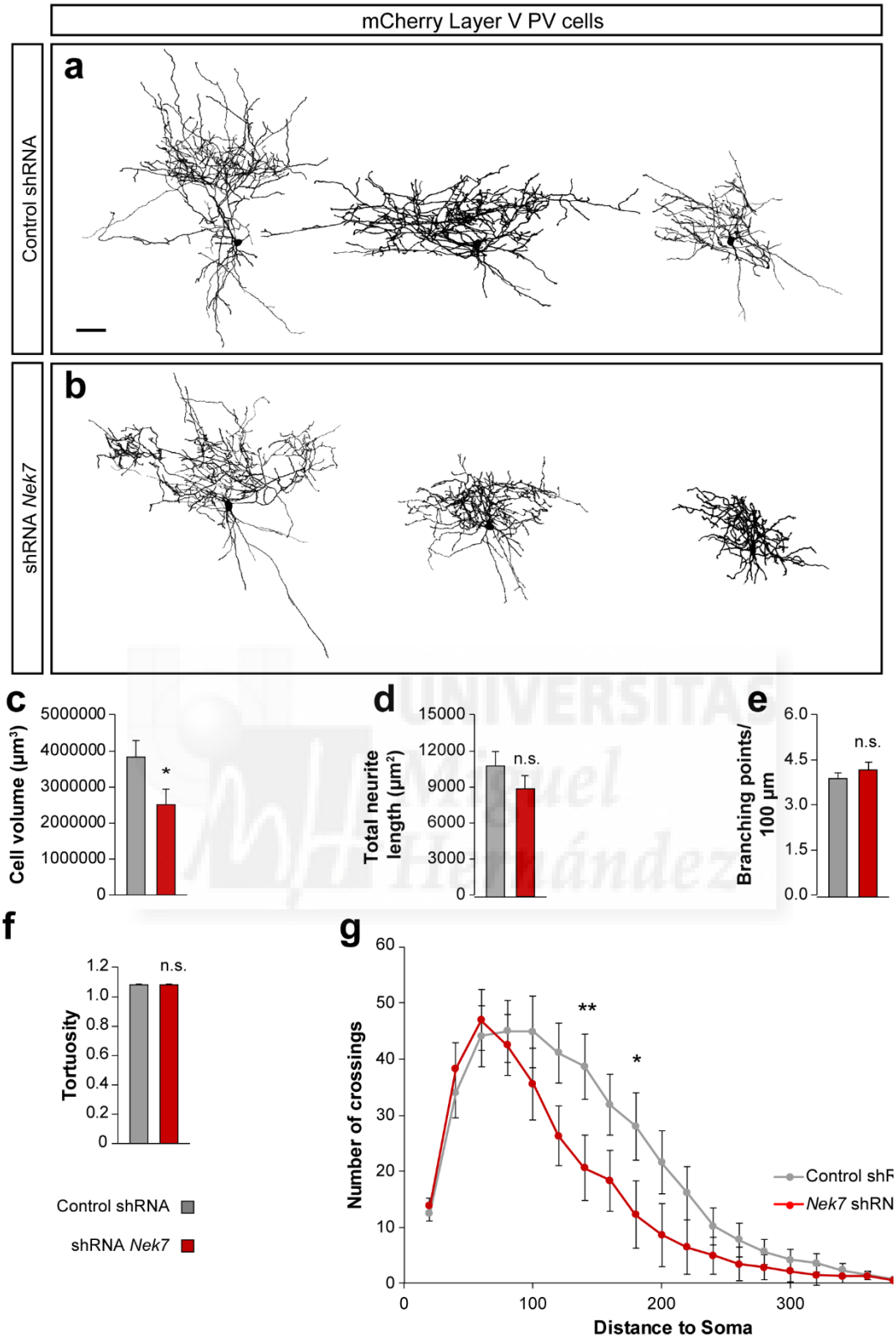

Figure 5.8. Loss of Nek7 alters neuronal morphology in PV interneurons. (a,b) Examples of PV interneurons reconstructed from SSC layer V of P21 *Lhx6Cre* mice infected with the AAVs expressing shRNA and mCherry (black). (c) Total cell volume occupied by the convex hull containing the reconstructed cells. (d) Total length of the reconstructed neurites. p=0.265. (e) Branching points per unit length of neurites. p=0.898. (f) Neurite tortuosity. p=0.413. (g) Sholl analysis, number of crossings between neurites and concentric circles centred in the soma. (c-f) T-test. (g) Two-way ANOVA with

(legend from figure 5.8) Bonferroni correction. *p<0.05, **p<0.01, n.s. not significant. Scale bar: 50 µm. Data are expressed as mean±s.e.m.

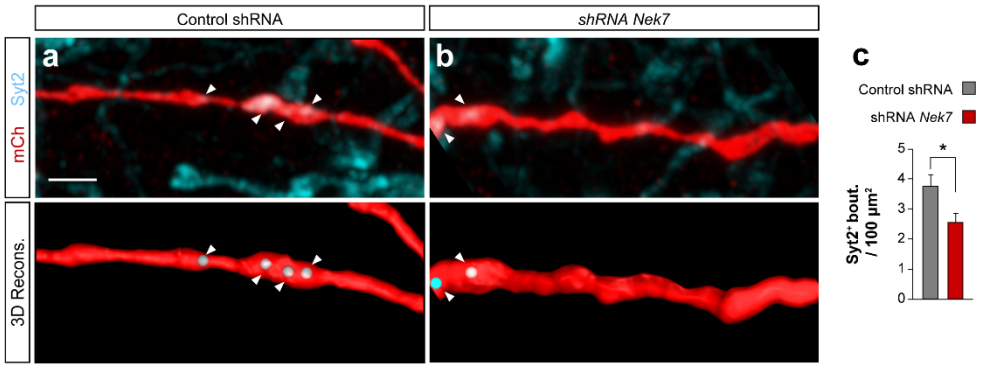

Figure 5.9. Loss of Nek7 alters axonal bouton density. (a-b) Top, confocal Z-projections of infected PV cells expressing mCherry (red). Boutons are labelled by Syt2 (blue). Bottom, Imaris 3D reconstruction used for quantification. (c) Syt2 bouton density per unit area of neurite. T-test. *p<0.05. Scale bar: 2 µm. Data are expressed as mean±s.e.m.

5.7. Loss of Nek7 affects axonal growth cone dynamics in vitro

Axonal arborisation and synapse formation are two developmental processes highly interrelated. For example, axonal branches stabilise through the formation of synapses with postsynaptic targets (Meyer and Smith, 2006; Ruthazer *et al.*, 2006). Based on this, it is plausible that the synaptic and arborisation phenotypes found in our study could be mechanistically linked. For this reason, we carried out primary cortical cultures of *Nkx2.1Cre* and transfected them with the shRNA constructs. Using time-lapse imaging, we recorded growth cones in culture when they still have an active growth (DIV7). Since PV has a very late temporal expression, we decided to quantify growth cones from all Nkx2.1-expressing cells labelled with mCherry and examine the behaviour of the whole population.

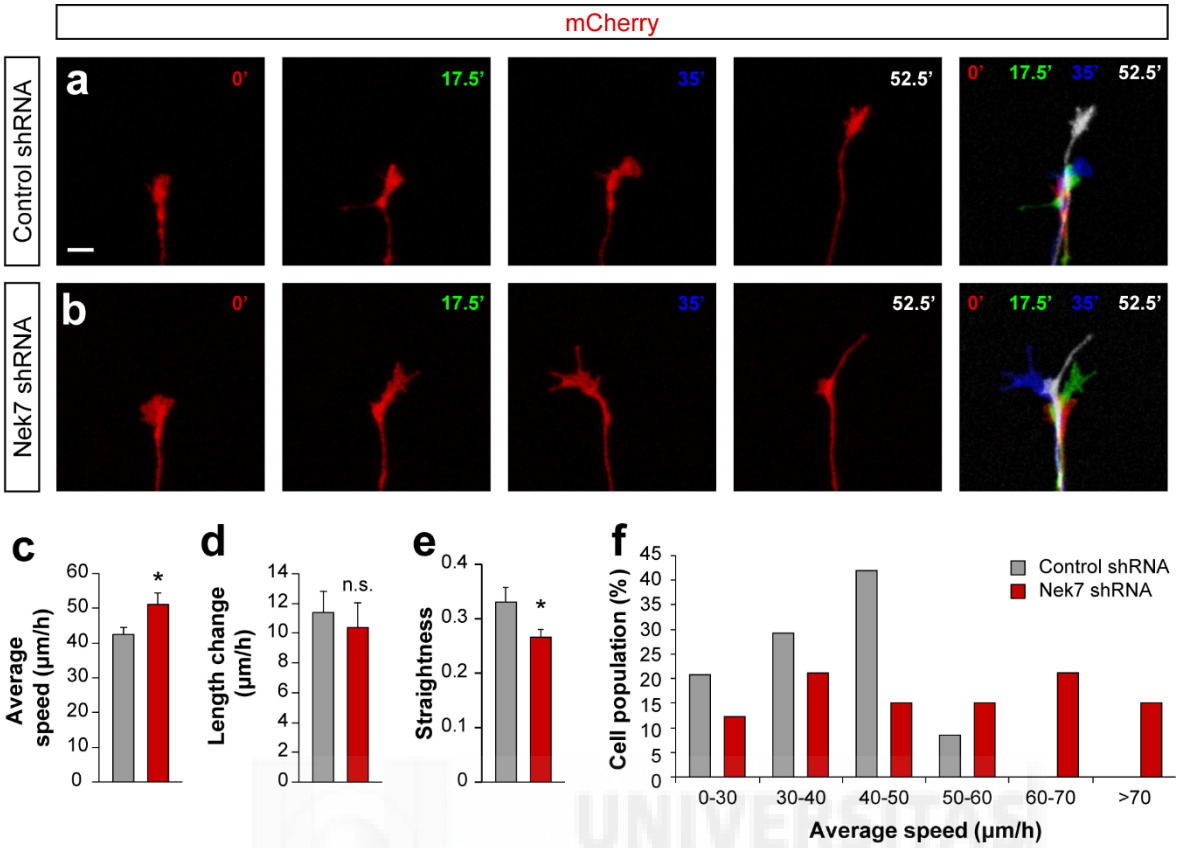

Figure 5.10. *Nek7* depletion impairs axonal growth cone dynamics *in vitro*. (a,b) Confocal Z-projection frames from axons growing in DIV 7 cultures of *Lhx6Cre* mice transfected with the shRNA-mCherry (red) plasmids. (c) Average speed of the recorded growth cones in µm progressed per hour. (d) Total axonal length change per hour. P=0.564. (e) Path straightness. (f) Distribution of growth cone average speed with the control shRNA and *Nek7* shRNA. (c,d) Mann-Whitney U test. (e) T-test. (f) X^2 test $p<0.05$, n.s. not significant. Scale bar: 5 µm. (c,d,e) Data are express as mean±s.e.m. (f) Data are express as total cell percentage.

Depleting Nek7 from the *Nkx2.1* population caused a significant increase in the average axonal moving speed compared to controls (control shRNA, 42.36±2.12 µm/h; Nek7 shRNA, 51.14±3.20 µm/h; Fig.5.10c). These differences can only be observed in a subpopulation of the recorded cells as showed in the distribution, suggesting that only some cells are affected by Nek7 knockdown (Fig. 5.10f). However, the total axonal length change was similar (control shRNA, 11.38±1.46 µm/h; Nek7 shRNA, 10.40±1.63 µm/h; Fig.5.10d). This discrepancy is supported by a less straight path while the axon senses its surrounding in Nek7 knockdown compare to control (Fig. 5.10e). Namely, the axon extended in a more meandering manner when Nek7 was not present. Two main features can be studied in growth cone dynamics: growth cone turning, where the axon actively search for neighbouring cues, and growth cone advance (Geraldo and Gordon-Weeks, 2009). The observed change in global moving speed without a change in total growth suggests that growth cone turning but not its advance is affected in *Nek7* knockdown.

In conclusion, these results suggest that Nek7 is involved in axonal growth that could lead to a deficiency in axonal arborisation and synapse formation. Alternatively, a deficit in the initial processes of synapse formation and, therefore, in branch point stabilisation could trigger a more random growth of the axon.

RESULTS

6. Role of Galectin-1 in synapse formation

6.1. Introduction

Galectins are a family of proteins that share a characteristic β-galactoside binding domain with a conserved aminoacidic sequence called carbohydrate recognition domain (CRD) (Barondes *et al.*, 1994). This family is composed by three different subtypes: a) prototype galectins that contain a CRD, Galectin-1 (Gal-1), b) chimera-type, like Galectin-3 (Gal-3), consisting on a CRD and a non-lectin domain and c) tandem-repeat galectins that contain two CRDs. Gal-1 is a prototype galectin and, as other members of this subtype, form homodimers (Cho and Cummings, 1995; Lobsanov *et al.*, 1993).

Given their common CRD, all galectins share affinity for the monosaccharide galactose (Gal). However, this interaction is weak and they bound with increased affinity to disaccharides containing galactose and glucosamine (Glc), N-acetylglucosamine (GlcNAc) or N-acetylgalactosamine (GalNAc) (Carlsson *et al.*, 2007; Knibbs *et al.*, 1993; Salameh *et al.*, 2010). Gal-1 binds preferentially to Gal-GlcNAc disaccharides (lactosamine) when they are located in the terminal part of glycans (Carlsson *et al.*, 2007; Ideo *et al.*, 2011; Leppänen *et al.*, 2005; Salomonsson *et al.*, 2010). Other extensions such as sulphate or neuraminic acid increase Gal-1 affinity (Carlsson *et al.*, 2007; Sörme *et al.*, 2002; Stowell *et al.*, 2004). Moreover, Gal-1 glycan binding activity depends on the reduced state of the protein, i.e. oxidised Gal-1 does not bind to glycans (Horie and Kadoya, 2004)).

Glycan moieties are present in secreted proteins and the extracellular domains of transmembrane proteins. For this reason, galectins would be expected to exert their function as secreted molecules. Nevertheless, galectins can be found both intra- and extracellularly. They are thought to be secreted via a non-classical pathway because they lack a secretion signal peptide (Hughes, 1999). The main molecular pathways where galectins have been found are still extracellular.

Galectins interact with extracellular matrix and membrane-bound glycoproteins that mediate the activation of different molecular pathways. Specifically, Gal-1 binds to proteins like thrombospondin, fibronectin and laminin that are present in the extracellular matrix (Moiseeva *et al.*, 2003). Regarding transmembrane proteins, the main known partners of Gal-1 are integrins α7β1 and α1β1 (Gu *et al.*, 1994; Moiseeva *et al.*, 1999). Interestingly, Gal-3 have been proven to interact with NCAM but this has not been assayed with Gal-1 (Probstmeier *et al.*, 2002). Through these interactions, galectins can either facilitate adhesion by crosslinking glycosylated proteins or reduce it by blocking receptors. For Gal-1, this modulation depends on protein levels (Cho and Cummings, 1995; Morris *et al.*, 2004).

As the rest of galectins, Gal-1 is quite ubiquitous being expressed by various neural tissues where it seems to be functionally polyvalent. For example, it can be found in dorsal root ganglia and spinal cord where it is expressed by sensory and motor neurons (Akazawa *et al.*, 2004; Horie *et al.*, 1999). When these axons are sectioned, Gal-1 is upregulated and promotes nerve regeneration (Crandall *et al.*, 2000; Horie *et al.*, 1999; McGraw *et al.*, 2005). This effect is mediated by Gal-1 in its oxidized form, being therefore independent on their lectin activity (Horie *et al.*, 1999). Its interaction with neuropilin-1/plexinA4 complex interferes with growth inhibitory Sema3A signals (Quintá *et al.*, 2014). Gal-1 also influences the growth of nociceptive afferents. For this reason, *Lgals1* full knock out (*Lgals1* KO) has impaired nociception (McGraw *et al.*, 2005).

A similar function on axonal growth can be found in the olfactory system. Sensory olfactory axons project from the olfactory neuroepithelium to the olfactory bulb via the olfactory nerve (Tenne-Brown *et al.*, 1998). Gal-1 is expressed by the cells ensheathing these nerves and lactosamine glycans are present in olfactory axons (Crandall *et al.*, 2000; Mahanthappa *et al.*, 1994). Gal-1 is thought to promote the growth or guidance of these axons through its interaction with glycans and β2-laminin, present as well in the axonal path (Crandall *et al.*, 2000; Puche *et al.*, 1996). In cultured primary cerebellar granular neurons, Gal-1 promotes neuritogenesis cross-linking GM1 ganglioside and α5β1-integrin. This activates a signalling cascade that involves focal adhesion kinase (Sango *et al.*, 2004).

Several studies have revealed the expression of Gal-1 in interneurons of the neocortex and the hippocampus, supporting our screening data. In both regions, Gal-1 is expressed by a high proportion of SST cells while the number of PV cells is low (Bischoff *et al.*, 2012; Kajitani *et al.*, 2014; Winden *et al.*, 2009). Both SST and PV populations are known to die after the induction of epileptic seizures (Kobayashi and Buckmaster, 2003). Interestingly, Gal-1 levels increase their expression in astrocytes after this and in *Lgals1* KO neuronal death is abolished. Conversely, Gal-3 does not have this effect (Bischoff *et al.*, 2012). Moreover, *Lgals1* KO has impaired spatial and contextual fear learning (Sakaguchi *et al.*, 2011) which may be related to its expression in interneurons.

Gal-1 function in cell adhesion together with its interaction with extracellular matrix proteins makes it a good candidate to be participating in synaptogenesis through these molecular mechanisms. Moreover, its involvement in axonal growth and guidance in several systems suggests that it could have the same effect in interneurons, affecting the formation of their synapses through this cellular mechanism.

6.2. Developmental time course of Gal-1 expression

To confirm and validate the relative transcript levels obtained in the microarray experiments, we carried out qPCR with specific primers for *Lgals1*. To perform this validation, pyramidal cells and interneurons were sorted again using the same previous conditions. As it was conducted for Nek7, a new time point at P5 was introduced for interneurons to increase the time resolution of the analysis of *Lgals1* levels.

There is a higher increase in *Lgals1* levels in interneurons than in pyramidal cells during synapse formation (Fold change 59.01±10.80 and 0.97±0.44, respectively; Fig. 6.1a). This data supports the specificity in the expression of *Lgals1* in interneurons compared to pyramidal cells. This increase was observed also in the microarray data where interneurons increase expression levels 12.64 times during synaptogenesis and, compared to pyramidal cells, they have 19.70 times more *Lgals1* (Fig. 6.1a). There is a considerable difference between the increments found in the microarray and qPCR data, namely, qPCR values are higher than microarray values (Fig. 6.1a). This can be explained by a different resolution between both techniques to detect small or high levels of the transcript. Thus, we can conclude that there is a real enrichment of *Lgals1* in interneuron during synapse formation.

Whereas the levels of *Lgals1* increased from P0 to P10 in interneurons, the levels of the transcript were almost undetectable in pyramidal cells at both ages (InP0, 1.88±0.35%; PyrP0, 2.03±0.15%; PyrP12, 2.10±1.04% relative to levels in InP10; Fig. 6.1b). Slightly higher levels are already detected at P5, the new time point added (InP5 14.87±4.25% relative to InP10; Fig. 6.1b).

However, are these changes along development a consequence of an increment of transcript within the cell or to more cells expressing the gene? To address this question, we quantified the number of Gal-1 positive cells in somatosensory cortex of P0, P5, P10 and P30 mice (N=1). Our preliminary data suggests that the number of cells expressing Gal-1 increase along the first 10 days of postnatal development and decreases slightly during the following days (Fig. 6.1c, d). It is possible that the peak at P10 followed by a decrease in the number of cells expressing Gal-1 could be due to a function of the gene at this particular stage that is no longer required later. Alternatively, since interneurons undergo apoptosis around P7-P10, the reduction of cells at later stages during development might be indicative of a natural cortical cell pruning (Southwell *et al.*, 2012).

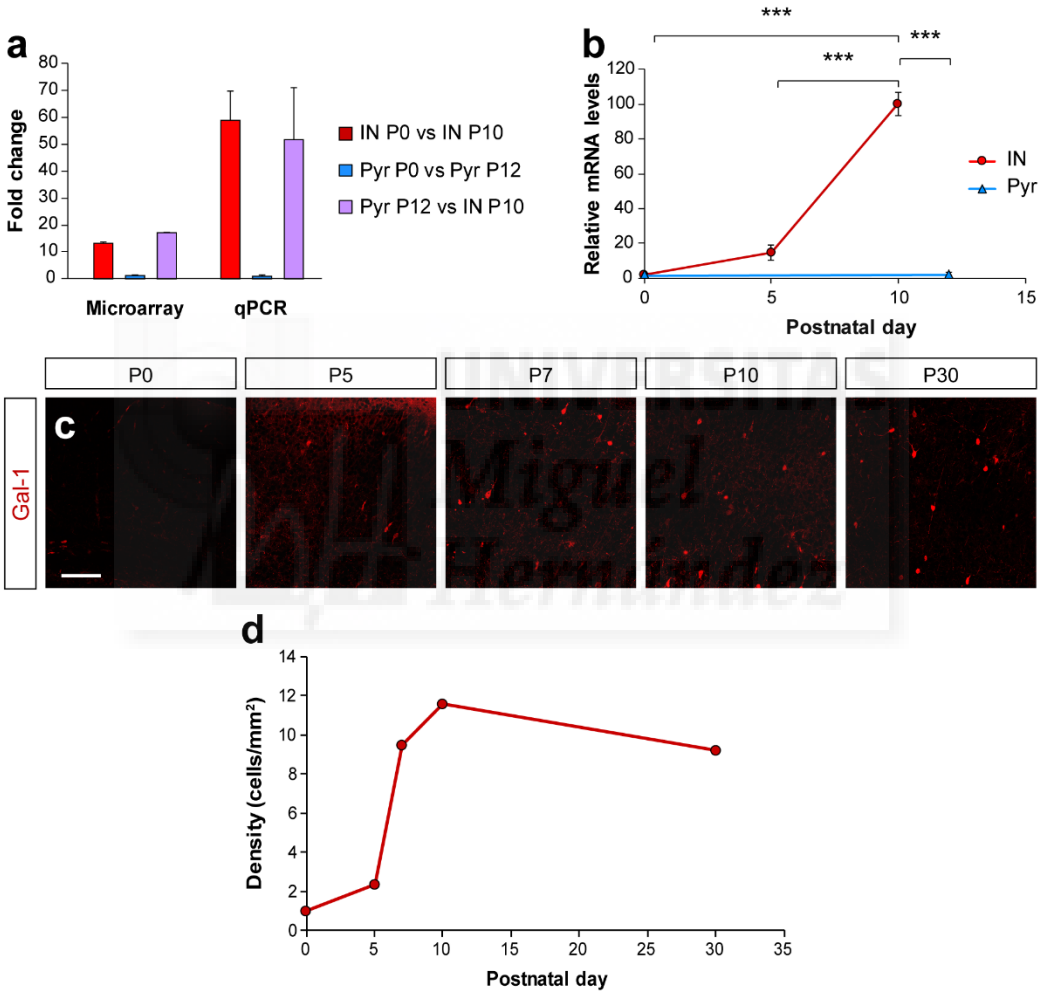

Figure 6.1. *Lgals1* expression levels along development. (a) Fold changes in the different comparisons carried out bioinformatically between the sorted experimental groups [interneurons at P0 and P10 (IN P0, IN P10) and pyramidal cells at P0 and P12 (Pyr P0, Pyr P12)]. Both the data from microarray experiments and qPCR are shown. (b) *Lgals1* mRNA levels measured by qPCR in sorted cortices from *Nkx2.1Cre;RCE* (IN, red) and *NexCre;RCE* (Pyr, blue) mice. One-way ANOVA, Post hoc Bonferroni, ***p<0.01 , n=3 brains per age. (c) Single confocal planes showing the density of cells labelled with Gal-1 in SSC from C57BL/6 mice at different developmental time points. (d) (legend from figure 6.1) Gal-1 positive cell density along development N=1 brain per age. (a-b) Data are expressed as mean±s.e.m. (d) Data are expressed as density of n=1. Scale bar: 100 µm.

6.3. Interneurons expressing Gal-1

The restriction of Gal-1 expression to the *Nkx2.1* positive population could be due to the expression of the gene in either SST or PV positive cells (Gelman and Marín, 2010). To identify the interneuron populations expressing Gal-1, we colocalized the lectin with these two population markers using immunohistochemistry. Gal-1 was expressed in a high proportion of SST positive cells in somatosensory cortex as previously described (Bischoff *et al.*, 2012; Kajitani *et al.*, 2014; Winden *et al.*, 2009). A 60.54±5.07% of Gal-1 positive cells express SST and, similarly, a 42.06±3.27% of SST positive interneurons are Gal-1 positive (Fig. 6.2a, d, e). There is also a small population of Gal-1+ cells expressing PV: 24.69±1.05%, which accounts for 13.32±1.87% of the PV population (Fig. 6.2b, c, d, e).

To know whether there was some expression bias in these subpopulations towards specific cortical layers, we quantified cell densities and colocalization percentages per layer. As illustrated in the graph, there is a higher density of Gal-1 positive cells in lower layer, V and VI, than in upper layers, II/III and IV, following the pattern of PV and SST interneurons (Fig. 6.2f). Comparing with SST cell density, we found that in layer II/III, IV and V the relative densities follow the above-mentioned percentage of colocalization (Fig. 6.2f). However, in layer VI Gal-1 and SST densities were quite similar (SST 76.01±16.22 cells/mm^2, Gal-1 68.27±3.92 cells/mm^2; Fig. 6.2f). Looking at the proportion of Gal-1 cells expressing SST per layer, we could observe that there was a drop from upper layers to lower layers, suggesting that there was other cell population expressing Gal-1 and it concentrated more in this area (Fig. 6.2g).

Finally, we focused in PV cells to analyse the layering expression pattern of Gal-1 in this population. Interestingly, there was almost no expression of Gal-1 in upper layer PV cells while most of the colocalization resides in layer VI (layer II/III N/A, layer IV 1.16±1.16%, layer V 8.18±2.75%, layer VI 53.39±0.45%; Fig. 6.2b, c, i). Percentages of PV positive cells in Gal-1 population were rather similar to the previous percentages (Fig. 6.2b, c, h). This pattern partially explained the higher density of Gal-1 in layer VI and the drop in SST expressing percentage (Fig. 6.2g). To conclude, Gal-1 was expressed by both SST and PV interneurons. While the protein is present in half of the SST population along the cortex, its expression in PV cells is restricted to lower layers, mainly layer VI.

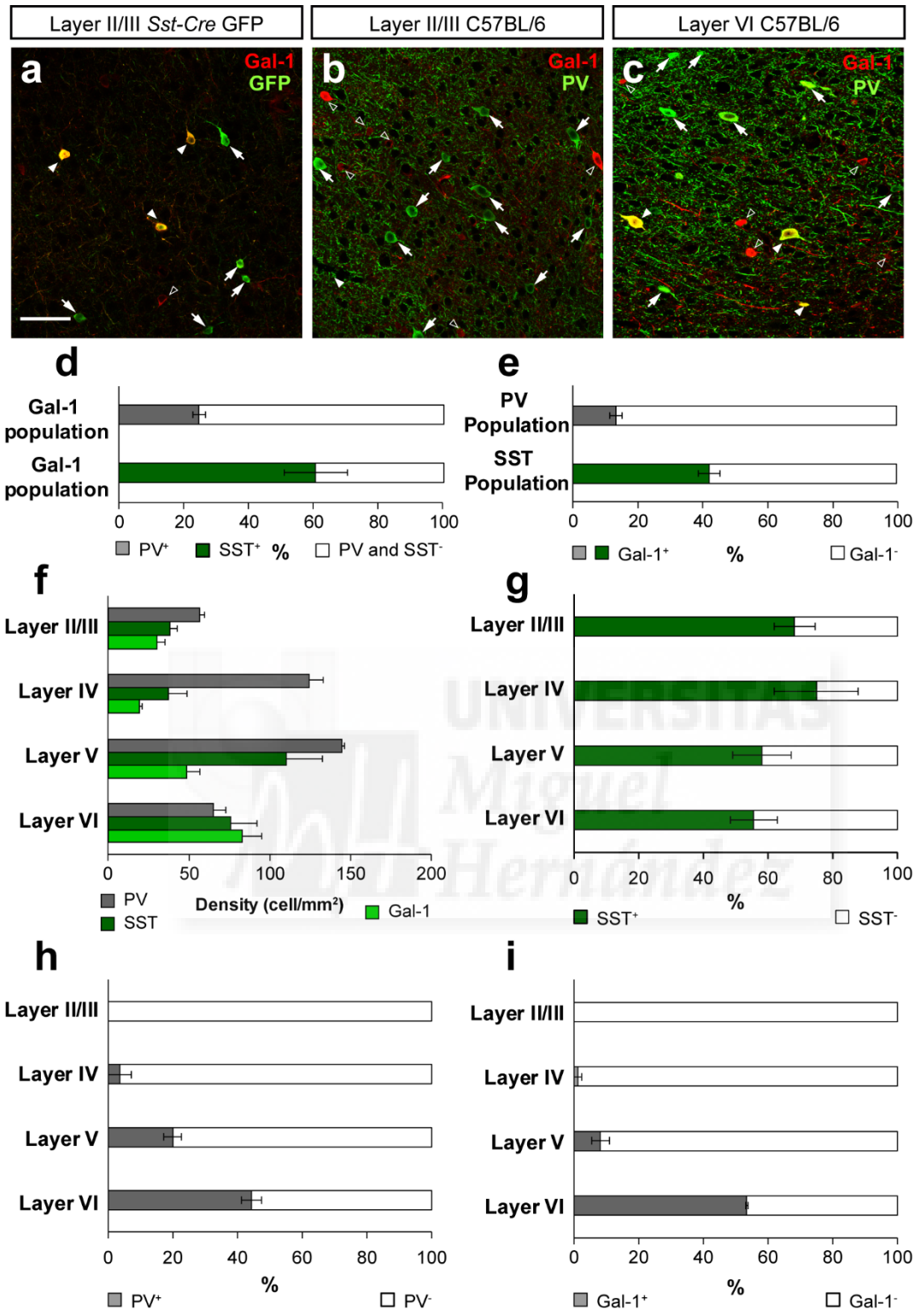

Figure 6.2. Interneuron populations expressing Gal-1. (a) Single confocal images showing immunohistochemistry labelling for Gal-1 (red) and GFP (green) in SSC from P30 *SstCre;RCE* mice. Colocalizing cells (filled arrowheads), GFP+ Gal-1-$^{-}$ (arrows), GFP- Gal-1+ (open arrowheads). (b) Same as in (a) but with the interneuron marker PV (green) in layer II/III of C57BL/6 mice. (c) Same as in (b) in layer VI. (d) Percentage of PV (Grey) and SST (Dark green) among all Gal-1+ cortical cells. (e) Percentage of Gal-1+ cells among all PV (Grey) and SST (Green) cortical populations. (f) Cell density of PV (Grey), SST (Light green) and Gal-1 (green) expressing cells in the different cortical layers. (g) Percentage of SST cells among all Gal-1+ population in all cortical layers. (h) Percentage of Gal-1+

(legend from figure 6.2) cells among PV population in the different cortical layers. (i) Same as in (g) for PV cells. N=3 brains. Scale bar: 50 µm.

6.4. Loss of function in somatostatin interneurons

To evaluate the possible involvement of Gal-1 in synapse formation of somatostatin cells, we analysed the density of somatostatin outputs and inputs in *Lgals1* knockout (KO) mice compared with their wild type littermates. Although the expression of Gal-1 is very low at perinatal stages (Fig. 6.1), we quantified SST cell density in somatosensory cortex to confirm that the migration of interneurons was normal in absence of Gal-1. As expected, SST cell density remained unaltered in *Lgals1* KO (Fig. 6.3).

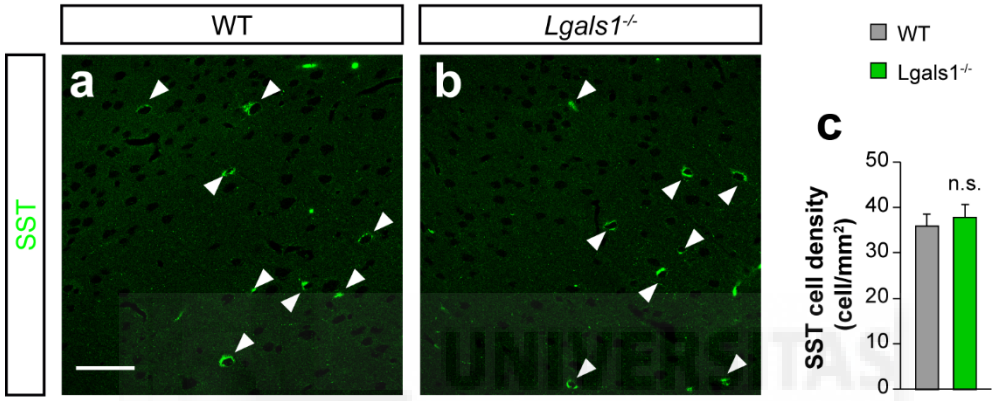

Figure 6.3. SST cell density in *Lgals1 KO* and WT mice. (a,b) Single confocal images showing SST labelling in SSC layer II/III of *Lgals1* KO and WT mice. Filled arrowheads: SST cells. (c) SST cell density in all cortical layers. N=4 and 5 *Lgals1* KO and WT brains respectively. Scale bar: 50 µm. T-test. n.s. not significant P=0.661. Data are expressed as mean±s.e.m.

6.4.1. Somatostatin cell output

A large number of somatostatin interneurons belong to the morphological type known as Martinotti cells. These are cells that have their soma in different layers of the cortex and extend their axon to layer I where they form most of their arborisation and synapses (Wang *et al.*, 2004). Gal-1 seemed to be present at all the subcellular compartments of somatostatin neurons (Fig. 6.4 a, b, d) and the presence of Gal-1 expressing neurites was higher in layer I compared to the rest of the layers (Fig. 6.4c). This, together with the fact that Gal-1 was expressed in 48% (N=1) of the GFP positive cells in the GIN mouse suggested that Gal-1 was expressed in the Martinotti cell population.

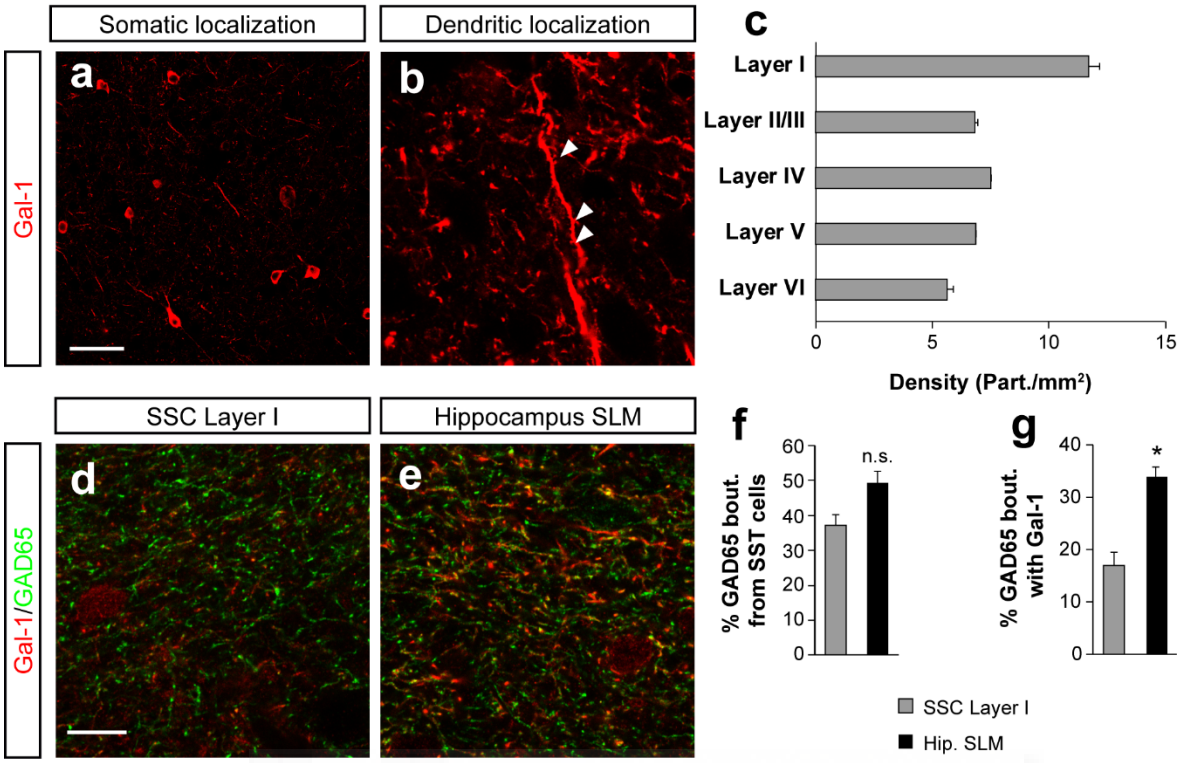

Figure 6.4. Galectin-1 subcellular expression pattern. (a, b) Confocal images showing the expression of Gal-1 in subcellular structures like the soma (a) and dendritic spines (b). Filled arrowheads: dendritic spines. (c) Density of Gal-1 particles across cortical layers. N=3 brains. (d, e) Single confocal planes colocalizing Gal-1 particles (red) with GAD65 (green) in SSC layer I (d) and hippocampus (SLM, e). (f) Percentage of GAD65 boutons from SST cells in SSC layer I (grey) and hippocampus (black). N=2 and 3 brains for SSC and SLM respectively. (g) Same as in (f) for GAD65/Gal-1 particles. Data showed in images (d, e). N=2 and 3 brains for SSC and SLM respectively. Scale bars: (a, b) 100 µm, (d, e) 10 µm. T-test. *p<0.05, n.s. not significant P=0.220. Data are expressed as mean±s.e.m.

GAD65 is enriched in the synaptic boutons formed by somatostatin cells (Fish *et al.*, 2011). However, whether the source of these GAD65 boutons in layer I is the somatostatin population is not known. We tried to answer this question by colocalising GAD65 with Tomato expressed by the reporter line *Sst-Cre;Tomato*. A 37.2±2.9% of GAD65 boutons were formed by SST cell axons in this area (Fig. 6.4d, f). Moreover, when colocalizing GAD65 boutons to neurites expressing Gal-1, we found that 16.9±2.5% of them were positive for Gal-1 (Fig. 6.4g). Thus, considering all the advantages and limitations of the approach, this was used as a readout to assess the possible involvement of Gal-1 in the formation of inhibitory presynaptic terminals by SST interneurons (Fig. 6.5 a). We found that GAD65 bouton density did not significantly change in layer I (WT, 11.36±0.76 bout/100 µm^2; *Lgals1* KO, 11.06±0.93 bout/100 µm^2; Fig. 6.5b, c, d). No differences were found either when comparing the number of boutons apposed to Geph-containing postsynaptic densities, which are putative mature boutons (WT, 3.32±0.92 bout/100 µm^2; *Lgals1* KO, 2.82±0.81 bout/100 µm^2; Fig. 6.5e, f, g). Beyond the number of boutons, Gal-1 could be affecting other synaptic properties that affect the size or GAD65 intensity of these boutons. Yet, no differences were found in these two variables (Fig. 6.5k, l). However, the small population of Gal-1 positive terminals within the GAD65 population could compromise our resolution to detect any potential phenotype.

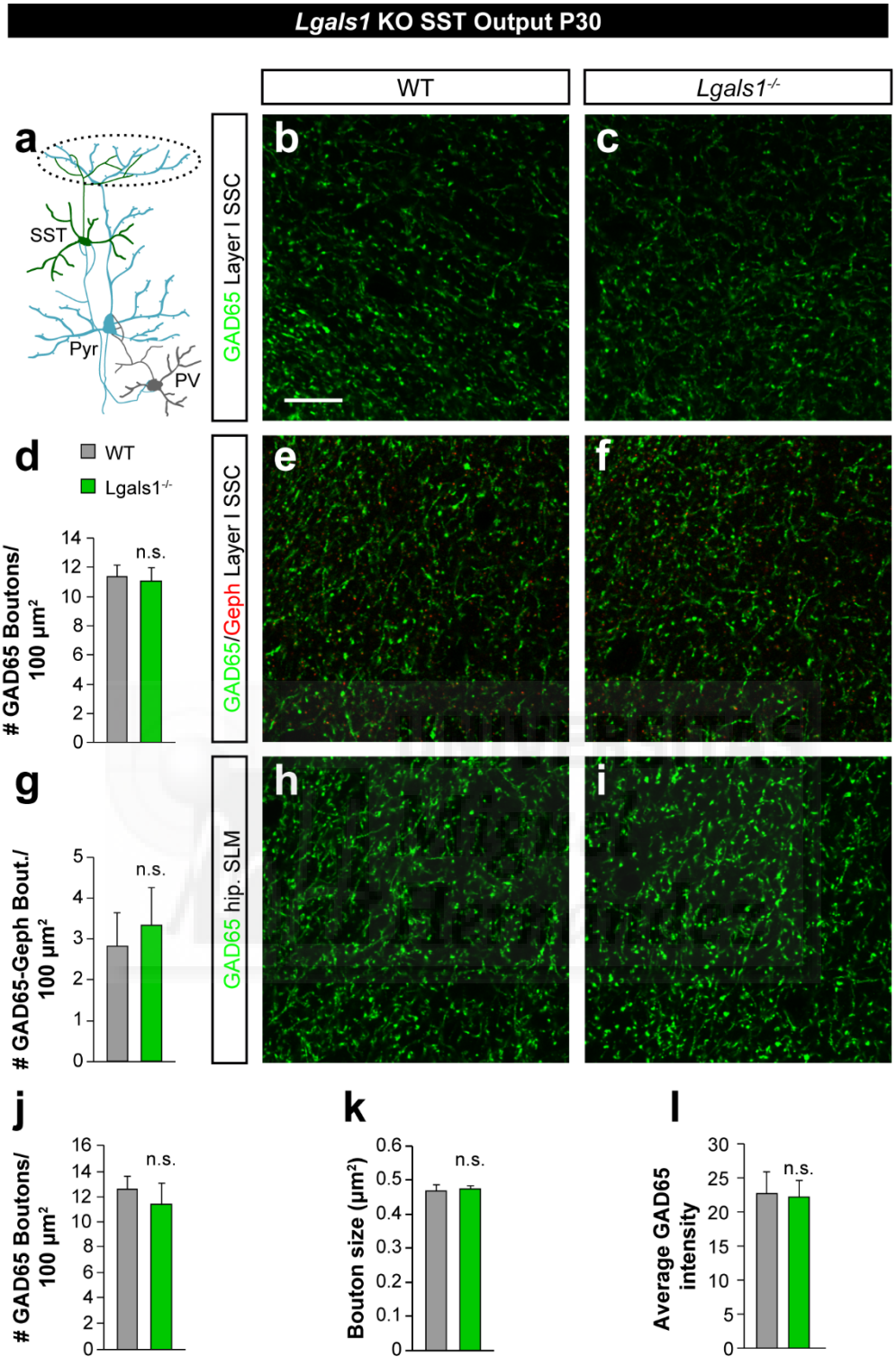

Figure 6.5. Synaptic output of SST cells in *Lgals1* KO mouse. (a) Schematic of the circuitry involving Gal-1. The dashed ovoid indicates the synapses analysed in this experiment: SST cell output in layer I of SSC. (b,c) Single confocal planes showing GAD65 staining in Layer I of SSC in *Lgals1* KO and WT mice at P30. (d) Density of GAD65 boutons in 100 µm^2 of layer I neuropil. P=0.713. (e, f) Same as in (b,c) adding Gephrin (red). (g) Same as in (d) with boutons colabelled with GAD65 and Geph. P=0.698. (h,i) Same as in (c,d) in hippocampus SLM. P=0.563. (j) Same as in (d) in SLM. P= (k) Size of the boutons labelled with GAD65 in layer I SSC. P=0.739. (l) Average intensity of the boutons labelled with GAD65 in layer I SSC.

(legend from figure 6.5) P=0.903. Scale bar: 10 µm. T-test. n.s. not significant. N= 5 and 6 brains for WT and *Lgals1* KO respectively. Data are expressed as mean±s.e.m.

In the hippocampus, OLM cells are Somatostatin interneurons located in the stratum oriens that have a similar connectivity to Martinotti cells in the cortex. As Martinotti cells sent their axons to layer I, the OLM cells target the stratum lacunosum moleculare (SLM), where there was a high density of GAD65 boutons (Fig. 6.5h, i). Moreover, Gal-1 is expressed in 80% of SST cells in hippocampus (Bischoff, Deogracias *et al.*, 2012). The percentage of GAD65 boutons that are SST positive and/or Gal-1 positive in the SLM of the hippocampus is higher than in somatosensory cortex layer I (49.31±3.32% and 33.85±1.97% of GAD65 boutons are SST positive or Gal-1 positive, respectively; Fig. 6.4e, f, g). Thus, we conducted the same analysis carried out in cortical layer I in hippocampus SLM, where a higher proportion of Gal-1 putative dependent boutons can be analysed. However, no difference was found in the number of boutons (Fig. 6.5h, i, j). These results suggest that inhibitory output provided by SST cells do not require Gal-1 to be formed.

6.4.2. Somatostatin cell input

We next examined whether Gal-1 was contributing to the formation of the synaptic input received by SST interneurons. First, we assessed excitatory synapse formation by quantifying the number of VGlut1 boutons apposed to the soma of SST expressing cells. We found no difference in synaptic density between *Lgals1* KO and WT mice (WT, 25.05±1.74 bout/100 µm; *Lgals1* KO, 26.19±1.25 bout/100 µm; Fig. 6.6b, c, d). Since Gal-1 was only expressed in a subpopulation of SST^+ cells, we analysed the distribution of the synaptic density frequencies. However, frequencies remained also unaltered in Gal-1 deficient mice (Fig. 6.6h).

SST cells receive mainly inhibitory input from VIP cells (Pfeffer *et al.*, 2013) that express GAD65 (Xu and Callaway, 2009). To evaluate the effect of Gal-1 deficiency in the formation of these inputs onto SST cells, we quantified their number in the soma of these cells. The density of GAD65 somatic bouton were similar in *Lgals1* KO and WT (WT, 13.74±0.86 bout/100 µm; *Lgals1* KO, 2.82±0.81 bout/100 µm; Fig. 6.6e, f, g). This data suggests that Gal-1 is not essential in the formation of neither excitatory nor inhibitory inputs in SST cells.

It is possible that our analysis in mature networks could preclude unveiling a potential developmental delay in synapse formation. For example, compensatory homeostatic mechanisms could restore the number of boutons masking early synaptic phenotypes. To overcome this problem, we assessed synaptic densities at early stages of synaptogenesis, more specifically, when the highest synaptogenetic rate was reached and a delay would be more noticeable: P10. We observed that both inhibitory outputs and excitatory inputs did not have a delay in their formation (Fig. 6.7). This further confirms that Gal-1 is not participating in synapse formation in SST interneurons.

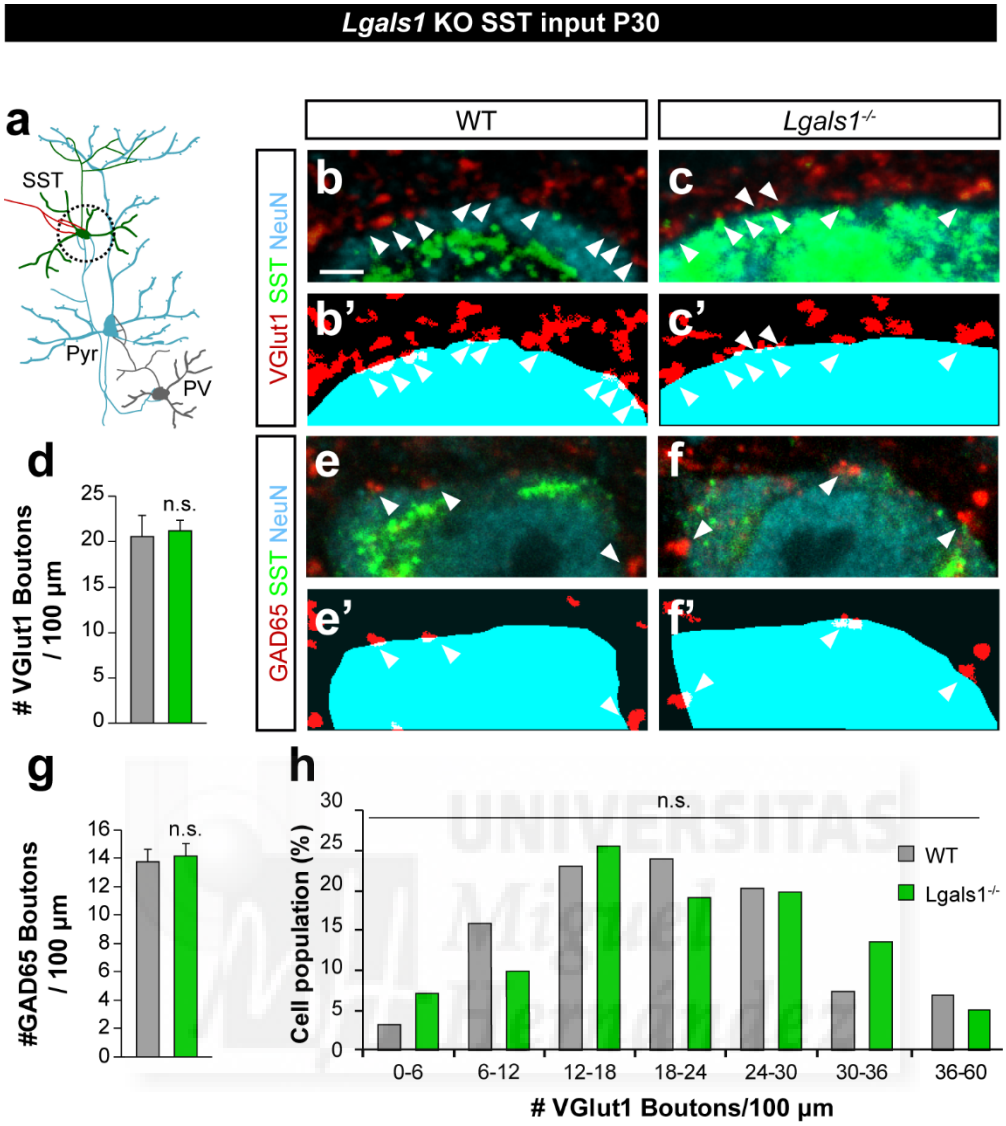

Figure 6.6. Synaptic input of SST cells in *Lgals1* KO mouse. (a) Schematic of the circuitry involving Gal-1. The dashed circle indicates the synapses analysed in this experiment: SST cell excitatory (blue axon) and inhibitory (red axon) input. (b,c) High magnification of confocal images showing VGlut1 (red) boutons apposed to SST (green) somas delimited by NeuN (cyan) in WT and *Lgals1* KO mice at P30. Apposed boutons: arrowheads. (b', c') Binary mask used for quantification. Apposed boutons: white pixels. (d) Density of apposed VGlut1 boutons in 100 µm of SST cell soma. T-test. P=0.821. (e,e', f,f') Same as in (b, b' and c, c') with GAD65 boutons (inhibitory). (g) Same as in (d) with GAD65 boutons. T-test. P=0.571. (h) Distribution of VGlut1 bouton density on SST cells in WT and *Lgals1* KO. X^2 test p=0.330. n.s. not significant. WT: n=5 brains. Lgals1 KO: n=7 brains. Scale bar: 2 µm. (d,g) Data are expressed as mean±s.e.m. (h) Data are expressed as total cell percentage.

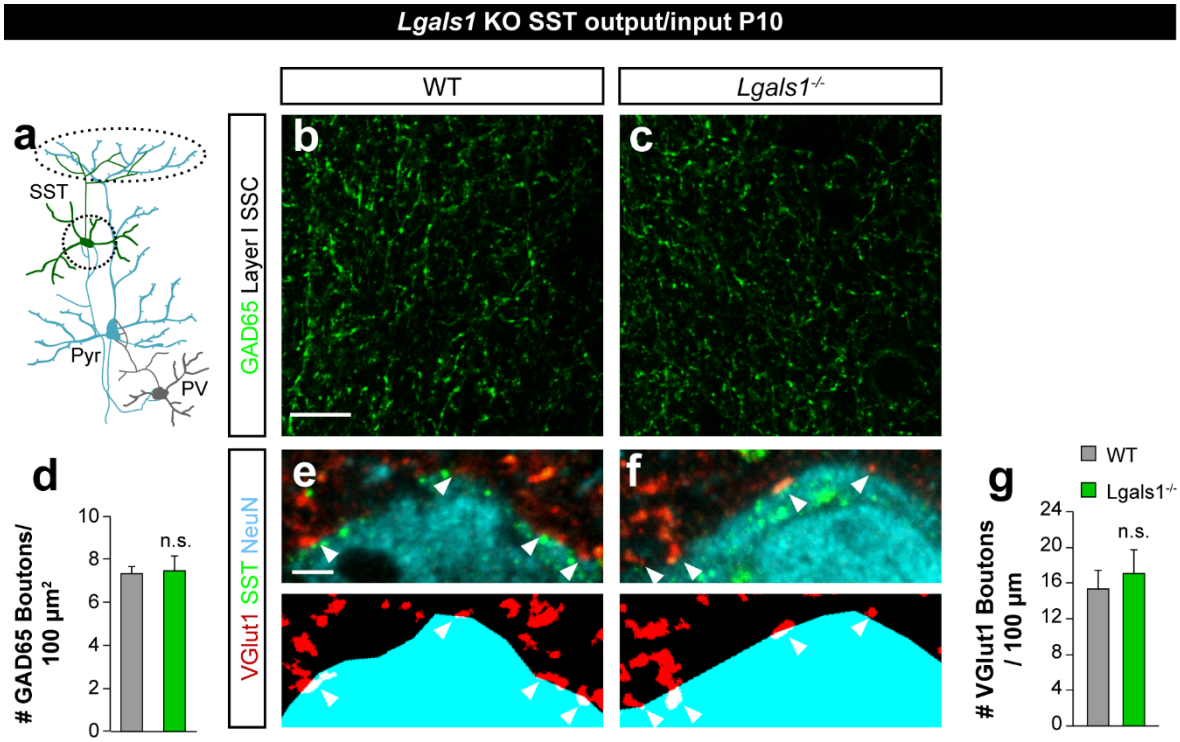

Figure 6.7. Synaptic input and output of SST cells in *Lgals1* KO mouse at P10. (a) Schematic of the circuitry involving Gal-1. The dashed circles indicate the synapses analysed in this experiment: SST cell output (upper ovoid) and excitatory input (lower circle). (b,c) Single confocal planes showing GAD65 staining in Layer I of SSC in *Lgals1* KO and WT mice at P10. (d) Density of GAD65 boutons in 100 µm^2 of layer I neuropil. P=0.865. (e,f) Top, high magnification of confocal images showing VGlut1 (red) boutons apposed to SST (green) somas delimited by NeuN (cyan) in WT and *Lgals1* KO mice at P10. Apposed boutons: arrowheads. Bottom, binary mask used for quantification. Apposed boutons: white pixels. (g) Density of apposed VGlut1 boutons in 100 µm of SST cell soma. P=0.636. Scale bars: (b,c) 10 µm, (e,f) 2 µm. T-test. n.s. not significant. N= 3 and 3 brains for WT and *Lgals1* KO respectively. Data are expressed as mean±s.e.m.

6.5. Loss of function in parvalbumin interneurons

Although the overall proportion of PV cells expressing Gal-1 is low in the cortex, they concentrate in layer VI where they become a considerable percentage (Fig. 6.2). As described for SST interneurons, there were no differences in the density of PV cells when *Lgals1* KO and WT mice were compared, indicating that migration and proliferation were not affected (Fig. 6.8a-c).

To test whether Gal-1 was involved in the formation of synaptic input and output of PV interneurons in layer VI, we followed up a similar approach to the previously performed for the somatostatin population. PV positive neurons form most of their inhibitory synapses onto pyramidal cells located in the same layer, as explained for *Nek7* experiments. Gal-1 was present in PV inhibitory boutons, labelled with the specific PV cell synaptic marker Syt2, and its distribution along cortical layers followed the distribution of PV$^+$/Gal-1$^+$ cells (Fig. 6.8d, e). Specifically, in layer VI 66% of these boutons were in a Gal-1 positive labelled area (Fig. 6.8d, e), suggesting that quantifying these boutons is a good proxy to detect presynaptic deficits in this population. We quantified Syt2 boutons onto pyramidal cell somas stained with NeuN$^+$, finding no differences in somatic synaptic densities (WT, 14.94±0.64 bout/100 µm; *Lgals1* KO, 15.96±0.73 bout/100 µm; Fig.6.9a-d). Different pyramidal cells in lower layers seem to be engaged into distinct pyramidal cell subnetworks (Vélez-Fort *et al.*, 2014). It is possible that

the inhibitory inputs targeting different pyramidal cells are also segregated. Indeed, cortico-fugal and cortico-cortical pyramidal cells seem to receive different inhibitory inputs (Bortone *et al.*, 2014; Sohal *et al.*, 2009). Therefore, one possibility is that PV positive interneurons expressing Gal-1 may innervate different population of pyramidal cells. However, when analysing the distribution of somatic synaptic densities, we did not find any differences between WT and *Lgals1* KO (Fig. 6.9e). Likewise, we did not observe any developmental deficit in the early assembly of PV outputs, since these synapses were not altered by the loss of Gal-1 at P10 (WT, 7.77±0.60 bout/100 µm; *Lgals1* KO, 8.01±0.35 bout/100 µm; Fig. 6.9f-g). These results confirm that Gal-1 is not participating in inhibitory presynaptic terminal formation.

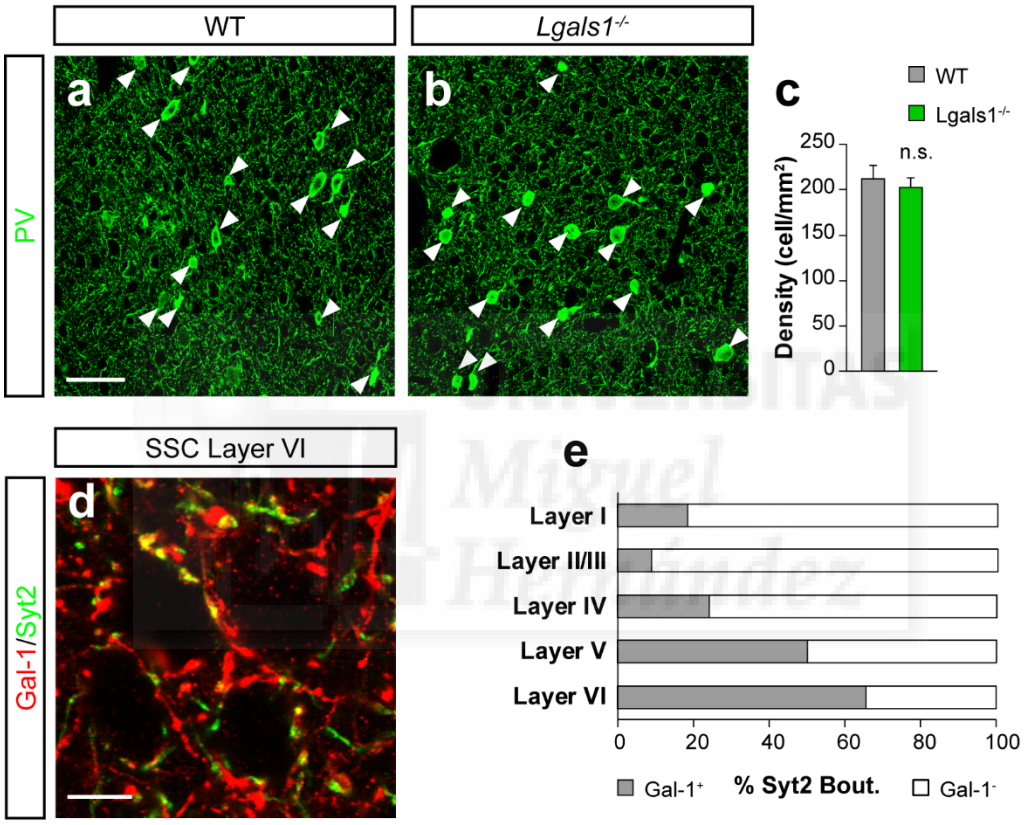

Figure 6.8. PV cell density in *Lgals1* KO and WT mice. (a,b) Single confocal images showing PV staining in SSC layer VI of *Lgals1* KO and WT mice. Filled arrowheads: PV cells. (c) SST cell density in all cortical layers. N=4 and 5 WT and *Lgals1* KO brains respectively. (d) Single confocal plane colocalizing Gal-1 particles (red) with Syt2 (green) in SSC layer VI of C57BL/6 mice. (e) Percentage of Gal-1 particles colocalizing with Syt2 across cortical layers. T-test. n.s. not significant P=0.604. (c) Data are expressed as mean±s.e.m. (e) Data are expressed as percentage of n=1. Scale bars: (a,b) 50 µm, (c) 10 µm.

Finally, we assessed the possible involvement of the protein in the formation of excitatory synapses onto PV interneurons. Similar to the results shown for SST interneurons, VGlut1 bouton somatic densities or frequency distribution onto PV cells remained unaltered in *Lgals1* KO (WT, 33.83±1.16 bout/100 µm; *Lgasl1* KO, 35.66±1.32 bout/100 µm; Fig. 6.10a-e). Another synaptic target of PV interneurons are other PV expressing cells (Pfeffer *et al.*, 2013). Different genes may be necessary presynaptically to reach different synaptic targets, namely, Gal-1 could be involved in the formation of synapses that target other PV interneurons specifically. To test this hypothesis, we counted the number

of Syt2 boutons onto PV cell somas. Yet, there was no difference in somatic bouton densities between control and mutant mice (WT, 14.25±0.95 bout/100 µm; *Lgals1* KO, 15.67±0.91 bout/100 µm; Fig. 6.10f-h).

Altogether, these results demonstrate that Gal-1 is not required for the wiring of SST or PV cells, the main population expressing the gene.

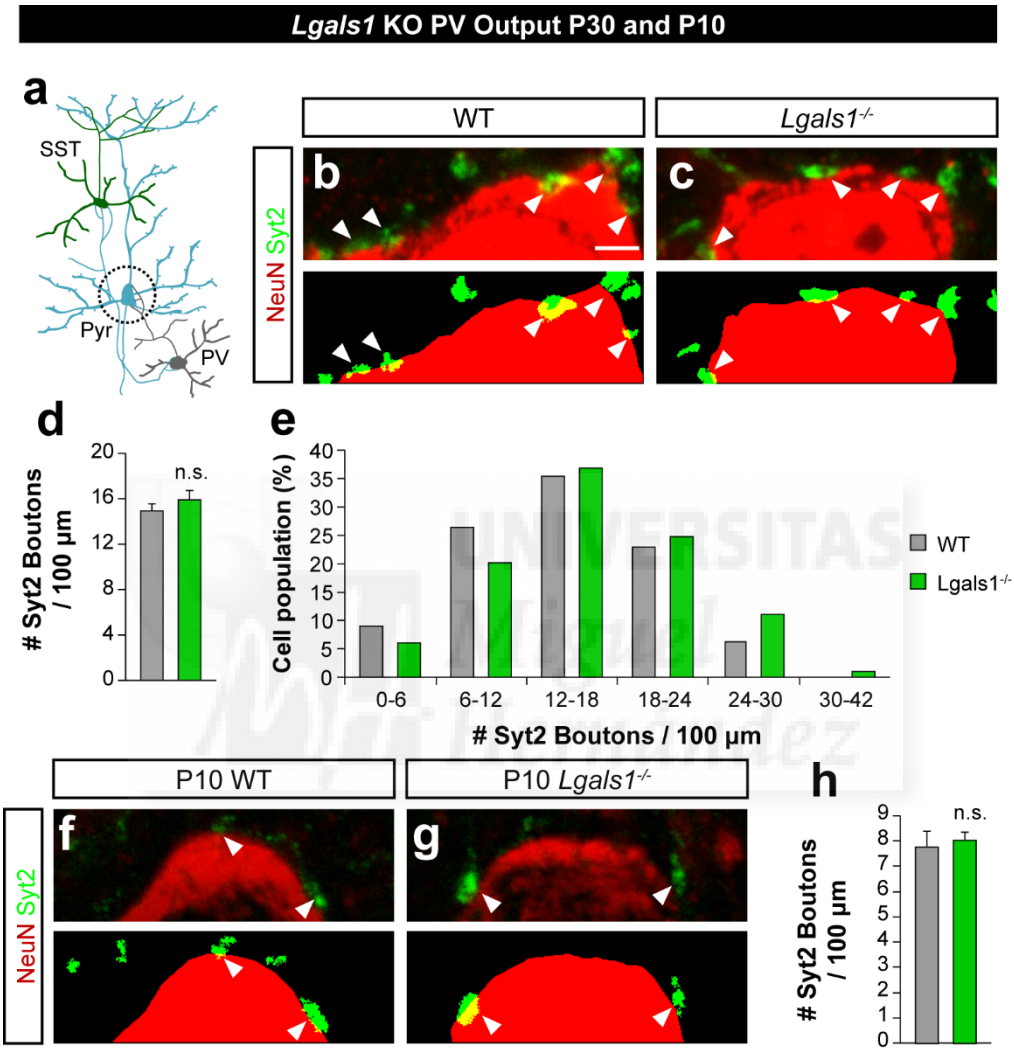

Figure 6.9. Synaptic output of PV cells in *Lgals1* KO mouse. (a) Schematic of the circuitry involving Gal-1. The dashed circle indicates the synapses analysed in this experiment: PV cell output onto Pyramidal cell soma. (b,c) Top, high magnification of confocal images showing Syt2 (green) boutons apposed to somas delimited by NeuN (red) in WT and *Lgals1* KO mice at P30. Apposed boutons: arrowheads. Bottom, binary mask used for quantification. Apposed boutons: yellow pixels. (d) Density of apposed Syt2 boutons in 100 µm of SST cell soma. T-test, P=0.340. N=5 and 7 WT and *Lgals1* KO brains respectively. (e) Distribution of Syt2 bouton density on SST cells in WT and *Lgals1* KO. X^2 test p=0.759. (f, g) Same as in (b, c) at P10. (h) Same as in (d) at P10. P=0.378. N=4 and 3 WT and *Lgals1* KO brains respectively. Scale bar: 2 µm. n.s. not significant. (d,h) Data are expressed as mean±s.e.m. (e) Data are expressed as total cell percentage.

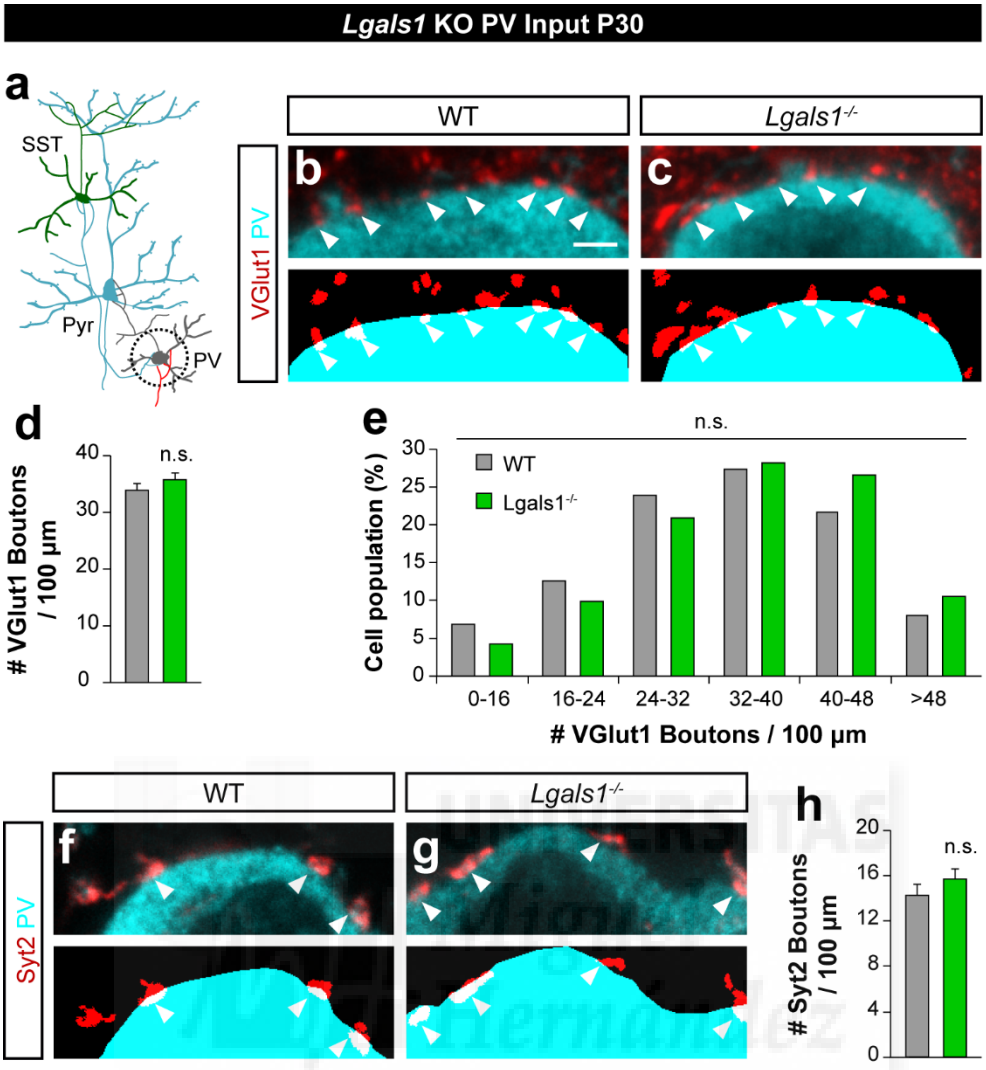

Figure 6.10. Synaptic input of PV cells in *Lgals1* KO mouse. (a) Schematic of the circuitry involving Gal-1. The dashed circle indicates the synapses analysed in this experiment: PV cell excitatory (blue axon) and inhibitory (red axon) input. (b, c). Top, high magnification of confocal images showing VGlut1 (red) boutons apposed to somas delimited by NeuN (cyan) in WT and *Lgals1* KO mice at P30. Apposed boutons: arrowheads. Bottom, binary mask used for quantification. Apposed boutons: white pixels. (d) Density of apposed VGlut1 boutons in 100 µm of SST cell soma. T-test. P=0.325. (e) Distribution of VGlut1 bouton density on SST cells in WT and *Lgals1* KO. X^2 test p=0.886. (f, g) Same as in (b,c) with Syt2 boutons (inhibitory). (h) Same as in (d) with Syt2 boutons. T-test. P=0.313. Scale bar: 2 µm. n.s. not significant. N=6 and 7 WT and *Lgals1* KO brains respectively. (d,h) Data are expressed as mean±s.e.m. (e) Data are expressed as total cell percentage.

7. DISCUSSION

Pyramidal cells and interneurons form their synapses through a series of partly differential events that include targeted axonal pathfinding. While glutamatergic axons are rather straight and form their synapses through the extension of protrusions, GABAergic axonal paths are more tortuous and form a greater number of crossings with their synaptic targets (Huang *et al.*, 2007; Stepanyants *et al.*, 2004; Wierenga *et al.*, 2008). This suggests that GABAergic axons look for their synaptic targets more actively when growing. However, little is known about the molecular mechanisms that generate such divergence. In the present study, we carry out for the first time a high-throughput screening for genes differentially upregulated during synaptogenesis in both populations. We found that Nek7, a kinase involved in microtubule polymerization, is specifically expressed in a high proportion of PV cells during synaptogenesis. Interestingly, Nek7 specific elimination from PV interneurons causes a decrease in the number of synaptic boutons they form onto pyramidal cells, as well as a reduction in the size of their neuritic arbour *in vivo*. When grown *in vitro*, Nek7 lacking axons show a more meandering path. Conversely, no synaptic deficits were found when removing Gal-1, another gene found in the screening that is expressed by PV and SST interneurons. Altogether, these data show that our screening is able to identify molecules differentially involved in GABAergic interneuron wiring. Moreover, Nek7 findings suggest that the kinase may be involved in a singular molecular mechanism by which PV interneuron axons guide their growth through the formation of synapses.

7.1. Identification of genes upregulated during GABAergic synapse formation

GABAergic interneurons have important roles in many cognitive cortical functions (Tremblay *et al.*, 2016). Furthermore, increasing evidence suggests that GABAergic neurotransmission is linked to several neurodevelopmental disorders (Dani *et al.*, 2005; Levitt, 2005; Lewis *et al.*, 2005; Marín, 2016; Rubenstein and Merzenich, 2003; Ting *et al.*, 2011). Consequently, factors that affect the development of interneurons are of special relevance for both understanding how circuits that allow high cognitive functions are formed, and for shedding some light on the aetiology of psychiatric disorders. Synapse formation during postnatal development is one of the most essential processes in brain circuit wiring. Previous studies *in vitro*, have tried to identify selected genes for their specific involvement in GABAergic synapse formation but the high number of available genes that can be tested made it difficult to have a complete picture of the whole set of genes that mediate this process (Paradis *et al.*, 2007). Here we carried out a novel high throughput genetic screening searching for genes involved in GABAergic synaptogenesis, focusing mainly in specific genes that are not mediating glutamatergic synapse formation. This analysis discloses a gene set formed by 140 genes that are specifically expressed in interneurons and upregulated during synapse formation. GO analysis of this gene set revealed cellular compartments and biological processes related to synaptogenesis confirming the validity of our approach. A final ranking of the genes by a non-biased criteria highlighted new genes that could be participating in synaptogenesis. Interestingly, one of the first genes in the list, Nek7, was proven to have a role in synapse formation in this study. These results support the validity of our approach to identify GABAergic synaptogenic genes and provide a solid database to further expand the analysis to new research avenues, e.g. specific Glutamatergic synaptogenic genes.

7.1.1. GABAergic and glutamatergic synapse formation time course

Previous studies had assessed how the number of GABAergic and glutamatergic synapses changes along development in mouse cortex (De Felipe *et al.*, 1997; Gozlan and Ben-Ari, 2003) using electron microscopy or functional studies. Electron microscopy quantification is based on the presence of morphologically defined symmetric (glutamatergic) or asymmetric (GABAergic) synapses, requiring the synapse to be mature to be identified. Our experimental approach using the accumulation of presynaptic markers to analyse the number of inputs is able to identify synapses in earlier stages of synapse formation. This, together with the increase in time resolution, make our approach more suitable to identify when there is the first increase in synapse formation and thus in the expression of synaptic genes involved in the wiring process. Both studies consistently identify a remarkable increase during the first postnatal weeks in synapse formation. However, while a slightly earlier increase is found in glutamatergic synaptogenesis compared with GABAergic using electron microscopy, we found the opposite sequence (De Felipe *et al.*, 1997, Fig. 4.1). It is important to mention that our study does not assess the development of functional synapses. Functional GABAergic connections already seem to be present as early as P3, however, they function as excitatory at these early stages (Agmon *et al.*, 1996; Ben-Ari, 2002; Gozlan and Ben-Ari, 2003; Pangratz-Fuehrer and Hestrin, 2011). In Gozlan 2003, they find, consistently with our study, that GABAergic synapses form before glutamatergic synapses. The discrepancy between these results and the results seen by electron microscopy may be also due to temporal differences between the initial stages of synapse formation and the latest stages of morphological differentiation.

7.1.2. Microarray data analysis

Our main analysis focused on genes specific for GABAergic interneurons that are upregulated during synapse formation. We obtained 140 genes that were matched with the available literature using databases like GO and subsequently ranked by population specificity, expression levels and cell densities.

GO identified different ontological terms that can be grouped in two main clusters: axon/presynapse and extracellular matrix. Both clusters contain plausible genes that can play a role in synapse formation. Indeed, genes encoding proteins that are present in the axon and, more specifically, in the presynaptic terminal are ideal candidates to contribute to synaptogenesis. Also, several extracellular matrix proteins have been associated with synapse formation (Dityatev and Schachner, 2006; Paradis *et al.*, 2007). Thus, our screening design has generated a solid database to search for genes involved in the wiring of cortical neurons. Each of the tested genes in our top gene set belong to one of these two clusters and as expected one of them, Nek7, is playing a role in axon development and GABAergic synapse formation.

Several GO biological process terms were specially enriched in the gene set as well. Linked with interneuron role in the cortex (Tremblay *et al.*, 2016), we find many GO terms related to cognitive function. The other big cluster that can be defined with GO is neurotransmission where, interestingly, we find many genes involved in neuropeptide signalling also found with KEGG and Reactome. Altogether, these data confirm that GABAergic interneurons use this type of transmission more than pyramidal cells as previously shown (Baraban and Tallent, 2004).

Finally, some molecular processes were identified with GO. Interestingly, GO highlighted 3 genes related to the Wnt pathway, a signalling cascade that has been extensively linked with synapse formation before (Ahmad-Annuar *et al.*, 2006; Hall *et al.*, 2000; Scheiffele, 2003). Many other genes were related to the synthesis of sulphur components, like glutathione, which are related to oxidative stress (Yang *et al.*, 2002). This is likely consistent with the high metabolisms of interneurons, in particular parvalbumin cells that are susceptible to oxidative stress (Hu *et al.*, 2010; Powell *et al.*, 2012). The relevance of these GO terms is of limited relevance given their low p-value and, in the case of sulphur compounds, the broad spectrum of processes that the genes may be mediating.

The potential of the generated data set has not been fully exploited in this thesis. For example, it would be very interesting to explore in the future: specific genes involved in glutamatergic synaptogenesis, common mechanisms between GABAergic and glutamatergic synapse formation or genes downregulated during these processes. Furthermore, genes expressed in both populations that are differentially mediating synapse formation could be found. An example of this kind of differential mechanisms is mediated by Npas4, a transcription factor that is expressed by both pyramidal cells and interneurons but activates distinct transcriptional programs in each cell type (Lin *et al.*, 2008; Spiegel *et al.*, 2014).

7.2. Role of the kinase Nek7 in parvalbumin interneuron wiring

Our experimental approach has been able to identify a novel role for the protein Nek7 in axonal development and synapse formation that is specific for interneurons. Nek7 depletion causes an impairment in PV cell synapse formation and a change in their putative axonal spatial distribution *in vivo*. Previous studies have shown that axonal arbors are stabilized by the formation of synapses (Meyer and Smith, 2006). Interestingly, we found that axonal pathfinding is altered in Nek7 knockdown, suggesting that a deficit in synaptogenesis might preclude synaptic stabilization and as consequence the formation of a normal axonal arbor. Alternatively, a misrouted axon could lose the precise window of time for synapse formation and fail to reach the proper target.

7.2.1. Developmental time course of Nek7 expression

Using a high throughput screening we found that *Nek7* is a kinase specifically expressed in interneurons and upregulated during GABAergic synaptogenesis. These data were further confirmed by qPCR showing that the microarray data is reliable (Fig. 5.1a). Detection of *Nek7* transcript levels at more time points showed a growing curve that resembles that of synaptic proteins like GAD65 (Fig. 4.1c and Fig. 5.1). After the first postnatal weeks, *Nek7* levels increase up to the end of synapse formation, P30. This developmental increase matches with the increment in mature synapses number that has been observed using electron microscopy (De Felipe *et al.*, 1997).

Although the main phenotype described in our study points out a role of Nek7 in neuritic arborisation and synapse formation, it is possible that the kinase plays an additional role after the wiring of these interneurons. Indeed, most of the proteins involved in synaptogenesis keep their expression levels during adulthood to mediate synaptic maintenance like Nrg1/ErbB4 (Barros *et al.*, 2009). Nek7 might also be present in the synapse after postnatal development to participate in synaptic maintenance.

7.2.2. Nek7 is expressed by PV and SST interneurons in the cortex

Several studies has previously detected *Nek7* transcript in the brain (Feige and Motro, 2002) as well as the protein in dentate gyrus (Li *et al.*, 2014). Moreover, recent high throughput transcriptional analysis in single cells show that Nek7 is expressed in virtually all PV interneurons and in some SST cells (Tasic *et al.*, 2016). We studied the precise layer localization of *Nek7* and its overlap with several interneuron markers, finding that 60% of PV and 25% of SST interneurons express the transcript. However we did not find any expression of Nek7 in the dentate gyrus using in situ hybridization or the same antibody used before to localize Nek7 in the hippocampal areas, suggesting that the previously reported expression in the dentate gyrus may be unspecific.

The differences found in the PV population expressing Nek7 transcript in our study and Tasic *et al.*, could be explained by the low sensitivity of *in situ* hybridization (present study), compared to single cell sequencing (Tasic *et al.*,). Therefore, we would be able to detect just those cells with higher *Nek7* levels. The existence of PV cells with different levels of *Nek7* suggests that further functional differences could exist between these two interneuron populations. Alternatively, PV cells could vary *Nek7* transcript levels according to their immediate needs.

Since PV and SST have been described as not overlapping populations in the neocortex (Rudy *et al.*, 2011), Nek7 population would be composed by 80% PV cells and 10% SST cells. The remaining 10% can account for cells expressing other markers or, more probably, for cells expressing low levels of PV or GFP (*SstCre;RCE:loxP)* not detected due to the stringent experimental conditions in the in situ hybridization protocols. We found that a small population of GFP positive cells (4%) is co-stained with PV in lower layers (Data not shown). It is possible that some of the SST (GFP) positive cells may have expressed SST at some point and switched on the expression of GFP. However, the proportion of SST cells expressing *Nek7* is higher and must reflect a real expression of the transcript in this interneuron population.

It is plausible that interneurons expressing Nek7 share some morphological features. Interestingly, the majority of the Parvalbumin interneurons are basket cells and 21% of SST positive cells have also a basket like morphology in the cortex (Jiang *et al.*, 2015). Nek7 may be required for a specific basket morphology that is common between PV basket cells and SST but differ from other basket populations, like the CCK expressing basket cells. It would be interesting to test this hypothesis in the future.

7.2.3. Loss of Nek7 impairs PV interneuron inhibitory synapse formation

Nek7 depletion with shRNA causes a reduction in the number of inhibitory somatic boutons formed by PV interneurons onto pyramidal cells. The decrease in synaptic terminals was confirmed by a reduction in bouton density of PV cell axons. Therefore, Nek7 is involved in synapse formation independently of axonal length. Nek7 main known molecular roles are the formation of microtubule-based structures and the regulation of microtubule dynamics (Bajar *et al.*, 2016; Cohen *et al.*, 2013; O'Regan and Fry, 2009; Salem *et al.*, 2010; Yissachar *et al.*, 2006). Interestingly, synaptic architecture and function are sensitive to changes in microtubule dynamics. Proteins like *futsch,* that is involved in the formation of a microtubule loop in the neuromuscular junction of *Drosophila melanogaster*, also

affect the formation of these synapses (Roos *et al.*, 2000). Thus, Nek7 may be participating in synapse formation through the regulation of microtubule dynamics.

We also found that the GABAergic synaptic deficit observed in pyramidal cells is somehow compensated by other non-targeted wildtype PV cells contacting them. We ignore whether such compensation comes from other PV cells that have kept their expression of Nek7 or from cells that express low levels of Nek7. Although it was thought that the inhibition of interneurons onto pyramidal cells was homogeneous (Fino *et al.*, 2013), many studies have shown that there is a preference for inhibiting specific pyramidal cell subsets across or within different layers; this has been shown particularly in layer V (Hilscher *et al.*, 2017; Lee *et al.*, 2014; Ye *et al.*, 2015). One possibility is that different populations of PV cells are targeting distinct pyramidal cell subnetworks providing to them different levels of inhibition. It is very appealing to hypothesize that Nek7-expressing PV cells could be assembling specific pyramidal cell subnetworks. The lack of Nek7 in PV cells depending on the kinase might be triggering a compensation for the synaptic loss from Nek7 intact cells. Conversely, if the connectivity between PV and pyramidal cells is not specific the compensation may be emerging from any other PV cell. The identification of specific features confined to Nek7 positive cells will be key to understand not only their contribution to the circuit but the compensatory mechanisms by which PV interneurons contribute to form subnetworks.

The nature of our screening make it possible to identify molecules that can be potentially involved in formation of both postsynaptic and presynaptic compartments. However, the possible postsynaptic role of Nek7 in PV interneurons was not assessed in the present thesis project and future experiments should address this question. Moreover, Nek7 may have a similar synaptogenetic role in the 25% of SST cells expressing the kinase. Although this population is small, they could have specific features that differentiate them from the not expressing Nek7 interneurons.

7.2.4. Loss of Nek7 alters PV interneuron arborisation *in vivo*

A change in microtubule dynamics can alter axon development (Conde and Cáceres, 2009). A member of the Nek family, Nek3, was proven to be involved in axonal formation (Chang *et al.*, 2009) and Nek7 may be exerting a similar function by accelerating microtubule dynamic instability (Cohen *et al.*, 2013). We found that Nek7 knockdown alters PV interneuron neuritic arbour extension. This alteration is not explained by differences in neurite length, branching points or path tortuosity (Fig. 5.8). However, the complexity of interneuron morphologies makes these averaged variables insufficient to be able to grasp fine differences and see how these are related among them ((Petilla Interneuron Nomenclature Group *et al.*, 2008).

The diversity of PV interneurons in layer V raises the question of whether the observed change in neuritic extension takes place in all PV interneurons or just in a subset of morphologically defined cells. The actual classification method for interneurons is merely empirical and more unambiguous criteria are needed to define the diverse morphological classes (De Felipe *et al.*, 1997). For example, using the current criteria is very difficult to classify cells whose morphology have been altered, like Nek7 knockdown neurons. Many more unbiased variables could be analysed by using recent algorithms that allow to compare tridimensional neuronal reconstructions among them (Costa *et al.*, 2016). This would allow to cluster cells by their morphological tree, *e.g.* to distinguish whether a given PV morphological type has its arbour altered by Nek7 loss.

As stated above, the deficient neuritic arbour observed in PV interneurons lacking Nek7 in our study cannot be the only cause of the synaptic phenotype found since a decrease of the synaptic density is found along the axon. Nonetheless, this does not necessarily prove that both phenotypes are completely independent. Although arbor structure and synapse formation could be independent events (Alsina, Cohen-Cory 2001), several studies have shown that synaptogenesis promote the stabilization of extending axonal processes (Meyer and Smith, 2006). Since microtubules have a central role in axon guidance (Geraldo and Gordon-Weeks, 2009), it is tempting to speculate that this kinase could be a molecular player mediating the stabilization of axonal growth cones by synapse formation.

7.2.5. Loss of Nek7 affects axonal growth cone dynamics *in vitro*

We attempt to prove this hypothesis by analysing interneuron growth cone dynamics using time-lapse imaging. Nek7 depleted cells have growth cones that move faster but their growth rate is not altered (Fig. 5.10). Two well-differentiated processes can be distinguished in axon guidance: growth cone turning, where the axon is sensing the neighbouring cues, and growth cone advance (Geraldo and Gordon-Weeks, 2009). Hence, the observed dynamics in Nek7 knockdown can be interpreted as an increase in growth cone turning but no alteration in the progression of the growth cone. There are some limitations to these experiments. First, the Cre expressing cells in *Lhx6Cre* mouse include PV cells, however, we cannot distinguish them from the SST population since they do not express PV at this stage. Our analysis on the cell distribution of path lengths shows that just a subpopulation of the imaged cells are affected by loss of Nek7, suggesting that only the Nek7 dependent interneurons, most of which are putatively PV, exhibit impaired axonal dynamics (fig. 5.10f). Further studies will need to confirm that the Nek7 dependent population is indeed PV positive.

7.2.6. Concluding remarks

Growth cone motility is associated with the extension of filopodia and lamellipodia. Filopodia are one of the main structures responsible for axonal detection of guidance cues by making the growth cone turn or grow in response to them. These events are mediated by the interaction between dynamic microtubules and actin filaments in the filopodia (Geraldo and Gordon-Weeks, 2009). By controlling microtubule dynamics, Nek7 might be regulating the axonal response to these guidance cues orchestrating axonal turning. *In vitro* manipulation of Nek7 levels in interneurons disrupts this process. *In vivo*, the axon could be misguided affecting its final arborisation. However, axonal growth would not be altered and its total length would remain unchanged.

Interestingly, the alteration in axonal pathfinding might be closely linked to synapse formation. Since synapse formation stabilizes growing axons, Nek7 depleted cells may have difficulties finding their proper path due to an impaired synapse formation. Guidance molecules like semaphorins, netrins or ephrins could be mediating this mechanism (Paradis *et al.*, 2007). Molecules, like Sema4d, that stimulate axonal outgrowth (Masuda *et al.*, 2004) are also involved in synapse formation (Paradis *et al.*, 2007). Interestingly, two semaphorins (Sema5a and Sema3c) are present in our screening as differentially expressed genes in interneurons at the time of synapse formation. These or others guidance molecules might be upstream of Nek7 mediating synapse formation and axonal turning.

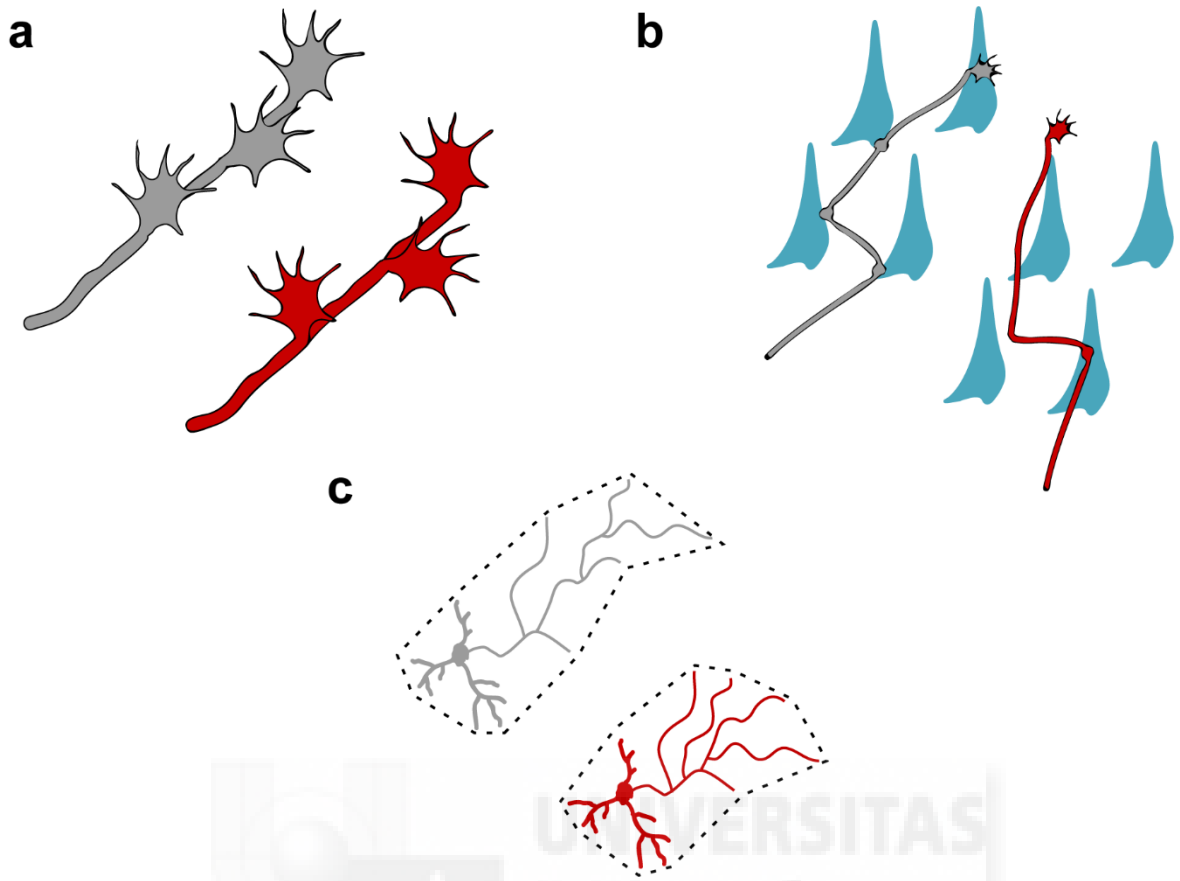

Figure 7.1. Summary and model of alterations in Nek7 knockdown. (a) Growth cones with reduced levels of Nek7 (red) make more turnings while keeping a normal growth rates compare to controls (grey). (b) Axons form less synapses than in normal conditions what may alter their normal paths. (c) Consequently, Nek7 depleted cells have a smaller axonal arbour.

The molecular mechanisms, by which Nek7 mediates microtubule dynamics in PV interneurons and as consequence axonal pathfinding, remain to be investigated. One plausible candidate mediating this process is γ-tubulin that localizes at the centrosome and interacts with Nek7 (Kim *et al.*, 2007). During neuron maturation, the centrosome loses its microtubule nucleating capacity but γ-tubulin still nucleates microtubules (Sánchez-Huertas *et al.*, 2016). Consistent with this idea, loss of γ-tubulin alters axonal arborisation *in vitro*. Although there are prominent differences between both studies, Nek7 could be mediating axonal pathfinding through γ-tubulin in interneurons. Alternatively, the plus-end-directed motor protein Eg5 has a role in axonal growth and is phosphorylated by Nek6, closely related to Nek7 (Bertran *et al.*, 2011; Myers and Baas, 2007). Nek7 could thus phosphorylate Eg5 and exert its effect in the growth cone through this kinesin.

The specificity of Nek7 expression in interneurons implies that the suggested mechanism should not be found or, alternatively, it should be differently mediated in pyramidal cells. As opposed to glutamatergic axons, GABAergic axonal paths are more tortuous and form a greater number of crossings with their synaptic targets (Huang *et al.*, 2007; Stepanyants *et al.*, 2004; Wierenga *et al.*, 2008), suggesting that GABAergic axons look for their synaptic targets more actively when growing. Given the data shown in this study, we propose a differential mechanism by which GABAergic axons stabilize their axonal paths through the formation of synapses mediated by microtubules. In order to

prove this model, differences in growth cone and microtubule dynamics must be analysed in pyramidal cells and compared with GABAergic interneurons. Furthermore, exogenous expression of Nek7 in pyramidal cells would give us information about how the protein can alter pyramidal cell axon or microtubule dynamics.

Previous studies have unveiled molecular processes that mediate both synapse formation and arborisation in PV basket cells (Berryer *et al.*, 2016; Chattopadhyaya *et al.*, 2007, 2013; Wu *et al.*, 2012). NCAM depletion during somatic synapse formation alters the formation of synaptic boutons and axonal branching (Chattopadhyaya *et al.*, 2013). Conversely, GABA release blockade not only increases bouton and axonal density in fixed tissue but also increases bouton stability and filopodia density in live imaging experiments. Thus, Nek7 might share common signalling pathways with NCAM or GABA to exert its effect.

The alteration of basket cell circuitry have been shown to be linked to cognitive deficits in several studies (Berryer *et al.*, 2016; Del Pino *et al.*, 2013). On the one hand, depletion of the Ras GTPase-activating protein SYNGAP1 reduces the formation of somatic boutons in PV basket cells (Berryer *et al.*, 2016), reducing inhibitory synaptic activity, cortical gamma oscillations and causing cognitive deficits (Berryer *et al.*, 2016). On the other hand, lack of *Erbb4* reduces the number of excitatory boutons formed onto basket and chandelier cells, reduces gamma band oscillations and impairs cognitive function (Del Pino *et al.*, 2013). These effects recapitulate pathophysiological features of schizophrenia because gamma band oscillations and cognitive functions are altered in this disease (Marín, 2012). Therefore, a cellular specific mechanism involving basket cells is thought to be linked with schizophrenia aetiology. Nek7 might also be participating in the formation of functional basket cell circuits to hold normal cognitive functions. Other neurodevelopmental disorders, like autism spectrum disorders (ASD) or intellectual disabilities, may not be cell specific but be a result of an imbalance between excitation and inhibition (Marín, 2012). Nek7 might contribute to keep this balance in PV cells. Further experiments are necessary to clarify the possible role of Nek7 in neurodevelopmental disorders and cognitive function.

7.3. Role of galectin-1 in synapse formation

In this study, we identified *Lgals1* as a gene specifically upregulated in interneurons during synapse formation. Gal-1 is located in the extracellular matrix and has been previously associated with axonal growth (Crandall *et al.*, 2000; Horie *et al.*, 1999; McGraw *et al.*, 2005; Sango *et al.*, 2004), pointing out this lectin as a good candidate to play a role in synapse formation. In particular, since Gal-1 protein is expressed in 60% of SST interneurons and 40% of layer VI parvalbumin interneurons, we explored whether the wiring of these interneurons depended on *Lgas-1* gene. However, we did not find a change in the number of the most remarkable synaptic inputs and outputs of either SST or PV interneurons. Its lack of involvement in synapse formation further suggests the presence in our screening of genes that might be involved in other processes like axon formation or neurotransmission.

7.3.1. Lgals1 expression

We found in our screening that *Lgals1* is specifically expressed by interneurons and upregulated during synapse formation in these cells. This increase is related to a higher density of cells expressing the protein from P0 to P10 (Fig. 3.1). The protein expression is kept until P30 suggesting that Gal-1 may have a role in the adult brain. Previous studies have identified the expression of Gal-1 in SST

interneurons in neocortex and hippocampus (Bischoff *et al.*, 2012; Kajitani *et al.*, 2014; Winden *et al.*, 2009). Our work confirms previous studies reporting that around 60% of the SST interneurons express Gal-1 and provides new data in neocortex showing that a small population of PV cells also contain Gal-1 protein. We found that 40% of PV interneurons express Gal-1 in layer VI. Interestingly, a similar population of PV cells located in layer VI was shown to mediate translaminar inhibition through an axonal arbour that extends up to layer I (Bortone *et al.*, 2014). Given the similar percentages, Gal-1+ PV+ population might be this translaminar population.

Around 70% of the SST expressing cells are Martinotti (Jiang *et al.*, 2015). Therefore, it is also tempting to hypothesize that Somatostatin cells classically targeting distal dendrites and PV cells from layer VI that contact distal dendrites as well have a common function in the circuitry and therefore may share some molecular programs, including *Lgas-1* gene expression. Further future experiments will be required to test this hypothesis.

A role for *Lgals1* in adult neurogenesis was previously described in the dentate gyrus (Sakaguchi *et al.*, 2006). In contrast, no changes were found neither in SST or PV cell densities in the KO (Fig. 6.7 and 6.9), suggesting that the protein is not mediating embryonic interneuron neurogenesis.

7.3.2. LOF in somatostatin and parvalbumin interneurons

SST interneurons synapse formation seems independent of Gal-1 (Fig. 6.5 and 6.7). The main limitation of our results consists on the reduced number of GAD65 boutons that originate from *Lgals1* expressing cells in layer I, conferring low resolution to our analysis (Fig. 6.4). In this area GAD65 labels synapses not only coming from all SST cells but also from any other interneuron that project to this layer (Jiang *et al.*, 2015; Wall *et al.*, 2016). Although the contribution from SST cells to the GAD65 boutons is higher in hippocampus (SLM), we observed similar results. Still, a 70% of the boutons would never be affected by Gal-1 elimination in SLM since they do not express the protein. This suggests that if any, a possible alteration in the number of these boutons would not be big enough to be detected with our approach. A further experiment labelling SST cells and quantifying synaptic boutons within the labelled axons, would be needed to get a more precise comparison.

Both the excitatory and inhibitory inputs received by SST were not altered in *Lgals1* KO. The main inhibitory input received by SST interneurons comes from bipolar and neurogliaform cells (Jiang *et al.*, 2015). Although there is no direct evidence showing that GAD65 is localized in the inhibitory boutons of these cells, both morphological types are labeled in the GAD65-GFP transgenic mouse (G30) (López-Bendito *et al.*, 2004; Xu and Callaway, 2009). This suggests that the synaptic marker used in our analysis, GAD65, is an adequate proxy to evaluate SST inhibitory input.

Similar results were observed when assessing PV interneuron inputs and outputs in layer VI. The absence of any phenotype in *Lgals1* KO can also be due to the redundancy of the protein, whose lack may be compensated by expression of *Lgals3* or, alternatively, by expression of other proteins. Gal-3 is structurally related to Gal-1 but mice lacking Gal-1 do not exhibit an increment of Gal-3 expression (Bischoff *et al.*, 2012; Hsu *et al.*, 2009). Although we cannot discard that our level of analysis does not have enough power to detect small changes in subpopulation of interneurons depending on Gal-1, we can conclude that Gal-1 is likely not involved in GABAergic synaptogenesis.

7.3.3. Alternative roles for Gal-1

The known role of Gal-1 in axonal growth and guidance and the upregulation we found in interneurons during the first postnatal weeks, suggests that the protein might be playing a similar role in interneurons (Crandall *et al.*, 2000; Horie *et al.*, 1999; McGraw *et al.*, 2005; Sango *et al.*, 2004). Gal-1 complexes with neuropilin-1 and plexinA4 (Quintá *et al.*, 2014), which have been shown to be associated with axonal growth and guidance. One possibility is that Gal-1 may be orchestrating the growth of interneuron axons towards their targets. Alternatively, since Gal-1 is present in the extracellular matrix, it could be acting in axons approaching interneurons as a guidance cue.

Beyond development, Gal-1 is still present in interneurons and it may play a specific role in these cells during adulthood. Exogenous Gal-1 increases the expression of NMDA receptor NR1 and modulates de desensitization of several AMPA and kainite receptors (Copits *et al.*, 2014; Lekishvili *et al.*, 2006). Furthermore, *Lgals1* KO mice have alterations in spatial and contextual learning (Sakaguchi *et al.*, 2011). These data suggest that Gal-1 may be playing a role in neurotransmission or neuronal plasticity in GABAergic interneurons and, consequently, in cognitive function.

A totally different role of Gal-1 consist on interneuron neurodegeneration following epileptic seizures (Bischoff *et al.*, 2012; Plachta *et al.*, 2007). Gal-1 is required for neuronal death in SST interneurons after epileptic induction. A large population of interneurons are known to die after the first two weeks of postnatal development (Southwell *et al.*, 2012). Therefore, lack of Gal-1 could preclude interneuron death during development. However, we found no difference in neither SST nor PV cell densities (Fig. 6.2 and 6.8a-c). The expression of Gal-1 during cell death may be exclusively linked to the cell response to epileptic induction but not to natural cell death. Similarly to Nek7, Gal-1 expression by GABAergic interneurons could be related to a potential role in cognitive function and neurodevelopomental disorders (Marín, 2012).

To conclude, the lack of involvement of *Lgals1* in synapse formation shows that although our high throughput screening has proven valid to identify genes involved in GABAergic synaptogenesis, like *Nek7;* genes involved in other processes are upregulated as well during this postnatal period. These other processes include axonal (and dendritic) formation and synaptic transmission. Further studies aimed at identifying Gal-1 role in the cortex will shed light on its potential function in other aspects of GABAergic interneurons development or function.

8. CONCLUSIONS / CONCLUSIONES

1. Cortical GABAergic interneurons and glutamatergic pyramidal cells undergo a transcriptional change during the first postnatal weeks (P0-P10).

2. Cortical GABAergic interneurons differentially upregulate genes that are putatively involved in synapse formation but also some that may be required for other aspects of neuronal differentiation during the first postnatal weeks. These mainly include genes involved in neurite formation and synaptic transmission, like neuropeptides.

3. *Nek7* is specifically expressed and upregulated during synapse formation in a subpopulation of GABAergic interneurons. This subpopulation includes 60% of all PV interneurons and 25% of all SST interneurons in the neocortex.

4. *Nek7* depletion causes a decrease in the number of inhibitory somatic boutons formed by PV interneurons in pyramidal cells. This decrease is observed in both synaptic compartment: a reduction in the inhibitory boutons contacting the pyramidal cells and a decrease in the synaptic density within PV cell axons. This confirms that Nek7 has a role in synapse formation that is not attributable exclusively to axonal formation.

5. *Nek7* knockdown alters the PV interneuron neuritic arbour extension *in vivo* and axonal growth cone turning *in vitro*. By altering microtubule dynamics, Nek7 might be regulating the response to guidance cues that affect axonal turning and, consequently, the formation of an adequate axonal arbour.

6. We hypothesise a differential mechanism by which GABAergic axons stabilize their paths through the formation of synapses mediated by microtubules. However, in order to prove this model, differences in growth cone and microtubule dynamics must be analysed in both interneurons and pyramidal cells. Investigating this mechanism will be key to understand the specific features of GABAergic wiring.

7. The gene *Lgals1* is specifically expressed by GABAergic interneurons and upregulated during synapse formation. This interneuron population comprises 60% of all SST interneurons and 40% of layer VI PV interneurons.

8. The absence of Gal-1, the protein encoding by *Lgals1* gene, does not affect the synaptic inputs and outputs of SST and layer VI PV interneurons. This suggests that *Lgals1* is not involved in synapse formation. However, previous studies and its upregulation during the first postnatal weeks suggest that Gal-1 may probably be involved in other aspects of interneuron maturation. Studying Gal-1 role in the cortex will shed light on the development and adult function of GABAergic interneurons.

1. Las interneuronas GABAergicas y las células piramidales glutamatérgicas sufren un acusado cambio transcripcional durante las dos primeras semanas de desarrollo postnatal (P0-P10)

2. Las interneuronas GABAérgicas regulan positivamente genes que están supuestamente involucrados en sinaptogénesis de forma diferencial, así como algunos genes que podrían ser requeridos en otros aspectos de la diferenciación neuronal durante las dos primeras semanas de desarrollo postnatal. Estos últimos incluyen principalmente genes involucrados en la formación neurítica y transmisión sináptica, como los neuropéptidos.

3. *Nek7* está específicamente expresado y regulado positivamente durante sinaptogénesis en una subpoblación de interneuronas GABAérgicas. Dicha subpoblación incluye un 60% de toas las interneuronas PV y un 25% de todas las interneuronas SST en la neocorteza.

4. La disminución en los niveles de *Nek7* produce una reducción en el número de botones inhibitorios somáticos formados por las interneuronas PV en las células piramidales. Este decremento fue observado en ambos compartimentos sinápticos: una reducción en el número de botones inhibitorios contactando a las células piramidales y una disminución en la densidad sináptica dentro de los axones de las células PV. Esto confirma que Nek7 juega un papel en sinaptogénesis que no es atribuible exclusivamente a la formación del axón.

5. La reducción de *Nek7* altera la extensión del árbol neurítico de las interneuronas *in vivo* y el giro durante el crecimiento del cono axonal *in vitro*. Mediante la alteración de la dinámica de los microtúbulos, Nek7 podría estar regulando la respuesta a señales de guía que afectan al giro del axón y, en consecuencia, a la formación de un árbol axonal adecuado.

6. Hipotetizamos un mecanismo diferencial mediante el cual los axones GABAergicos estabilizan sus rutas de crecimiento a través de la formación de sinápsis mediado por los microtúbulos. Sin embargo, con el fin de probar este modelo, las diferencias en la dinámica de crecimiento axonal y microtúbulos entre interneuronas y células piramidales deben ser analizadas. Investigar este mecanismo será clave para comprender las características específicas de la formación de circuitos GABAérgicos.

7. El gen *Lgals1* es expresado específicamente por interneuronas GABAérgicas y regulado positivamente durante sinaptogénesis. Esta población de interneuronas comprende un 60% de todas las interneuronas SST así como un 40% de las interneuronas PV de la capa VI.

8. La ausencia de Gal-1, la proteína codificada por el gen *Lgals1*, no afecta a los inputs y outputs sinápticos de las interneuronas SST o PV en la capa VI. Esto sugiere que *Lgals1* no participa en sinaptogénesis. Sin embargo, estudios previos así como sus niveles de expresión durante las dos primeras semanas de desarrollo postnatal sugieren que Gal-1 podría probablemente estar involucrada en otros aspectos de la maduración de las interneuronas. Estudiar el papel de Gal-1 en la corteza arrojará luz sobre la función de las interneuronas GABAergicas tanto durante el desarrollo como en el adulto.

9. REFERENCES

Aakalu, G., Smith, W.B., Nguyen, N., Jiang, C., and Schuman, E.M. (2001). Dynamic visualization of local protein synthesis in hippocampal neurons. Neuron *30*, 489–502.

Abe, I., Ochiai, N., Ichimura, H., Tsujino, A., Sun, J., and Hara, Y. (2004). Internodes can nearly double in length with gradual elongation of the adult rat sciatic nerve. J Orthop Res *22*, 571–577.

Aberle, H., Haghighi, A.P., Fetter, R.D., McCabe, B.D., Magalhães, T.R., and Goodman, C.S. (2002). wishful thinking encodes a BMP type II receptor that regulates synaptic growth in Drosophila. Neuron *33*, 545–558.

Adler, C.E., Fetter, R.D., and Bargmann, C.I. (2006). UNC-6/Netrin induces neuronal asymmetry and defines the site of axon formation. Nat Neurosci *9*, 511–518.

Agmon, A., Hollrigel, G., and O'Dowd, D.K. (1996). Functional GABAergic synaptic connection in neonatal mouse barrel cortex. J Neurosci *16*, 4684–4695.

Aguado, F., Carmona, M.A., Pozas, E., Aguiló, A., Martínez-Guijarro, F.J., Alcantara, S., Borrell, V., Yuste, R., Ibañez, C.F., and Soriano, E. (2003). BDNF regulates spontaneous correlated activity at early developmental stages by increasing synaptogenesis and expression of the K+/Cl- co-transporter KCC2. Development *130*, 1267–1280.

Ahmad, F.J., He, Y., Myers, K.A., Hasaka, T.P., Francis, F., Black, M.M., and Baas, P.W. (2006). Effects of dynactin disruption and dynein depletion on axonal microtubules. Traffic *7*, 524–537.

Ahmad-Annuar, A., Ciani, L., Simeonidis, I., Herreros, J., Fredj, N.B., Rosso, S.B., Hall, A., Brickley, S., and Salinas, P.C. (2006). Signaling across the synapse: a role for Wnt and Dishevelled in presynaptic assembly and neurotransmitter release. J Cell Biol *174*, 127–139.

Ahmari, S.E., and Smith, S.J. (2002). Knowing a nascent synapse when you see it. Neuron *34*, 333–336.

Ahmari, S.E., Buchanan, J., and Smith, S.J. (2000). Assembly of presynaptic active zones from cytoplasmic transport packets. Nat Neurosci *3*, 445–451.

Akazawa, C., Nakamura, Y., Sango, K., Horie, H., and Kohsaka, S. (2004). Distribution of the galectin-1 mRNA in the rat nervous system: its transient upregulation in rat facial motor neurons after facial nerve axotomy. Neuroscience *125*, 171–178.

Alcamo, E.A., Chirivella, L., Dautzenberg, M., Dobreva, G., Fariñas, I., Grosschedl, R., and McConnell, S.K. (2008). Satb2 regulates callosal projection neuron identity in the developing cerebral cortex. Neuron *57*, 364–377.

Allen, N.J., Bennett, M.L., Foo, L.C., Wang, G.X., Chakraborty, C., Smith, S.J., and Barres, B.A. (2012). Astrocyte glypicans 4 and 6 promote formation of excitatory synapses via GluA1 AMPA receptors. Nature *486*, 410–414.

Alsina, B., Vu, T., and Cohen-Cory, S. (2001). Visualizing synapse formation in arborizing optic axons in vivo: dynamics and modulation by BDNF. Nat Neurosci *4*, 1093–1101.

De Anda, F.C., Pollarolo, G., Da Silva, J.S., Camoletto, P.G., Feiguin, F., and Dotti, C.G. (2005). Centrosome localization determines neuronal polarity. Nature *436*, 704–708.

De Anda, F.C., Meletis, K., Ge, X., Rei, D., and Tsai, L.-H. (2010). Centrosome motility is essential for initial axon formation in the neocortex. J Neurosci *30*, 10391–10406.

Andersen, P. (2007). The' ' hippocampus book (Oxford: Oxford University Press).

Andrews, S.B., Leapman, R.D., Landis, D.M., and Reese, T.S. (1988). Activity-dependent accumulation of calcium in Purkinje cell dendritic spines. Proc Natl Acad Sci U S A *85*, 1682–1685.

Ango, F., di Cristo, G., Higashiyama, H., Bennett, V., Wu, P., and Huang, Z.J. (2004). Ankyrin-based subcellular gradient of neurofascin, an immunoglobulin family protein, directs GABAergic innervation at purkinje axon initial segment. Cell *119*, 257–272.

Arikkath, J., and Reichardt, L.F. (2008). Cadherins and catenins at synapses: roles in synaptogenesis and synaptic plasticity. Trends Neurosci *31*, 487–494.

Arlotta, P., Molyneaux, B.J., Chen, J., Inoue, J., Kominami, R., and Macklis, J.D. (2005). Neuronal subtype-specific genes that control corticospinal motor neuron development in vivo. Neuron *45*, 207–221.

Ashburner, M., Ball, C.A., Blake, J.A., Botstein, D., Butler, H., Cherry, J.M., Davis, A.P., Dolinski, K., Dwight, S.S., Eppig, J.T., *et al.* (2000). Gene ontology: tool for the unification of biology. The Gene Ontology Consortium. Nat Genet *25*, 25–29.

Baas, P.W., Deitch, J.S., Black, M.M., and Banker, G.A. (1988). Polarity orientation of microtubules in hippocampal neurons: uniformity in the axon and nonuniformity in the dendrite. Proc Natl Acad Sci U S A *85*, 8335–8339.

Bagri, A., Gurney, T., He, X., Zou, Y.-R., Littman, D.R., Tessier-Lavigne, M., and Pleasure, S.J. (2002). The chemokine SDF1 regulates migration of dentate granule cells. Development *129*, 4249–4260.

Bajar, B.T., Wang, E.S., Lam, A.J., Kim, B.B., Jacobs, C.L., Howe, E.S., Davidson, M.W., Lin, M.Z., and Chu, J. (2016). Improving brightness and photostability of green and red fluorescent proteins for live cell imaging and FRET reporting. Sci Rep *6*, 20889.

Bamji, S.X. (2005). Cadherins: actin with the cytoskeleton to form synapses. Neuron *47*, 175–178.

Bamji, S.X., Shimazu, K., Kimes, N., Huelsken, J., Birchmeier, W., Lu, B., and Reichardt, L.F. (2003). Role of beta-catenin in synaptic vesicle localization and presynaptic assembly. Neuron *40*, 719–731.

Bandler, R.C., Mayer, C., and Fishell, G. (2017). Cortical interneuron specification: the juncture of genes, time and geometry. Curr Opin Neurobiol *42*, 17–24.

Baraban, S.C., and Tallent, M.K. (2004). Interneuron Diversity series: Interneuron neuropeptides--endogenous regulators of neuronal excitability. Trends Neurosci *27*, 135–142.

Barnes, A.P., Lilley, B.N., Pan, Y.A., Plummer, L.J., Powell, A.W., Raines, A.N., Sanes, J.R., and Polleux, F. (2007). LKB1 and SAD kinases define a pathway required for the polarization of cortical neurons. Cell *129*, 549–563.

Barondes, S.H., Cooper, D.N., Gitt, M.A., and Leffler, H. (1994). Galectins. Structure and function of a large family of animal lectins. J Biol Chem *269*, 20807–20810.

Barros, C.S., Calabrese, B., Chamero, P., Roberts, A.J., Korzus, E., Lloyd, K., Stowers, L., Mayford, M., Halpain, S., and Müller, U. (2009). Impaired maturation of dendritic spines without disorganization of cortical cell layers in mice lacking NRG1/ErbB signaling in the central nervous system. Proc Natl Acad Sci U S A *106*, 4507–4512.

Barros, C.S., Franco, S.J., and Müller, U. (2011). Extracellular matrix: functions in the nervous system. Cold Spring Harb Perspect Biol *3*, a005108.

Bastmeyer, M., and O'Leary, D.D. (1996). Dynamics of target recognition by interstitial axon branching along developing cortical axons. J Neurosci *16*, 1450–1459.

Ben-Ari, Y. (2002). Excitatory actions of gaba during development: the nature of the nurture. Nat Rev Neurosci *3*, 728–739.

Benson, D.L., and Tanaka, H. (1998). N-cadherin redistribution during synaptogenesis in hippocampal neurons. J Neurosci *18*, 6892–6904.

Benson, D.L., Colman, D.R., and Huntley, G.W. (2001). Molecules, maps and synapse specificity. Nat Rev Neurosci *2*, 899–909.

Bentley, D., and Toroian-Raymond, A. (1986). Disoriented pathfinding by pioneer neurone growth cones deprived of filopodia by cytochalasin treatment. Nature *323*, 712–715.

Berryer, M.H., Chattopadhyaya, B., Xing, P., Riebe, I., Bosoi, C., Sanon, N., Antoine-Bertrand, J., Lévesque, M., Avoli, M., Hamdan, F.F., *et al.* (2016). Decrease of SYNGAP1 in GABAergic cells impairs inhibitory synapse connectivity, synaptic inhibition and cognitive function. Nat Commun *7*, 13340.

Bertran, M.T., Sdelci, S., Regué, L., Avruch, J., Caelles, C., and Roig, J. (2011). Nek9 is a Plk1-activated kinase that controls early centrosome separation through Nek6/7 and Eg5. EMBO J *30*, 2634–2647.

Biederer, T., Sara, Y., Mozhayeva, M., Atasoy, D., Liu, X., Kavalali, E.T., and Südhof, T.C. (2002). SynCAM, a synaptic adhesion molecule that drives synapse assembly. Science *297*, 1525–1531.

Bischoff, V., Deogracias, R., Poirier, F., and Barde, Y.-A. (2012). Seizure-induced neuronal death is suppressed in the absence of the endogenous lectin Galectin-1. J Neurosci *32*, 15590–15600.

Black, M.M., Slaughter, T., and Fischer, I. (1994). Microtubule-associated protein 1b (MAP1b) is concentrated in the distal region of growing axons. J Neurosci *14*, 857–870.

Bliss, T.V., and Collingridge, G.L. (1993). A synaptic model of memory: long-term potentiation in the hippocampus. Nature *361*, 31–39.

Böckers, T.M., Segger-Junius, M., Iglauer, P., Bockmann, J., Gundelfinger, E.D., Kreutz, M.R., Richter, D., Kindler, S., and Kreienkamp, H.-J. (2004). Differential expression and dendritic transcript localization of Shank family members: identification of a dendritic targeting element in the 3' untranslated region of Shank1 mRNA. Mol Cell Neurosci *26*, 182–190.

Bolshakov, V.Y., and Siegelbaum, S.A. (1995). Regulation of hippocampal transmitter release during development and long-term potentiation. Science *269*, 1730–1734.

Bormann, J., Hamill, O.P., and Sakmann, B. (1987). Mechanism of anion permeation through channels gated by glycine and gamma-aminobutyric acid in mouse cultured spinal neurones. J Physiol (Lond) *385*, 243–286.

Bortone, D.S., Olsen, S.R., and Scanziani, M. (2014). Translaminar inhibitory cells recruited by layer 6 corticothalamic neurons suppress visual cortex. Neuron *82*, 474–485.

Boucard, A.A., Chubykin, A.A., Comoletti, D., Taylor, P., and Südhof, T.C. (2005). A splice code for trans-synaptic cell adhesion mediated by binding of neuroligin 1 to alpha- and beta-neurexins. Neuron *48*, 229–236.

Bowery, N. (1989). GABAB receptors and their significance in mammalian pharmacology. Trends Pharmacol Sci *10*, 401–407.

Bozdagi, O., Valcin, M., Poskanzer, K., Tanaka, H., and Benson, D.L. (2004). Temporally distinct demands for classic cadherins in synapse formation and maturation. Mol Cell Neurosci *27*, 509–521.

Bradke, F., and Dotti, C.G. (1997). Neuronal polarity: vectorial cytoplasmic flow precedes axon formation. Neuron *19*, 1175–1186.

Bresler, T., Shapira, M., Boeckers, T., Dresbach, T., Futter, M., Garner, C.C., Rosenblum, K., Gundelfinger, E.D., and Ziv, N.E. (2004). Postsynaptic density assembly is fundamentally different from presynaptic active zone assembly. J Neurosci *24*, 1507–1520.

Britanova, O., de Juan Romero, C., Cheung, A., Kwan, K.Y., Schwark, M., Gyorgy, A., Vogel, T., Akopov, S., Mitkovski, M., Agoston, D., *et al.* (2008). Satb2 is a postmitotic determinant for upper-layer neuron specification in the neocortex. Neuron *57*, 378–392.

Brose, K., Bland, K.S., Wang, K.H., Arnott, D., Henzel, W., Goodman, C.S., Tessier-Lavigne, M., and Kidd, T. (1999). Slit proteins bind Robo receptors and have an evolutionarily conserved role in repulsive axon guidance. Cell *96*, 795–806.

Brünig, I., Suter, A., Knuesel, I., Lüscher, B., and Fritschy, J.-M. (2002). GABAergic terminals are required for postsynaptic clustering of dystrophin but not of GABA(A) receptors and gephyrin. J Neurosci *22*, 4805–4813.

Buchanan, J., Sun, Y.A., and Poo, M.M. (1989). Studies of nerve-muscle interactions in Xenopus cell culture: fine structure of early functional contacts. J Neurosci *9*, 1540–1554.

Burgess, T.L., and Kelly, R.B. (1987). Constitutive and regulated secretion of proteins. Annu Rev Cell Biol *3*, 243–293.

Burkhardt, C., Müller, M., Badde, A., Garner, C.C., Gundelfinger, E.D., and Püschel, A.W. (2005). Semaphorin 4B interacts with the post-synaptic density protein PSD-95/SAP90 and is recruited to synapses through a C-terminal PDZ-binding motif. FEBS Lett *579*, 3821–3828.

Buzsáki, G., and Wang, X.-J. (2012). Mechanisms of gamma oscillations. Annu Rev Neurosci *35*, 203–225.

Cabelli, R.J., Allendoerfer, K.L., Radeke, M.J., Welcher, A.A., Feinstein, S.C., and Shatz, C.J. (1996). Changing patterns of expression and subcellular localization of TrkB in the developing visual system. J Neurosci *16*, 7965–7980.

Cadwell, C.R., Palasantza, A., Jiang, X., Berens, P., Deng, Q., Yilmaz, M., Reimer, J., Shen, S., Bethge, M., Tolias, K.F., *et al.* (2016). Electrophysiological, transcriptomic and morphologic profiling of single neurons using Patch-seq. Nat Biotechnol *34*, 199–203.

Cajigas, I.J., Tushev, G., Will, T.J., tom Dieck, S., Fuerst, N., and Schuman, E.M. (2012). The local transcriptome in the synaptic neuropil revealed by deep sequencing and high-resolution imaging. Neuron *74*, 453–466.

Cardin, J.A., Carlén, M., Meletis, K., Knoblich, U., Zhang, F., Deisseroth, K., Tsai, L.-H., and Moore, C.I. (2009). Driving fast-spiking cells induces gamma rhythm and controls sensory responses. Nature *459*, 663–667.

Carlsson, S., Carlsson, M.C., and Leffler, H. (2007). Intracellular sorting of galectin-8 based on carbohydrate fine specificity. Glycobiology *17*, 906–912.

Celio, M.R., Spreafico, R., De Biasi, S., and Vitellaro-Zuccarello, L. (1998). Perineuronal nets: past and present. Trends Neurosci *21*, 510–515.

Cellerino, A., and Maffei, L. (1996). The action of neurotrophins in the development and plasticity of the visual cortex. Prog Neurobiol *49*, 53–71.

Chacón, M.R., Fernández, G., and Rico, B. (2010). Focal adhesion kinase functions downstream of Sema3A signaling during axonal remodeling. Mol Cell Neurosci *44*, 30–42.

Chacón, M.R., Navarro, A.I., Cuesto, G., del Pino, I., Scott, R., Morales, M., and Rico, B. (2012). Focal adhesion kinase regulates actin nucleation and neuronal filopodia formation during axonal growth. Development *139*, 3200–3210.

Chang, J., Baloh, R.H., and Milbrandt, J. (2009). The NIMA-family kinase Nek3 regulates microtubule acetylation in neurons. J Cell Sci *122*, 2274–2282.

Chang, M.C., Park, J.M., Pelkey, K.A., Grabenstatter, H.L., Xu, D., Linden, D.J., Sutula, T.P., McBain, C.J., and Worley, P.F. (2010). Narp regulates homeostatic scaling of excitatory synapses on parvalbumin-expressing interneurons. Nat Neurosci *13*, 1090–1097.

Chattopadhyaya, B., Di Cristo, G., Wu, C.Z., Knott, G., Kuhlman, S., Fu, Y., Palmiter, R.D., and Huang, Z.J. (2007). GAD67-mediated GABA synthesis and signaling regulate inhibitory synaptic innervation in the visual cortex. Neuron *54*, 889–903.

Chattopadhyaya, B., Baho, E., Huang, Z.J., Schachner, M., and Di Cristo, G. (2013). Neural cell adhesion molecule-mediated Fyn activation promotes GABAergic synapse maturation in postnatal mouse cortex. J Neurosci *33*, 5957–5968.

Chavis, P., and Westbrook, G. (2001). Integrins mediate functional pre- and postsynaptic maturation at a hippocampal synapse. Nature *411*, 317–321.

Chen, A.I., Nguyen, C.N., Copenhagen, D.R., Badurek, S., Minichiello, L., Ranscht, B., and Reichardt, L.F. (2011a). TrkB (tropomyosin-related kinase B) controls the assembly and maintenance of GABAergic synapses in the cerebellar cortex. J Neurosci *31*, 2769–2780.

Chen, C., Arai, I., Satterfield, R., Young, S.M., and Jonas, P. (2017). Synaptotagmin 2 is the fast ca(2+) sensor at a central inhibitory synapse. Cell Rep *18*, 723–736.

Chen, Y., Tian, X., Kim, W.-Y., and Snider, W.D. (2011b). Adenomatous polyposis coli regulates axon arborization and cytoskeleton organization via its N-terminus. PLoS ONE *6*, e24335.

Chen, Z., Lee, H., Henle, S.J., Cheever, T.R., Ekker, S.C., and Henley, J.R. (2013). Primary neuron culture for nerve growth and axon guidance studies in zebrafish (Danio rerio). PLoS ONE *8*, e57539.

Cho, M., and Cummings, R.D. (1995). Galectin-1, a beta-galactoside-binding lectin in Chinese hamster ovary cells. I. Physical and chemical characterization. J Biol Chem *270*, 5198–5206.

Cho, Y.T., Fudge, J.L., and Ross, D.A. (2016). The Architecture of Cortex-in Illness and in Health. Biol Psychiatry *80*, e95–e97.

Christopherson, K.S., Ullian, E.M., Stokes, C.C.A., Mullowney, C.E., Hell, J.W., Agah, A., Lawler, J., Mosher, D.F., Bornstein, P., and Barres, B.A. (2005). Thrombospondins are astrocyte-secreted proteins that promote CNS synaptogenesis. Cell *120*, 421–433.

Chrominski, K., and Tkacz, M. (2015). Comparison of High-Level Microarray Analysis Methods in the Context of Result Consistency. PLoS ONE *10*, e0128845.

Chubykin, A.A., Atasoy, D., Etherton, M.R., Brose, N., Kavalali, E.T., Gibson, J.R., and Südhof, T.C. (2007). Activity-dependent validation of excitatory versus inhibitory synapses by neuroligin-1 versus neuroligin-2. Neuron *54*, 919–931.

Cline, H.T. (2001). Dendritic arbor development and synaptogenesis. Curr Opin Neurobiol *11*, 118–126.

Cohen, S., Aizer, A., Shav-Tal, Y., Yanai, A., and Motro, B. (2013). Nek7 kinase accelerates microtubule dynamic instability. Biochim Biophys Acta *1833*, 1104–1113.

Conde, C., and Cáceres, A. (2009). Microtubule assembly, organization and dynamics in axons and dendrites. Nat Rev Neurosci *10*, 319–332.

Copits, B.A., Vernon, C.G., Sakai, R., and Swanson, G.T. (2014). Modulation of ionotropic glutamate receptor function by vertebrate galectins. J Physiol (Lond) *592*, 2079–2096.

Costa, M., Manton, J.D., Ostrovsky, A.D., Prohaska, S., and Jefferis, G.S.X.E. (2016). NBLAST: rapid, sensitive comparison of neuronal structure and construction of neuron family databases. Neuron *91*, 293–311.

Courchet, J., Lewis, T.L., Lee, S., Courchet, V., Liou, D.-Y., Aizawa, S., and Polleux, F. (2013). Terminal axon branching is regulated by the LKB1-NUAK1 kinase pathway via presynaptic mitochondrial capture. Cell *153*, 1510–1525.

Couteaux, R., and Pecot-Dechavassine, M. (1970). Vesicules synaptiques et poches au niveau des zones actives de Ia jonction neuromusculaire. CR Acad Sci Ser D Paris 2346–9.

Craig, A.M., and Kang, Y. (2007). Neurexin-neuroligin signaling in synapse development. Curr Opin Neurobiol *17*, 43–52.

Craig, A.M., Graf, E.R., and Linhoff, M.W. (2006). How to build a central synapse: clues from cell culture. Trends Neurosci *29*, 8–20.

Crandall, J., Dibble, C., Butler, D., Pays, L., Ahmad, N., Kostek, C., Püschel, A.W., and Schwarting, G. (2000). Patterning of olfactory sensory connections is mediated by extracellular matrix proteins in the nerve layer of the olfactory bulb. Dev Neurobiol.

Dai, Z., Luo, X., Xie, H., and Peng, H.B. (2000). The actin-driven movement and formation of acetylcholine receptor clusters. J Cell Biol *150*, 1321–1334.

Dajas-Bailador, F., Bonev, B., Garcez, P., Stanley, P., Guillemot, F., and Papalopulu, N. (2012). microRNA-9 regulates axon extension and branching by targeting Map1b in mouse cortical neurons. Nat Neurosci.

Dalva, M.B., Takasu, M.A., Lin, M.Z., Shamah, S.M., Hu, L., Gale, N.W., and Greenberg, M.E. (2000). EphB receptors interact with NMDA receptors and regulate excitatory synapse formation. Cell *103*, 945–956.

Dalva, M.B., McClelland, A.C., and Kayser, M.S. (2007). Cell adhesion molecules: signalling functions at the synapse. Nat Rev Neurosci *8*, 206–220.

Dani, V.S., Chang, Q., Maffei, A., Turrigiano, G.G., Jaenisch, R., and Nelson, S.B. (2005). Reduced cortical activity due to a shift in the balance between excitation and inhibition in a mouse model of Rett syndrome. Proc Natl Acad Sci U S A *102*, 12560–12565.

Daniels, D., Eklof Spink, K., and Weis, W. (2001). beta-catenin: molecular plasticity and drug design. Trends Biochem Sci *26*, 672–678.

Dean, C., and Dresbach, T. (2006). Neuroligins and neurexins: linking cell adhesion, synapse formation and cognitive function. Trends Neurosci *29*, 21–29.

Dean, C., Scholl, F.G., Choih, J., DeMaria, S., Berger, J., Isacoff, E., and Scheiffele, P. (2003). Neurexin mediates the assembly of presynaptic terminals. Nat Neurosci *6*, 708–716.

DeFelipe, J., López-Cruz, P.L., Benavides-Piccione, R., Bielza, C., Larrañaga, P., Anderson, S., Burkhalter, A., Cauli, B., Fairén, A., Feldmeyer, D., *et al.* (2013). New insights into the classification and nomenclature of cortical GABAergic interneurons. Nat Rev Neurosci *14*, 202–216.

Dent, E.W., and Kalil, K. (2001). Axon branching requires interactions between dynamic microtubules and actin filaments. J Neurosci *21*, 9757–9769.

Dent, E.W., Callaway, J.L., Szebenyi, G., Baas, P.W., and Kalil, K. (1999). Reorganization and movement of microtubules in axonal growth cones and developing interstitial branches. J Neurosci *19*, 8894–8908.

Dent, E.W., Tang, F., and Kalil, K. (2003). Axon Guidance by Growth Cones and Branches: Common Cytoskeletal and Signaling Mechanisms. Neuroscientist *9*, 343–353.

Desai, A., Verma, S., Mitchison, T.J., and Walczak, C.E. (1999). Kin I kinesins are microtubule-destabilizing enzymes. Cell *96*, 69–78.

Dieni, S., Matsumoto, T., Dekkers, M., Rauskolb, S., Ionescu, M.S., Deogracias, R., Gundelfinger, E.D., Kojima, M., Nestel, S., Frotscher, M., *et al.* (2012). BDNF and its pro-peptide are stored in presynaptic dense core vesicles in brain neurons. J Cell Biol *196*, 775–788.

Dillon, C., and Goda, Y. (2005). The actin cytoskeleton: integrating form and function at the synapse. Annu Rev Neurosci *28*, 25–55.

Distel, M., Hocking, J.C., Volkmann, K., and Köster, R.W. (2010). The centrosome neither persistently leads migration nor determines the site of axonogenesis in migrating neurons in vivo. J Cell Biol *191*, 875–890.

Dityatev, A., and El-Husseini, A. (2006). Molecular mechanisms of synaptogenesis (New York, NY: Springer).

Dityatev, A., and Schachner, M. (2006). The extracellular matrix and synapses. Cell Tissue Res *326*, 647–654.

Dityatev, A., Dityateva, G., and Schachner, M. (2000). Synaptic strength as a function of post- versus presynaptic expression of the neural cell adhesion molecule NCAM. Neuron *26*, 207–217.

Dityatev, A., Dityateva, G., Sytnyk, V., Delling, M., Toni, N., Nikonenko, I., Muller, D., and Schachner, M. (2004). Polysialylated neural cell adhesion molecule promotes remodeling and formation of hippocampal synapses. J Neurosci *24*, 9372–9382.

Dotti, C.G., and Banker, G.A. (1987). Experimentally induced alteration in the polarity of developing neurons. Nature *330*, 254–256.

Drake, C.T., Milner, T.A., and Patterson, S.L. (1999). Ultrastructural localization of full-length trkB immunoreactivity in rat hippocampus suggests multiple roles in modulating activity-dependent synaptic plasticity. J Neurosci *19*, 8009–8026.

Dufour, A., Seibt, J., Passante, L., Depaepe, V., Ciossek, T., Frisén, J., Kullander, K., Flanagan, J.G., Polleux, F., and Vanderhaeghen, P. (2003). Area specificity and topography of thalamocortical projections are controlled by ephrin/Eph genes. Neuron *39*, 453–465.

Elia, L.P., Yamamoto, M., Zang, K., and Reichardt, L.F. (2006). p120 catenin regulates dendritic spine and synapse development through Rho-family GTPases and cadherins. Neuron *51*, 43–56.

Elmariah, S.B., Hughes, E.G., Oh, E.J., and Balice-Gordon, R.J. (2004). Neurotrophin signaling among neurons and glia during formation of tripartite synapses. Neuron Glia Biol *1*, 1–11.

Endo, M., and Yamashita, T. (2009). Inactivation of Ras by p120GAP via focal adhesion kinase dephosphorylation mediates RGMa-induced growth cone collapse. J Neurosci *29*, 6649–6662.

Engqvist-Goldstein, A.E.Y., and Drubin, D.G. (2003). Actin assembly and endocytosis: from yeast to mammals. Annu Rev Cell Dev Biol *19*, 287–332.

Etienne-Manneville, S., and Hall, A. (2003). Cdc42 regulates GSK-3beta and adenomatous polyposis coli to control cell polarity. Nature *421*, 753–756.

Fabregat, A., Sidiropoulos, K., Garapati, P., Gillespie, M., Hausmann, K., Haw, R., Jassal, B., Jupe, S., Korninger, F., McKay, S., *et al.* (2016). The Reactome pathway Knowledgebase. Nucleic Acids Res *44*, D481–7.

Fazzari, P., Paternain, A.V., Valiente, M., Pla, R., Luján, R., Lloyd, K., Lerma, J., Marín, O., and Rico, B. (2010). Control of cortical GABA circuitry development by Nrg1 and ErbB4 signalling. Nature *464*, 1376–1380.

Fdez, E., and Hilfiker, S. (2006). Vesicle pools and synapsins: new insights into old enigmas. Brain Cell Biol *35*, 107–115.

Featherstone, D.E., and Broadie, K. (2000). Surprises from Drosophila: genetic mechanisms of synaptic development and plasticity. Brain Res Bull *53*, 501–511.

Feige, E., and Motro, B. (2002). The related murine kinases, Nek6 and Nek7, display distinct patterns of expression.

De Felipe, J., Marco, P., Fairén, A., and Jones, E.G. (1997). Inhibitory synaptogenesis in mouse somatosensory cortex. Cereb Cortex *7*, 619–634.

Feng, G., Tintrup, H., Kirsch, J., Nichol, M.C., Kuhse, J., Betz, H., and Sanes, J.R. (1998). Dual requirement for gephyrin in glycine receptor clustering and molybdoenzyme activity. Science *282*, 1321–1324.

Fino, E., Packer, A.M., and Yuste, R. (2013). The logic of inhibitory connectivity in the neocortex. Neuroscientist *19*, 228–237.

Fish, K.N., Sweet, R.A., and Lewis, D.A. (2011). Differential distribution of proteins regulating GABA synthesis and reuptake in axon boutons of subpopulations of cortical interneurons. Cereb Cortex *21*, 2450–2460.

Flavell, S.W., Cowan, C.W., Kim, T.-K., Greer, P.L., Lin, Y., Paradis, S., Griffith, E.C., Hu, L.S., Chen, C., and Greenberg, M.E. (2006). Activity-dependent regulation of MEF2 transcription factors suppresses excitatory synapse number. Science *311*, 1008–1012.

Fogarty, M., Grist, M., Gelman, D., Marín, O., Pachnis, V., and Kessaris, N. (2007). Spatial genetic patterning of the embryonic neuroepithelium generates GABAergic interneuron diversity in the adult cortex. J Neurosci *27*, 10935–10946.

Fogel, A.I., Akins, M.R., Krupp, A.J., Stagi, M., Stein, V., and Biederer, T. (2007). SynCAMs organize synapses through heterophilic adhesion. J Neurosci *27*, 12516–12530.

Fogel, A.I., Stagi, M., Perez de Arce, K., and Biederer, T. (2011). Lateral assembly of the immunoglobulin protein SynCAM 1 controls its adhesive function and instructs synapse formation. EMBO J *30*, 4728–4738.

Fremeau, R.T., Kam, K., Qureshi, T., Johnson, J., Copenhagen, D.R., Storm-Mathisen, J., Chaudhry, F.A., Nicoll, R.A., and Edwards, R.H. (2004). Vesicular glutamate transporters 1 and 2 target to functionally distinct synaptic release sites. Science *304*, 1815–1819.

Friedman, H.V., Bresler, T., Garner, C.C., and Ziv, N.E. (2000). Assembly of new individual excitatory synapses: time course and temporal order of synaptic molecule recruitment. Neuron *27*, 57–69.

Fritschy, J.-M., Panzanelli, P., Kralic, J.E., Vogt, K.E., and Sassoè-Pognetto, M. (2006). Differential dependence of axo-dendritic and axo-somatic GABAergic synapses on GABAA receptors containing the alpha1 subunit in Purkinje cells. J Neurosci *26*, 3245–3255.

Fritschy, J.-M., Harvey, R.J., and Schwarz, G. (2008). Gephyrin: where do we stand, where do we go? Trends Neurosci *31*, 257–264.

Fry, A.M., O'Regan, L., Sabir, S.R., and Bayliss, R. (2012). Cell cycle regulation by the NEK family of protein kinases. J Cell Sci *125*, 4423–4433.

Fukata, M., Watanabe, T., Noritake, J., Nakagawa, M., Yamaga, M., Kuroda, S., Matsuura, Y., Iwamatsu, A., Perez, F., and Kaibuchi, K. (2002). Rac1 and Cdc42 capture microtubules through IQGAP1 and CLIP-170. Cell *109*, 873–885.

Fux, C.M., Krug, M., Dityatev, A., Schuster, T., and Schachner, M. (2003). NCAM180 and glutamate receptor subtypes in potentiated spine synapses: an immunogold electron microscopic study. Mol Cell Neurosci *24*, 939–950.

Fuzik, J., Zeisel, A., Máté, Z., Calvigioni, D., Yanagawa, Y., Szabó, G., Linnarsson, S., and Harkany, T. (2016). Integration of electrophysiological recordings with single-cell RNA-seq data identifies neuronal subtypes. Nat Biotechnol *34*, 175–183.

Galarreta, M., and Hestrin, S. (1999). A network of fast-spiking cells in the neocortex connected by electrical synapses. Nature *402*, 72–75.

Gallo, G. (2011). The cytoskeletal and signaling mechanisms of axon collateral branching. Dev Neurobiol *71*, 201–220.

Gallo, G., and Letourneau, P.C. (1998). Localized sources of neurotrophins initiate axon collateral sprouting. J Neurosci *18*, 5403–5414.

Gallo, G., and Letourneau, P.C. (1999). Different contributions of microtubule dynamics and transport to the growth of axons and collateral sprouts. J Neurosci *19*, 3860–3873.

Garcia, R.A., Vasudevan, K., and Buonanno, A. (2000). The neuregulin receptor ErbB-4 interacts with PDZ-containing proteins at neuronal synapses. Proc Natl Acad Sci U S A *97*, 3596–3601.

Garner, C.C., Waites, C.L., and Ziv, N.E. (2006). Synapse development: still looking for the forest, still lost in the trees. Cell Tissue Res *326*, 249–262.

Gasic, G.P., and Hollmann, M. (1992). Molecular neurobiology of glutamate receptors. Annu Rev Physiol *54*, 507–536.

Gelman, D.M., and Marín, O. (2010). Generation of interneuron diversity in the mouse cerebral cortex. Eur J Neurosci *31*, 2136–2141.

Gentet, L.J. (2012). Functional diversity of supragranular GABAergic neurons in the barrel cortex. Front Neural Circuits *6*, 52.

Geraldo, S., and Gordon-Weeks, P.R. (2009). Cytoskeletal dynamics in growth-cone steering. J Cell Sci *122*, 3595–3604.

Geraldo, S., Khanzada, U.K., Parsons, M., Chilton, J.K., and Gordon-Weeks, P.R. (2008). Targeting of the F-actin-binding protein drebrin by the microtubule plus-tip protein EB3 is required for neuritogenesis. Nat Cell Biol *10*, 1181–1189.

Gerrow, K., Romorini, S., Nabi, S.M., Colicos, M.A., Sala, C., and El-Husseini, A. (2006). A preformed complex of postsynaptic proteins is involved in excitatory synapse development. Neuron *49*, 547–562.

Giancotti, F.G., and Ruoslahti, E. (1999). Integrin signaling. Science *285*, 1028–1032.

Gibson, J.R., Beierlein, M., and Connors, B.W. (1999). Two networks of electrically coupled inhibitory neurons in neocortex. Nature *402*, 75–79.

Gil, O.D., Needleman, L., and Huntley, G.W. (2002). Developmental patterns of cadherin expression and localization in relation to compartmentalized thalamocortical terminations in rat barrel cortex. J Comp Neurol *453*, 372–388.

Goebbels, S., Bormuth, I., Bode, U., Hermanson, O., Schwab, M.H., and Nave, K.-A. (2006). Genetic targeting of principal neurons in neocortex and hippocampus of NEX-Cre mice. Genesis *44*, 611–621.

Goldman, J.S., Ashour, M.A., Magdesian, M.H., Tritsch, N.X., Harris, S.N., Christofi, N., Chemali, R., Stern, Y.E., Thompson-Steckel, G., Gris, P., *et al.* (2013). Netrin-1 promotes excitatory synaptogenesis between cortical neurons by initiating synapse assembly. J Neurosci *33*, 17278–17289.

Gómez-Climent, M.Á., Guirado, R., Castillo-Gómez, E., Varea, E., Gutierrez-Mecinas, M., Gilabert-Juan, J., García-Mompó, C., Vidueira, S., Sanchez-Mataredona, D., Hernández, S., *et al.* (2011). The polysialylated form of the neural cell adhesion molecule (PSA-NCAM) is expressed in a subpopulation of mature cortical interneurons characterized by reduced structural features and connectivity. Cereb Cortex *21*, 1028–1041.

Gordon-Weeks, P.R. (2004). Microtubules and growth cone function. J Neurobiol *58*, 70–83.

Gozlan, H., and Ben-Ari, Y. (2003). Interneurons are the source and the targets of the first synapses formed in the rat developing hippocampal circuit. Cereb Cortex *13*, 684–692.

Graf, E.R., Zhang, X., Jin, S.-X., Linhoff, M.W., and Craig, A.M. (2004). Neurexins induce differentiation of GABA and glutamate postsynaptic specializations via neuroligins. Cell *119*, 1013–1026.

Gross, C.G. (2007). The discovery of motor cortex and its background. J Hist Neurosci *16*, 320–331.

Gu, M., Wang, W., Song, W.K., Cooper, D.N., and Kaufman, S.J. (1994). Selective modulation of the interaction of alpha 7 beta 1 integrin with fibronectin and laminin by L-14 lectin during skeletal muscle differentiation. J Cell Sci *107 (Pt 1)*, 175–181.

Guez-Barber, D., Fanous, S., Harvey, B.K., Zhang, Y., Lehrmann, E., Becker, K.G., Picciotto, M.R., and Hope, B.T. (2012). FACS purification of immunolabeled cell types from adult rat brain. J Neurosci Methods *203*, 10–18.

Guirado, R., Perez-Rando, M., Sanchez-Matarredona, D., Castillo-Gómez, E., Liberia, T., Rovira-Esteban, L., Varea, E., Crespo, C., Blasco-Ibáñez, J.M., and Nacher, J. (2014). The dendritic spines of interneurons are dynamic structures influenced by PSA-NCAM expression. Cereb Cortex *24*, 3014–3024.

Gurden, H., Takita, M., and Jay, T.M. (2000). Essential role of D1 but not D2 receptors in the NMDA receptor-dependent long-term potentiation at hippocampal-prefrontal cortex synapses in vivo. J Neurosci *20*, RC106.

Hall, A., and Lalli, G. (2010). Rho and Ras GTPases in axon growth, guidance, and branching. Cold Spring Harb Perspect Biol *2*, a001818.

Hall, A.C., Lucas, F.R., and Salinas, P.C. (2000). Axonal remodeling and synaptic differentiation in the cerebellum is regulated by WNT-7a signaling. Cell *100*, 525–535.

Hannah, M.J., Schmidt, A.A., and Huttner, W.B. (1999). Synaptic vesicle biogenesis. Annu Rev Cell Dev Biol *15*, 733–798.

Haq, T., Richards, M.W., Burgess, S.G., Gallego, P., Yeoh, S., O'Regan, L., Reverter, D., Roig, J., Fry, A.M., and Bayliss, R. (2015). Mechanistic basis of Nek7 activation through Nek9 binding and induced dimerization. Nat Commun *6*, 8771.

Harris, K.M., and Kater, S.B. (1994). Dendritic spines: cellular specializations imparting both stability and flexibility to synaptic function. Annu Rev Neurosci *17*, 341–371.

Harris, K.M., and Stevens, J.K. (1989). Dendritic spines of CA 1 pyramidal cells in the rat hippocampus: serial electron microscopy with reference to their biophysical characteristics. J Neurosci *9*, 2982–2997.

Hartsock, A., and Nelson, W.J. (2008). Adherens and tight junctions: structure, function and connections to the actin cytoskeleton. Biochim Biophys Acta *1778*, 660–669.

Harvey, V.L., and Stephens, G.J. (2004). Mechanism of GABA receptor-mediated inhibition of spontaneous GABA release onto cerebellar Purkinje cells. Eur J Neurosci *20*, 684–700.

Hata, K., Kaibuchi, K., Inagaki, S., and Yamashita, T. (2009). Unc5B associates with LARG to mediate the action of repulsive guidance molecule. J Cell Biol *184*, 737–750.

Hayashi, T., and Su, T.-P. (2004). Sigma-1 receptors at galactosylceramide-enriched lipid microdomains regulate oligodendrocyte differentiation. Proc Natl Acad Sci U S A *101*, 14949–14954.

Hayashi, M.K., Tang, C., Verpelli, C., Narayanan, R., Stearns, M.H., Xu, R.-M., Li, H., Sala, C., and Hayashi, Y. (2009). The postsynaptic density proteins Homer and Shank form a polymeric network structure. Cell *137*, 159–171.

Hayashi, Y., Shi, S.H., Esteban, J.A., Piccini, A., Poncer, J.C., and Malinow, R. (2000). Driving AMPA receptors into synapses by LTP and CaMKII: requirement for GluR1 and PDZ domain interaction. Science *287*, 2262–2267.

He, Z., Wang, K.C., Koprivica, V., Ming, G., and Song, H.-J. (2002). Knowing how to navigate: mechanisms of semaphorin signaling in the nervous system. Sci STKE *2002*, re1.

Heidemann, S.R., Landers, J.M., and Hamborg, M.A. (1981). Polarity orientation of axonal microtubules. J Cell Biol *91*, 661–665.

Henkemeyer, M., Itkis, O.S., Ngo, M., Hickmott, P.W., and Ethell, I.M. (2003). Multiple EphB receptor tyrosine kinases shape dendritic spines in the hippocampus. J Cell Biol *163*, 1313–1326.

Herb, A., Wisden, W., Lüddens, H., Puia, G., Vicini, S., and Seeburg, P.H. (1992). The third gamma subunit of the gamma-aminobutyric acid type A receptor family. Proc Natl Acad Sci U S A *89*, 1433–1437.

Hida, Y., and Ohtsuka, T. (2010). CAST and ELKS proteins: structural and functional determinants of the presynaptic active zone. J Biochem *148*, 131–137.

Hilscher, M.M., Leão, R.N., Edwards, S.J., Leão, K.E., and Kullander, K. (2017). Chrna2-Martinotti Cells Synchronize Layer 5 Type A Pyramidal Cells via Rebound Excitation. PLoS Biol *15*, e2001392.

Hioki, H., Fujiyama, F., Taki, K., Tomioka, R., Furuta, T., Tamamaki, N., and Kaneko, T. (2003). Differential distribution of vesicular glutamate transporters in the rat cerebellar cortex. Neuroscience *117*, 1–6.

Hioki, H., Fujiyama, F., Nakamura, K., Wu, S.-X., Matsuda, W., and Kaneko, T. (2004). Chemically specific circuit composed of vesicular glutamate transporter 3- and preprotachykinin B-producing interneurons in the rat neocortex. Cereb Cortex *14*, 1266–1275.

Hirokawa, N., Niwa, S., and Tanaka, Y. (2010). Molecular motors in neurons: transport mechanisms and roles in brain function, development, and disease. Neuron *68*, 610–638.

Hofer, S.B., Ko, H., Pichler, B., Vogelstein, J., Ros, H., Zeng, H., Lein, E., Lesica, N.A., and Mrsic-Flogel, T.D. (2011). Differential connectivity and response dynamics of excitatory and inhibitory neurons in visual cortex. Nat Neurosci *14*, 1045–1052.

Holtmaat, A.J.G.D., Trachtenberg, J.T., Wilbrecht, L., Shepherd, G.M., Zhang, X., Knott, G.W., and Svoboda, K. (2005). Transient and persistent dendritic spines in the neocortex in vivo. Neuron *45*, 279–291.

Homma, N., Takei, Y., Tanaka, Y., Nakata, T., Terada, S., Kikkawa, M., Noda, Y., and Hirokawa, N. (2003). Kinesin superfamily protein 2A (KIF2A) functions in suppression of collateral branch extension. Cell *114*, 229–239.

Horie, H., and Kadoya, T. (2004). Galectin-1 plays essential roles in adult mammalian nervous tissues. Roles of oxidized galectin-1. Glycoconj J *19*, 479–489.

Horie, H., Inagaki, Y., Sohma, Y., Nozawa, R., Okawa, K., Hasegawa, M., Muramatsu, N., Kawano, H., Horie, M., Koyama, H., *et al.* (1999). Galectin-1 regulates initial axonal growth in peripheral nerves after axotomy. J Neurosci *19*, 9964–9974.

Hruska, M., and Dalva, M.B. (2012). Ephrin regulation of synapse formation, function and plasticity. Mol Cell Neurosci *50*, 35–44.

Hsu, D.K., Chen, H.-Y., and Liu, F.-T. (2009). Galectin-3 regulates T-cell functions. Immunol Rev *230*, 114–127.

Hu, J., Bai, X., Bowen, J.R., Dolat, L., Korobova, F., Yu, W., Baas, P.W., Svitkina, T., Gallo, G., and Spiliotis, E.T. (2012). Septin-driven coordination of actin and microtubule remodeling regulates the collateral branching of axons. Curr Biol *22*, 1109–1115.

Hu, W., Zhang, M., Czéh, B., Flügge, G., and Zhang, W. (2010). Stress impairs GABAergic network function in the hippocampus by activating nongenomic glucocorticoid receptors and affecting the integrity of the parvalbumin-expressing neuronal network. Neuropsychopharmacology *35*, 1693–1707.

Huang, Z.J., and Scheiffele, P. (2008). GABA and neuroligin signaling: linking synaptic activity and adhesion in inhibitory synapse development. Curr Opin Neurobiol *18*, 77–83.

Huang, Z.J., Kirkwood, A., Pizzorusso, T., Porciatti, V., Morales, B., Bear, M.F., Maffei, L., and Tonegawa, S. (1999). BDNF regulates the maturation of inhibition and the critical period of plasticity in mouse visual cortex. Cell *98*, 739–755.

Huang, Z.J., Di Cristo, G., and Ango, F. (2007). Development of GABA innervation in the cerebral and cerebellar cortices. Nat Rev Neurosci *8*, 673–686.

Huber, K.M., Gallagher, S.M., Warren, S.T., and Bear, M.F. (2002). Altered synaptic plasticity in a mouse model of fragile X mental retardation. Proc Natl Acad Sci U S A *99*, 7746–7750.

Hughes, R.C. (1999). Secretion of the galectin family of mammalian carbohydrate-binding proteins. Biochim Biophys Acta *1473*, 172–185.

Huttner, W.B., Ohashi, M., Kehlenbach, R.H., Barr, F.A., Bauerfeind, R., Bräunling, O., Corbeil, D., Hannah, M., Pasolli, H.A., and Schmidt, A. (1995). Biogenesis of neurosecretory vesicles. Cold Spring Harb Symp Quant Biol *60*, 315–327.

Ichtchenko, K., Hata, Y., Nguyen, T., Ullrich, B., Missler, M., Moomaw, C., and Südhof, T.C. (1995). Neuroligin 1: a splice site-specific ligand for beta-neurexins. Cell *81*, 435–443.

Ideo, H., Matsuzaka, T., Nonaka, T., Seko, A., and Yamashita, K. (2011). Galectin-8-N-domain recognition mechanism for sialylated and sulfated glycans. J Biol Chem *286*, 11346–11355.

Ihaka, R., and Gentleman, R. (1996). R: A Language for Data Analysis and Graphics. Journal of Computational and Graphical Statistics *5*, 299.

Inoue, A., and Sanes, J.R. (1997). Lamina-specific connectivity in the brain: regulation by N-cadherin, neurotrophins, and glycoconjugates. Science *276*, 1428–1431.

Ivanov, D., Philippova, M., Antropova, J., Gubaeva, F., Iljinskaya, O., Tararak, E., Bochkov, V., Erne, P., Resink, T., and Tkachuk, V. (2001). Expression of cell adhesion molecule T-cadherin in the human vasculature. Histochem Cell Biol *115*, 231–242.

Jackson, J., Bland, B.H., and Antle, M.C. (2009). Nonserotonergic projection neurons in the midbrain raphe nuclei contain the vesicular glutamate transporter VGLUT3. Synapse *63*, 31–41.

Javaherian, A., and Cline, H.T. (2005). Coordinated motor neuron axon growth and neuromuscular synaptogenesis are promoted by CPG15 in vivo. Neuron *45*, 505–512.

Jiang, X., Shen, S., Cadwell, C.R., Berens, P., Sinz, F., Ecker, A.S., Patel, S., and Tolias, A.S. (2015). Principles of connectivity among morphologically defined cell types in adult neocortex. Science *350*, aac9462.

Jiménez-Mateos, E.M., Paglini, G., González-Billault, C., Cáceres, A., and Avila, J. (2005). End binding protein-1 (EB1) complements microtubule-associated protein-1B during axonogenesis. J Neurosci Res *80*, 350–359.

Jin, H., Wu, H., Osterhaus, G., Wei, J., Davis, K., Sha, D., Floor, E., Hsu, C.-C., Kopke, R.D., and Wu, J.-Y. (2003). Demonstration of functional coupling between gamma -aminobutyric acid (GABA) synthesis and vesicular GABA transport into synaptic vesicles. Proc Natl Acad Sci U S A *100*, 4293–4298.

Jones, E.G. (1986). Neurotransmitters in the cerebral cortex. J Neurosurg *65*, 135–153.

Jontes, J.D., Buchanan, J., and Smith, S.J. (2000). Growth cone and dendrite dynamics in zebrafish embryos: early events in synaptogenesis imaged in vivo. Nat Neurosci *3*, 231–237.

Ju, W., Morishita, W., Tsui, J., Gaietta, G., Deerinck, T.J., Adams, S.R., Garner, C.C., Tsien, R.Y., Ellisman, M.H., and Malenka, R.C. (2004). Activity-dependent regulation of dendritic synthesis and trafficking of AMPA receptors. Nat Neurosci *7*, 244–253.

Kajitani, K., Kobayakawa, Y., Nomaru, H., Kadoya, T., Horie, H., and Nakabeppu, Y. (2014). Characterization of galectin-1-positive cells in the mouse hippocampus. Neuroreport *25*, 171–176.

Kalil, K., and Dent, E.W. (2014). Branch management: mechanisms of axon branching in the developing vertebrate CNS. Nat Rev Neurosci *15*, 7–18.

Kandel, E.R. (2013). Principles of neural science (New York: McGraw-Hill).

Kanehisa, M., Furumichi, M., Tanabe, M., Sato, Y., and Morishima, K. (2017). KEGG: new perspectives on genomes, pathways, diseases and drugs. Nucleic Acids Res *45*, D353–D361.

Kennedy, M.B. (1993). The postsynaptic density. Curr Opin Neurobiol *3*, 732–737.

Kennedy, M.J., and Ehlers, M.D. (2006). Organelles and trafficking machinery for postsynaptic plasticity. Annu Rev Neurosci *29*, 325–362.

Kerlin, A.M., Andermann, M.L., Berezovskii, V.K., and Reid, R.C. (2010). Broadly tuned response properties of diverse inhibitory neuron subtypes in mouse visual cortex. Neuron *67*, 858–871.

Kessaris, N., Fogarty, M., Iannarelli, P., Grist, M., Wegner, M., and Richardson, W.D. (2006). Competing waves of oligodendrocytes in the forebrain and postnatal elimination of an embryonic lineage. Nat Neurosci *9*, 173–179.

Ketschek, A., and Gallo, G. (2010). Nerve growth factor induces axonal filopodia through localized microdomains of phosphoinositide 3-kinase activity that drive the formation of cytoskeletal precursors to filopodia. J Neurosci *30*, 12185–12197.

Kim, E., and Sheng, M. (2004). PDZ domain proteins of synapses. Nat Rev Neurosci *5*, 771–781.

Kim, S., Lee, K., and Rhee, K. (2007). NEK7 is a centrosomal kinase critical for microtubule nucleation. Biochem Biophys Res Commun *360*, 56–62.

Kim, S., Kim, S., and Rhee, K. (2011). NEK7 is essential for centriole duplication and centrosomal accumulation of pericentriolar material proteins in interphase cells. J Cell Sci *124*, 3760–3770.

Kins, S., Betz, H., and Kirsch, J. (2000). Collybistin, a newly identified brain-specific GEF, induces submembrane clustering of gephyrin. Nat Neurosci *3*, 22–29.

Knable, M.B., Barci, B.M., Bartko, J.J., Webster, M.J., and Torrey, E.F. (2002). Molecular abnormalities in the major psychiatric illnesses: Classification and Regression Tree (CRT) analysis of post-mortem prefrontal markers. Mol Psychiatry *7*, 392–404.

Knibbs, R.N., Osborne, S.E., Glick, G.D., and Goldstein, I.J. (1993). Binding determinants of the sialic acid-specific lectin from the slug Limax flavus. J Biol Chem *268*, 18524–18531.

Knuesel, I., Mastrocola, M., Zuellig, R.A., Bornhauser, B., Schaub, M.C., and Fritschy, J.M. (1999). Short communication: altered synaptic clustering of GABAA receptors in mice lacking dystrophin (mdx mice). Eur J Neurosci *11*, 4457–4462.

Ko, J., Kim, S., Chung, H.S., Kim, K., Han, K., Kim, H., Jun, H., Kaang, B.-K., and Kim, E. (2006). SALM synaptic cell adhesion-like molecules regulate the differentiation of excitatory synapses. Neuron *50*, 233–245.

Kobayashi, M., and Buckmaster, P.S. (2003). Reduced inhibition of dentate granule cells in a model of temporal lobe epilepsy. J Neurosci *23*, 2440–2452.

Kornack, D.R., and Giger, R.J. (2005). Probing microtubule +TIPs: regulation of axon branching. Curr Opin Neurobiol *15*, 58–66.

Korobova, F., and Svitkina, T. (2008). Arp2/3 complex is important for filopodia formation, growth cone motility, and neuritogenesis in neuronal cells. Mol Biol Cell *19*, 1561–1574.

Kryuchkova-Mostacci, N., and Robinson-Rechavi, M. (2017). A benchmark of gene expression tissue-specificity metrics. Brief Bioinformatics *18*, 205–214.

Kurusu, M., Cording, A., Taniguchi, M., Menon, K., Suzuki, E., and Zinn, K. (2008). A screen of cell-surface molecules identifies leucine-rich repeat proteins as key mediators of synaptic target selection. Neuron *59*, 972–985.

Kuzirian, M.S., and Paradis, S. (2011). Emerging themes in GABAergic synapse development. Prog Neurobiol *95*, 68–87.

Kuzirian, M.S., Moore, A.R., Staudenmaier, E.K., Friedel, R.H., and Paradis, S. (2013). The class 4 semaphorin Sema4D promotes the rapid assembly of GABAergic synapses in rodent hippocampus. J Neurosci *33*, 8961–8973.

Kvitsiani, D., Ranade, S., Hangya, B., Taniguchi, H., Huang, J.Z., and Kepecs, A. (2013). Distinct behavioural and network correlates of two interneuron types in prefrontal cortex. Nature *498*, 363–366.

Kwiatkowski, A.V., Maiden, S.L., Pokutta, S., Choi, H.-J., Benjamin, J.M., Lynch, A.M., Nelson, W.J., Weis, W.I., and Hardin, J. (2010). In vitro and in vivo reconstitution of the cadherin-catenin-actin complex from Caenorhabditis elegans. Proc Natl Acad Sci U S A *107*, 14591–14596.

Lagler, M., Ozdemir, A.T., Lagoun, S., Malagon-Vina, H., Borhegyi, Z., Hauer, R., Jelem, A., and Klausberger, T. (2016). Divisions of Identified Parvalbumin-Expressing Basket Cells during Working Memory-Guided Decision Making. Neuron *91*, 1390–1401.

Landis, D.M., Weinstein, L.A., and Reese, T.S. (1987). Substructure in the postsynaptic density of Purkinje cell dendritic spines revealed by rapid freezing and etching. Synapse *1*, 552–558.

Lee, A.T., Gee, S.M., Vogt, D., Patel, T., Rubenstein, J.L., and Sohal, V.S. (2014). Pyramidal neurons in prefrontal cortex receive subtype-specific forms of excitation and inhibition. Neuron *81*, 61–68.

Lee, C.H., Herman, T., Clandinin, T.R., Lee, R., and Zipursky, S.L. (2001). N-cadherin regulates target specificity in the Drosophila visual system. Neuron *30*, 437–450.

Lee, R.C., Clandinin, T.R., Lee, C.-H., Chen, P.-L., Meinertzhagen, I.A., and Zipursky, S.L. (2003). The protocadherin Flamingo is required for axon target selection in the Drosophila visual system. Nat Neurosci *6*, 557–563.

Lein, E.S., Hawrylycz, M.J., Ao, N., Ayres, M., Bensinger, A., Bernard, A., Boe, A.F., Boguski, M.S., Brockway, K.S., Byrnes, E.J., *et al.* (2007). Genome-wide atlas of gene expression in the adult mouse brain. Nature *445*, 168–176.

Lekishvili, T., Hesketh, S., Brazier, M.W., and Brown, D.R. (2006). Mouse galectin-1 inhibits the toxicity of glutamate by modifying NR1 NMDA receptor expression. Eur J Neurosci *24*, 3017–3025.

Leppänen, A., Stowell, S., Blixt, O., and Cummings, R.D. (2005). Dimeric galectin-1 binds with high affinity to alpha2,3-sialylated and non-sialylated terminal N-acetyllactosamine units on surface-bound extended glycans. J Biol Chem *280*, 5549–5562.

Leshchyns'ka, I., and Sytnyk, V. (2016). Reciprocal Interactions between Cell Adhesion Molecules of the Immunoglobulin Superfamily and the Cytoskeleton in Neurons. Frontiers in Cell and Developmental Biology *4*, 9.

Letourneau, P.C., Shattuck, T.A., and Ressler, A.H. (1987). Pull" and "push" in neurite elongation: observations on the effects of different concentrations of cytochalasin B and taxol. Cell Motil Cytoskeleton *8*, 193–209.

Levitt, P. (2005). Disruption of interneuron development. Epilepsia *46 Suppl 7*, 22–28.

Lewis, D.A., Hashimoto, T., and Volk, D.W. (2005). Cortical inhibitory neurons and schizophrenia. Nat Rev Neurosci *6*, 312–324.

Lewis, T.L., Mao, T., Svoboda, K., and Arnold, D.B. (2009). Myosin-dependent targeting of transmembrane proteins to neuronal dendrites. Nat Neurosci *12*, 568–576.

Lewis, T.L., Courchet, J., and Polleux, F. (2013). Cell biology in neuroscience: Cellular and molecular mechanisms underlying axon formation, growth, and branching. J Cell Biol *202*, 837–848.

Li, L., Wan, J., Sase, S., Gröger, M., Pollak, A., Korz, V., and Lubec, G. (2014). Protein kinases paralleling late-phase LTP formation in dorsal hippocampus in the rat. Neurochem Int *76*, 50–58.

Li, W., Lee, J., Vikis, H.G., Lee, S.-H., Liu, G., Aurandt, J., Shen, T.-L., Fearon, E.R., Guan, J.-L., Han, M., *et al.* (2004). Activation of FAK and Src are receptor-proximal events required for netrin signaling. Nat Neurosci *7*, 1213–1221.

Lin, Y., Bloodgood, B.L., Hauser, J.L., Lapan, A.D., Koon, A.C., Kim, T.-K., Hu, L.S., Malik, A.N., and Greenberg, M.E. (2008). Activity-dependent regulation of inhibitory synapse development by Npas4. Nature *455*, 1198–1204.

Liu, Y., and Edwards, R.H. (1997). The role of vesicular transport proteins in synaptic transmission and neural degeneration. Annu Rev Neurosci *20*, 125–156.

Liu, G., Beggs, H., Jürgensen, C., Park, H.-T., Tang, H., Gorski, J., Jones, K.R., Reichardt, L.F., Wu, J., and Rao, Y. (2004). Netrin requires focal adhesion kinase and Src family kinases for axon outgrowth and attraction. Nat Neurosci *7*, 1222–1232.

Liu, T.T., Bannatyne, B.A., and Maxwell, D.J. (2010). Organization and neurochemical properties of intersegmental interneurons in the lumbar enlargement of the adult rat. Neuroscience *171*, 461–484.

Llinás, R., Steinberg, I.Z., and Walton, K. (1981). Relationship between presynaptic calcium current and postsynaptic potential in squid giant synapse. Biophys J *33*, 323–351.

Lobsanov, Y.D., Gitt, M.A., Leffler, H., Barondes, S.H., and Rini, J.M. (1993). X-ray crystal structure of the human dimeric S-Lac lectin, L-14-II, in complex with lactose at 2.9-A resolution. J Biol Chem *268*, 27034–27038.

Lodato, S., and Arlotta, P. (2015). Generating neuronal diversity in the mammalian cerebral cortex. Annu Rev Cell Dev Biol *31*, 699–720.

López-Bendito, G., Sturgess, K., Erdélyi, F., Szabó, G., Molnár, Z., and Paulsen, O. (2004). Preferential origin and layer destination of GAD65-GFP cortical interneurons. Cereb Cortex *14*, 1122–1133.

Lorente de Nó, R. (1922). La corteza cerebral de ratón. Trabajos de Laboratorio de Investigaciones Biológicas de La Universidad de Madrid 41–78.

Loverde, J.R., Tolentino, R.E., and Pfister, B.J. (2011). Axon stretch growth: the mechanotransduction of neuronal growth. J Vis Exp.

Lupo, G., Harris, W.A., and Lewis, K.E. (2006). Mechanisms of ventral patterning in the vertebrate nervous system. Nat Rev Neurosci *7*, 103–114.

Ma, Y., Hu, H., Berrebi, A.S., Mathers, P.H., and Agmon, A. (2006). Distinct subtypes of somatostatin-containing neocortical interneurons revealed in transgenic mice. J Neurosci *26*, 5069–5082.

Magdaleno, S., Jensen, P., Brumwell, C.L., Seal, A., Lehman, K., Asbury, A., Cheung, T., Cornelius, T., Batten, D.M., Eden, C., *et al.* (2006). BGEM: an in situ hybridization database of gene expression in the embryonic and adult mouse nervous system. PLoS Biol *4*, e86.

Mahanthappa, N.K., Cooper, D.N., Barondes, S.H., and Schwarting, G.A. (1994). Rat olfactory neurons can utilize the endogenous lectin, L-14, in a novel adhesion mechanism. Development *120*, 1373–1384.

Malsam, J., Kreye, S., and Söllner, T.H. (2008). Membrane fusion: SNAREs and regulation. Cell Mol Life Sci *65*, 2814–2832.

Man, H.Y., Ju, W., Ahmadian, G., and Wang, Y.T. (2000). Intracellular trafficking of AMPA receptors in synaptic plasticity. Cell Mol Life Sci *57*, 1526–1534.

Marín, O. (2012). Interneuron dysfunction in psychiatric disorders. Nat Rev Neurosci *13*, 107–120.

Marín, O. (2016). Developmental timing and critical windows for the treatment of psychiatric disorders. Nat Med *22*, 1229–1238.

Marín, O., and Rubenstein, J.L.R. (2003). Cell migration in the forebrain. Annu Rev Neurosci *26*, 441–483.

Markram, H., Toledo-Rodriguez, M., Wang, Y., Gupta, A., Silberberg, G., and Wu, C. (2004). Interneurons of the neocortical inhibitory system. Nat Rev Neurosci *5*, 793–807.

Marsh, L., and Letourneau, P.C. (1984). Growth of neurites without filopodial or lamellipodial activity in the presence of cytochalasin B. J Cell Biol *99*, 2041–2047.

Martínez, A., and Soriano, E. (2005). Functions of ephrin/Eph interactions in the development of the nervous system: emphasis on the hippocampal system. Brain Res Brain Res Rev *49*, 211–226.

Masuda, K., Furuyama, T., Takahara, M., Fujioka, S., Kurinami, H., and Inagaki, S. (2004). Sema4D stimulates axonal outgrowth of embryonic DRG sensory neurones. Genes Cells *9*, 821–829.

Matheson, S.F., and Levine, R.B. (1999). Steroid hormone enhancement of neurite outgrowth in identified insect motor neurons involves specific effects on growth cone form and function. J Neurobiol *38*, 27–45.

Mauch, D.H., Nägler, K., Schumacher, S., Göritz, C., Müller, E.C., Otto, A., and Pfrieger, F.W. (2001). CNS synaptogenesis promoted by glia-derived cholesterol. Science *294*, 1354–1357.

Maximov, A., Südhof, T.C., and Bezprozvanny, I. (1999). Association of neuronal calcium channels with modular adaptor proteins. J Biol Chem *274*, 24453–24456.

McAllister, A.K. (2007). Dynamic aspects of CNS synapse formation. Annu Rev Neurosci *30*, 425–450.

McGraw, J., Gaudet, A.D., Oschipok, L.W., Steeves, J.D., Poirier, F., Tetzlaff, W., and Ramer, M.S. (2005). Altered primary afferent anatomy and reduced thermal sensitivity in mice lacking galectin-1. Pain *114*, 7–18.

McLaughlin, T., and O'Leary, D.D.M. (2005). Molecular gradients and development of retinotopic maps. Annu Rev Neurosci *28*, 327–355.

Megías, M., Emri, Z., Freund, T.F., and Gulyás, A.I. (2001). Total number and distribution of inhibitory and excitatory synapses on hippocampal CA1 pyramidal cells. Neuroscience *102*, 527–540.

Mei, L., and Nave, K.-A. (2014). Neuregulin-ERBB signaling in the nervous system and neuropsychiatric diseases. Neuron *83*, 27–49.

Meyer, M.P., and Smith, S.J. (2006). Evidence from in vivo imaging that synaptogenesis guides the growth and branching of axonal arbors by two distinct mechanisms. J Neurosci *26*, 3604–3614.

Meyer, A.H., Katona, I., Blatow, M., Rozov, A., and Monyer, H. (2002). In vivo labeling of parvalbumin-positive interneurons and analysis of electrical coupling in identified neurons. J Neurosci *22*, 7055–7064.

Mingorance-Le Meur, A., and O'Connor, T.P. (2009). Neurite consolidation is an active process requiring constant repression of protrusive activity. EMBO J *28*, 248–260.

Minoguchi, S., Minoguchi, M., and Yoshimura, A. (2003). Differential control of the NIMA-related kinases, Nek6 and Nek7, by serum stimulation. Biochem Biophys Res Commun *301*, 899–906.

Miranda, R.C., Sohrabji, F., and Toran-Allerand, C.D. (1993). Neuronal colocalization of mRNAs for neurotrophins and their receptors in the developing central nervous system suggests a potential for autocrine interactions. Proc Natl Acad Sci U S A *90*, 6439–6443.

Missler, M., and Südhof, T.C. (1998). Neurexophilins form a conserved family of neuropeptide-like glycoproteins. J Neurosci *18*, 3630–3638.

Miyoshi, G., Hjerling-Leffler, J., Karayannis, T., Sousa, V.H., Butt, S.J.B., Battiste, J., Johnson, J.E., Machold, R.P., and Fishell, G. (2010). Genetic fate mapping reveals that the caudal ganglionic eminence produces a large and diverse population of superficial cortical interneurons. J Neurosci *30*, 1582–1594.

Mizoguchi, A., Nakanishi, H., Kimura, K., Matsubara, K., Ozaki-Kuroda, K., Katata, T., Honda, T., Kiyohara, Y., Heo, K., Higashi, M., *et al.* (2002). Nectin: an adhesion molecule involved in formation of synapses. J Cell Biol *156*, 555–565.

Mizuno, H., Hirano, T., and Tagawa, Y. (2007). Evidence for activity-dependent cortical wiring: formation of interhemispheric connections in neonatal mouse visual cortex requires projection neuron activity. J Neurosci *27*, 6760–6770.

Moiseeva, E.P., Spring, E.L., Baron, J.H., and de Bono, D.P. (1999). Galectin 1 modulates attachment, spreading and migration of cultured vascular smooth muscle cells via interactions with cellular receptors and components of extracellular matrix. J Vasc Res *36*, 47–58.

Moiseeva, E.P., Williams, B., and Samani, N.J. (2003). Galectin 1 inhibits incorporation of vitronectin and chondroitin sulfate B into the extracellular matrix of human vascular smooth muscle cells. Biochim Biophys Acta *1619*, 125–132.

Molyneaux, B.J., Arlotta, P., Menezes, J.R.L., and Macklis, J.D. (2007). Neuronal subtype specification in the cerebral cortex. Nat Rev Neurosci *8*, 427–437.

Morales, M., Colicos, M.A., and Goda, Y. (2000). Actin-dependent regulation of neurotransmitter release at central synapses. Neuron *27*, 539–550.

Morris, N.R. (1976). Nucleosome structure in Aspergillus nidulans. Cell *8*, 357–363.

Morris, M., Maeda, S., Vossel, K., and Mucke, L. (2011). The many faces of tau. Neuron *70*, 410–426.

Morris, S., Ahmad, N., André, S., Kaltner, H., Gabius, H.-J., Brenowitz, M., and Brewer, F. (2004). Quaternary solution structures of galectins-1, -3, and -7. Glycobiology *14*, 293–300.

Murai, K.K., and Pasquale, E.B. (2003). Eph 'ective signaling: forward, reverse and crosstalk. J Cell Sci *116*, 2823–2832.

Murthy, V.N., Sejnowski, T.J., and Stevens, C.F. (1997). Heterogeneous release properties of visualized individual hippocampal synapses. Neuron *18*, 599–612.

Myers, J.P., and Gomez, T.M. (2011). Focal adhesion kinase promotes integrin adhesion dynamics necessary for chemotropic turning of nerve growth cones. J Neurosci *31*, 13585–13595.

Myers, K.A., and Baas, P.W. (2007). Kinesin-5 regulates the growth of the axon by acting as a brake on its microtubule array. J Cell Biol *178*, 1081–1091.

Myers, J.P., Robles, E., Ducharme-Smith, A., and Gomez, T.M. (2012). Focal adhesion kinase modulates Cdc42 activity downstream of positive and negative axon guidance cues. J Cell Sci *125*, 2918–2929.

Navarro, A.I., and Rico, B. (2014). Focal adhesion kinase function in neuronal development. Curr Opin Neurobiol *27*, 89–95.

Nery, S., Wichterle, H., and Fishell, G. (2001). Sonic hedgehog contributes to oligodendrocyte specification in the mammalian forebrain. Development *128*, 527–540.

Ngo, V.N., Davis, R.E., Lamy, L., Yu, X., Zhao, H., Lenz, G., Lam, L.T., Dave, S., Yang, L., Powell, J., *et al.* (2006). A loss-of-function RNA interference screen for molecular targets in cancer. Nature *441*, 106–110.

Nguyen, M.M., Stone, M.C., and Rolls, M.M. (2011). Microtubules are organized independently of the centrosome in Drosophila neurons. Neural Dev *6*, 38.

Niell, C.M., Meyer, M.P., and Smith, S.J. (2004). In vivo imaging of synapse formation on a growing dendritic arbor. Nat Neurosci *7*, 254–260.

Nitkin, R.M., Smith, M.A., Magill, C., Fallon, J.R., Yao, Y.M., Wallace, B.G., and McMahan, U.J. (1987). Identification of agrin, a synaptic organizing protein from Torpedo electric organ. J Cell Biol *105*, 2471–2478.

O'Brien, R.J., Xu, D., Petralia, R.S., Steward, O., Huganir, R.L., and Worley, P. (1999). Synaptic clustering of AMPA receptors by the extracellular immediate-early gene product Narp. Neuron *23*, 309–323.

O'Connell, M.J., Krien, M.J.E., and Hunter, T. (2003). Never say never. The NIMA-related protein kinases in mitotic control. Trends Cell Biol *13*, 221–228.

O'Regan, L., and Fry, A.M. (2009). The Nek6 and Nek7 protein kinases are required for robust mitotic spindle formation and cytokinesis. Mol Cell Biol *29*, 3975–3990.

Ohtsuka, T., Takao-Rikitsu, E., Inoue, E., Inoue, M., Takeuchi, M., Matsubara, K., Deguchi-Tawarada, M., Satoh, K., Morimoto, K., Nakanishi, H., *et al.* (2002). Cast: a novel protein of the cytomatrix at the active zone of synapses that forms a ternary complex with RIM1 and munc13-1. J Cell Biol *158*, 577–590.

Okabe, S., Miwa, A., and Okado, H. (2001). Spine formation and correlated assembly of presynaptic and postsynaptic molecules. J Neurosci *21*, 6105–6114.

Okaty, B.W., Sugino, K., and Nelson, S.B. (2011). A quantitative comparison of cell-type-specific microarray gene expression profiling methods in the mouse brain. PLoS ONE *6*, e16493.

Olsen, R.W., and Tobin, A.J. (1990). Molecular biology of GABAA receptors. FASEB J *4*, 1469–1480.

Paddison, P.J., Caudy, A.A., Bernstein, E., Hannon, G.J., and Conklin, D.S. (2002). Short hairpin RNAs (shRNAs) induce sequence-specific silencing in mammalian cells. Genes Dev *16*, 948–958.

Pandya, D., Seltzer, B., Petrides, M., and Cipolloni, P.B. (2015). Cerebral cortex: architecture, connections, and the dual origin concept (Oxford University Press).

Pangratz-Fuehrer, S., and Hestrin, S. (2011). Synaptogenesis of electrical and GABAergic synapses of fast-spiking inhibitory neurons in the neocortex. J Neurosci *31*, 10767–10775.

Panzer, J.A., Song, Y., and Balice-Gordon, R.J. (2006). In vivo imaging of preferential motor axon outgrowth to and synaptogenesis at prepatterned acetylcholine receptor clusters in embryonic zebrafish skeletal muscle. J Neurosci *26*, 934–947.

Papadopoulos, T., Eulenburg, V., Reddy-Alla, S., Mansuy, I.M., Li, Y., and Betz, H. (2008). Collybistin is required for both the formation and maintenance of GABAergic postsynapses in the hippocampus. Mol Cell Neurosci *39*, 161–169.

Paradis, S., Harrar, D.B., Lin, Y., Koon, A.C., Hauser, J.L., Griffith, E.C., Zhu, L., Brass, L.F., Chen, C., and Greenberg, M.E. (2007). An RNAi-based approach identifies molecules required for glutamatergic and GABAergic synapse development. Neuron *53*, 217–232.

Pascual, M., Pozas, E., Barallobre, M.J., Tessier-Lavigne, M., and Soriano, E. (2004). Coordinated functions of Netrin-1 and Class 3 secreted Semaphorins in the guidance of reciprocal septohippocampal connections. Mol Cell Neurosci *26*, 24–33.

Peng, H.B., Baker, L.P., and Chen, Q. (1991). Induction of synaptic development in cultured muscle cells by basic fibroblast growth factor. Neuron *6*, 237–246.

Peters, A., Palay, S.L., and Webster, H. deF. (1991). The' ' fine structure of the nervous system: Neurons and their supporting cells (New York: Oxford University Press).

Petilla Interneuron Nomenclature Group, Ascoli, G.A., Alonso-Nanclares, L., Anderson, S.A., Barrionuevo, G., Benavides-Piccione, R., Burkhalter, A., Buzsáki, G., Cauli, B., Defelipe, J., *et al.* (2008). Petilla terminology: nomenclature of features of GABAergic interneurons of the cerebral cortex. Nat Rev Neurosci *9*, 557–568.

Pfeffer, C.K., Xue, M., He, M., Huang, Z.J., and Scanziani, M. (2013). Inhibition of inhibition in visual cortex: the logic of connections between molecularly distinct interneurons. Nat Neurosci *16*, 1068–1076.

Pfister, B.J., Iwata, A., Meaney, D.F., and Smith, D.H. (2004). Extreme stretch growth of integrated axons. J Neurosci *24*, 7978–7983.

Phillips, G.R., Huang, J.K., Wang, Y., Tanaka, H., Shapiro, L., Zhang, W., Shan, W.S., Arndt, K., Frank, M., Gordon, R.E., *et al.* (2001). The presynaptic particle web: ultrastructure, composition, dissolution, and reconstitution. Neuron *32*, 63–77.

Phillips, G.R., Tanaka, H., Frank, M., Elste, A., Fidler, L., Benson, D.L., and Colman, D.R. (2003). Gamma-protocadherins are targeted to subsets of synapses and intracellular organelles in neurons. J Neurosci *23*, 5096–5104.

Phipson, B., Lee, S., Majewski, I.J., Alexander, W.S., and Smyth, G.K. (2016). Robust hyperparameter estimation protects against hypervariable genes and improves power to detect differential expression. Ann Appl Stat *10*, 946–963.

Pierce, J.P., and Mendell, L.M. (1993). Quantitative ultrastructure of Ia boutons in the ventral horn: scaling and positional relationships. J Neurosci *13*, 4748–4763.

Del Pino, I., García-Frigola, C., Dehorter, N., Brotons-Mas, J.R., Alvarez-Salvado, E., Martínez de Lagrán, M., Ciceri, G., Gabaldón, M.V., Moratal, D., Dierssen, M., *et al.* (2013). Erbb4 deletion from fast-spiking interneurons causes schizophrenia-like phenotypes. Neuron *79*, 1152–1168.

Del Pino, I., Brotons-Mas, J.R., Marques-Smith, A., Marighetto, A., Frick, A., Marín, O., and Rico, B. (2017). Abnormal wiring of CCK(+) basket cells disrupts spatial information coding. Nat Neurosci *20*, 784–792.

Plachta, N., Annaheim, C., Bissière, S., Lin, S., Rüegg, M., Hoving, S., Müller, D., Poirier, F., Bibel, M., and Barde, Y.-A. (2007). Identification of a lectin causing the degeneration of neuronal processes using engineered embryonic stem cells. Nat Neurosci *10*, 712–719.

Portera-Cailliau, C., Weimer, R.M., De Paola, V., Caroni, P., and Svoboda, K. (2005). Diverse modes of axon elaboration in the developing neocortex. PLoS Biol *3*, e272.

Posse De Chaves, E.I., Vance, D.E., Campenot, R.B., Kiss, R.S., and Vance, J.E. (2000). Uptake of lipoproteins for axonal growth of sympathetic neurons. J Biol Chem *275*, 19883–19890.

Poulopoulos, A., Aramuni, G., Meyer, G., Soykan, T., Hoon, M., Papadopoulos, T., Zhang, M., Paarmann, I., Fuchs, C., Harvey, K., *et al.* (2009). Neuroligin 2 drives postsynaptic assembly at perisomatic inhibitory synapses through gephyrin and collybistin. Neuron *63*, 628–642.

Powell, S.B., Sejnowski, T.J., and Behrens, M.M. (2012). Behavioral and neurochemical consequences of cortical oxidative stress on parvalbumin-interneuron maturation in rodent models of schizophrenia. Neuropharmacology *62*, 1322–1331.

Probstmeier, R., Montag, D., and Schachner, M. (2002). Galectin-3, a β-Galactoside-Binding Animal Lectin, Binds to Neural Recognition Molecules. Journal of Neurochemistry *64*, 2465–2472.

Puche, A.C., Poirier, F., Hair, M., Bartlett, P.F., and Key, B. (1996). Role of galectin-1 in the developing mouse olfactory system. Dev Biol *179*, 274–287.

Purves, D. (2011). Neuroscience (Sunderland, Mass: Sinauer Associates).

Qiang, L., Yu, W., Liu, M., Solowska, J.M., and Baas, P.W. (2010). Basic fibroblast growth factor elicits formation of interstitial axonal branches via enhanced severing of microtubules. Mol Biol Cell *21*, 334–344.

Quarmby, L.M., and Mahjoub, M.R. (2005). Caught Nek-ing: cilia and centrioles. J Cell Sci *118*, 5161–5169.

Quintá, H.R., Pasquini, J.M., Rabinovich, G.A., and Pasquini, L.A. (2014). Glycan-dependent binding of galectin-1 to neuropilin-1 promotes axonal regeneration after spinal cord injury. Cell Death Differ *21*, 941–955.

Raissi, A.J., Staudenmaier, E.K., David, S., Hu, L., and Paradis, S. (2013). Sema4D localizes to synapses and regulates GABAergic synapse development as a membrane-bound molecule in the mammalian hippocampus. Mol Cell Neurosci *57*, 23–32.

Rallu, M., Machold, R., Gaiano, N., Corbin, J.G., McMahon, A.P., and Fishell, G. (2002). Dorsoventral patterning is established in the telencephalon of mutants lacking both Gli3 and Hedgehog signaling. Development *129*, 4963–4974.

Ramón y Cajal, S. (1899). Textura del sistema nervioso del hombre y de los vertebrados. Moya, Madrid.

Randlett, O., Poggi, L., Zolessi, F.R., and Harris, W.A. (2011). The oriented emergence of axons from retinal ganglion cells is directed by laminin contact in vivo. Neuron *70*, 266–280.

Rapley, J., Nicolàs, M., Groen, A., Regué, L., Bertran, M.T., Caelles, C., Avruch, J., and Roig, J. (2008). The NIMA-family kinase Nek6 phosphorylates the kinesin Eg5 at a novel site necessary for mitotic spindle formation. J Cell Sci *121*, 3912–3921.

Régnier-Vigouroux, A., Tooze, S.A., and Huttner, W.B. (1991). Newly synthesized synaptophysin is transported to synaptic-like microvesicles via constitutive secretory vesicles and the plasma membrane. EMBO J *10*, 3589–3601.

Rettig, J., and Neher, E. (2002). Emerging roles of presynaptic proteins in Ca++-triggered exocytosis. Science *298*, 781–785.

Revel, J.P., and Karnovsky, M.J. (1967). Hexagonal array of subunits in intercellular junctions of the mouse heart and liver. J Cell Biol *33*, C7–C12.

Richards, M.W., O'Regan, L., Mas-Droux, C., Blot, J.M.Y., Cheung, J., Hoelder, S., Fry, A.M., and Bayliss, R. (2009). An autoinhibitory tyrosine motif in the cell-cycle-regulated Nek7 kinase is released through binding of Nek9. Mol Cell *36*, 560–570.

Rico, B., Xu, B., and Reichardt, L.F. (2002). TrkB receptor signaling is required for establishment of GABAergic synapses in the cerebellum. Nat Neurosci *5*, 225–233.

Rico, B., Beggs, H.E., Schahin-Reed, D., Kimes, N., Schmidt, A., and Reichardt, L.F. (2004). Control of axonal branching and synapse formation by focal adhesion kinase. Nat Neurosci *7*, 1059–1069.

Ritchie, M.E., Phipson, B., Wu, D., Hu, Y., Law, C.W., Shi, W., and Smyth, G.K. (2015). limma powers differential expression analyses for RNA-sequencing and microarray studies. Nucleic Acids Res *43*, e47.

Riveros, N., Fiedler, J., Lagos, N., Muñoz, C., and Orrego, F. (1986). Glutamate in rat brain cortex synaptic vesicles: influence of the vesicle isolation procedure. Brain Res *386*, 405–408.

Rizzoli, S.O., and Jahn, R. (2007). Kiss-and-run, collapse and "readily retrievable" vesicles. Traffic *8*, 1137–1144.

Robitaille, R., Adler, E.M., and Charlton, M.P. (1990). Strategic location of calcium channels at transmitter release sites of frog neuromuscular synapses. Neuron *5*, 773–779.

Rocca, J. (2003). Galen on the brain: anatomical knowledge and physiological speculation in the second century AD. Stud Anc Med *26*, 1–313.

Rodenas-Ruano, A., Perez-Pinzon, M.A., Green, E.J., Henkemeyer, M., and Liebl, D.J. (2006). Distinct roles for ephrinB3 in the formation and function of hippocampal synapses. Dev Biol *292*, 34–45.

Rodriguez, O.C., Schaefer, A.W., Mandato, C.A., Forscher, P., Bement, W.M., and Waterman-Storer, C.M. (2003). Conserved microtubule-actin interactions in cell movement and morphogenesis. Nat Cell Biol *5*, 599–609.

Roos, J., Hummel, T., Ng, N., Klämbt, C., and Davis, G.W. (2000). Drosophila Futsch regulates synaptic microtubule organization and is necessary for synaptic growth. Neuron *26*, 371–382.

Rubenstein, J.L.R., and Merzenich, M.M. (2003). Model of autism: increased ratio of excitation/inhibition in key neural systems. Genes Brain Behav *2*, 255–267.

Rudy, B., Fishell, G., Lee, S., and Hjerling-Leffler, J. (2011). Three groups of interneurons account for nearly 100% of neocortical GABAergic neurons. Dev Neurobiol *71*, 45–61.

Runyan, C.A., and Sur, M. (2013). Response selectivity is correlated to dendritic structure in parvalbumin-expressing inhibitory neurons in visual cortex. J Neurosci *33*, 11724–11733.

Ruthazer, E.S., Li, J., and Cline, H.T. (2006). Stabilization of axon branch dynamics by synaptic maturation. J Neurosci *26*, 3594–3603.

Ruthel, G., and Hollenbeck, P.J. (2000). Growth cones are not required for initial establishment of polarity or differential axon branch growth in cultured hippocampal neurons. J Neurosci *20*, 2266–2274.

Sabo, S.L., Gomes, R.A., and McAllister, A.K. (2006). Formation of presynaptic terminals at predefined sites along axons. J Neurosci *26*, 10813–10825.

Sakaguchi, M., Shingo, T., Shimazaki, T., Okano, H.J., Shiwa, M., Ishibashi, S., Oguro, H., Ninomiya, M., Kadoya, T., Horie, H., *et al.* (2006). A carbohydrate-binding protein, Galectin-1, promotes proliferation of adult neural stem cells. Proc Natl Acad Sci U S A *103*, 7112–7117.

Sakaguchi, M., Arruda-Carvalho, M., Kang, N.H., Imaizumi, Y., Poirier, F., Okano, H., and Frankland, P.W. (2011). Impaired spatial and contextual memory formation in galectin-1 deficient mice. Mol Brain *4*, 33.

Salameh, B.A., Cumpstey, I., Sundin, A., Leffler, H., and Nilsson, U.J. (2010). 1H-1,2,3-triazol-1-yl thiodigalactoside derivatives as high affinity galectin-3 inhibitors. Bioorg Med Chem *18*, 5367–5378.

Salem, H., Rachmin, I., Yissachar, N., Cohen, S., Amiel, A., Haffner, R., Lavi, L., and Motro, B. (2010). Nek7 kinase targeting leads to early mortality, cytokinesis disturbance and polyploidy. Oncogene *29*, 4046–4057.

Salomonsson, E., Carlsson, M.C., Osla, V., Hendus-Altenburger, R., Kahl-Knutson, B., Oberg, C.T., Sundin, A., Nilsson, R., Nordberg-Karlsson, E., Nilsson, U.J., *et al.* (2010). Mutational tuning of galectin-3 specificity and biological function. J Biol Chem *285*, 35079–35091.

Sambrook, J., and Russell, D.W. (David W. (2001). Molecular cloning: A laboratory manual (Cold Spring Harbor, N.Y: Cold Spring Harbor Laboratory Press).

Sánchez-Huertas, C., and Rico, B. (2011). CREB-Dependent Regulation of GAD65 Transcription by BDNF/TrkB in Cortical Interneurons. Cereb Cortex *21*, 777–788.

Sánchez-Huertas, C., Freixo, F., Viais, R., Lacasa, C., Soriano, E., and Lüders, J. (2016). Non-centrosomal nucleation mediated by augmin organizes microtubules in post-mitotic neurons and controls axonal microtubule polarity. Nat Commun *7*, 12187.

Sando, R., Bushong, E., Zhu, Y., Huang, M., Considine, C., Phan, S., Ju, S., Uytiepo, M., Ellisman, M., and Maximov, A. (2017). Assembly of excitatory synapses in the absence of glutamatergic neurotransmission. Neuron *94*, 312–321.e3.

Sango, K., Tokashiki, A., Ajiki, K., Horie, M., Kawano, H., Watabe, K., Horie, H., and Kadoya, T. (2004). Synthesis, localization and externalization of galectin-1 in mature dorsal root ganglion neurons and Schwann cells. Eur J Neurosci *19*, 55–64.

Sankaranarayanan, S., Atluri, P.P., and Ryan, T.A. (2003). Actin has a molecular scaffolding, not propulsive, role in presynaptic function. Nat Neurosci *6*, 127–135.

Schaefer, A.M., Hadwiger, G.D., and Nonet, M.L. (2000). rpm-1, a conserved neuronal gene that regulates targeting and synaptogenesis in C. elegans. Neuron *26*, 345–356.

Scheiffele, P. (2003). Cell-cell signaling during synapse formation in the CNS. Annu Rev Neurosci *26*, 485–508.

Scheiffele, P., Fan, J., Choih, J., Fetter, R., and Serafini, T. (2000). Neuroligin expressed in nonneuronal cells triggers presynaptic development in contacting axons. Cell *101*, 657–669.

Schikorski, T., and Stevens, C.F. (1997). Quantitative ultrastructural analysis of hippocampal excitatory synapses. J Neurosci *17*, 5858–5867.

Schindelin, J., Arganda-Carreras, I., Frise, E., Kaynig, V., Longair, M., Pietzsch, T., Preibisch, S., Rueden, C., Saalfeld, S., Schmid, B., *et al.* (2012). Fiji: an open-source platform for biological-image analysis. Nat Methods *9*, 676–682.

Schneider, C.A., Rasband, W.S., and Eliceiri, K.W. (2012). NIH Image to ImageJ: 25 years of image analysis. Nat Methods *9*, 671–675.

Schweizer, F.E., and Ryan, T.A. (2006). The synaptic vesicle: cycle of exocytosis and endocytosis. Curr Opin Neurobiol *16*, 298–304.

Scolding (1999). Greenfield's neuropathology. Sixth edition. J Neurol Neurosurg Psychiatr *66*, 696.

Shalom, O., Shalva, N., Altschuler, Y., and Motro, B. (2008). The mammalian Nek1 kinase is involved in primary cilium formation. FEBS Lett *582*, 1465–1470.

Shapira, M., Zhai, R.G., Dresbach, T., Bresler, T., Torres, V.I., Gundelfinger, E.D., Ziv, N.E., and Garner, C.C. (2003). Unitary assembly of presynaptic active zones from Piccolo-Bassoon transport vesicles. Neuron *38*, 237–252.

Shapiro, L., and Colman, D.R. (1999). The diversity of cadherins and implications for a synaptic adhesive code in the CNS. Neuron *23*, 427–430.

Sharma, K., Choi, S.-Y., Zhang, Y., Nieland, T.J.F., Long, S., Li, M., and Huganir, R.L. (2013). High-throughput genetic screen for synaptogenic factors: identification of LRP6 as critical for excitatory synapse development. Cell Rep *5*, 1330–1341.

Shelly, M., Cancedda, L., Heilshorn, S., Sumbre, G., and Poo, M.-M. (2007). LKB1/STRAD promotes axon initiation during neuronal polarization. Cell *129*, 565–577.

Shelly, M., Cancedda, L., Lim, B.K., Popescu, A.T., Cheng, P., Gao, H., and Poo, M. (2011). Semaphorin3A regulates neuronal polarization by suppressing axon formation and promoting dendrite growth. Neuron *71*, 433–446.

Sheng, M., and Sala, C. (2001). PDZ domains and the organization of supramolecular complexes. Annu Rev Neurosci *24*, 1–29.

Shetty, A., Sytnyk, V., Leshchyns'ka, I., Puchkov, D., Haucke, V., and Schachner, M. (2013). The neural cell adhesion molecule promotes maturation of the presynaptic endocytotic machinery by switching synaptic vesicle recycling from adaptor protein 3 (AP-3)- to AP-2-dependent mechanisms. J Neurosci *33*, 16828–16845.

Shi, S.-H., Jan, L.Y., and Jan, Y.-N. (2003). Hippocampal neuronal polarity specified by spatially localized mPar3/mPar6 and PI 3-kinase activity. Cell *112*, 63–75.

Shi, S.-H., Cheng, T., Jan, L.Y., and Jan, Y.-N. (2004). APC and GSK-3beta are involved in mPar3 targeting to the nascent axon and establishment of neuronal polarity. Curr Biol *14*, 2025–2032.

Sholl, D.A. (1953). Dendritic organization in the neurons of the visual and motor cortices of the cat. J Anat *87*, 387–406.

Sigler, A., Oh, W.C., Imig, C., Altas, B., Kawabe, H., Cooper, B.H., Kwon, H.-B., Rhee, J.-S., and Brose, N. (2017). Formation and maintenance of functional spines in the absence of presynaptic glutamate release. Neuron *94*, 304–311.e4.

Siksou, L., Varoqueaux, F., Pascual, O., Triller, A., Brose, N., and Marty, S. (2009). A common molecular basis for membrane docking and functional priming of synaptic vesicles. Eur J Neurosci *30*, 49–56.

Singh, J., and Kaur, G. (2009). Transcriptional regulation of PSA-NCAM expression by NMDA receptor activation in RA-differentiated C6 glioma cultures. Brain Res Bull *79*, 157–168.

Smith, D.H., Wolf, J.A., and Meaney, D.F. (2001). A new strategy to produce sustained growth of central nervous system axons: continuous mechanical tension. Tissue Eng *7*, 131–139.

Sohal, V.S., Zhang, F., Yizhar, O., and Deisseroth, K. (2009). Parvalbumin neurons and gamma rhythms enhance cortical circuit performance. Nature *459*, 698–702.

Sohya, K., Kameyama, K., Yanagawa, Y., Obata, K., and Tsumoto, T. (2007). GABAergic neurons are less selective to stimulus orientation than excitatory neurons in layer II/III of visual cortex, as revealed by in vivo functional Ca2+ imaging in transgenic mice. J Neurosci *27*, 2145–2149.

Sommeijer, J.-P., and Levelt, C.N. (2012). Synaptotagmin-2 is a reliable marker for parvalbumin positive inhibitory boutons in the mouse visual cortex. PLoS ONE *7*, e35323.

Somogyi, P., and Klausberger, T. (2005). Defined types of cortical interneurone structure space and spike timing in the hippocampus. J Physiol (Lond) *562*, 9–26.

Somogyi, J., Baude, A., Omori, Y., Shimizu, H., El Mestikawy, S., Fukaya, M., Shigemoto, R., Watanabe, M., and Somogyi, P. (2004). GABAergic basket cells expressing cholecystokinin contain vesicular glutamate transporter type 3 (VGLUT3) in their synaptic terminals in hippocampus and isocortex of the rat. Eur J Neurosci *19*, 552–569.

Song, A.-H., Wang, D., Chen, G., Li, Y., Luo, J., Duan, S., and Poo, M.-M. (2009). A selective filter for cytoplasmic transport at the axon initial segment. Cell *136*, 1148–1160.

Sörme, P., Qian, Y., Nyholm, P., Leffler, H., and Nilsson, U.J. (2002). Low Micromolar Inhibitors of Galectin-3 Based on 3′-Derivatization of N-Acetyllactosamine. ChemBioChem.

Southwell, D.G., Paredes, M.F., Galvao, R.P., Jones, D.L., Froemke, R.C., Sebe, J.Y., Alfaro-Cervello, C., Tang, Y., Garcia-Verdugo, J.M., Rubenstein, J.L., *et al.* (2012). Intrinsically determined cell death of developing cortical interneurons. Nature *491*, 109–113.

De Souza, E.E., Meirelles, G.V., Godoy, B.B., Perez, A.M., Smetana, J.H.C., Doxsey, S.J., McComb, M.E., Costello, C.E., Whelan, S.A., and Kobarg, J. (2014). Characterization of the human NEK7 interactome suggests catalytic and regulatory properties distinct from those of NEK6. J Proteome Res *13*, 4074–4090.

Spencer, K.M., Nestor, P.G., Niznikiewicz, M.A., Salisbury, D.F., Shenton, M.E., and McCarley, R.W. (2003). Abnormal neural synchrony in schizophrenia. J Neurosci *23*, 7407–7411.

Spiegel, I., Mardinly, A.R., Gabel, H.W., Bazinet, J.E., Couch, C.H., Tzeng, C.P., Harmin, D.A., and Greenberg, M.E. (2014). Npas4 regulates excitatory-inhibitory balance within neural circuits through cell-type-specific gene programs. Cell *157*, 1216–1229.

Stark, E., Eichler, R., Roux, L., Fujisawa, S., Rotstein, H.G., and Buzsáki, G. (2013). Inhibition-induced theta resonance in cortical circuits. Neuron *80*, 1263–1276.

Stark, E., Roux, L., Eichler, R., Senzai, Y., Royer, S., and Buzsáki, G. (2014). Pyramidal cell-interneuron interactions underlie hippocampal ripple oscillations. Neuron *83*, 467–480.

Stepanyants, A., Tamás, G., and Chklovskii, D.B. (2004). Class-specific features of neuronal wiring. Neuron *43*, 251–259.

Steward, O., and Levy, W.B. (1982). Preferential localization of polyribosomes under the base of dendritic spines in granule cells of the dentate gyrus. J Neurosci *2*, 284–291.

Steward, O., and Schuman, E.M. (2001). Protein synthesis at synaptic sites on dendrites. Annu Rev Neurosci *24*, 299–325.

Stowell, S.R., Dias-Baruffi, M., Penttilä, L., Renkonen, O., Nyame, A.K., and Cummings, R.D. (2004). Human galectin-1 recognition of poly-N-acetyllactosamine and chimeric polysaccharides. Glycobiology *14*, 157–167.

Sudhof, T.C. (2004). The synaptic vesicle cycle. Annu Rev Neurosci *27*, 509–547.

Südhof, T.C., and Rizo, J. (2011). Synaptic vesicle exocytosis. Cold Spring Harb Perspect Biol *3*.

Südhof, T.C., and Rothman, J.E. (2009). Membrane fusion: grappling with SNARE and SM proteins. Science *323*, 474–477.

Sun, Y., Paşca, S.P., Portmann, T., Goold, C., Worringer, K.A., Guan, W., Chan, K.C., Gai, H., Vogt, D., Chen, Y.-J.J., *et al.* (2016). A deleterious Nav1.1 mutation selectively impairs telencephalic inhibitory neurons derived from Dravet Syndrome patients. Elife *5*.

Sussel, L., Marin, O., Kimura, S., and Rubenstein, J.L. (1999). Loss of Nkx2.1 homeobox gene function results in a ventral to dorsal molecular respecification within the basal telencephalon: evidence for a transformation of the pallidum into the striatum. Development *126*, 3359–3370.

Suter, D.M., and Miller, K.E. (2011). The emerging role of forces in axonal elongation. Prog Neurobiol *94*, 91–101.

Suter, D.M., Schaefer, A.W., and Forscher, P. (2004). Microtubule dynamics are necessary for SRC family kinase-dependent growth cone steering. Curr Biol *14*, 1194–1199.

Sutton, M.A., and Schuman, E.M. (2005). Local translational control in dendrites and its role in long-term synaptic plasticity. J Neurobiol *64*, 116–131.

Sytnyk, V., Leshchyns'ka, I., Nikonenko, A.G., and Schachner, M. (2006). NCAM promotes assembly and activity-dependent remodeling of the postsynaptic signaling complex. J Cell Biol *174*, 1071–1085.

Szebenyi, G., Callaway, J.L., Dent, E.W., and Kalil, K. (1998). Interstitial branches develop from active regions of the axon demarcated by the primary growth cone during pausing behaviors. J Neurosci *18*, 7930–7940.

Tada, T., and Sheng, M. (2006). Molecular mechanisms of dendritic spine morphogenesis. Curr Opin Neurobiol *16*, 95–101.

Takai, Y., and Nakanishi, H. (2003). Nectin and afadin: novel organizers of intercellular junctions. J Cell Sci *116*, 17–27.

Takasu, M.A., Dalva, M.B., Zigmond, R.E., and Greenberg, M.E. (2002). Modulation of NMDA receptor-dependent calcium influx and gene expression through EphB receptors. Science *295*, 491–495.

Takei, Y., Teng, J., Harada, A., and Hirokawa, N. (2000). Defects in axonal elongation and neuronal migration in mice with disrupted tau and map1b genes. J Cell Biol *150*, 989–1000.

Takeichi, M., and Abe, K. (2005). Synaptic contact dynamics controlled by cadherin and catenins. Trends Cell Biol *15*, 216–221.

Tallon-Baudry, C., Bertrand, O., Peronnet, F., and Pernier, J. (1998). Induced gamma-band activity during the delay of a visual short-term memory task in humans. J Neurosci *18*, 4244–4254.

Tamagnone, L., Artigiani, S., Chen, H., He, Z., Ming, G.I., Song, H., Chedotal, A., Winberg, M.L., Goodman, C.S., Poo, M., *et al.* (1999). Plexins are a large family of receptors for transmembrane, secreted, and GPI-anchored semaphorins in vertebrates. Cell *99*, 71–80.

Taniguchi, H., Lu, J., and Huang, Z.J. (2013). The spatial and temporal origin of chandelier cells in mouse neocortex. Science *339*, 70–74.

Tasic, B., Menon, V., Nguyen, T.N., Kim, T.K., Jarsky, T., Yao, Z., Levi, B., Gray, L.T., Sorensen, S.A., Dolbeare, T., *et al.* (2016). Adult mouse cortical cell taxonomy revealed by single cell transcriptomics. Nat Neurosci *19*, 335–346.

Tenne-Brown, J., Puche, A.C., and Key, B. (1998). Expression of galectin-1 in the mouse olfactory system. Int J Dev Biol *42*, 791–799.

Terauchi, A., Johnson-Venkatesh, E.M., Toth, A.B., Javed, D., Sutton, M.A., and Umemori, H. (2010). Distinct FGFs promote differentiation of excitatory and inhibitory synapses. Nature *465*, 783–787.

Tessier-Lavigne, M. (1995). Eph receptor tyrosine kinases, axon repulsion, and the development of topographic maps. Cell *82*, 345–348.

Tillo, M., Ruhrberg, C., and Mackenzie, F. (2012). Emerging roles for semaphorins and VEGFs in synaptogenesis and synaptic plasticity. Cell Adh Migr *6*, 541–546.

Ting, A.K., Chen, Y., Wen, L., Yin, D.-M., Shen, C., Tao, Y., Liu, X., Xiong, W.-C., and Mei, L. (2011). Neuregulin 1 promotes excitatory synapse development and function in GABAergic interneurons. J Neurosci *31*, 15–25.

Togashi, H., Abe, K., Mizoguchi, A., Takaoka, K., Chisaka, O., and Takeichi, M. (2002). Cadherin regulates dendritic spine morphogenesis. Neuron *35*, 77–89.

Togashi, H., Miyoshi, J., Honda, T., Sakisaka, T., Takai, Y., and Takeichi, M. (2006). Interneurite affinity is regulated by heterophilic nectin interactions in concert with the cadherin machinery. J Cell Biol *174*, 141–151.

Tortosa, E., Galjart, N., Avila, J., and Sayas, C.L. (2013). MAP1B regulates microtubule dynamics by sequestering EB1/3 in the cytosol of developing neuronal cells. EMBO J *32*, 1293–1306.

Trachtenberg, J.T., Chen, B.E., Knott, G.W., Feng, G., Sanes, J.R., Welker, E., and Svoboda, K. (2002). Long-term in vivo imaging of experience-dependent synaptic plasticity in adult cortex. Nature *420*, 788–794.

Tran, T.S., Rubio, M.E., Clem, R.L., Johnson, D., Case, L., Tessier-Lavigne, M., Huganir, R.L., Ginty, D.D., and Kolodkin, A.L. (2009). Secreted semaphorins control spine distribution and morphogenesis in the postnatal CNS. Nature *462*, 1065–1069.

Tremblay, R., Lee, S., and Rudy, B. (2016). Gabaergic interneurons in the neocortex: from cellular properties to circuits. Neuron *91*, 260–292.

Tusher, V.G., Tibshirani, R., and Chu, G. (2001). Significance analysis of microarrays applied to the ionizing radiation response. Proc Natl Acad Sci U S A *98*, 5116–5121.

Uhlhaas, P.J., and Singer, W. (2010). Abnormal neural oscillations and synchrony in schizophrenia. Nat Rev Neurosci *11*, 100–113.

Ullian, E.M., Christopherson, K.S., and Barres, B.A. (2004). Role for glia in synaptogenesis. Glia *47*, 209–216.

Umemori, H., Linhoff, M.W., Ornitz, D.M., and Sanes, J.R. (2004). FGF22 and its close relatives are presynaptic organizing molecules in the mammalian brain. Cell *118*, 257–270.

Unwin, N. (1989). The structure of ion channels in membranes of excitable cells. Neuron *3*, 665–676.

Vaithianathan, T., Matthias, K., Bahr, B., Schachner, M., Suppiramaniam, V., Dityatev, A., and Steinhaüser, C. (2004). Neural cell adhesion molecule-associated polysialic acid potentiates alpha-amino-3-hydroxy-5-methylisoxazole-4-propionic acid receptor currents. J Biol Chem *279*, 47975–47984.

Valiente, M., Ciceri, G., Rico, B., and Marín, O. (2011). Focal adhesion kinase modulates radial glia-dependent neuronal migration through connexin-26. J Neurosci *31*, 11678–11691.

Varoqueaux, F., Jamain, S., and Brose, N. (2004). Neuroligin 2 is exclusively localized to inhibitory synapses. Eur J Cell Biol *83*, 449–456.

Varoqueaux, F., Aramuni, G., Rawson, R.L., Mohrmann, R., Missler, M., Gottmann, K., Zhang, W., Südhof, T.C., and Brose, N. (2006). Neuroligins determine synapse maturation and function. Neuron *51*, 741–754.

Vaughn, J.E. (1989). Fine structure of synaptogenesis in the vertebrate central nervous system. Synapse *3*, 255–285.

Vaughn, J.E., and Sims, T.J. (1978). Axonal growth cones and developing axonal collaterals form synaptic junctions in embryonic mouse spinal cord. J Neurocytol *7*, 337–363.

Vélez-Fort, M., Rousseau, C.V., Niedworok, C.J., Wickersham, I.R., Rancz, E.A., Brown, A.P.Y., Strom, M., and Margrie, T.W. (2014). The stimulus selectivity and connectivity of layer six principal cells reveals cortical microcircuits underlying visual processing. Neuron *83*, 1431–1443.

Verret, L., Mann, E.O., Hang, G.B., Barth, A.M.I., Cobos, I., Ho, K., Devidze, N., Masliah, E., Kreitzer, A.C., Mody, I., *et al.* (2012). Inhibitory interneuron deficit links altered network activity and cognitive dysfunction in Alzheimer model. Cell *149*, 708–721.

Vicario-Abejón, C., Collin, C., McKay, R.D., and Segal, M. (1998). Neurotrophins induce formation of functional excitatory and inhibitory synapses between cultured hippocampal neurons. J Neurosci *18*, 7256–7271.

Vogt Weisenhorn, D.M., Celio, M.R., and Rickmann, M. (1998). The onset of parvalbumin-expression in interneurons of the rat parietal cortex depends upon extrinsic factor(s). Eur J Neurosci *10*, 1027–1036.

Waites, C.L., Craig, A.M., and Garner, C.C. (2005). Mechanisms of vertebrate synaptogenesis. Annu Rev Neurosci *28*, 251–274.

Wall, N.R., De La Parra, M., Sorokin, J.M., Taniguchi, H., Huang, Z.J., and Callaway, E.M. (2016). Brain-Wide Maps of Synaptic Input to Cortical Interneurons. J Neurosci *36*, 4000–4009.

Wamsley, B., and Fishell, G. (2017). Genetic and activity-dependent mechanisms underlying interneuron diversity. Nat Rev Neurosci *18*, 299–309.

Wang, C.-Y., Chang, K., Petralia, R.S., Wang, Y.-X., Seabold, G.K., and Wenthold, R.J. (2006). A novel family of adhesion-like molecules that interacts with the NMDA receptor. J Neurosci *26*, 2174–2183.

Wang, W., Mullikin-Kilpatrick, D., Crandall, J.E., Gronostajski, R.M., Litwack, E.D., and Kilpatrick, D.L. (2007). Nuclear factor I coordinates multiple phases of cerebellar granule cell development via regulation of cell adhesion molecules. J Neurosci *27*, 6115–6127.

Wang, Y., Toledo-Rodriguez, M., Gupta, A., Wu, C., Silberberg, G., Luo, J., and Markram, H. (2004). Anatomical, physiological and molecular properties of Martinotti cells in the somatosensory cortex of the juvenile rat. J Physiol (Lond) *561*, 65–90.

Washbourne, P., Bennett, J.E., and McAllister, A.K. (2002). Rapid recruitment of NMDA receptor transport packets to nascent synapses. Nat Neurosci *5*, 751–759.

Wickham, H. (2009). Ggplot2: Elegant graphics for data analysis (New York: Springer).

Wierenga, C.J., Becker, N., and Bonhoeffer, T. (2008). GABAergic synapses are formed without the involvement of dendritic protrusions. Nat Neurosci *11*, 1044–1052.

Williams, M.E., Wilke, S.A., Daggett, A., Davis, E., Otto, S., Ravi, D., Ripley, B., Bushong, E.A., Ellisman, M.H., Klein, G., *et al.* (2011). Cadherin-9 regulates synapse-specific differentiation in the developing hippocampus. Neuron *71*, 640–655.

Winckler, B., Forscher, P., and Mellman, I. (1999). A diffusion barrier maintains distribution of membrane proteins in polarized neurons. Nature *397*, 698–701.

Winden, K.D., Oldham, M.C., Mirnics, K., Ebert, P.J., Swan, C.H., Levitt, P., Rubenstein, J.L., Horvath, S., and Geschwind, D.H. (2009). The organization of the transcriptional network in specific neuronal classes. Mol Syst Biol *5*, 291.

Wittmann, T., Bokoch, G.M., and Waterman-Storer, C.M. (2003). Regulation of leading edge microtubule and actin dynamics downstream of Rac1. J Cell Biol *161*, 845–851.

Wittmann, T., Bokoch, G.M., and Waterman-Storer, C.M. (2004). Regulation of microtubule destabilizing activity of Op18/stathmin downstream of Rac1. J Biol Chem *279*, 6196–6203.

Wobst, H., Schmitz, B., Schachner, M., Diestel, S., Leshchyns'ka, I., and Sytnyk, V. (2015). Kinesin-1 promotes post-Golgi trafficking of NCAM140 and NCAM180 to the cell surface. J Cell Sci *128*, 2816–2829.

Wu, H., Reuver, S.M., Kuhlendahl, S., Chung, W.J., and Garner, C.C. (1998). Subcellular targeting and cytoskeletal attachment of SAP97 to the epithelial lateral membrane. J Cell Sci *111 (Pt 16)*, 2365–2376.

Wu, X., Fu, Y., Knott, G., Lu, J., Di Cristo, G., and Huang, Z.J. (2012). GABA signaling promotes synapse elimination and axon pruning in developing cortical inhibitory interneurons. J Neurosci *32*, 331–343.

Xia, C.-H., Roberts, E.A., Her, L.-S., Liu, X., Williams, D.S., Cleveland, D.W., and Goldstein, L.S.B. (2003). Abnormal neurofilament transport caused by targeted disruption of neuronal kinesin heavy chain KIF5A. J Cell Biol *161*, 55–66.

Xu, X., and Callaway, E.M. (2009). Laminar specificity of functional input to distinct types of inhibitory cortical neurons. J Neurosci *29*, 70–85.

Xu, D., Hopf, C., Reddy, R., Cho, R.W., Guo, L., Lanahan, A., Petralia, R.S., Wenthold, R.J., O'Brien, R.J., and Worley, P. (2003). Narp and NP1 form heterocomplexes that function in developmental and activity-dependent synaptic plasticity. Neuron *39*, 513–528.

Xu, Q., Wonders, C.P., and Anderson, S.A. (2005). Sonic hedgehog maintains the identity of cortical interneuron progenitors in the ventral telencephalon. Development *132*, 4987–4998.

Yabe, J.T., Pimenta, A., and Shea, T.B. (1999). Kinesin-mediated transport of neurofilament protein oligomers in growing axons. J Cell Sci *112 (Pt 21)*, 3799–3814.

Yang, Y., Dieter, M.Z., Chen, Y., Shertzer, H.G., Nebert, D.W., and Dalton, T.P. (2002). Initial characterization of the glutamate-cysteine ligase modifier subunit Gclm(-/-) knockout mouse. Novel model system for a severely compromised oxidative stress response. J Biol Chem *277*, 49446–49452.

Yau, H.-J., Wang, H.-F., Lai, C., and Liu, F.-C. (2003). Neural development of the neuregulin receptor ErbB4 in the cerebral cortex and the hippocampus: preferential expression by interneurons tangentially migrating from the ganglionic eminences. Cereb Cortex *13*, 252–264.

Ye, Z., Mostajo-Radji, M.A., Brown, J.R., Rouaux, C., Tomassy, G.S., Hensch, T.K., and Arlotta, P. (2015). Instructing perisomatic inhibition by direct lineage reprogramming of neocortical projection neurons. Neuron *88*, 475–483.

Yi, J.J., Barnes, A.P., Hand, R., Polleux, F., and Ehlers, M.D. (2010). TGF-beta signaling specifies axons during brain development. Cell *142*, 144–157.

Yissachar, N., Salem, H., Tennenbaum, T., and Motro, B. (2006). Nek7 kinase is enriched at the centrosome, and is required for proper spindle assembly and mitotic progression. FEBS Lett *580*, 6489–6495.

Yoshii, A., and Constantine-Paton, M. (2010). Postsynaptic BDNF-TrkB signaling in synapse maturation, plasticity, and disease. Dev Neurobiol *70*, 304–322.

Yu, G., Wang, L.-G., Han, Y., and He, Q.-Y. (2012). clusterProfiler: an R package for comparing biological themes among gene clusters. OMICS *16*, 284–287.

Yu, W., Qiang, L., Solowska, J.M., Karabay, A., Korulu, S., and Baas, P.W. (2008). The microtubule-severing proteins spastin and katanin participate differently in the formation of axonal branches. Mol Biol Cell *19*, 1485–1498.

Yuste, R., and Bonhoeffer, T. (2004). Genesis of dendritic spines: insights from ultrastructural and imaging studies. Nat Rev Neurosci *5*, 24–34.

Zeisel, A., Muñoz-Manchado, A.B., Codeluppi, S., Lönnerberg, P., La Manno, G., Juréus, A., Marques, S., Munguba, H., He, L., Betsholtz, C., *et al.* (2015). Brain structure. Cell types in the mouse cortex and hippocampus revealed by single-cell RNA-seq. Science *347*, 1138–1142.

Zhai, R.G., Vardinon-Friedman, H., Cases-Langhoff, C., Becker, B., Gundelfinger, E.D., Ziv, N.E., and Garner, C.C. (2001). Assembling the presynaptic active zone: a characterization of an active one precursor vesicle. Neuron *29*, 131–143.

Zhang, S. (2007). A comprehensive evaluation of SAM, the SAM R-package and a simple modification to improve its performance. BMC Bioinformatics *8*, 230.

Zhang, S.J., and Jackson, M.B. (1993). GABA-activated chloride channels in secretory nerve endings. Science *259*, 531–534.

Zhang, W., and Benson, D.L. (2001). Stages of synapse development defined by dependence on F-actin. J Neurosci *21*, 5169–5181.

Zhang, W., and Benson, D.L. (2002). Developmentally regulated changes in cellular compartmentation and synaptic distribution of actin in hippocampal neurons. J Neurosci Res *69*, 427–436.

Zhang, C., Atasoy, D., Araç, D., Yang, X., Fucillo, M.V., Robison, A.J., Ko, J., Brunger, A.T., and Südhof, T.C. (2010). Neurexins physically and functionally interact with GABA(A) receptors. Neuron *66*, 403–416.

Zhou, F.-Q., Zhou, J., Dedhar, S., Wu, Y.-H., and Snider, W.D. (2004). NGF-induced axon growth is mediated by localized inactivation of GSK-3beta and functions of the microtubule plus end binding protein APC. Neuron *42*, 897–912.

Zhu, P.C., Thureson-Klein, A., and Klein, R.L. (1986). Exocytosis from large dense cored vesicles outside the active synaptic zones of terminals within the trigeminal subnucleus caudalis: a possible mechanism for neuropeptide release. Neuroscience *19*, 43–54.

Zito, K., Knott, G., Shepherd, G.M.G., Shenolikar, S., and Svoboda, K. (2004). Induction of spine growth and synapse formation by regulation of the spine actin cytoskeleton. Neuron *44*, 321–334.

Ziv, N.E., and Garner, C.C. (2004). Cellular and molecular mechanisms of presynaptic assembly. Nat Rev Neurosci *5*, 385–399.

Ziv, N.E., and Smith, S.J. (1996). Evidence for a role of dendritic filopodia in synaptogenesis and spine formation. Neuron *17*, 91–102.

Zuo, Y., Yang, G., Kwon, E., and Gan, W.-B. (2005a). Long-term sensory deprivation prevents dendritic spine loss in primary somatosensory cortex. Nature *436*, 261–265.

Zuo, Y., Lin, A., Chang, P., and Gan, W.-B. (2005b). Development of long-term dendritic spine stability in diverse regions of cerebral cortex. Neuron *46*, 181–189.